43322

NAME OF AUTHOR/*NOM DE L'AUTEUR* __REZA AHMADI__

TITLE OF THESIS/*TITRE DE LA THÈSE* __AN EXPERIMENTAL STUDY OF INTERACTION BETWEEN MAIN CHANNEL AND FLOOD PLAIN FLOWS__

UNIVERSITY/*UNIVERSITÉ* __University of Alberta, EDMONTON, ALBERTA__

DEGREE FOR WHICH THESIS WAS PRESENTED/
GRADE POUR LEQUEL CETTE THÈSE FUT PRÉSENTÉE __DOCTOR OF PHILOSOPHY__

YEAR THIS DEGREE CONFERRED/*ANNÉE D'OBTENTION DE CE GRADE* __FALL 1979__

NAME OF SUPERVISOR/*NOM DU DIRECTEUR DE THÈSE* __Dr. N. RAJARATNAM__

DATED/*DATÉ* __July 11/1979__ SIGNED/*SIGNÉ* __Reza Ahmadi__

PERMANENT ADDRESS/*RÉSIDENCE FIXÉ* __777 SUMMIT AVENUE HACKENSACK New Jersey United State__

NOTICE

AVIS

The quality of this microfiche is heavily dependent upon the quality of the original thesis submitted for microfilming. Every effort has been made to ensure the highest quality of reproduction possible.

If pages are missing, contact the university which granted the degree.

Some pages may have indistinct print especially if the original pages were typed with a poor typewriter ribbon or if the university sent us a poor photocopy.

Previously copyrighted materials (journal articles, published tests, etc.) are not filmed.

Reproduction in full or in part of this film is governed by the Canadian Copyright Act, R.S.C. 1970, c. C-30. Please read the authorization forms which accompany this thesis.

La qualité de cette microfiche dépend grandement de la qualité de la thèse soumise au microfilmage. Nous avons tout fait pour assurer une qualité supérieure de reproduction.

S'il manque des pages, veuillez communiquer avec l'université qui a conféré le grade.

La qualité d'impression de certaines pages peut laisser à désirer, surtout si les pages originales ont été dactylographiées à l'aide d'un ruban usé ou si l'université nous a fait parvenir une photocopie de mauvaise qualité.

Les documents qui font déjà l'objet d'un droit d'auteur (articles de revue, examens publiés, etc.) ne sont pas microfilmés.

La reproduction, même partielle, de ce microfilm est soumise à la Loi canadienne sur le droit d'auteur, SRC 1970, c. C-30. Veuillez prendre connaissance des formules d'autorisation qui accompagnent cette thèse.

THIS DISSERTATION
HAS BEEN MICROFILMED
EXACTLY AS RECEIVED

LA THÈSE A ÉTÉ
MICROFILMÉE TELLE QUE
NOUS L'AVONS REÇUE

THE UNIVERSITY OF ALBERTA

AN EXPERIMENTAL STUDY OF INTERACTION BETWEEN MAIN CHANNEL

AND FLOOD PLAIN FLOWS

by

Reza Ahmadi

Ⓒ

A THESIS

SUBMITTED TO THE FACULTY OF GRADUATE STUDIES AND RESEARCH

IN PARTIAL FULFILMENT OF THE REQUIREMENTS FOR THE DEGREE

OF Doctor of Philosophy

Civil Engineering

EDMONTON, ALBERTA

Fall 1979

THE UNIVERSITY OF ALBERTA

FACULTY OF GRADUATE STUDIES AND RESEARCH

The undersigned certify that they have read, and
recommend to the Faculty of Graduate Studies and Research,
for acceptance, a thesis entitled AN EXPERIMENTAL STUDY OF
INTERACTION BETWEEN MAIN CHANNEL AND FLOOD PLAIN FLOWS
submitted by Reza Ahmadi in partial fulfilment of the
requirements for the degree of Doctor of Philosophy.

....
Supervisor

....
John Shaw

....

....
External Examiner

Date...10 July 79.............................

Abstract

This study presents a method to analyse the interaction between flow in the main channel and the flood plain channel of a model river. The basic concept of this method has been supported by observation of the velocity field and shear stresses. The study was started by investigating the flow in a straight rectangular channel with smooth and rough boundaries. The effect of the aspect ratio on the distribution of the shear stresses on the bed and walls for both types of boundaries was investigated. More precise values of the aspect ratio and related shear stresses were obtained for better definition of a broad channel, which was wide enough to ensure that the presence of walls did not interfere with the main core of the flow. A straight and symmetrical compound cross-section with rectangular main and flood plain channels was tested and the results showed that momentum is transferred from the main channel to the flood plain channel thereby disturbing the velocity field and bed shear stress. It was found that the most important parameters for slowing down the flow in the main channel and increasing the flow in the flood plain channel are the relative width and depth of the main and flood plain channels. It was also found that the lateral variation of the longitudinal velocity is similar for various depths of flow. A suitable form of non-dimensional velocity distribution was introduced. A relationship for relative depth and length scale in the main and the flood plain channels was established suggesting that they are a measure

iv

of lateral penetration of momentum exchange in the main and flood plain channels.

Asymmetrical straight channels with wide main and flood plain channels were tested and it was determined that the flow pattern did not differ in principle from symmetrical straight channels and that the results for the symmetrical channels can be used for practical purposes.

The analysis was extended to include flow in meandering channels within a straight valley. Experimental results showed that helicoidal motion was not confined to the main curved channel. The upper part of the flow above the flood plain level has an effective width approximately equal to twice the amplitude of the meandering channel. In the main channel the flow retained the secondary flow characteristic by exhibiting higher velocity along the radially innermost (convex wall) wall and lower velocity along the outermost wall (concave wall). The tangential velocity profiles were approximately uniform and the logarithmic law was not valid, even as a rough approximation. The exchange of momentum was observed to take place between the channels with the breadth of twice the amplitude of the main channel curve and the flood plain channel. Comparison of the flow characteristics with and without the flood plain channel presented a number of interesting points and showed that it is possible to determine the zone of increasing velocity, length of penetration, and similarity of lateral velocity profiles. Because the velocity of the flow has a tendency to persist in one direction, it accelerates inside the curve wave over the flood plain and decelerates in the main channel. Isovel

maps showed that high velocity would occur on top of the flood plain close to the convex region suggesting that it is the excess shear stress associated with higher velocity which erodes the channel. This mechanism appears to be the principal reason for the straightening-out of the main meandering channel during the time of high flood in a river.

Qualitative tests were also conducted in the straight and meandering channels using dye to observe the flow direction. Eddy viscosity computations were made in a few cases.

ACKNOWLEDGMENTS

Table of Contents

ix

Tables

xi

Table of Figures

1. Introduction

1.1 General

If high flow in a river rises above the natural or
artificial banks in any reach, water from the overtopped
banks spreads out over the flood plain. Since the
characteristics of the flood plain make it a desirable
location for a variety of activities, it is important to
develop a method to determine the rating curve for high
discharges.

1.1.1 Introduction to Problem

Measures to control flood flows are only one set of
adjustments that can be made to combat the flood hazard. The
appraisal of such engineering measures, if they are to be
viewed in relation to their full consequences, requires the
analysis of other possible adjustments. Experience shows
that the construction and operation of engineering works to
control flood flows may reduce or curb flows without
necessarily reducing the threat of erosion to the river bed
and banks or the flood plain area. Little is known of the
shear stress distribution on a river bed and flood plain
bed. Rise of flow over the flood plain area together with
the increase of shear stress is capable of eroding the edge
of the flood plain and the main channel. The redistribution
of velocity and shear stress will affect the amount of
sediment transported in both channels as well as the
stability of the main channel bank and the flood plain beds.

1.2 Review of Flow in Channels with Flood Plain

When the depth of flow D in the main channel exceeds the depth of the main channel h, the flood plain carries a part of the total discharge. In the preparation of rating curves for rivers when D is much larger than d (where d is the depth of flow in the flood plain) the general practice (Chow, 1959) is to divide the compound flow section into a number of homogeneous sub-areas by the introduction of shear-free vertical boundaries which are the extension of the banks of the main channel. The flow is then computed for each subsection and the sum of the flow in all of the subsections is the total discharge Q. When D is only slightly larger than d, the division is done by introducing a horizontal plane as an extension of the bed of the flood plain (Smith, 1978, and Toebes & Sooky, 1967). The first method of sub-division is the one most frequently used since the majority of the practical cases have a large value of D/d. It has been generally recognized (Goncharov, 1964, Sellin, 1964, and Zheleznyakov, 1971) that appreciable interaction and turbulent mixing occurs between the faster main channel flow and the slower flood plain flow. Because of the transport of the longitudinal momentum to the flood plain, the vertical plane between the main channel and flood plain experiences significant (turbulent) shear stress in the longitudinal (or flow) direction. Wright & Carstens (1970) demonstrated the existence of this shear stress in an air-duct of a compound cross-section. A similar observation could be made from the study of Myers & Elsawy (1975) on a

rectangular main channel with an asymmetrical flood plain.

Sellin (1964) found that when the depth of flow D just exceeds the depth of the main channel h, the rate of increase of the discharge Q with the total depth of flow D becomes very small. For cases with a large value of D/d the discharge Q of the compound cross-section could be considerably less than the sum of the individual discharges of the homogeneous sub-areas, obtained by the introduction of the shear-free vertical separating walls. A few researchers (Sellin, 1964, Zheleznyakov, 1971, and Myers & Elsawy, 1975) found that in a channel with an asymmetric flood plain, the bed shear stress in the flood plain would be much larger than its undisturbed value, which would exist if there were no interaction with the main channel flow. Similarly, the main channel bed would experience a reduction of the bed shear stress from its undisturbed value. Some further observations on the interaction in straight channel have been made by Sellin (1964), Zheleznyakov (1971) and Ghosh & Jena (1971).

1.3 Effect of Curvature of Main Channel

It is well known that natural channels are neither straight and symmetrical nor are the boundaries hydraulically smooth. L.B. Leopold and W.B. Langbein in a United States Geological Survey report, "River Meanders" (1966) wrote:

"Is there such a thing as a straight river? Almost
anyone can think of a river that is more or less
straight for a certain distance, but it is unlikely
that the straight portion is either very straight or
very long. In fact, it is almost certain that the
distance any river is straight does not exceed 10
times its width at that point."

1.3.1 Review of the Literature on Curved Channels

Thomson in 1876 observed the spiral motion in a river

bend. Boussinesq theoretically solved the equations of

motion for the case of laminar flow in a curved pipe. Many

investigations have since been conducted on flow in bends.

B.C. Yen (1965) gives a brief summary of the important

experiments on flow in open-channel bends.

Fargue summarized his observation of the Garonne river

since 1849 and proposed a number of empirical laws dealing

with a meandering river and a mobile bed. Leliavsky verified

Fargue's laws from field observations. In 1934, Blue,

Herbert, and Lancefield published results of measurements in

the Iowa River. In 1935, Eakin published a study on the

curvature of the Mississippi River.

Among the analytical and experimental investigators,

Boss assumed free-vortex velocity distribution in the radial

direction. Yarnell and Woodward observed spiral motion.

Mockmore performed a theoretical study on flow in

open-channel bends by using assumed distributions of

velocity components. His study showed the streamlines to be

helicoidal.

Shukry (1949) presented the results of his experiments,

which covered a wide range of central angle, Froude number,

and aspect ratio.

Rozovskii (1957) reviewed the work of previous Russian investigators such as Ananyan and Milovich. With the aid of order-of-magnitude considerations and assumptions about eddy viscosity, vertical distribution of longitudinal velocity components, and zero net lateral discharge, Rozovskii was able to derive an approximate solution of the radial velocity component from Reynolds equations of motion. Using a number of other assumptions he attempted to solve for the radial distribution of the longitudinal velocity component and for the growth and decay of the spiral motion. The classical work in this area was done by Rozkovskii. More contemporary investigators have tended to accept Rozovskii's assumptions.

A widely accepted analytical and experimental investigation is that conducted by B.C. Yen in 1965. Yen proposed that, for fully developed flow in a bend, the loss of energy is the same for equal increments of the turning angle. Based on a logarithmic distribution of longitudinal velocity components along the vertical, and assuming that the eddy viscosity is a function of the depth and the radial distance, he derived an expression for the vertical distribution of the radial velocity component. However, by assuming that the coefficient of roughness in a curved channel is the same as that in a straight channel, he was able to derive an expression for the distribution of the average longitudinal velocity in the radial direction. He found that the average longitudinal velocity is approximately inversely proportional to the square root of

the radial distance from the center of the meander curve.

In 1974 Engelund assumed a constant tangential slope for fully developed flow in the curved channel and used similarity assumptions for radial and longitudinal velocity components. Further, he assumed that the longitudinal velocity followed the logarithmic distribution near the bed and parabolic distribution in the upper part of the flow. Based on these considerations, Engelund derived a fairly simple equations for the distribution of radial velocity over the depth and of longitudinal velocity over radial distance.

Ikeda's (1975) work closely followed that of Engelund. However, Ikeda proposed an arbitrary function for the distribution of tangential velocity over the width of the channel.

1.3.2 Comments on Assumptions in Flow Around Bends

In order to simplify the Reynolds equations of motion, certain general assumptions have been made by all investigators. An assumption which is frequently employed is the idea of fully developed flow around a bend. The fully developed flow in a pipe is reported after 300 degrees turn or more (Ellis & Joubert, 1974). In considering the flow in an open channel, it is impossible to reach fully developed flow because of the presence of the free water surface. If the bed slope of the valley is assumed constant throughout the entire reach as one can conclude from Figure 1.1, the bed slope of the main channel (in the straight portion) is the same as the valley slope. But as one moves along the

Flow ⟹

→ s

→ s

→ s
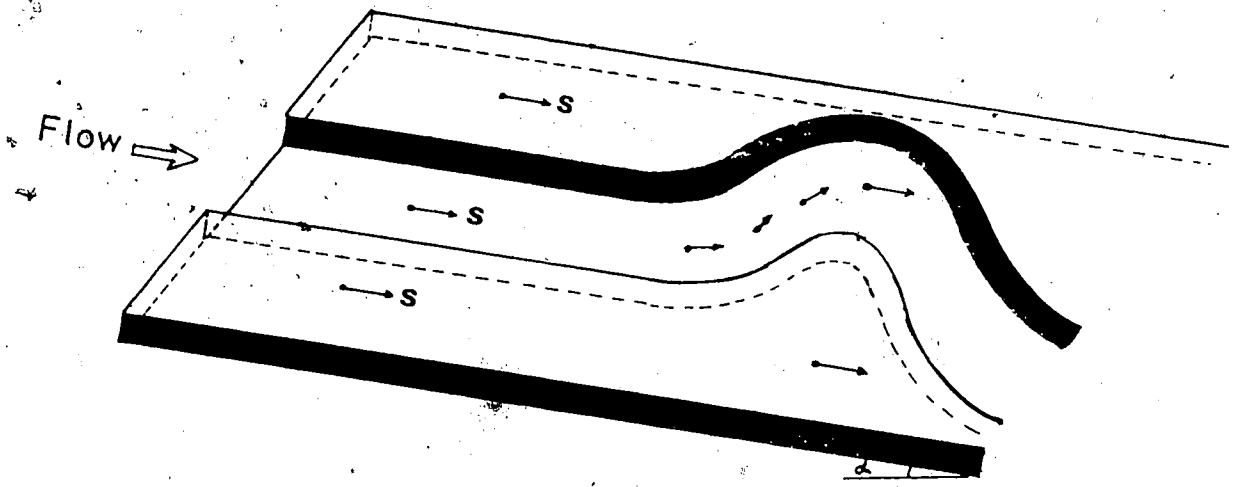
— Magnitude of Bed Slope

Figure 1.1 Variation of Bed Slope

U

U   U
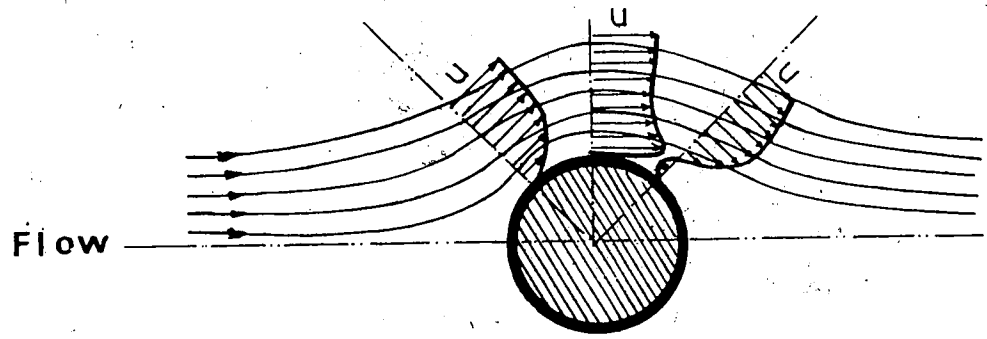
Flow

Figure 1.2 Flow Around Bluff Body

meandering path, the bed slope of the main channel changes accordingly. When the channel is running cross-wise, the bed slope is zero. If one assumes a flat bed, a water surface slope is required in order that the flow can take place, and since this means a drop in elevation the depth of flow will not be the same at all cross-sections. Thus, one cannot assume there is uniform flow, with a constant slope and depth of flow, even at the centerplane of the meandering channel. Choudhary et al. (1977) observed that in a 180 degree bend, of a narrow rectangular channel (aspect ratio of 5), and of a wide rectangular channel (aspect ratio of 20), the depth of flow changes with the angle of cross-section θ. Sieber & Gotz (1975) investigated the deviation of the tangential velocity from the mean velocity with θ. B.C. Yen and C.L. Yen (1971) studied the variation of the water surface slope with θ.

Another assumption is $S_o R = S r$ in which S_o represents the water surface slope along the channel centerline, R is radius of thee centerline and S is the water surface slope at a radial distance of r from the center of the bend. B.C. Yen (1965) arrives at this conclusion by setting the loss of energy equal for every segment of equal included angle. Further, it is well known that flow will not behave the same before and after it passes a bluff body (see Figure 1.2).

Even with these assumptions, the number of unknowns in the simplified equations of motion are still more than the number of equations of motion and continuity. To circumvent this difficulty, many investigators have had to assume a vertical distribution of the tangential velocity. With few

exceptions, investigators have assumed that the logarithmic law is adequate to describe the vertical distribution of this tangential velocity component. Rozovskii, unlike the others, considered the parabolic law, the elliptic law and the logarithmic law, but preferred to use the logarithmic law with the Von Karman constant equal to 0.5. If the momentum exchange can occur in the vertical direction from the upper layer to the lower layer, there is no reason to believe that a momentum exchange can not occur in horizontal direction from the inner region (generally a region of higher velocity) toward the outer region (the region of lower velocity). It is known that v', the vertical fluctuation velocity, which is only a small percentage of the tangential velocity u_θ, is responsible for the vertical mixing. Although the magnitude of the radial velocity v_r, depends upon many factors such as the radius of curvature, the aspect ratio, its order of magnitude is comparable to that of v'. Therefore, the tangential velocity must be redistributed in the lateral direction. As far as this author has been able to determine, no one has accounted for the effect of v_r on the redistribution of u_θ, over either the depth or the width of the flow.

Similarity assumptions for the distribution of u_θ and v_r appear to be unfounded. In sections beyond the crest of the bend (i.e. in a 180 degree bend, sections beyond 90 degrees), the trend of the predicted lateral distribution of u_θ is contrary to that existing in the flow (B. C. Yen, 1965, Choudhary, 1977, and Siebert & Gotz, 1975).

An adequate model should not only be able to predict

the distribution of radial velocity, but should also be able to account for the variation with θ as well as the effect of the secondary flow on the redistribution of the velocity field. To date, investigators are uncertain as to whether the kinematic eddy viscosities (ε_x, ε_y, ε_z) in a straight channel are the same as those (ε_θ, ε_r, ε_z) in a meandering channel. It is generally believed that secondary currents in a meandering channel are stronger than those in a similar straight channel. Therefore, there is no basis for assuming that the eddy viscosities are even approximately the same in straight and meandering channels.

1.4 Scope of Present Study

An understanding of the velocity field and shear stress distribution in the main and flood plain channels will be of great practical use, primarily for the protection of flood control structures. Erosion of the bed, river bank and surrounding flood area, conveyance of flow through the compound cross-section channel, magnitude of shear stress and eddy viscosity, both horizontal and vertical are required to predict the flood stage, erosion and deposition, and the amount of sediment transported in the system. Another factor is the momentum exchange between the main channel and flood plain channel. Even though a certain amount of work has already been done on some aspects of the problem, many questions remain to be answered.

The present investigation was undertaken in an effort to understand such characteristics of flow as the

distibution of velocity, the bed shear stress, the effective zone of momentum exchange and the variation of eddy viscosity. These, if properly understood, would enable the hydrologist to design flood control structures and predict the flood hazard zone with some degree of confidence.

The experiments began with the simplest possible case: a straight rectangular main channel with symmetrical flood plain. In an attempt to study a main channel of large width, an asymmetrical channel with larger main channel width was tested. The study was then extended to determine whether a one stage flood plain could be superimposed on another to provide a multi-stage flood plain.

Natural rivers, of course, differ significantly from the ideal case considered above. In nature, rivers are not straight, and the main channel meanders along its valley in a somewhat irregular manner. In order to assess the effect of the meandering main channel, the present investigation includes the case of a curved main channel in a straight valley. Some dye injection experiments were performed to explore the aspect of secondary flow in the main channel and the encroachment of secondary flow into the flood plain region. In the course of this study, some supplementary experiments were performed to study the variation of the bed shear stress with the aspect ratio for simple rectangular channels with smooth and rough beds.

1.4.1 Presentation of the Program

The experimental arrangements, the measuring techniques, the structure of the base flume and straight and

meandering channels are discussed in Chapter II. This
chapter also contains a description of the probes, the
calibration techniques and the method of using the
calibration charts. The limitations of the measurements are
developed fully in Chapter II as well. An x-y-z electric
coordinate system, in conjunction with a data acquisition
system were used to handle the mass of data obtained from
experiments. The data could be processed by computer with
great ease. The system is described without going into
details of the electronic design or programming of the
mini-computer (PDP8) or the main computer. A dye injector
was constucted for flow visualisation tests.

In Chapter III, investigations on the interaction
between a straight main channel and symmetrical flood plain
flows with smooth and rough beds are presented. This
preliminary study clarified the concept of momentum exchange
between the main channel and the flood plain flows. The
interaction region and reduction of shear stress in the main
channel and increase of the bed shear stress at the edge of
the flood plain are also studied.

Investigations of the effect of a wide main channel and
large width flood plain channel, are presented in Chapter
IV. Experimental findings on the asymmetrical channel
confirmed the basic concepts established in Chapter III.
Once again, it was possible to show that the lateral
velocity profiles are similar. The length scales in the
interaction region were correlated with D/d. Pedistribution
of shear stress in the main and flood plain channels was
examined.

In Chapter V, a preliminary investigation of the flow
in a curved channel without the flood plain is presented.
The experimental results of this run indicated the
inadequacy of the existing solutions to predict the velocity
profiles and the bed shear stress in curved open channels.
Therefore, the results of this study on curved channels are
presented in an empirical form. This chapter also presents
the results of two experiments with a curved main channel in
a straight valley.

A number of point velocities were measured with the use
of the data acquisition system in order that the data could
be fed to the computer. After plotting the velocity profiles
with the computer plotter, for better visualization of
secondary flow and acceleration and deceleration of flow,
isovel maps in the y-z and x-z planes were prepared. These
velocity profiles and isovel maps showed the interaction
between the main meandering channel and the flood plain
channel.

Based on the present studies, general conclusions are
presented in Chapter VI. A summary of the idea of
interaction in a wide main channel and wide flood plain, and
also, a general qualitative study of flow in the meandering
channel in a straight river valley are discussed. Some
recommendations are then made for further studies in this
field.

During the course of this investigation, some
supplementary experiments were conducted in rectangular
channels with smooth and rough beds. The results of the
correlation between maximum bed shear stress in a

rectangular channel with aspect ratio and distribution of
bed shear stresses are presented in Appendix A. Appendix B
presents the results of one experiment in a straight channel
with two asymmetrical flood plains at two different levels.

The present experimental investigations were carried
out at the T. Blench hydraulics laboratory of the University
of Alberta, Edmonton, Alberta, Canada, during the years 1977
and 1978.

2. Experimental Arrangement and Measurement Techniques

2.1 Introdution

This chapter describes the construction of the flume,
the experimental arrangements used, the limitation of the
measurements and physical limitation of the size of the
channels. The first set of experiments were conducted in a
main channel with symmetrical flood plain. The second set of
experiments were conducted in a straight but asymmetrical
channel to simulate a very wide main channel. The last set
of experiments were conducted in a meandering channel, in a
straight valley.

2.2 Experimental Flume

The experiments were conducted in a tilting rectangular
channel 4 feet (1.22 m) wide, 3 feet (0.90 m) deep, and 60
feet (18.29 m) long, with adjustable slope. The side walls
of the flume are made of plexiglass. The plywood bed is
covered with a smooth layer of fiberglass resin. This flume
was used as a base. All channels, consructed from concrete,
were placed within this rectangular flume. Considerable care
was taken to ensure that the concrete blocks were uniformly
laid on the bed of the flume and the bed was level prior to
adding roughness or tilting the flume.

The flume was supported on three sets of synchronized
screws which could be driven by an electric motor for slope
adjustment. Water was pumped from a sump into the head-tank
of the flume through a 12 inch (30.46 cm) overhead pipe,

fitted with an orifice meter, from which the discharge was obtained. The flume was fitted with a tilting tailgate for control of the depth of flow.

2.2.1 Boundary Roughnes

For most of the testing, the finished smooth surface of the concrete was used. In some tests, half inch (12.7 mm) diameter hemispheres, closely packed, were used as the roughness elements. This roughness was fabricated from hard rubber into rectangular sheets using a steel mold. The roughness height is 0.0208 feet (6.35 mm). These rubber mats were placed in the flume for a length of about 30 feet (9.15 m) and the velocity and shear measurements were carried out at a section located at least 20 feet (6.1 m) downstream from the start of the roughness.

2.2.2 Temperature Measurements

Water temperature was measured in order to determine the viscosity. The temperature was taken at fixed time intervals during tests using an electronic thermometer which was read to the nearest 0.01 degree celsius. Water temperature ranged from 17.0 degrees to 19.0 degrees Celsius.

2.3 Experimental Channel

All compound cross-sections simulating the main channel and the flood plain were made of concrete which was steel trowelled to ensure smooth surfaces.

2.3.1 Symmetrical Channel

The compound cross-section simulating the main channel and symmetrical flood plain was made of two rows of concrete blocks. For the first seven experiments, the depth of the main channel h below the flood plain level was about 4.3 inches (10.92 cm) and for the later experiments h was reduced to 3 inches (7.62 cm) by placing a layer of concrete in the main channel. The width of the main channel B was maintained at 8 inches (20.32 cm) for all these experiments. The total width of the flood plain b was equal to 40 inches (1.02 m) in all these experiments.

The measurements were made in the central part of the channel at a distance of approximately 30 feet (9.15 m) from the entrance, after making certain that the flow was fully developed and that the depth of the flow was approximately constant. For the first seven experiments, due to the presence of a small hump in the bed of the main channel, the effective slope for the main channel could be assessed only approximately. The slope given in Table 1 for experiments 1 - 7 is to be taken as the slope of the flood plain. For all further experiments, the effect of this hump was removed by adding a layer of thick cement to the main channel bed and by making it parallel to the flood plain bed.

The velocity measurements were made in one half of the compound section. Measurements of the bed shear stress in the main channel and flood plain were made by using the Prandtl tube as a Preston tube (Preston, 1954, Rajaratnam, 1965, and Rajaratnam & Muralidhar, 1968). A series of seven additional experiments were done mainly to obtain more data

on the bed shear stress distributions in the main channel and flood plain. In the first eight experiments (the significant details are recorded in Table 1), the boundary surfaces were generally smooth. For the ninth experiment, the bed of the flood plain was made rough by spreading the rubber mat with hemispherical projections of 0.5 inch (12.7 mm) diameter.

In addition, a number of special experiments were performed with the flow confined to the main channel, with smooth and rough boundaries to obtain some supplementary information on the distribution of the bed shear stress in rectangular channels of small and medium aspect ratios. These result will be presented in Appendix A.

2.3.2 Asymmetrical Channel

In order to asses the effect of aspect ratio in the main channel and flood plain channel three asymmetrical channels were tested. In addition, a multi-stage flood plain channel was also constructed.

2.3.2.1 Asymmetrical Channel Type A

One side wall of the main channel was extended by a row of concrete bricks. The depth of main channel h below the flood plain level was about 3 inches (7.62 cm). The width of the main channel B was maintained at 8 inches (20.3 cm). The flood plain width b was equal to 20 inches (50.8 cm), see Figure (2.1A). The velocity and shear measurements were made for the whole cross-section at a section, half way down the flume.

Rectangular Channel
B=8"

Symmetrical Chl.
b=40"   h=4"

b/2

Figure 2.1(a) Geometry of
Asymmetrical Channel Type A
A { B=8"   h=4"
    b=40"

Figure 2.1(b) Geometry of
Asymmetrical Channel Type B
B=20"   h=1-25" } B
b=16"

Figure 2.1(c) Geometry of
Asymmetrical Channel Type C

Asym. Chl. B=28"   h=4"
            b=40"   } C
b/2

Figure 2.1(d) Geometry of
Asymmetrical Channel Multi-Flood Plain Type

b/2   b/2

Multi-Flood-Plain Channel
B=20"   h=1.25"   } D
b=16"   h'=2.75"
b'=40"

Figure 2.1 Geometry of Straight Channels

2.3.2.2 Asymmetrical Channel Type B

Since, in the previous experiments, the width of the
main channel was not large enough and the depth of the main
channel from the flood plain level h was high, the concrete
blocks were removed (See Figure 2.1B). The depth of main
channel h, was 1.25 inches (3.2 cm), the width of main
channel 20 inches (50.8 cm) and the width of flood plain was
8 inches (20.3 cm). Measurements were conducted 30 feet from
the head-tank.

2.3.2.3 Asymmetrical Channel Type C

In order to simulate reasonably wide main and flood
plain channels, the bottom of the main channel was filled up
with mortar. The depth of main channel h below the flood
plain level was about 3 inches (7.6 cm). The width of the
main channel B was maintained at 28 inches (71.1 cm). The
flood plain width b was equal to 20 inches (50.8 cm).

Five experiments were conducted. The middle of the
flume was chosen for cross-sectional measurements. The
velocity and shear stress measurements were made over the
entire compound cross-section. Figure 2.1C shows the
dimensions of the channel and Table 2 shows the significant
details of experiments 1 to 5.

2.3.2.4 Asymmetrical Channel Type D

In addition, one test with multi-level flood plain was
conducted. The depth of main channel h, was 1.25 inches (3.2
cm) and the depth of first level of flood plain h', was 2.75
inches (7.0 cm). The main channel width B was 20 inches

(50.8 cm). The first level flood plain width was b/2=8 inches (20.3 cm) and the second level flood plain width was b'/2=20 inches (50.8 cm). Figure 2.1D shows the detailed dimensions of this channel.

2.3.3 Meandering Channel

In designing a meandering channel that is to be representative of a typical meandering river, one has to consider several parameters. The parameters involved can be classified into four groups:

1. The channel-geometry characteristics,
2. the flow characteristics,
3. the fluid properties,
4. the sediment properties.

Obviously, these are too many variables to be handled in the limited size of laboratory flume described previously. Therefore, sediment was eliminated from the study; clear water was used as the fluid; the movable bed was replaced by a smooth rigid boundary; the channel was built with a uniform rectangular cross-section. The meandering channel with constant curvature was constructed. Short tangents connected the reverse curves with one another.

With this simplified model (See Figure 2.2), the geometry of the curved channel can be defined by the central angle of the bend θ_c, centerline radius R, the tangent length T, the width of the channel B, and the depth of flow D.

B.C. Yen (1965) conducted a survey of the most
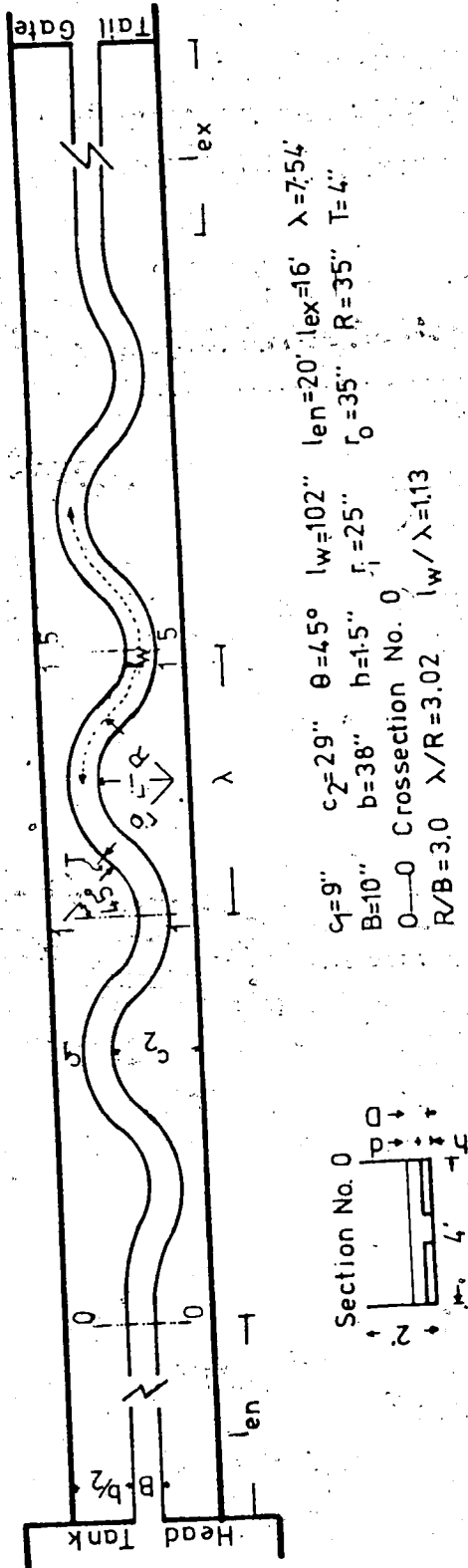
SCHEMATIC PLAN VIEW OF MEANDERING CHANNEL IN
STRAIGHT VALLEY

Figure 2.2 Geometry of Curved Channel

$c_1 = 9''$ $c_2 = 29''$ $\theta = 45°$ $l_w = 102''$ $l_{en} = 20''$ $l_{ex} = 16'$ $\lambda = 7.54'$

$B = 10''$ $b = 38''$ $h = 1.5''$ $r_o = 35''$ $R = 35''$ $T = 4''$

O—O Crossection No. 0 $r_i = 25''$

$R/B = 3.0$ $\lambda/R = 3.02$ $l_w/\lambda = 1.13$

PLAN VIEW
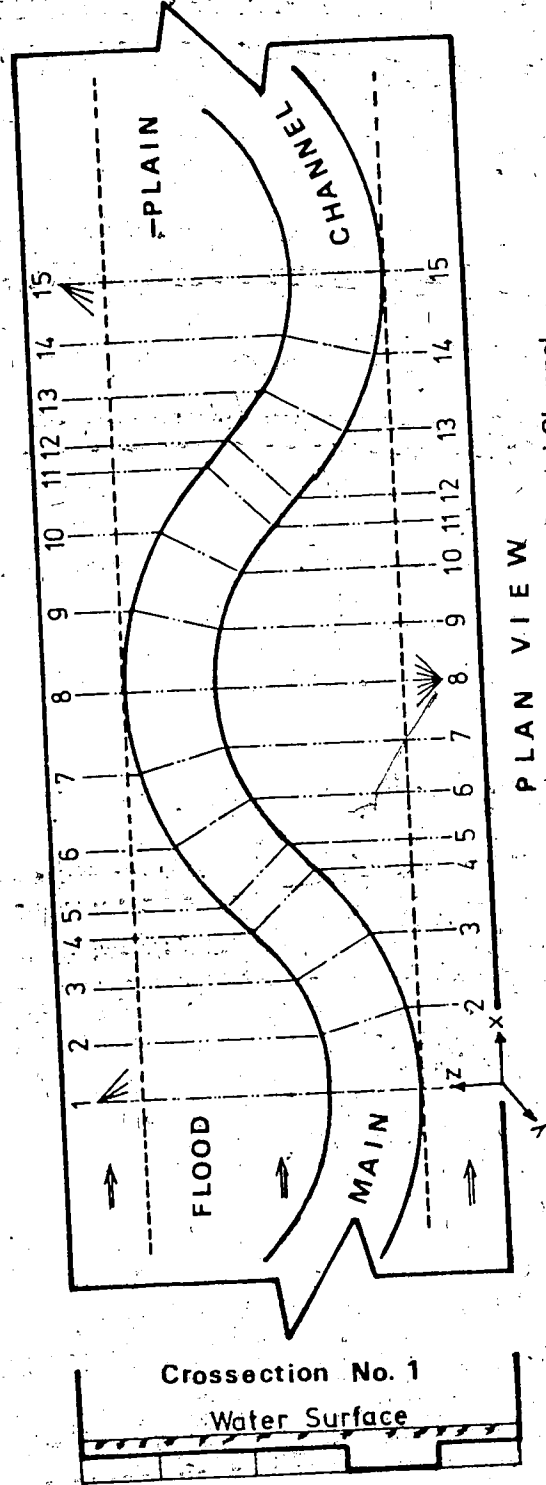
Figure 2.3 Location of Cross-Sections in Curved Channel

important experimental work on flow in open channel bends. Based on this survey, he maintained that those channels had a few short-comings. These short-comings include the fact the aspect ratio B/D was small, or if the channel had a large width, the total central angle θ_c is too large or too small. However, in most cases there was only one bend. Leopold & Langbein (1966) used a statistical analysis of rivers to give a range for sinuosity, or tightness of bend, which is expressed as the ratio of the length of the channel in a given curve l_w, to the wave length λ, between 1.3:1 and 4:1. Another property is the ratio of wave length of the curve and the radius of curvature. The appearance of regularity depends in part on how constant this ratio is. This value may change from the water surface to the bottom of the channel. The average value of l_w/λ is about 4.7:1. Also Leopold, Bagnold & Wolman (1960) gave an average value of R/B of 2.3 for many rivers and channels, and an average value of 3.24 for the few data they obtained for Mississippi River.

Based on all this information, and the limitation of the size of the available flume in the laboratory, the planimetric geometry of the model was chosen with $\theta_c=90$ degrees, R/B=3.0, $\lambda/R=3.02$, and $l_w/\lambda =1.13$. The model was built with the following dimensions: B=10 inches (25.4 cm), R=30 inches (76.2 cm), tangential length T=4 inches (10.2 cm), and h, the depth of the curved channel bed below the flood plain equal to 1.5 inches (3.8 cm). Seven identical 90 degree curves of reversed direction were connected by the 4 inches (10.16 cm) straight reach, where it formed total of

three loops. It was believed that developed flow would be obtained in the second loop. The channel was 60 feet (18.3 m) long. The first 18 feet (5.5 m) was a straight symmetrical main channel with flood plain width (l_{en}=18 feet, 5.5 m) of 19 inches (48.3 cm) on either side. The middle part 26.6 feet (8.1 m) of the flume contained three loops, and the rest was straight channel with a tail gate at the downsrteam end (l_{ex}=13.5 feet or 4.1 m). The general layout of the model is shown in Figure 2.2. As shown in this schematic plan view, the amplitude of the wave was 20 inches (50.8 cm) and the narrowest width of the flood plain in the meandering portion was 9 inches(c_1=22.9 cm).

The velocity and shear measurements were made in cross-sections at every 45 degree increment of θ in the second loop and at the entrance of the loop. Figure 2.3 shows a detailed plan view of these sections. The vertical profiles were located at 0.1 feet (3.05 cm) intervals in the flood plain and at 1 inch (2.54 cm) intervals in the main channel. Velocities were measured every 0.01 feet (3 mm) in vertical profiles.

2.4 Velocity Measurements

Prandtl and yaw probes were used for measuring the velocity field. In straight channels with very weak secondary currents, the velocity measurements were made using a 3 mm or 1.5 mm Prandtl type Pitot-static tube. The differential pressure was measured with a Pace model PID variable reluctance differential pressure transducer with

one inch of water for full scale diaphragm (zero to ten volts on the demodulator amplifier respectfully). Initially, readings were obtained from a direct reading Pace indicator (model CD 25). Later on, the outputs were recorded on a strip chart recorder and averaging was done by hand.

The calibration procedure consisted of applying static differential heads to the Prandtl tube and adjusting the demodulator for a linear output of zero to one inch of water. According to the manufacturer, the precision of these transducers is ±0.1%.

Each modulator was provided with a capacitor which damped the circuits to reduce the frequency responses of the output to a level suitable for input to the strip chart recorder. Instantaneous differential pressure between dynamic and static heads was recorded for one minute. Whenever the depth of flow on the flood plain was small, the requirement of depth of flow being at least five times the outside diameter of the probe could not be met with a 3mm OD probe. Therefore, for small depths of flow, the 1.5 mm OD Prandtl Pitot-static tube was used.

2.5 Velocity Vector Measurement

For velocity measurements in the curved channel with a flood plain, the conventional Pitot tube would not suffice as the angle of attack would be very large. In addition, the present investigation was aimed at measuring all the three components of a velocity vector which would require the measurement of the yaw and pitch angles. The obvious choice

was a five hole probe. After a preliminary study in the
curved channel it was found that the vertical component of
the velocity vector was rather small compared to the
horizontal component of the velocity vector and therefore
could be neglected. Besides, the outside diameter of five
hole probe was large and could not meet the requirement of
the depth of flow being at least five times the probe
diameter. Further, the complexity of the calibration curves
ruled out the possibility of using the five hole probe. In
two dimensional flows, when the velocity vector is in the
horizontal plane of the probe, its magnitude and direction
can be conveniently determined by means of the yaw probe.

The yaw probe was prepared from stainless steel tubes
of 1.5 mm outside diameter and had a 45 degree chamfer. At
the beginning of the experiment a rotating mechanism was
attached to the yaw probe. By rotating the yaw probe until
the differential pressures between center tube and the side
tube became the same, it was possible to obtain the
direction and magnitude of the velocity vector. The lag time
between rotating the yaw probe and the response of the
differential pressures kept the yaw probe in constant
motion. The fluctuation of direction of the velocity vector
added a greater problem. In order to overcome these
difficulties, an alternative method was used. Rajaratman &
Muralidhar (1968) gave the necessary calibration curves for
computation of magnitude and direction of the velocity
vector. The principle involved in this method of velocity
measurement is described briefly in the following
paragraphs.

For two-dimensional flows, if at any point the velocity is V at any angle of attack of $\bar{\theta}$ and the static piezometric head is h_o, the piezometric heads indicated by the three tubes of the probe set at that point are written as:

$$h_1 = h_o + k_1 \frac{V^2}{2g} \tag{2.1}$$

$$h_2 = h_o + k_2 \frac{V^2}{2g} \tag{2.2}$$

$$\text{and } h_3 = h_o + k_3 \frac{V^2}{2g} \tag{2.3}$$

where k_1, k_2, and k_3 are the calibration coefficients and are functions of $\bar{\theta}$ mainly, for a given probe neglecting viscous effects and other minor correction factors (see Figure 2.4). The mean calibration curves for k_1, k_2 and k_3 were obtained through a series of experiments, with $\bar{\theta}$ ranging from -60 to 60 degrees.

Using the three calibration factors k_1, k_2 an k_3 a fourth factor k is defined as:

$$k = \frac{k_3 - k_2}{k_1 - k_2} \tag{2.4}$$

and it could be seen that k is mainly a function of $\bar{\theta}$. Using the mean curves presented in Figure 2.4, the variation of k, with $\bar{\theta}$ is shown in Figure 2.5.

Equation 2.4 in combination with equations 2.1 to 2.3 could be rewritten as:
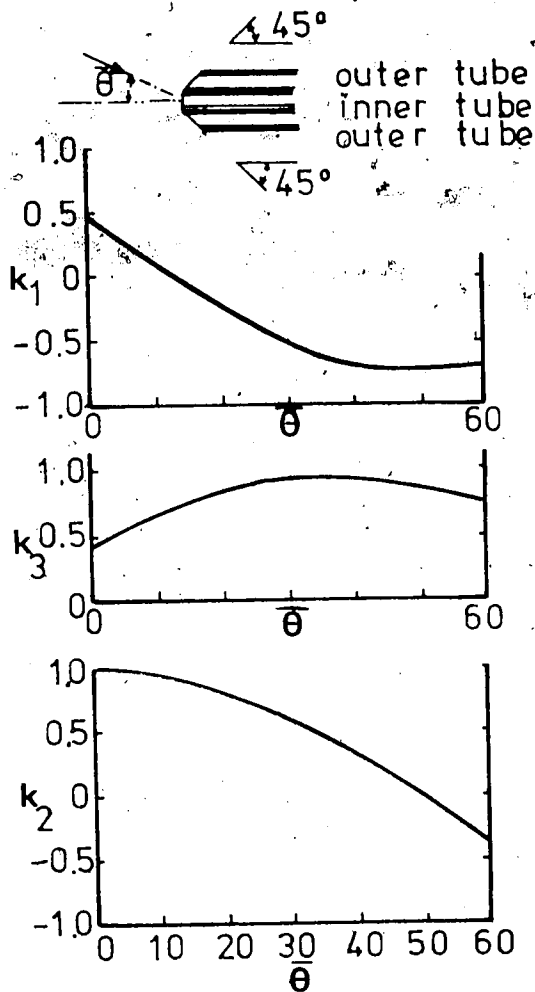
Figure 2.4 Yaw Probe Calibration
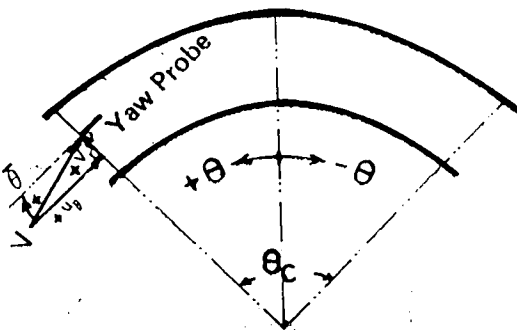Curve (variation of k_1, k_2 and k_3 with θ)

Figure 2.5 Yaw Probe
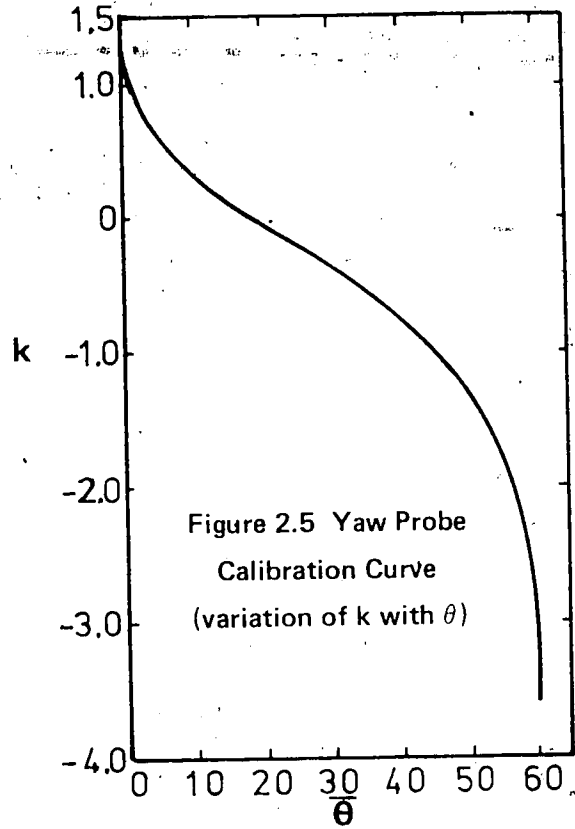Calibration Curve
(variation of k with θ)

Figure 2.6 Yaw Probe Calibration
Curve (variation of k_6 with θ)
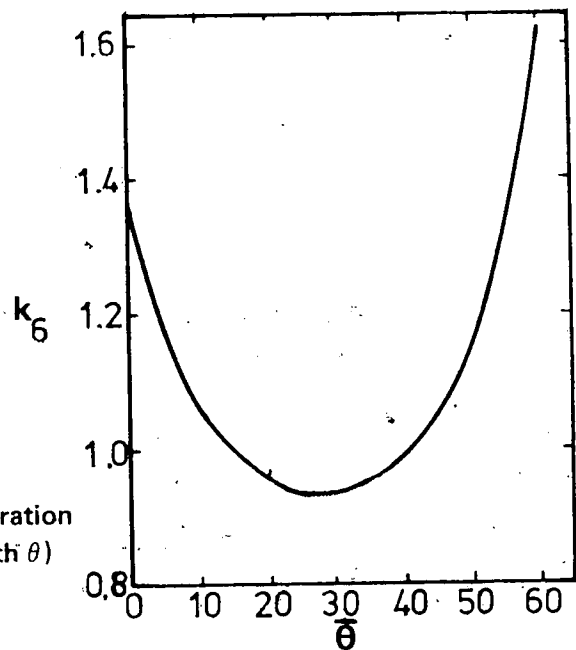
$$k = \frac{h_3 - h_2}{h_1 - h_2} \qquad\qquad (2.5)$$

From equation 2.5, k is found and hence the angle of the yaw is found by referring to Figure 2.5. It could be shown that

$$V = \sqrt{2g \ \frac{(h_1 - h_2)}{(k_1 - k_2)}} = [2g \ k_6 \ \Delta h]^{1/2} \qquad\qquad (2.6)$$

where

$$k_6 = \frac{1}{k_1 - k_2} \qquad\qquad (2.7)$$

and

$$\Delta h = h_1 - h_2 . \qquad\qquad (2.8)$$

It could be shown that k_6 is only a function of $\bar{\theta}$, and its variation with $\bar{\theta}$ is shown in Figure 2.6. Using this figure, k_6 could be found for the particular angle of attack $\bar{\theta}$ and the magnitude of the velocity vector is determined.

2.6 Boundary Shear Stress Measurements

The Preston tube is a total head tube resting on a boundary and facing the flow, with the tube in a zone where the law of the wall is valid. This requirement was met at all times and whenever the depth of flow was shallow, the 1.5 mm Pitot-static probe used. The Preston technique is a convenient method of measuring the boundary shear stress. The differential Δp pressure between the dynamic and the static pressures is correlated with the boundary shear stress τ_0. These correlation was developed by Preston (1954), mainly from similarity considerations and the

existence of the law of the wall. This correlation is given
in the form of

$$\frac{\Delta p\ d^2}{4 \rho\ \nu^2} = f \left(\frac{\tau_0\ d^2}{4\ \rho\ \nu^2} \right) \tag{2.9}$$

After Preston (1954) a number of investigators conducted
several experiments to check Preston's original calibration,
and to extend the use of the technique to developing
boundary layers and to study the effect of pressure
gradients (Hsu, 1955, and Bradshaw & Gregory, 1958).
Rajaratnam (1965) defined calibration curves theoretically
by assuming a suitable velocity distribution in the wall
region. The numerous smooth boundary calibrations showed
only a few percent difference. Rajaratnam & Muralidhar
(1968) showed that the Prandtl tube could be used as a
Preston tube. In the present investigation, Patel's curves
(Patel, 1965) were used to convert Δp to τ_0 and the required
calibration curves for the 3 mm and 1.5 mm Pitot-static
probe were prepared.

2.6.1 Yaw Probe as a Preston Tube

In the meandering channel, the direction of the bed
shear stress is not known beforehand. In principle, its
magnitude and direction can still be found by rotating the
Preston tube till the maximum dynamic pressure is indicated.
This method of rotating the probe is time consuming. In
order to overcome these difficulties, Rajaratnam and
Muralidhar (1968) used the yaw probe on the boundary and
gave the necessary calibration curves for obtaining the

direction and magnitude of the bed shear stress. The same yaw probe, described previously in connection with velocity measurement, was used as the Preston tube.

Combining various expressions in equation 2.4 and 2.5, the following can be written:

$$P_1 = P_0 + k_1 \left(\frac{4 \rho \nu^2}{d^2} \right) f(\tau_0 +) \qquad (2.10)$$

$$P_2 = P_0 + k_2 \left(\frac{4 \rho \nu^2}{d^2} \right) f(\tau_0 +) \qquad (2.11)$$

$$P_3 = P_0 + k_3 \left(\frac{4 \rho \nu^2}{d^2} \right) f(\tau_0 +) \qquad (2.12)$$

$$\text{where } (\tau_0 +) = \frac{\tau_0 d^2}{4 \rho \nu^2} \qquad (2.13)$$

and P_1, P_2 and P_3 are respectively the pressure at hole 1, 2 and 3.

By a suitable combination, the expressions in 2.5 can be written as the following:

$$\frac{(P_2 - P_1)}{4 \rho \nu^2} \frac{1}{(k_1 - k_2)} = f(\tau_0 +) \qquad (2.14)$$

In measuring shear stress at any point, P_1, P_2 and P_3 are known quantities so that k could be computed and then $\bar{\theta}$, could be found. Also k_1 and k_2 could be found from Figure 2.4. Since all the quantities on the left hand side of equation 2.14 are known, $f(\tau_0 +)$ can be determined. Using Patel's calibration curves $\tau_0 +$ and hence τ_0 were computed.

2.7 Depth and Slope of Water Surface

Depth was determined from manual gauge readings of the water surface along the flume centerline at every cross-section. These readings were referenced to their bed level datum. For subcritical flow conditions, the tailgate was adjusted to establish uniform flow by a trial and error process. The bed slope was set and uniform flow conditions were approached by manipulating the tailgate while observing the depth of flow. They were measured from 5 feet to 50 feet (1.52 to 15.25 m) from head-tank at 5 feet intervals.

After a few runs were conducted, it was found that the water surface measurement with a point gauge was not accurate enough for this study. Seven static probes were mounted over a reach betwen 15 to 45 feet from the entrance at intervals of 5 feet. The differential pressures between the static probes were measured with a pressure transducer Pace model P1D. Therefore, the uniform flow was established by manipulating the tailgate until the 6 differential pressures between the static probes became equal and the slope could be calculated by dividing the differential pressure reading over the distance between the two probes. Since the drop of the water surface could be read within a precision of 1/10,000th of a foot, the slope of the water surface could be measured accurately. In all cases, care was taken to see that the bed and the water surface slopes were essentially the same.

2.8 Special Instrumentation

In the straight channel a y-z electric coordinator and a one channel strip chart recorder were quite sufficient to take data manually. But, in the case of the meandering channel, obtaining data manually was quite time consuming. In addition to that, processing the data without computer help and plotting or mapping isovels was a great task by hand.

2.8.1 Coordinate Positions and Input Panel

The yaw probe was positioned within the flume by a x-y-z-θ electric coordinate system, where θ is the degree of rotation of the yaw probe with respect to the x direction. The origin of the x-y-z coordinate was selected in such a way that x=0.0 at cross-section NO. 1, z=0.0 at the right hand side corner of the flood plain and y or y'=0.0 upward from the bed. The location and rotation of the yaw probe (x-y-z-θ) could be controlled from a remote control switch box, which in turn drove a small DC electric motor to a desired position. The coordinate voltages were zeroed with the reference to the flume origin. The DC voltages representing the coordinates were then fed into the data acquisition system.
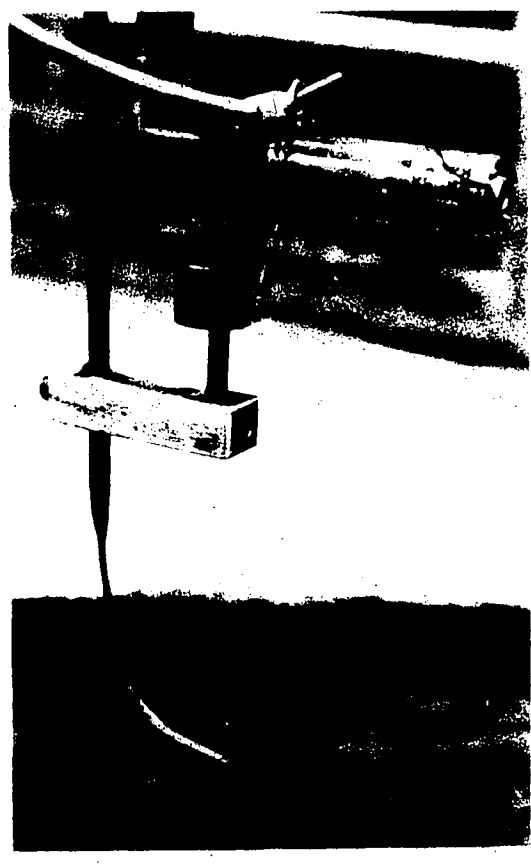
This system also was controlled from a small panel where coordinate datum planes could be set and calibrations performed. This equipment is indicated in the photograph in Figure 2.7.
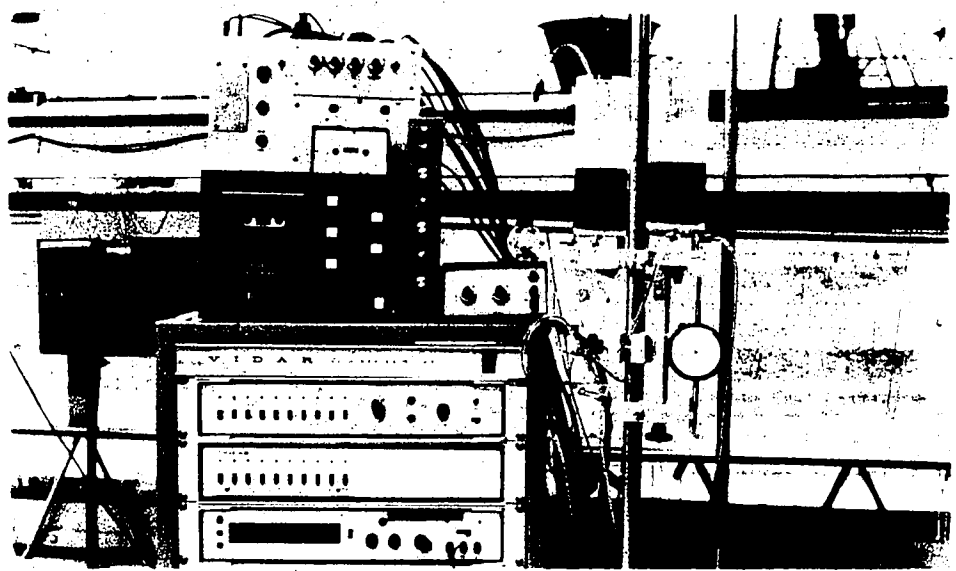
Data Aquisition System

Meandering Channel

Yaw Probe

Figure 2-7 Photograph of Data Aquisition System

2.8.2 Data Acquisition System

The acquisition system was made up of the following elements, which are represented in Figure 2.8.

1. 20 Channel Scanner (Vidar 604)
2. Integrating Digital Voltm (Vidar 500)
3. Data Coupler (Control Equipment Corporation model 310)
4. Scan Counter
5. Magnetic Tape Recorder (Techtran)

All inputs for the data acquisition system were in the range of -20.0 to 20.0 volts and each was assigned to a particular channel of the Scanner. The Scanner sequentially sampled selected channels, routing the analogue signals to the Digital Voltm where they were digitized and converted to a Binary Coded Decimal (BCD) Code. The Data Coupler formulated the BCD signal and routed it to the magnetic tape recorder (Techtran). The Techtran, on write mode, stored the information on a casset tape and, at a later period, the tape could be read to PDP8 computer.

The desired number of scan cycles were selected on the Scan Counter and the scan rate was selected on the Scanner. After several trials, 2400 characters per minute gave the best result, with approximately 80 samplings per minute in each channel.

Through a Basic language program, the information on the magnetic tape was read to the Digital Computer (PDP8) and the data was stored on the Flupy. Furthermore, PDP8 through several programs, was able to convert each set of readings to the desired average of that reading and, if
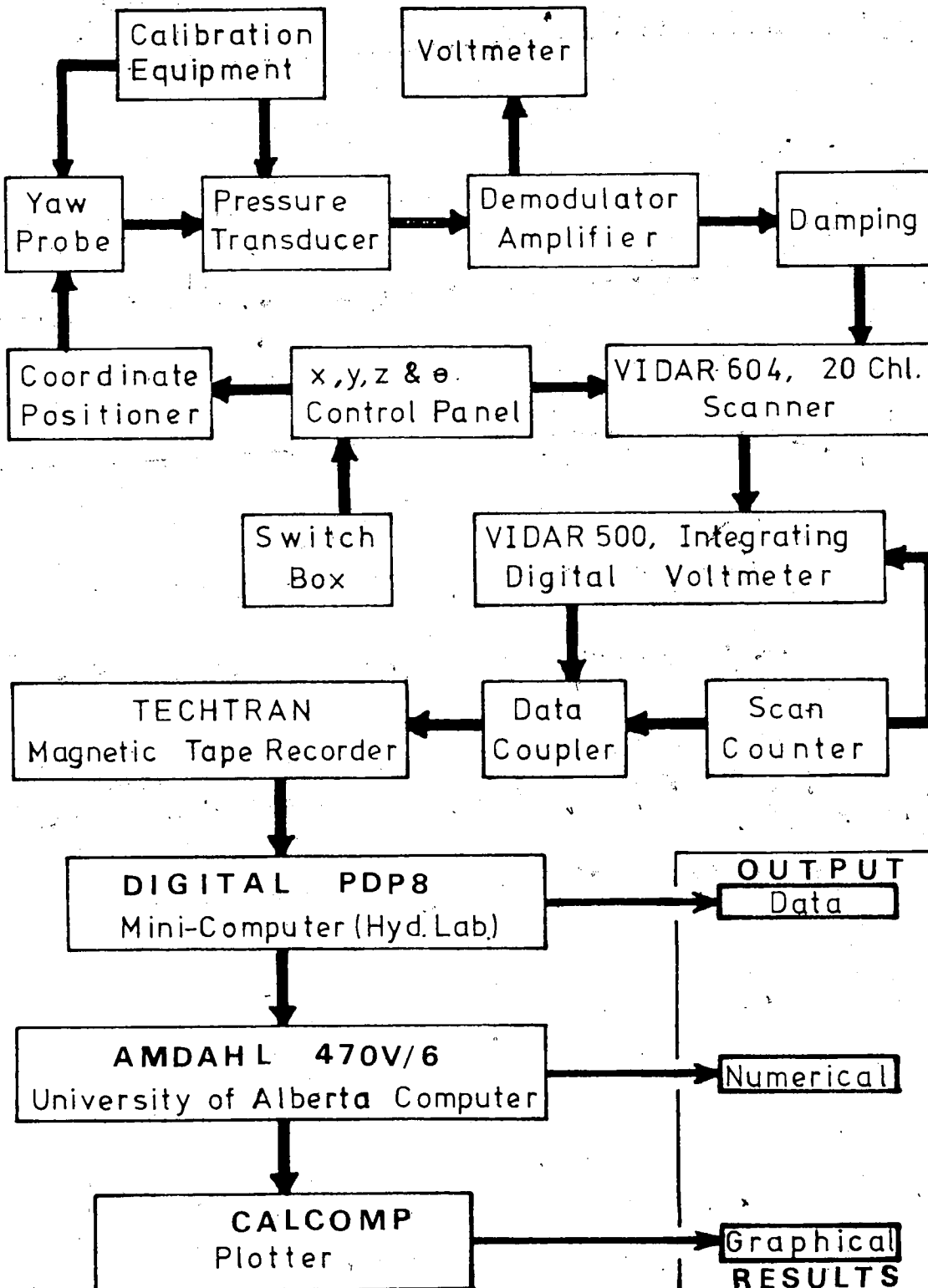
Figure 2.8 Flow Chart of Equipments

necessary, by going through a subroutine and applying

calibration curves to obtain the value of the variables.

Then, this information from the Hydraulic Laboratory was

transferred to the University Computer Center. From there

the data were stored in suitable matrices. It could be

called for under the Michigan Time Sharing System (MTS)

using an Amdahl 470V/6. All data processing and analyses

were carried out using Amdahl 470V/6 and the results were

plotted using a new version of Calcomp plotter. Surface II

Program (Sampson, 1978) had more capability for mapping,

therefore it was decided to use this program for isovel

maps.

2.8.3 Test Method

The following procedure was normally carried out to

complete a single test:

1. The channel slope was selected,

2. the flume slope was set,

3. a discharge was selected,

4. uniform flow was established by measuring water depth,
   and adjusting the tailgate elevation until the
   differential pressure between each pair of the static
   probes became equal,

5. final depths were measured, the water surface was
   plotted, and slope was determined,

6. the velocity distribution was measured by:
   a. selecting the cross-section,
   b. zeroing and calibrating the coordinate positioner,
      and the pressure transducers, and changing the angle

of the yaw probe if necessary,

7. making sure scan rate is set at 80 cycles,

8. positioning the velocity probe, selecting the channels
   to be scanned, and starting auto counter,

9. recording the data on magnetic tape,

10. shear measurements were carried out by following the
    same procedure as above with the yaw probe positioned on
    the boundary.

2.9 Flow Visualisation

Dye was injected parallel to the flow, by means of a 1
mm OD tube connected to a small constant pressure head-tank.
Dispersion of the dye was photographed from a fixed position
approximately 4 feet (1.2 m) above the flow. These photos
served many purposes such as measuring the rate of expansion
of the width of the dye plume, or the extent of the
intrusion of the main channel flow into the flood plain
region.

3. Interaction Between Straight Main Channel And Flood Plain

Flows in a Symmetrical Channel

A preliminary study was done in a narrow main channel with wide symmetrical flood plain.

The construction and dimensions of this symmetrical flume were described in detail in Chapter II, Section 2.3.1. Originally, it was used to check the basic idea of exchange of momentum between the main channel and the flood plain.

3.1 Concept of Momentum Exchange and Interaction Region

In a compound cross-section channel, composed of two similar channels with the same longitudinal slope, the one with a larger depth of flow at any given level will have a higher velocity than the one with a lower depth of flow at the same level. Therefore, it is obvious in a compound cross-section like a river with a flood plain, at any level above the flood plain, the main channel will have higher velocity because of greater depth of flow. It can be seen at any of these levels that there exists a lateral velocity gradient, higher velocity in the middle of the main channel and lower in the flood plain. The result of this difference will be that a part of the main flow near the flood plain will slow down and a part of the flow in the flood plain near the main channel will speed up. Perhaps this action will occur in such a way that the velocity of the main flow decreases smoothly toward the flood plain until it reaches the flood flow velocity. This is the result of transport of the longitudinal momentum to the flood plain and the

vertical plane between the main channel and flood plain will experience appreciable turbulent shear stress in the longitudinal direction.

In order to test the above ideas, data were taken from the isovel contours given by Sellin (1964) and plotted. A very simple calculation resulted in undisturbed velocity for the main channel and the flood plain channel. Comparison of these velocities with those obtained from the isovel showed main channel velocities were reduced and flood plain velocities increased.

In order to be able to pursue the forgoing idea, the symmetrical channel was tested for different depths of main channel and flood plain flows.

3.2 Experiments And Experimental Results

Measurements were made in the central part of the channel (at a distance of approximately 30 feet (9.15 m) from the entrance) after making certain that the flow was fully developed and that the depth of flow was approximately constant. As previously explained, for the first seven experiments, the effective slope for the main channel, could only be approximated. The slope given in Table 1 for experiments 1   to to be taken as the slope of the flood plain.

The velocity and shear stress measurements were made in one half of the compound section. A series of seven additional experiments were made, mainly to obtain more data on the bed shear in the main channel and the flood plain. In

TABLE 1

Significant Details of the Experiments

B = 0.67 feet, b = 3.33 feet

| Expt. No.	h(ft)	D(ft)	d(ft)	Q (cfs)	S x10³	D/d	F	Shear lbsx10³/sq.ft
1	0.346	0.483	0.137	0.98	0.70	3.53	0.52	18.37
2	0.358	0.410	0.052	0.50	0.40	7.88	0.59	90.96
3	0.358	0.584	0.226	2.00	1.14	2.58	0.59	16.56
4	0.358	0.538	0.180	1.50	1.07	2.99	0.56	17.59
5	0.358	0.407	0.129	0.58	0.29	3.16	0.31	23.32
6	0.358	0.518	0.160	0.18	0.03	3.24	0.08	1.50
7	0.358	0.450	0.092	0.18	0.04	4.89	0.13	8.50
8	0.245	0.360	0.115	0.54	1.18	3.13	0.39	2.79
9**	0.271	0.338	0.067	0.32	0.94	5.04	0.22	-
10 *	0.245	0.550	0.305	--	0.56	1.80	--	2.07
11 *	0.245	0.498	0.253	--	0.53	1.97	--	2.08
12 *	0.245	0.422	0.177	--	0.62	2.38	--	1.32
13 *	0.245	0.375	0.130	--	0.70	2.88	--	3.27
14 *	0.245	0.345	0.100	--	0.82	3.45	--	3.67
15 *	0.245	0.328	0.083	--	0.83	3.95	--	5.02
16 *	0.245	0.264	0.019	-	1.27	13.89	--	38.42

* Additional experiments.

** Rough flood plain 0.5 inch diameter hemi-spherical roughness.

the first eight experiments (see Table 1 for the significant details of the experiments), the boundary surfaces were generally smooth. For the ninth experiment only, the bed of the flood plain was made rough. In addition, a number of special experiments were made with the flow confined to the main channel, to obtain supplementary information on the distribution of the bed shear in rectangular channels of small aspect ratio. These results are presented in Appendix A.

The velocity profiles for three typical experiments are shown in Figure 3.2. Figure 3.2(a) shows the profiles for a large Froude number F of 0.52, wherein F is taken as the ratio of the mean velocity to the square root of the product of acceleration due to gravity and the depth of flow D. Figure 3.2(b) shows the profiles for F=0.08. Figure 3.2(c) shows the results for the ninth experiment which had a rough bed for the flood plain. Considering the flood plain, in Figure 3.2(a), the velocities increase continuously as one moves towards the main channel. This increase can be noticed in Figure 3.2(c) and to a lesser extent in Figure 3.2(b). In the main channel, Figure 3.2(a), the velocity increases with y, the distance from the bed up to some level, and decreases continuously to eventually become approximately constant near the water surface. This behaviour is noticeable in Figure 3.2(b) as well as Figure 3.2(c).

Figure 3.3(a) shows the variation of u with z from the centerplane for different horizontal planes (i.e. different values of y). From Figure 3.3(a) it can be seen that u

(a) (half) Sectional View

(b) Velocity Profiles

(c) Bed Shear Profiles
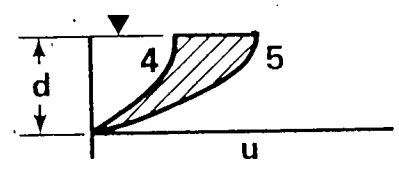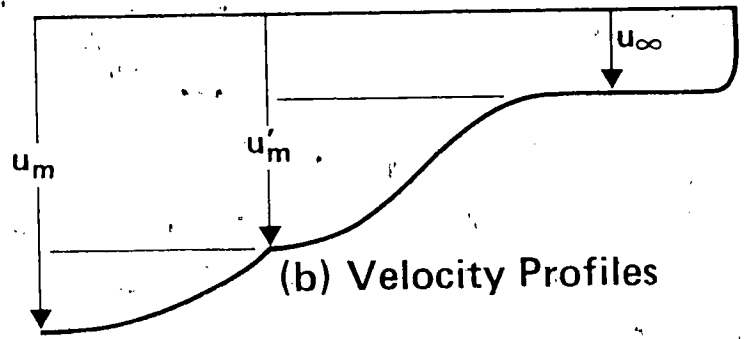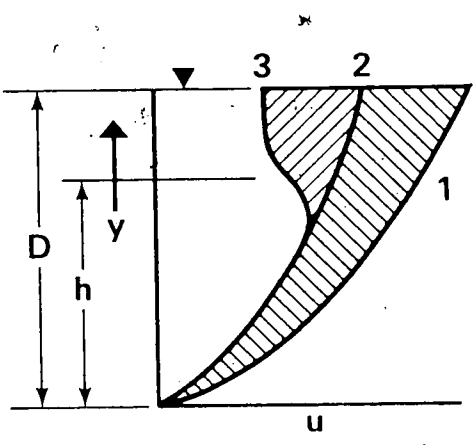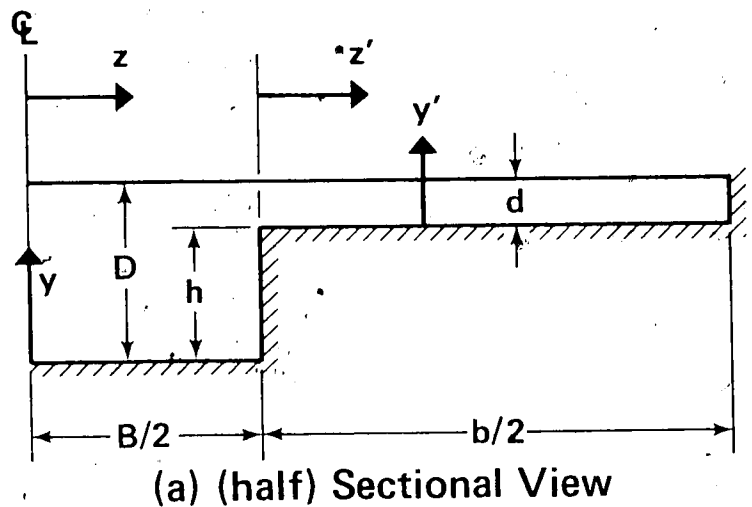
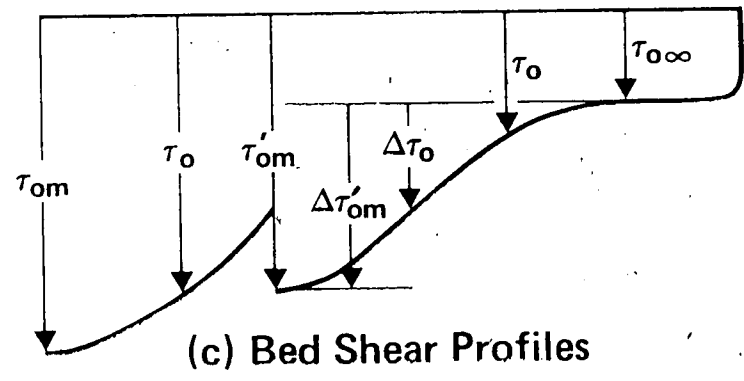(d) Concept of Flow Reduction
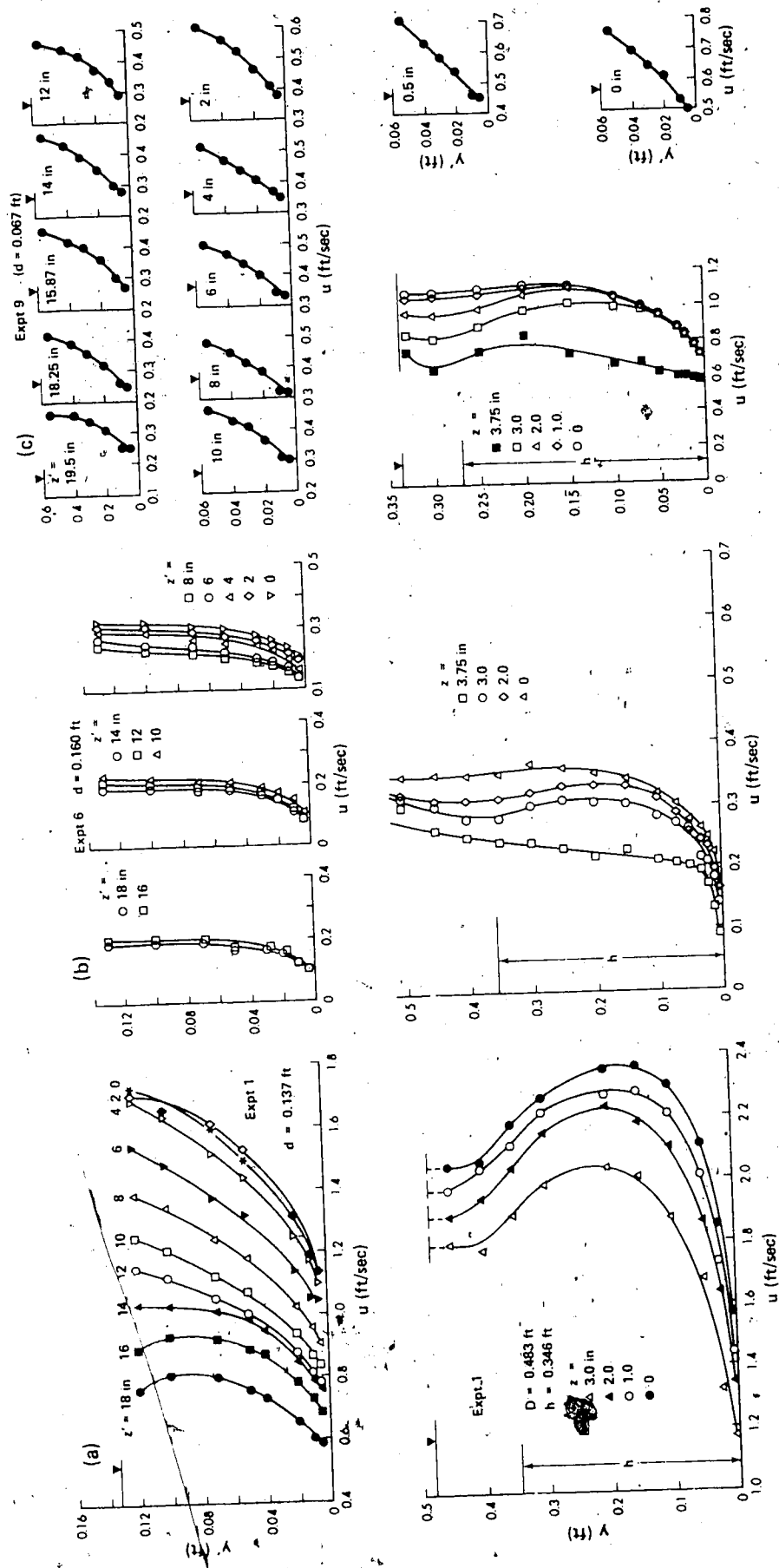
Figure 3.1 Definition Sketches

Figure 3.2a, b & c Typical Velocity Profiles (in y direction)

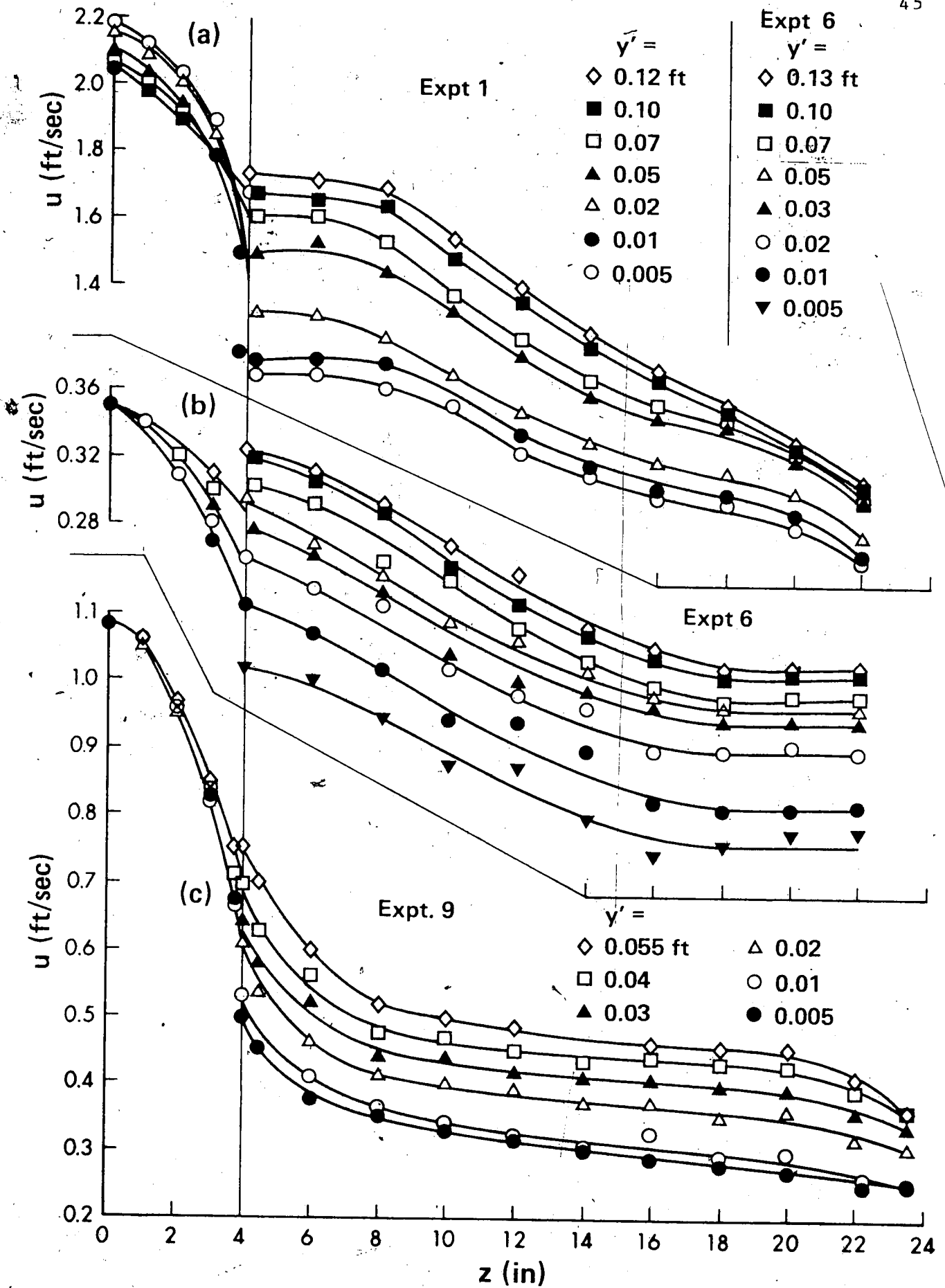Figure 3.3a, b & c Typical Velocity Profiles (in z direction)

decreases from a maximum value of u_m on the centerline rather rapidly to a value of u_m' at the junction plane between the main channel and flood plain and then decreases continuously from u_m' to eventually approach the undisturbed flood plain velocity of u. Figures 3.3(b) and 3.3(c) show two other typical profiles, one for low F and the other for a rough flood plain and similar variation can be noticed. In the immediate vicinity of the junction plane, in some experiments, a sharp increase in velocity was noticed (see for example Figure 3.3(b)). This sudden increase has also been reported by other observers (Goncharov, 1964).

The variation of the bed shear stress in the main channel and flood plain is shown in Figure 3.4 for the eight experiments as well as the additional series. In the main channel the bed shear decreases from a maximum value of τ_{om} to zero at the corner of the banks . In the flood plain, τ_o decreases continuously from a maximum at the junction plane to approach an undisturbed value of $\tau_{0\infty}$. $\tau_{0\infty}$ will again decrease as the bank of the flood plain is approached.

3.3 Analysis of Experimental Results

Some preliminary calculations indicated that in the part of the flow above the bed of the flood plain (i.e. y>h), the velocity profiles in the transverse direction (i.e. u(z)) if viewed with respect to u_∞, the undisturbed velocity in the flood plain, appeared to possess the property of similarity. After further analysis, it was found that the u(z) profiles could be split into two parts, one in
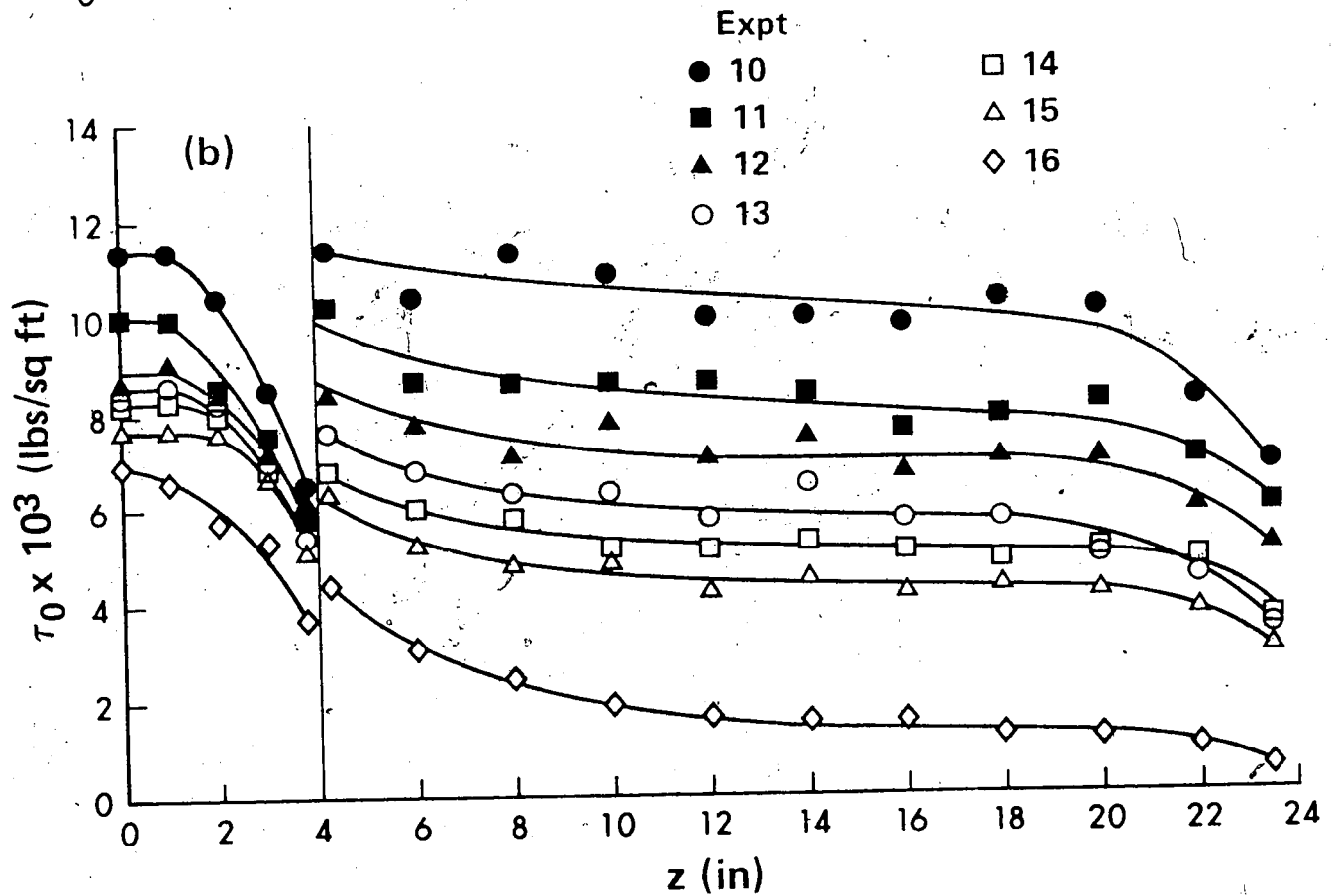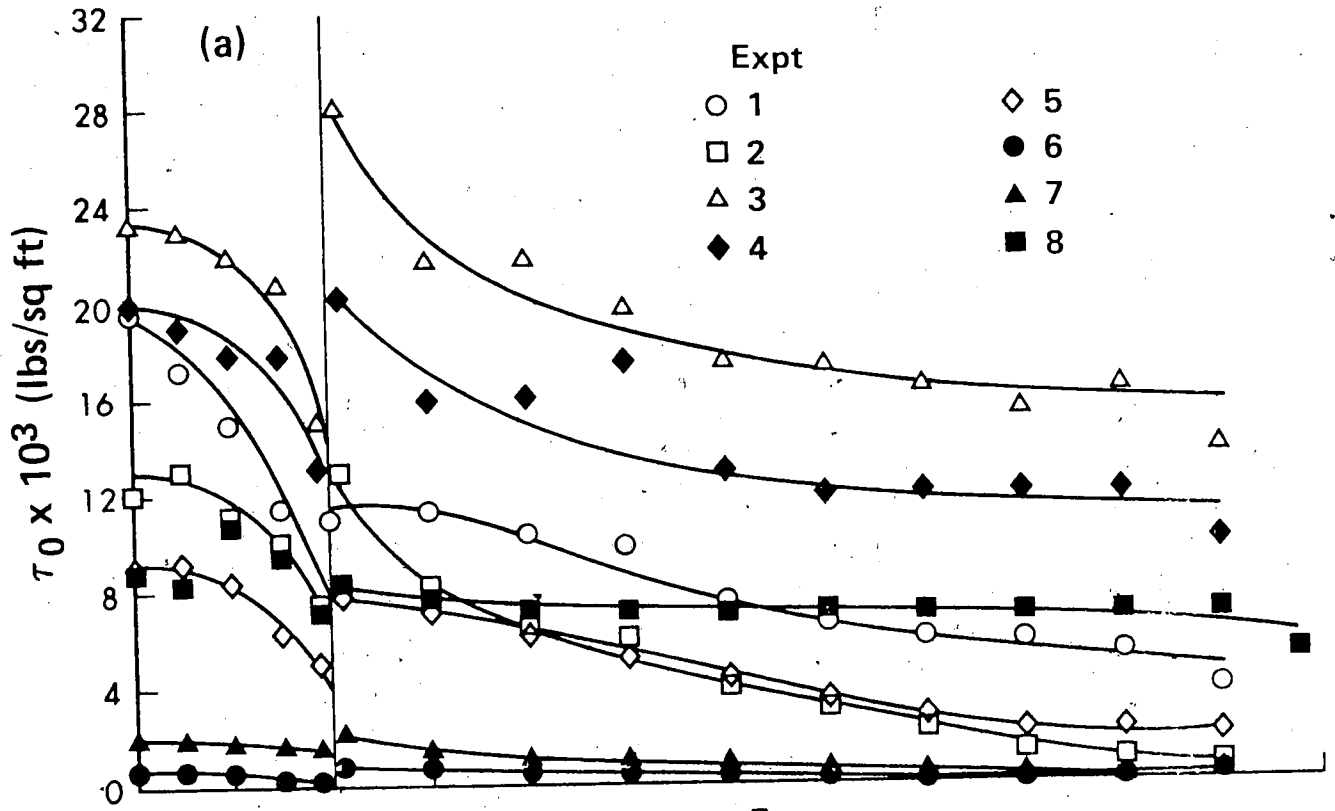
Figure 3.4a & b Bed Shear Stress Profiles

the main channel and the other in the flood plain. If u_m and u_m' are the values of the longitudinal velocity in the centerline of the main channel and at the junction of the main channel and flood plain for any given horizontal plane for which u_∞ is the corresponding undisturbed flood plain velocity, it was found that if $(u - u_m')/(u_m - u_m')$ is plotted against $\eta = z/b_m$ where b_m is the length scale, taken as equal to z where $(u - u_m')/(u_m - u_m') = 0.25$, the profiles are approximately similar as shown for a few typical experiments in Figure 3.5. The data are described by a curve of the equation:

$$f(\eta) = \frac{u - u_m'}{u_m - u_m'} = 1 - 0.75\eta^2 \tag{3.1}$$

In the above description, u_m and u_m' are the reference velocities and b_m is the length scale. If the main channel was sufficiently wide (Rajaratnam & Muralidhar 1969), u_m could be represented by the equation:

$$\frac{u_m}{u_*} = 5.75 \log\left(\frac{y\, u_*}{\nu}\right) + 5.5 \tag{3.2}$$

where $u_* = \sqrt{g\, D\, S_o}$, S_o is the slope of the channel and ν is the kinematic viscosity of water. The undisturbed flood plain velocity u_∞ would be given by the equation:

$$\frac{u_\infty}{u_{*\infty}} = 5.75 \log\left(\frac{y'\, u_{*\infty}}{\nu}\right) + 5.5 \tag{3.3}$$

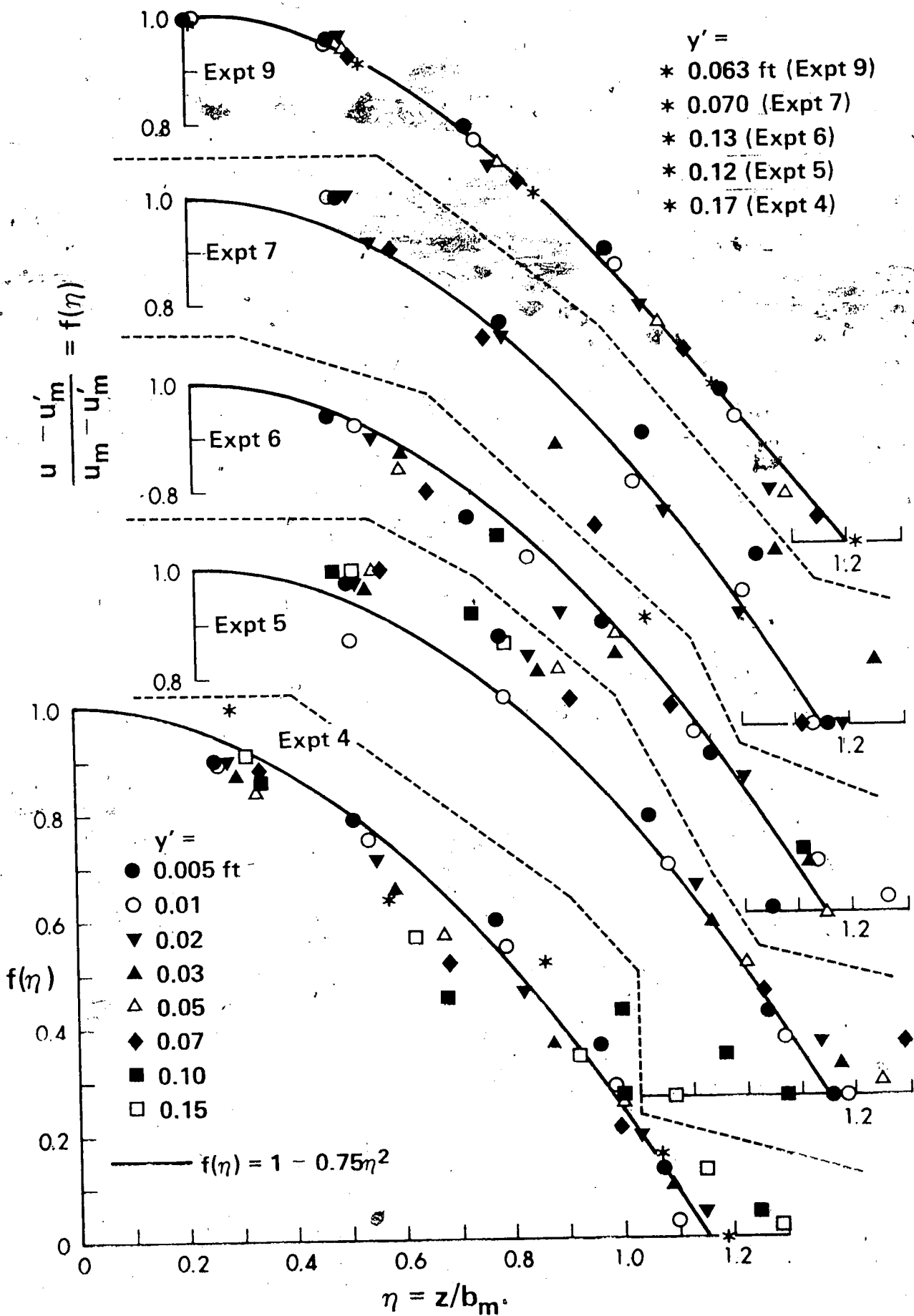where $u_{*\infty} = \sqrt{g\, d\, S_o}$, and y' is flood plain (see Figure 3.1).

Figure 3.5 Velocity Profile Similarity: Upper Part of Main Channel

Then it could be shown that:

$$\frac{u_m - u_\infty}{u_\infty} = \sqrt{\frac{D}{d}} \left[1 + \frac{\log \frac{y \sqrt{D}}{y' \sqrt{d}}}{\log \frac{C\, y \sqrt{g d S}}{\nu}} \right] - 1 \qquad (3.4a)$$

$$\frac{u_m - u_\infty}{u_\infty} = f\left[\frac{D}{d}, \frac{y'}{d}, \frac{d \sqrt{g\, D\, S_o}}{\nu} \right] \qquad (3.4b)$$

wherein C is a constant equal to 9.06.

In this study, the width of the main channel is not large and, as a result, the effects of mixing at the interface of the main channel and flood plain have permeated to the centerline of the main channel. Using equation 3.4 as a guide, a scheme was found for correlating u_m by plotting $(u_m - u_\infty)/(u_\infty)$ against y'/d (see Figure 3.6(a)). For any experiment, $(u_m - u_\infty)/(u_\infty)$ decreases with y'/d to eventually approach an asymptotic value as y'/d approaches unity. Using the results in Figure 3.6(a), Figure 3.6(b) was prepared which shows that $(u_m - u_\infty)/(u_\infty)$ for any given value of y'/d increases linearly with D/d. In any flood plain problem, if the flood plain is sufficiently wide, as was (approximately) the case in the present experiments, then u_∞ could be found. The behaviour of the length scale b_m is studied in Figure 3.7(a) wherein b_m/d is plotted against y'/d for different values of D/d. For any given value of D/d, variation of b_m/d with y'/d is not large and if an average value is adopted, this average value of b_m/D is seen to increase linearly with D/d as shown in Figure 3.7(b) and is described by the equation:
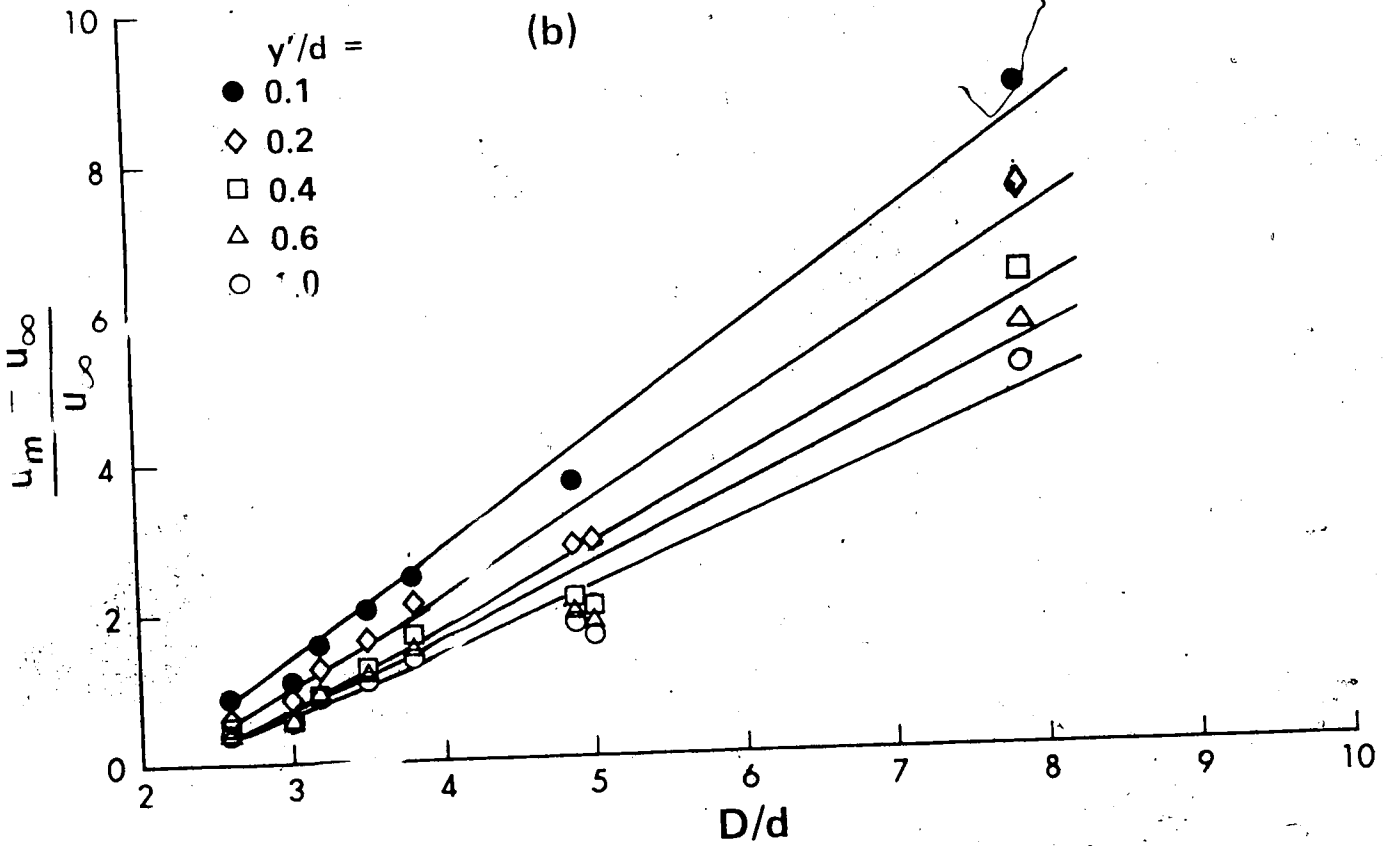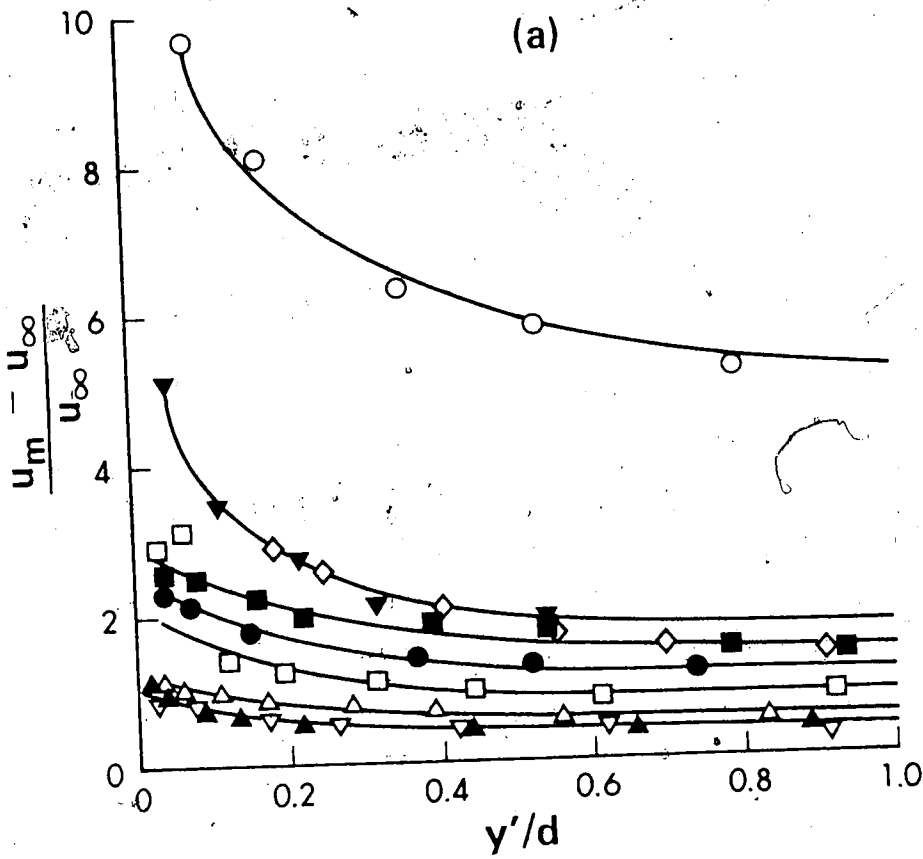
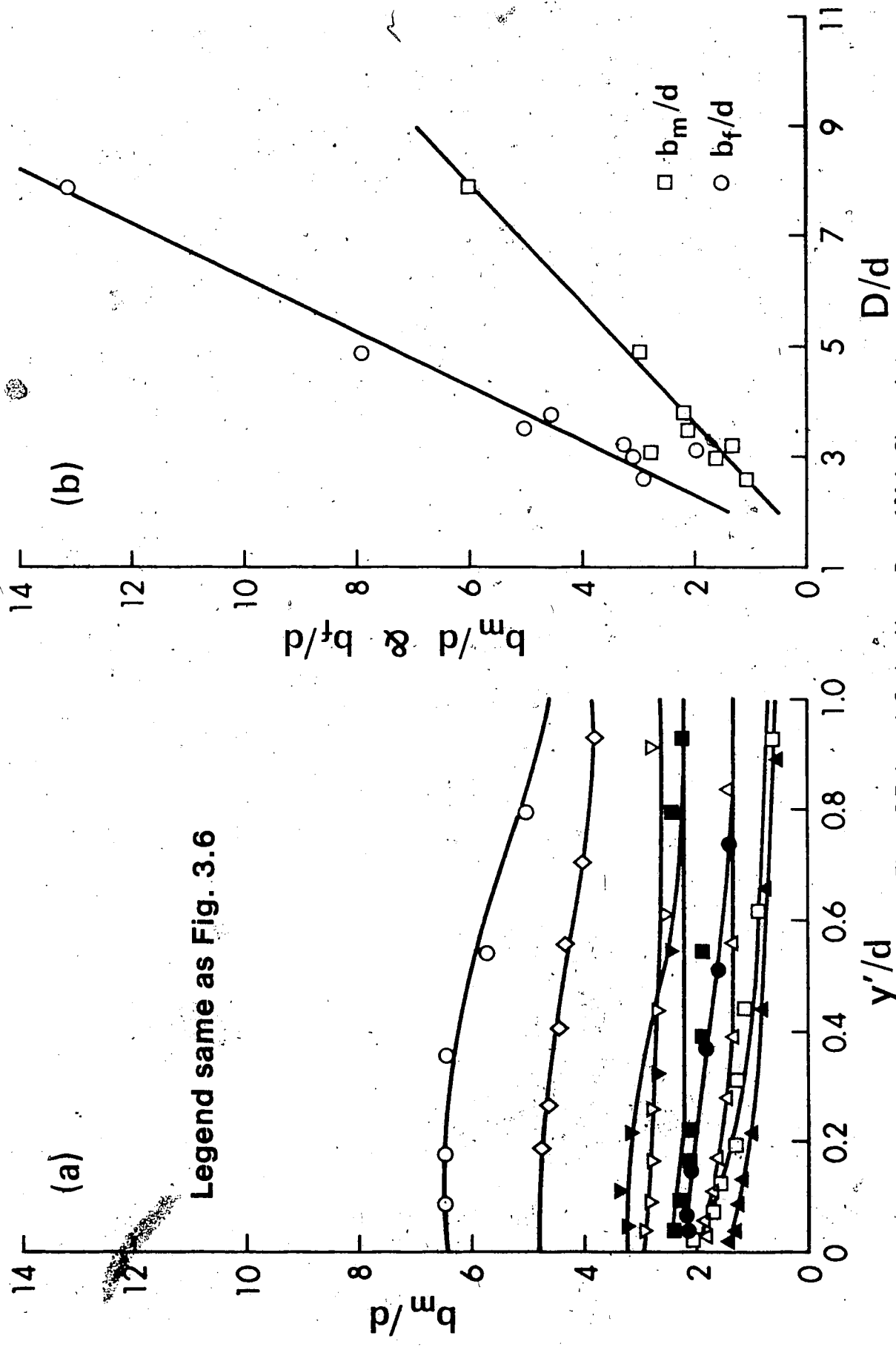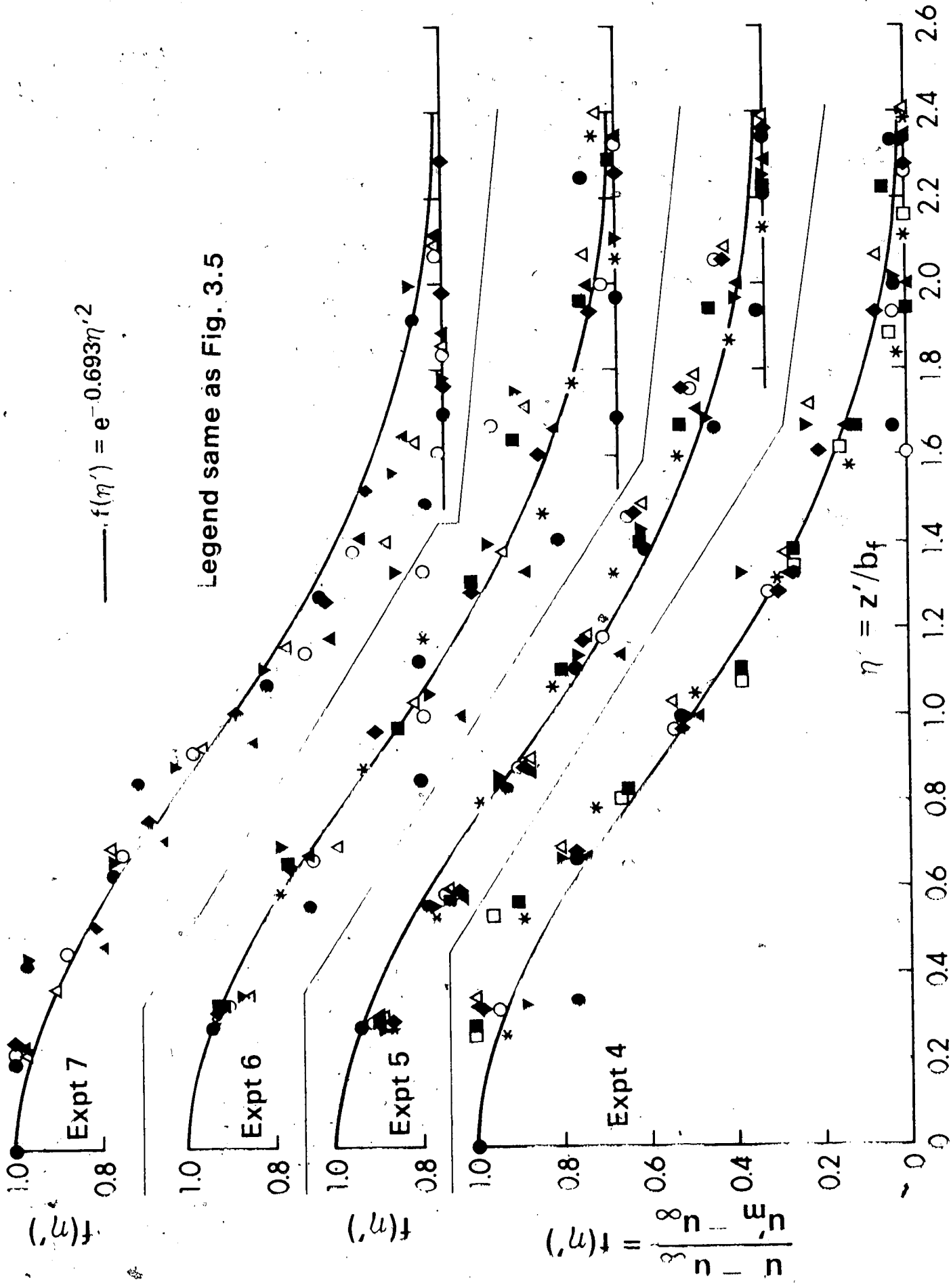Figure 3.6 Velocity Scale: Upper Part of Main Channel

Figure 3.7 Length Scale: Upper Part of Main Channel

$$\frac{b_m}{d} = 0.92 \frac{D}{d} - 1.32 \qquad\qquad (3.5)$$

The velocity profiles in the flood plain, when plotted with $(u_m - u_\infty)/(u_m' - u_\infty)$ against $\eta' = (z'/b_f)$ where $z' = (z - B/2)$ and $b_f = z'$ where $(u_m - u_\infty)/(u_m' - u_\infty) = 0.5$, were found to be (approximately) similar and a few typical plots are shown in Figure 3.8. These curves are satisfactorily described by the error function. In some plots of Figure 3.8, there is appreciable scatter, particularly for the lower most level, i.e. for the Pitot tube sitting on the bed of the flood plain. This observation will predict scatter in bed shear profiles. The behaviour of the velocity scale $(u_m' - u_\infty)/(u_\infty)$ is studied in Figure 3.9(a) wherein it is found that for $y'/d = 0.3$, it varies mainly with D/d and this variation is shown separately in Figure 3.9(b). In Figure 3.9(b), $(u_m' - u_\infty)/(u_\infty)$ is seen to increase linearly with D/d. Figure 3.9(c) shows that the length scale b_f/d is (almost) independent of y'/d and varies mainly with D/d. This variation is seen to be linear (see Figure 3.7(b)) and could be described by the equation:

$$\frac{b_f}{d} = 2.02 \frac{D}{d} - 2.71 \qquad\qquad (3.6)$$

The flow in the main channel below the bed level of the flood plain is analysed in an empirical manner. When the velocity profiles in this region were plotted with u/u_0 against y/h where u_0 is the value of u for $y = h$, as shown in Figure 3.10, it could be seen that for approximate

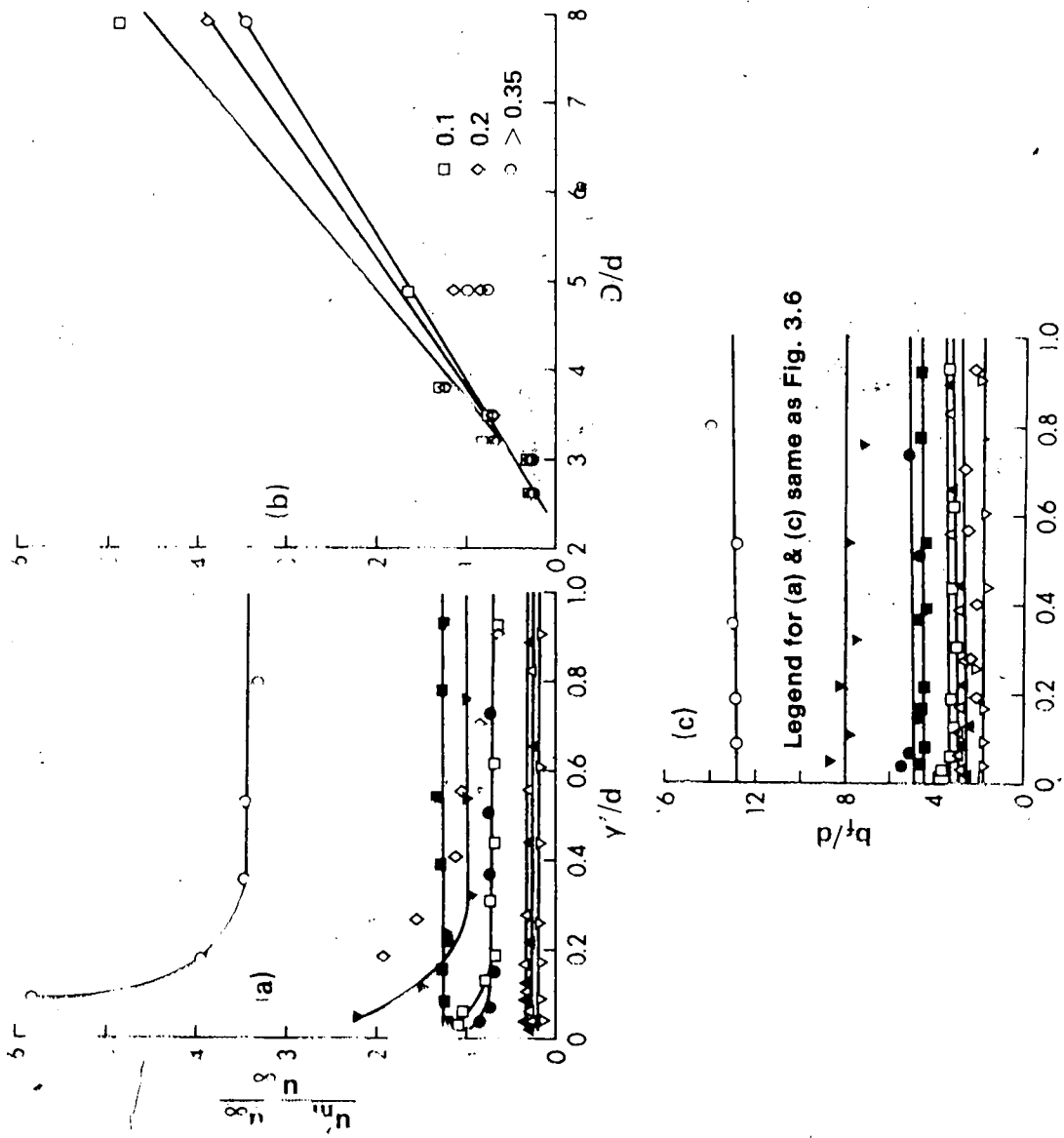Figure 3.8 Velocity Profile Similarity: Flood Plain

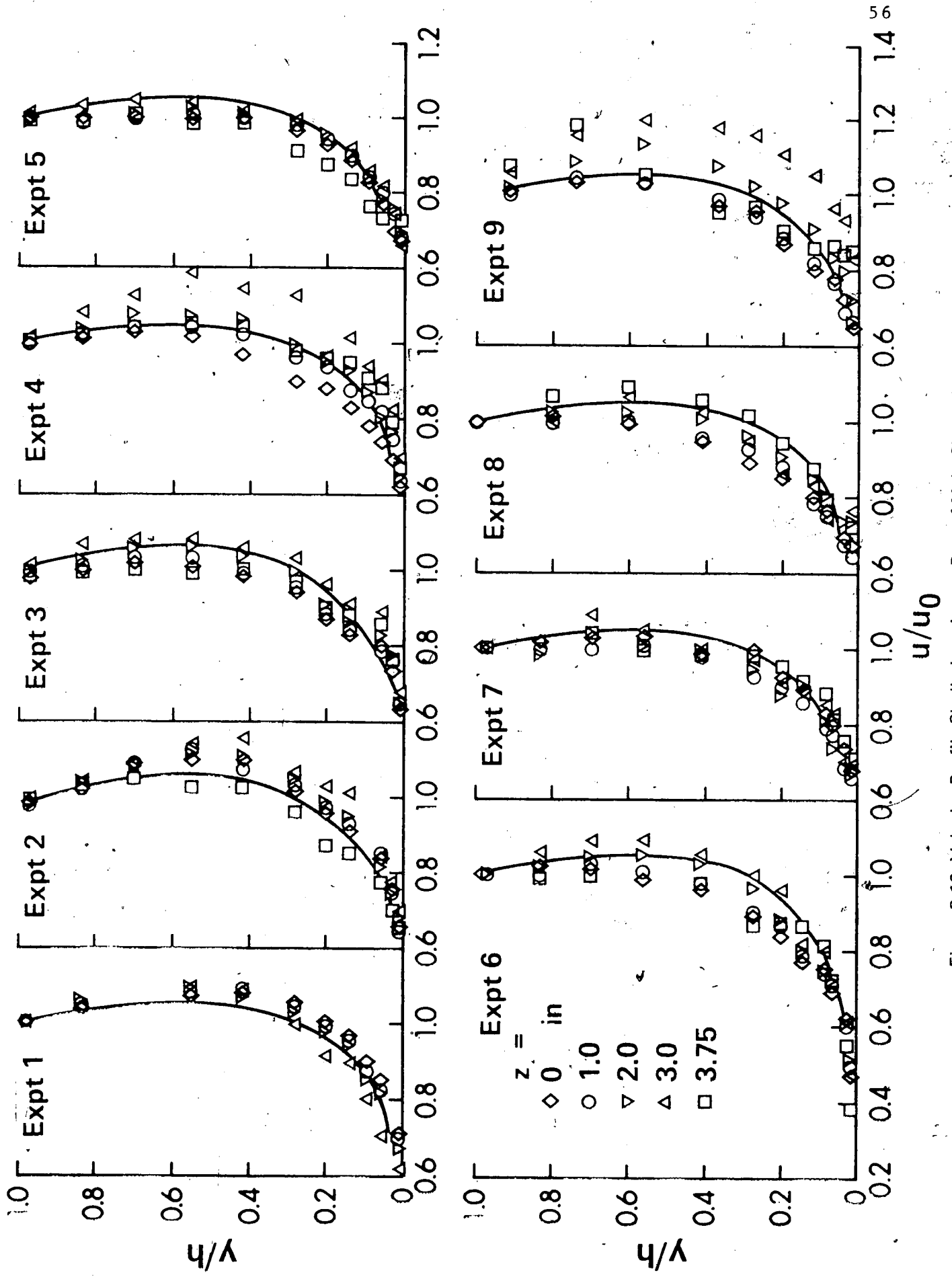Figure 3.9 Velocity and Length Scales: Flood Plain

Figure 3.10 Velocity Profile Similarity: Lower Part of Main Channel

calculation purposes, an average curve (shown by a continuous line in Figure 3.10) could be used. For this mean curve, the maximum value of $u/u_o = 1.06$ and occurs at $y/h = 0.5$. To use this curve, u_o could be obtained from Figure 3.6 for the lowest (experimental) value of y'/d. An alternate method of analysing the flow in this region is indicated later.

From the plot of the shear stress measurements, in the flood plain, (Figure 3.4) it is easy to see that the bed shear stress in the flood plain increases as the junction plane with the main channel is approached. If $\tau_{0\infty}$ is the undisturbed shear stress in the flood plain (occurring at points sufficiently away from the banks of the flood plain) and if τ_o is the shear stress at any distance z' the maximum value of $\Delta\tau_o = (\tau_o - \tau_{0\infty})$, written as $\Delta\tau_{om}$, occurs at the edge of the flood plain (i.e. for $z' = 0.0$). A plot of the variation of $\Delta\tau_o/\Delta\tau_{om}$ with z' in terms of a suitable length scale showed that for very approximate purposes, the distribution of this dimensionless excess bed shear stress could be considered to be similar but there was considerable scatter. If l_* is the value of z' where $\Delta\tau_o = 0.0$, the variation of l_*/d with D/d is shown in Figure 3.11(a). From Figure 3.11(a), it can be said that l_*/d increases almost linearly with D/d. Figure 3.11(b) shows a plot of the variation of τ_{om}/τ_o with D/d. Even though it is difficult to draw a trend-line in Figure 3.11(b), it can be seen that for $D/d = 10.0$, $\tau_{om} = 2\ \tau_{0\infty}$. Similar large increases have been reported by Myers and Elsawy (1975).

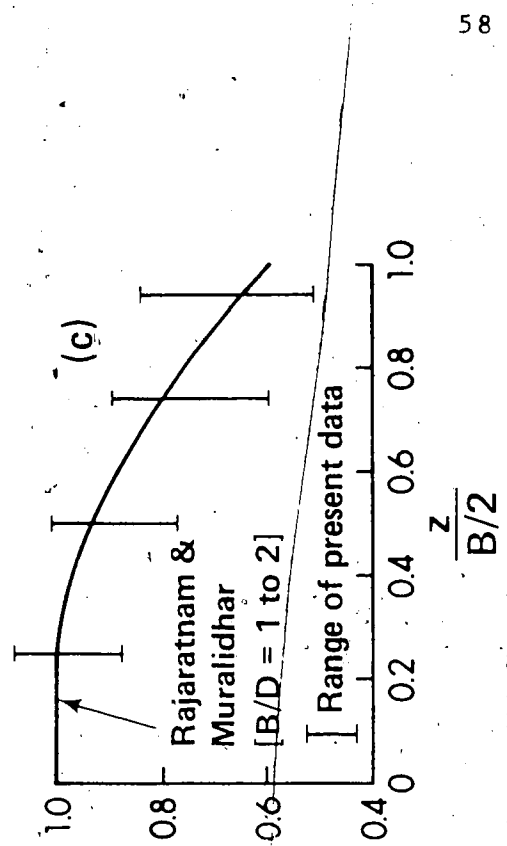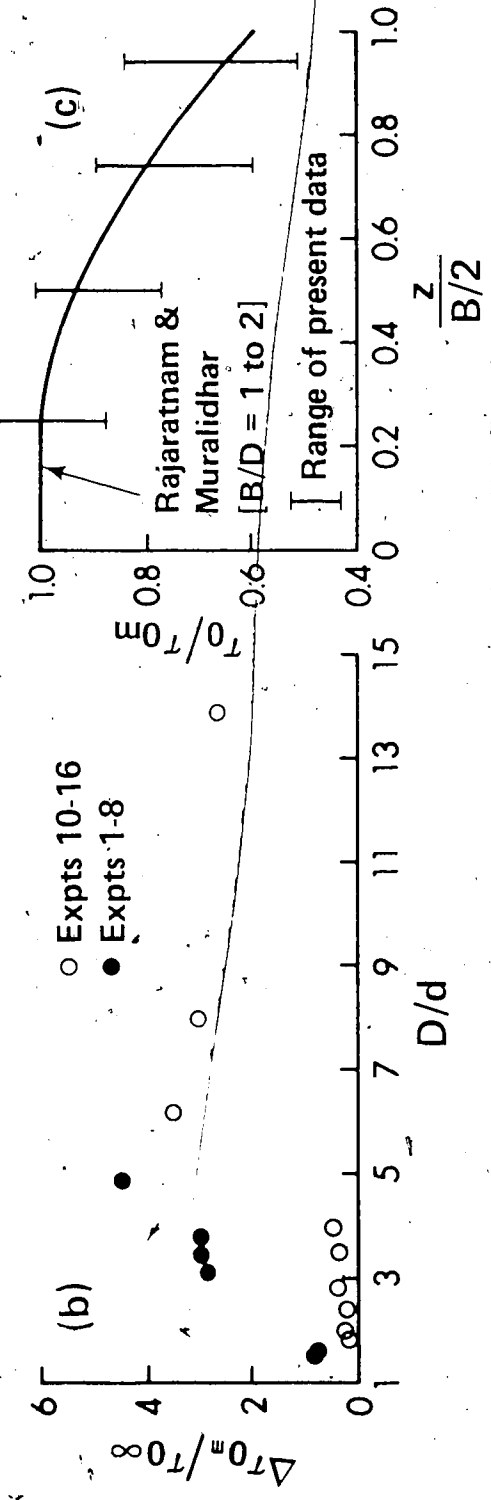Considering the bed shear stress in the main channel,
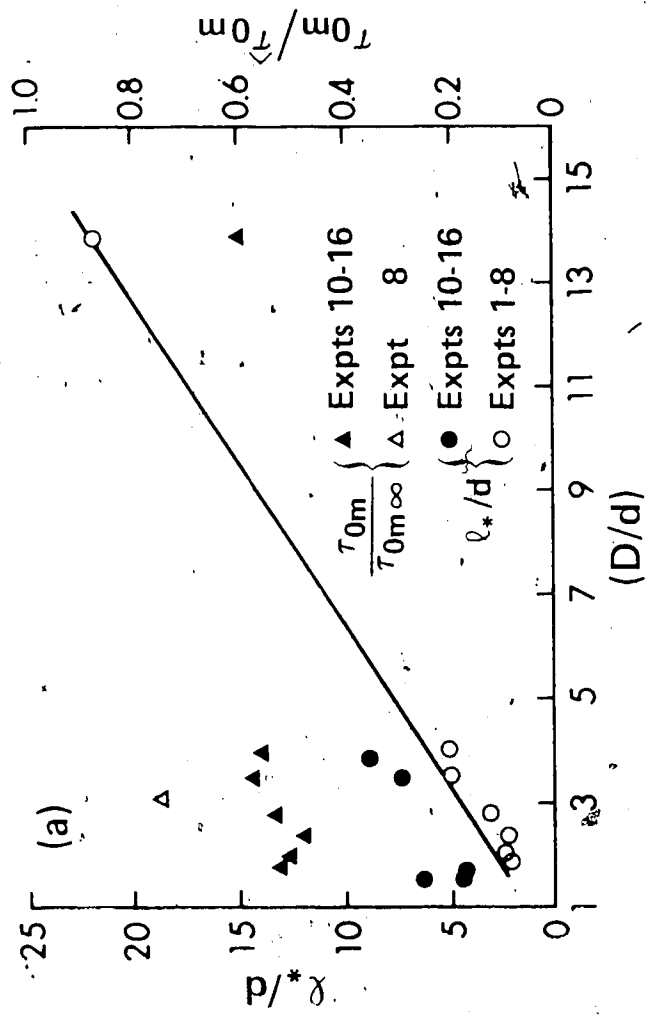
58

Figure 3.11 Bed Shear for Flood Plain and Defect in Main Channel

the results of the additional experiments as well as those of experiment 8 are shown in Figure 3.11(a) wherein τ_{om} is the corresponding τ_o which will exist if the side walls of the main channel were extended to a total depth of D. A curve for the variation of $\tau_{om}/\rho g D S_o$ with B/D based on the available results, with additional experiments performed by the author, is given in Figure 3.12. From Figure 3.11(a) it appears that the maximum bed shear stress in the main channel is reduced by about 40% because of the interaction with the flood plain flow. Similar decreases have been reported by Myers and Elsawy (1975). It was also found (see Figure 3.11(c)) that the variation of $\tau_o(z)/\tau_{om}$ in the main channel with z/B/2 was approximately the same as that of rectangular channels without flood plains. Hence, the main effect appears to be a reduction in the magnitude of the bed shear in the main channel.

If τ_* is the average shear stress exerted by the main channel flow on the flood plain flow at the junction plane, (τ_* d) could be recognized as equal to (Integral of $\Delta \tau_o dz'$ from 0 to z') where the upper limit is the value of z' where τ_o is reached. (If the flood plain wall shear is measured, τ_* could also be computed by considering all the forces acting on the flood plain flow for unit length.) The results for all the experiments are given in Table 1. Neglecting the experiments with small values of d (since in such cases, the error in τ_o measurements will be large), one general comment that could be made is that τ_o is of the same order as the maximum shear stress in the flood plain which occurs near the junction plane.
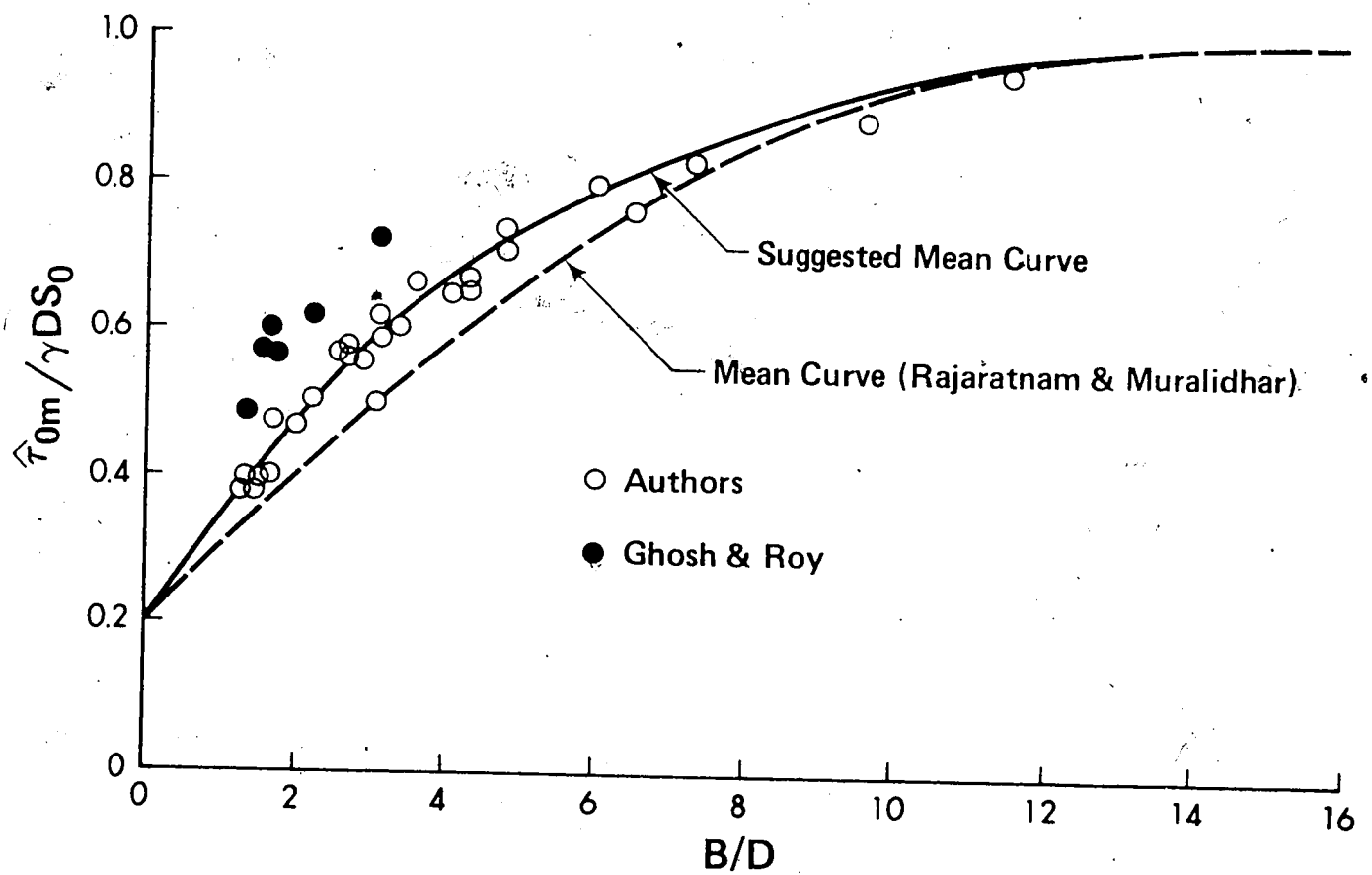
Figure 3.12 Centerline Bed Shear for Rectangular Channels

Using the results presented earlier, it is possible to present an analysis of the velocity profiles in the main channel. With reference to Figure 3.1(d), for any value of z, let curve 1 represent the profile of u with y that would exist when the side wall of the main channel is extended to a depth of D. If now the extension of the side wall is removed, the actual velocity profile has the shape of curve 3. Curve 3 predicts smaller velocities in the neighbourhood of the bed because of the reduction of τ_o. Further, as y approaches h and for y>h , due to the direct momentum loss to the flood plain, the velocity profile shows a dip or defect from curve 2, which is different from curve 1 because of only the reduction in τ_*. For the flood plain, in the region affected by the interaction, if curve 4 in Figure 3.1(d) is the undisturbed velocity distribution, curve 5 represents a typical velocity profile which includes an increase due to the momentum transport to the flood plain. It was found that for a number of the experiments, the shaded area between curves 2 and 3 integrated for the whole width of the main channel was approximately equal to the shaded area between curves 4 and 5 integrated for the whole width of the flood plain. That means the area between curves 1 and 2 integrated to cover the full width of the main channel will give the reduction in carrying capacity of the compound cross-section because of the flow interaction. It is possible to express this observation analytically.

3.4 Effect of Roughness

Two experiments, experiment 9 and 10, were performed with the flood plain roughened with a dense hemispherical roughness of diameter of 0.5 inch (12.7 mm). The equivalent sand roughness of this roughness has earlier been found equal to 0.028 feet (8.5 mm) (Hollingshead, 1972). The results of the velocity measurements showed that the momentum transport exists as in the case of a smooth bed. The velocity profiles in the main channel (for $y > h$) and in the flood plain were similar when considered relative to the undisturbed flood plain velocity and agreed with the results for the smooth bed.

Considering the velocity scale, Figure 3.6(a) shows that the variation of $(u_m - u_\infty)/(u_\infty)$ with y'/d is not at all affected by the roughness. The length scale b_m/d is increased by the roughness (see Figure 3.7(a)). The velocity scale $(u'_m - u_\infty)/(u_\infty)$ is affected to a certain extent (Figure 3.9(a)) and the length scale b_f/d is considerably reduced by the roughness (Figure 3.9(c)). It is necessary to perform more experiments with a range of roughness heights before the effects of the flood plain roughness on the momentum transport could be properly assessed.

3.5 Conclusions

Based on the experimental results presented in this chapter, the following conclusions could be made. The transport of the longitudinal momentum from the main channel to the flood plain as well as the existence of apprecieble

shear stresses in the junction plane between the main
channel and flood plain have been established. The lateral
distribution of the longitudinal velocity, in the upper part
of interaction region between the main channel and the flood
plain if viewed with respect to the proper velocity, has
been found to be separately similar in the main channel and
flood plain. In the main channel interaction region, the
velocity scale is the difference between the maximum
velocity u_m in the main channel and that in the junction
plane (u_m') and the base velocity (for similarity
considerations) is u_m'. The length scale b_m is the lateral
distance from the centerline where $(u - u_m') = 0.25(u_m - u_m')$.
The dimensionless velocity distribution is described by
equation 3.1. The dimensionless velocity $(u_m - u_\infty)/u_\infty$
varies with D/d and y'/d (see Figure 3.6). Futher,
$(u_m' - u_\infty)/u_\infty$ varies mainly with D/d and to a small extent
with y'/d for $y'/d > 0.35$. The dimensionless length scale
b_m/d, varies mainly with D/d and futher this variation is
linear and is described by equation 3.5.

For the interaction region in the flood plain, the
velocity scale is $(u_m' - u_\infty)$ and the length scale is b_f, the
distance from the junction plane to the point where
$(u - u_\infty) = 0.5(u_m' - u_\infty)$. The dimensionless length scale b_f/d
has been found to vary mainly with D/d and this variation
is described by equation 3.6. In the main channel below the
level of the flood plain, the velocity profiles have been
found to be approximately similar with u_o the velocity in
the main channel at $y=h$ as the velocity scale. The value of

u_0 could be obtained from the similarity profiles presented earlier.

The increase in the shear stress in the flood plain in terms of $\tau_{0\infty}$ as well as the extent of the affected region in terms of d appear to be mainly function of D/d. Most of the results in this chapter are concerned with smooth boundaries and hence more experiments should be performed with different kinds and heigths of roughness elements before the results presented in this chapter could be adopted for practical use.

4. Interaction Between Straight Main Channel and Straight Flood Plain Flows-Further Studies-Asymmetrical Channel

In Chapter III the results of the interaction between the main channel and the flood plain flows, for an idealized case of a straight channel in a straight valley, with the main channel being narrow so that the effects of interaction dominated the entire main channel, was studied. In this chapter the main channel is wide enough to have at least a section at the center in which the effects of lateral transfer of momentum are negligible. Hence, the results presented in this chapter have greater potential for applicability to practical problems.

In this chapter mainly the effect of the width of the channels on the structure of the flow is studied. Although, three types of asymmetrical channels (Type A,B and C) were studied, greater number of runs were made with type C because of its wide main channel and flood plain and this chapter presents the results on only the type C channel.

4.1 Experiments

The measurements were made in the middle cross-section of the channel at a distance of approximately 30 feet (9.15 m) from the entrance after making sure the flow was fully developed and that the depth of flow was constant. It was believed that uniform flow was established. This was accomplished by manipulating the tailgate and observing that the differential pressure reading between each consecutive pair of the seven static probes was the same up to one millivolt

reading on the modulator of the transducer. Also, care was taken to make sure the water surface slope and the bed slope were parallel. Five experiments were conducted in the type C channel, with different values for d or D. Table 2 shows the pertinent details of the dimensions and the experiments.

The velocity and shear stress measurements were made in the whole cross-section of the compound channel. The boundary surface was generally smooth. The interaction regions were studied first. It was found where the interaction would take place and this area was studied in detail. The vertical velocity profiles in the mixing zone were very close together. In addition, one special experiment was conducted with the multi-level flood plain and because of its special features the results of this experiment will be discussed in Appendix B.

4.2 Experimental Results

The velocity profile of a typical experiment are shown in Figure 4.2. Since the Froude number of all the experiments was around 0.35, it was decided to present the velocity profiles of one experiment (number 3 with D/d=4.76). It was found that the velocity will continuously increase as one moves from the flood plain towards the main channel and reaches a point where the disturbed velocity approaches the local undisturbed velocity. Figure 4.2 shows clearly this location of disturbed velocity approaching the undisturbed velocity. In the main channel the velocity increases with y, up to some level, and then decreases
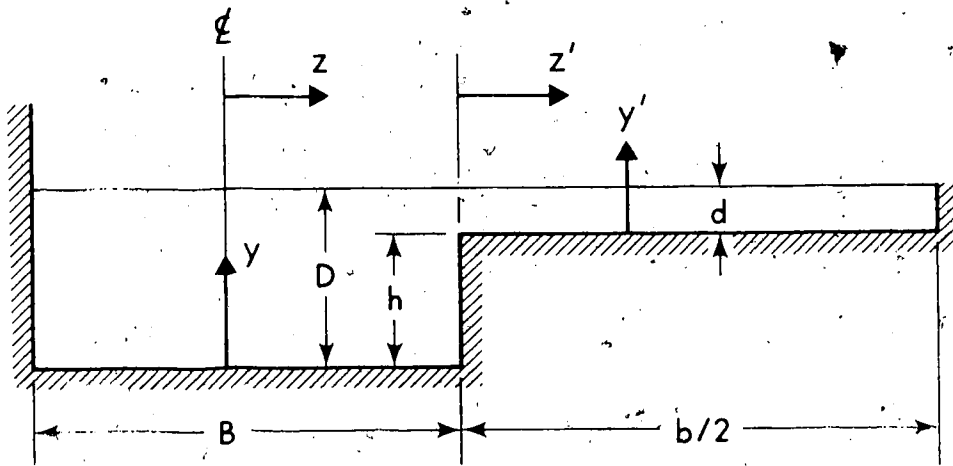
TABLE 2

Significant Details of the Experiments

B = 2.35 feet, b = 1.67 feet

Expt. No.	h(ft)	D(ft)	d(ft)	Q (cfs)	S $\times 10^3$	D/d	B/D	b/d
1	0.323	0.373	0.050	0.96	0.450	7.46	6.31	33.3
3	0.312	0.395	0.083	1.06	0.480	4.76	5.95	20.1
4	0.322	0.476	0.154	1.56	0.450	3.09	4.94	10.8
5	0.321	0.596	0.275	1.98	0.364	2.17	3.94	6.07
6	0.317	0.353	0.036	0.90	0.408	9.81	6.66	46.4
7*	0.318	0.420	0.102	1.26	0.724	4.12	5.61	16.3
8*	0.320	0.500	0.180	1.97	0.600	2.73	4.71	9.26

* Dye Test

(a) Sectional View
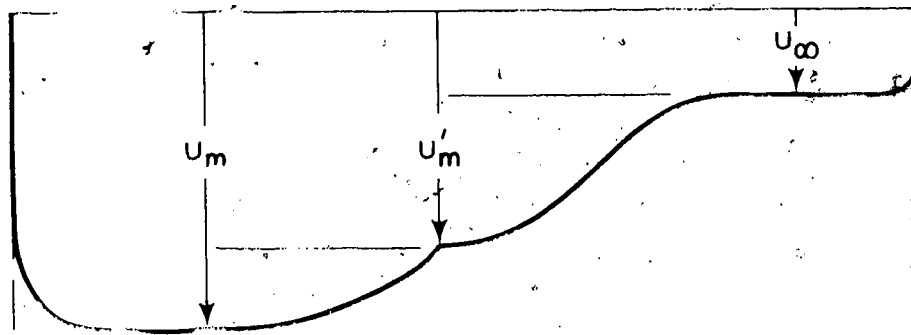
(b) Velocity Profiles
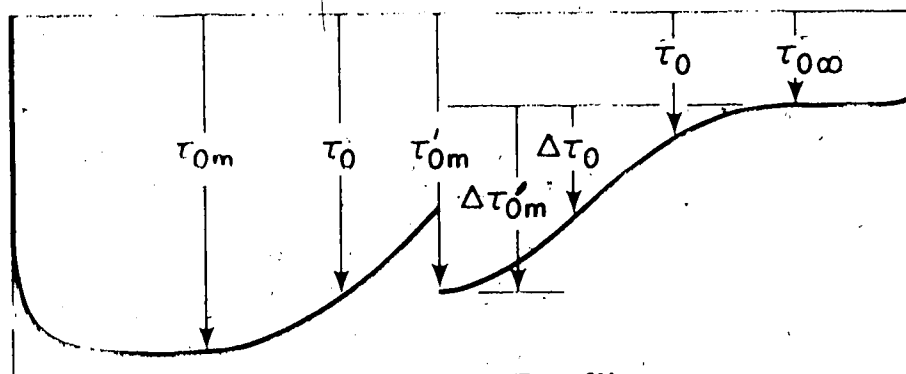
(c) Bed Shear Profiles

Figure 4.1 Definition Sketches
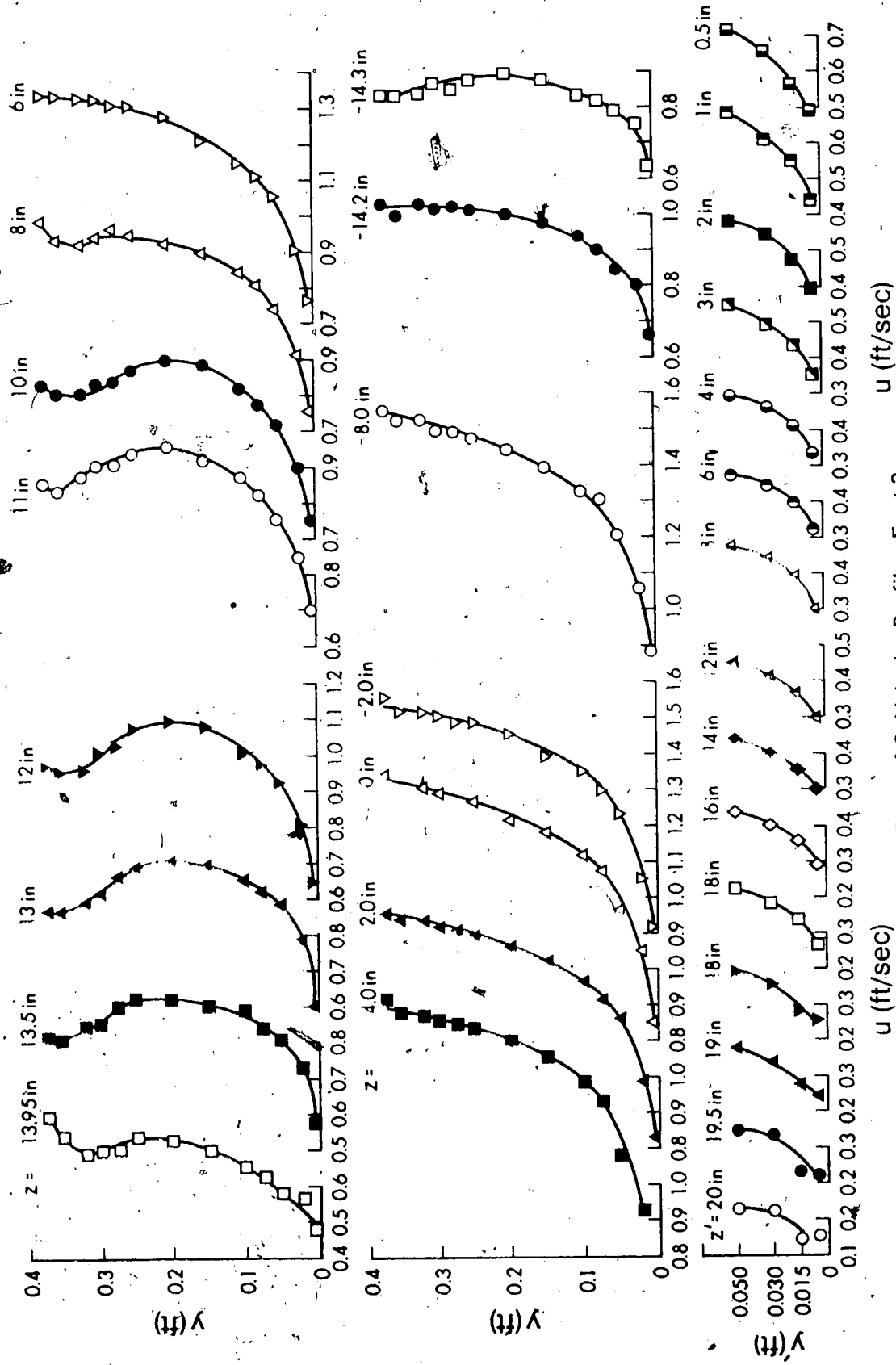
Figure 4.2 Velocity Profile; Expt-3

continuously to eventually become approximately constant

near the water surface. This behavior was also observed in

the previous chapter (Symmetrical Channel). In the central

region of the main channel, $\bar{u}$ increases continuously with y

up to (almost) the water surface whereas in the region near

the flood plain interface, a dip in the velocity profiles

due to lateral momentum transfer could be seen. At least in

principle, this dip is similar to the dip in velocity

profiles observed in narrow channels due to the lateral

momentum transfer to the side wall regions. In the flood

plain region, the velocity increases continuously with y'

until the water surface is reached except in the narrow

region near the side wall of the flood plain.

Although, velocity profiles in the lateral direction

(u(z)) in the region where y>h for a few values of y' (the

normal distance from the bed of the flood plain) were

prepared for all experiments, only three of those plots are

shown in Figure 4.3, for three typical experiments. In

Figure 4.3 for the three experiments, it is seen that u

decreases continuously from a maximum value of u_m at

approximately the centerline of the main channel to u'_m at

the interface between the main channel and the flood plain

and u further decreases with z' to reach u_∞ for some value

of z'. The value of u remains constant at u_∞ for a portion

of the flood plain until the section where influence of the

wall is felt. In the main channel for z<0.0, the u velocity

decreases due to the influence of the side wall. In the

immediate vicinity of the junction plane, in most of the

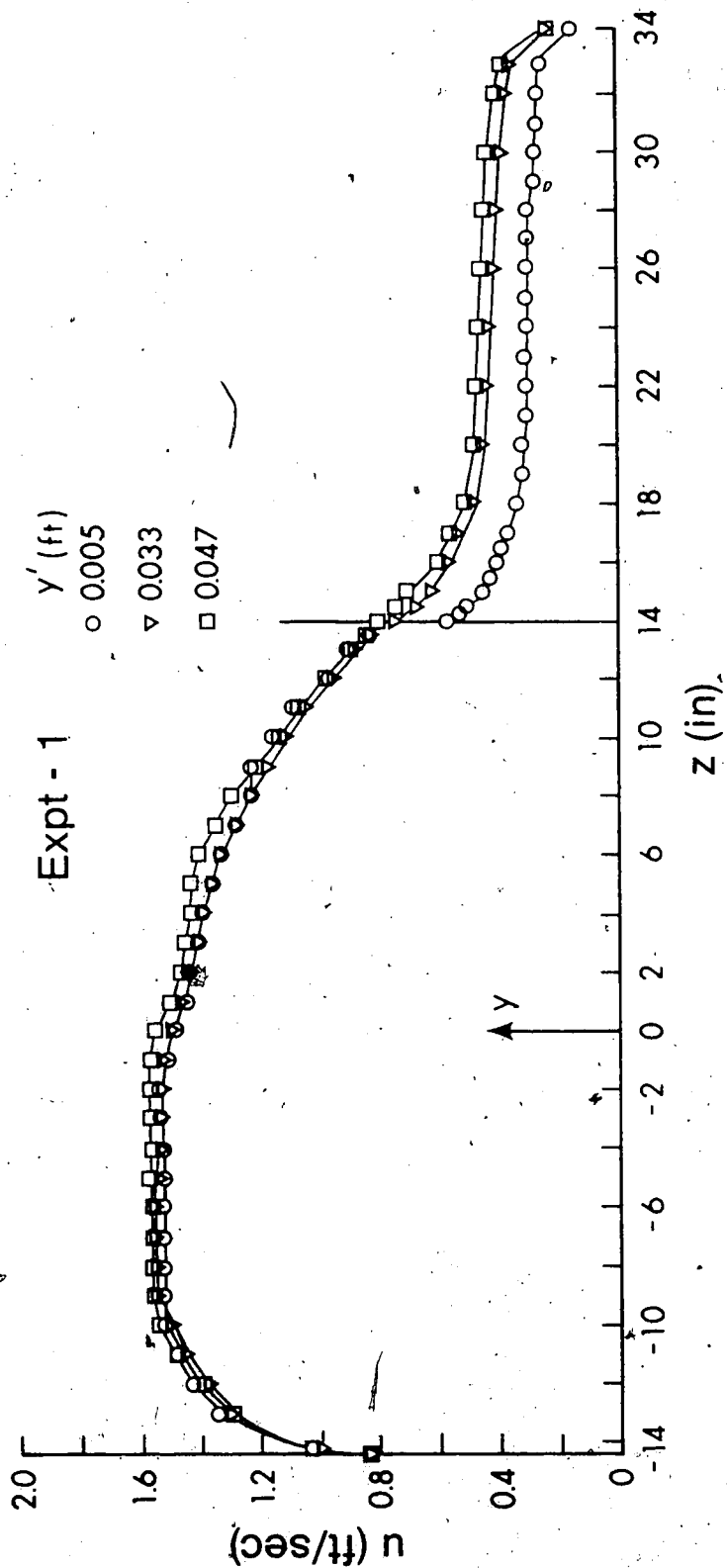experiments, a sharp increase in velocity was noticed. This

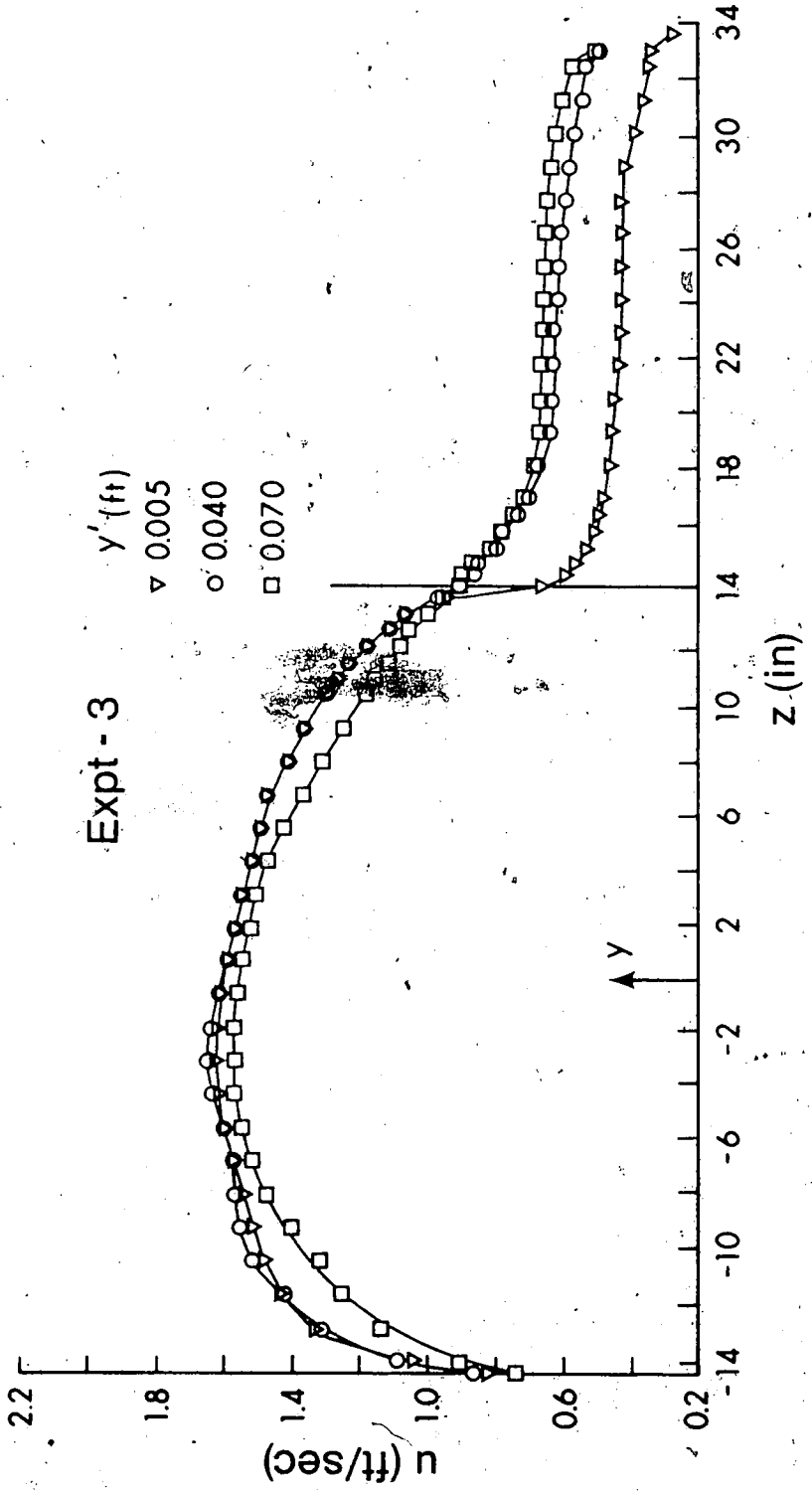Figure 4.3 Lateral Velocity Profiles: Expt-1
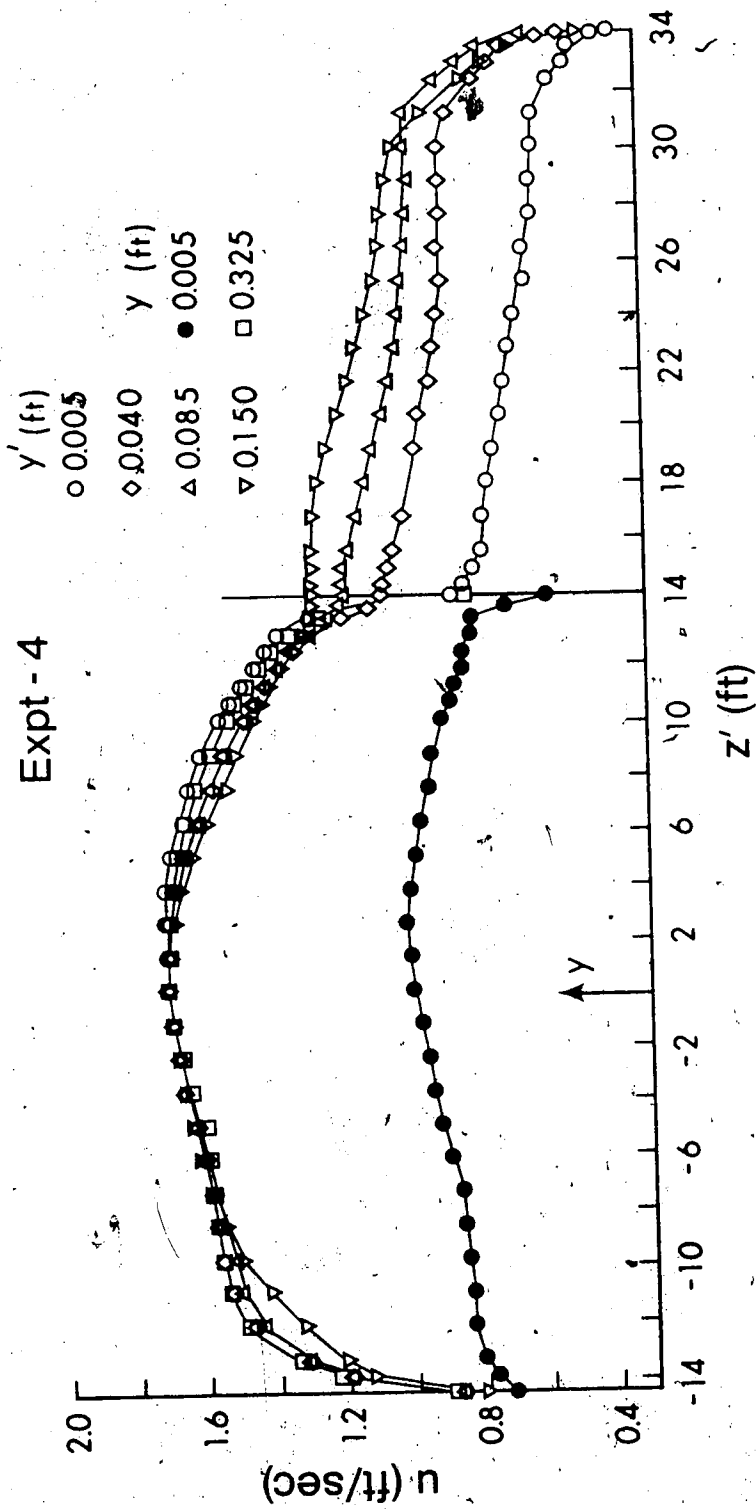
Figure 4.3 (cont.) Lateral Velocity Profiles: Expt-3

Figure 4.3 (cont.) - Lateral Velocity Profiles: Expt-4

sudden increase has also been reported by other observers such as Goncharov (1964).

Profiles of the boundary shear stress τ_0 for the experiments are shown in Figure 4.4. Considering the bed shear stress, it decreases from a maximum value of τ_{om} in the central region of the main channel to some value as the junction plane with the flood plain is reached. In the flood plain, τ_0 decreases from a large value at $z'=0.0$ until $\tau_{0\infty}$ is reached. The presence of the side walls causes a further decrease in the bed shear stress.

4.3 Analysis of Results

As indicated by an earlier study with a narrow main channel, u velocity profiles in the main channel, in the region for $y>h$, in the lateral direction, (i.e. $u(z)$) were plotted with $(u - u_m')/(u_m - u_m')$ versus $\eta = z/b_m$ wherein b_m is the length scale chosen in such a way that at $\eta=1.0$, $(u - u_m')/(u_m - u_m')=0.25$. The results, shown in Figure 4.5, indicate that, in general, for $y'/d=0.0$ to 1.0, the velocity profiles are similar and that they are well described by the equation:

$$f(\eta) = \frac{u - u_m'}{u_m - u_m'} = 1 - 0.75\eta^2 \qquad (4.1)$$

Considering the velocity scales, if the main channel and flood plain were so wide that sections where the velocity profiles ($u(y)$ or $u(y')$) are not affected to any (noticeable) extent by the momentum transfer to the flood
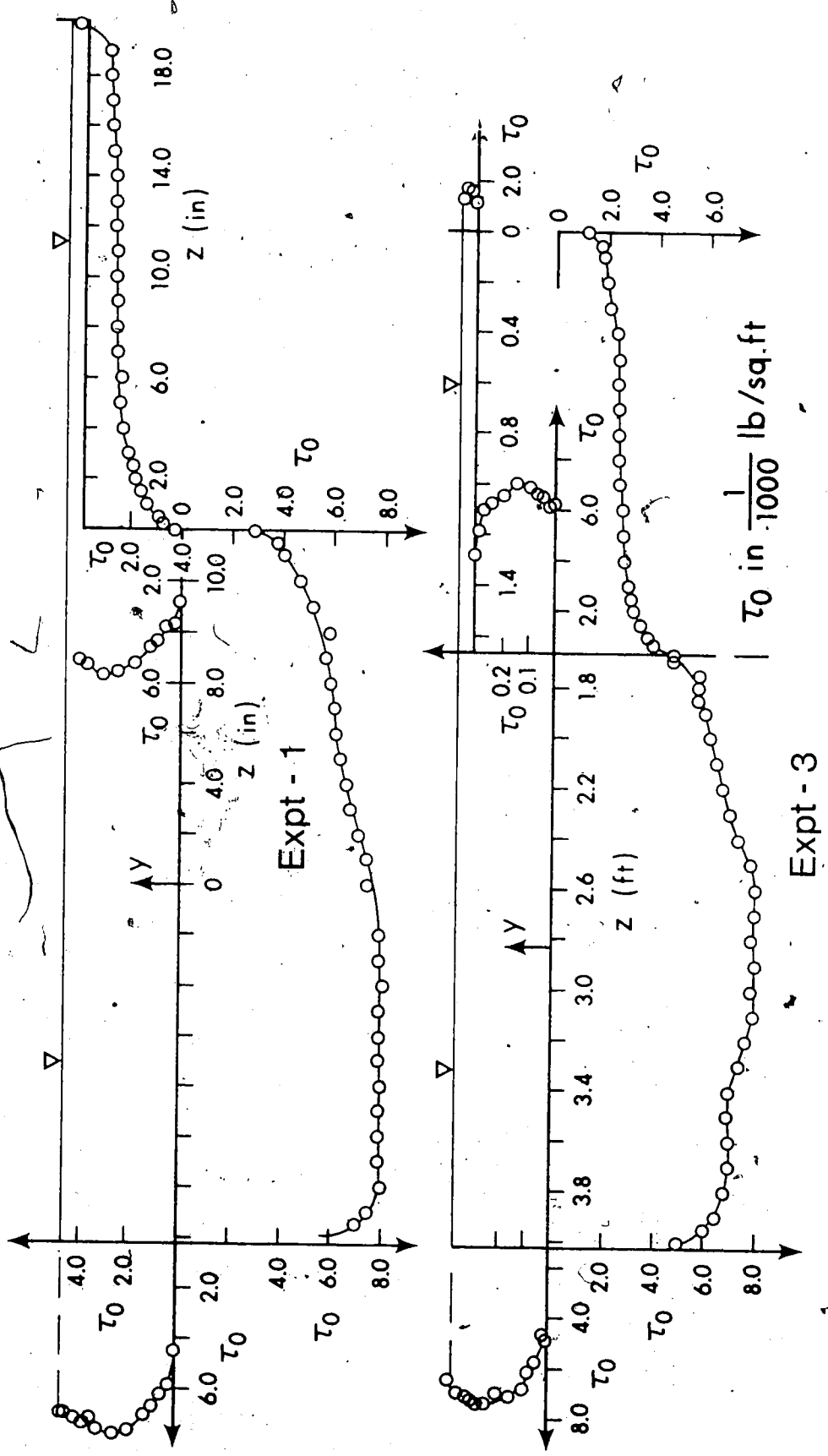
Figure 4.4 Bed Shear Stress: Expts 1 & 3

Expt - 4

Expt - 5

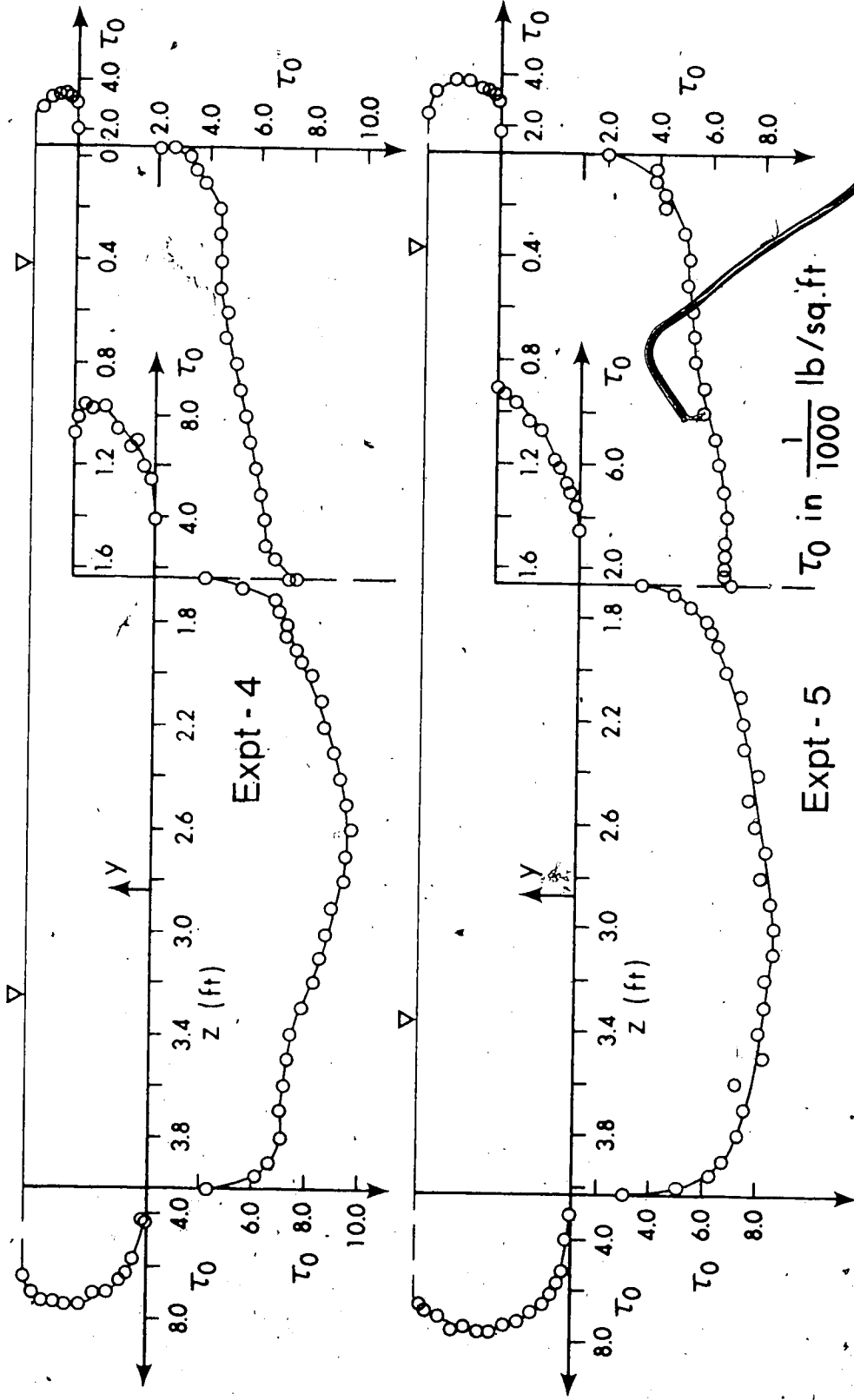τ_0 in $\frac{1}{1000}$ lb/sq.ft
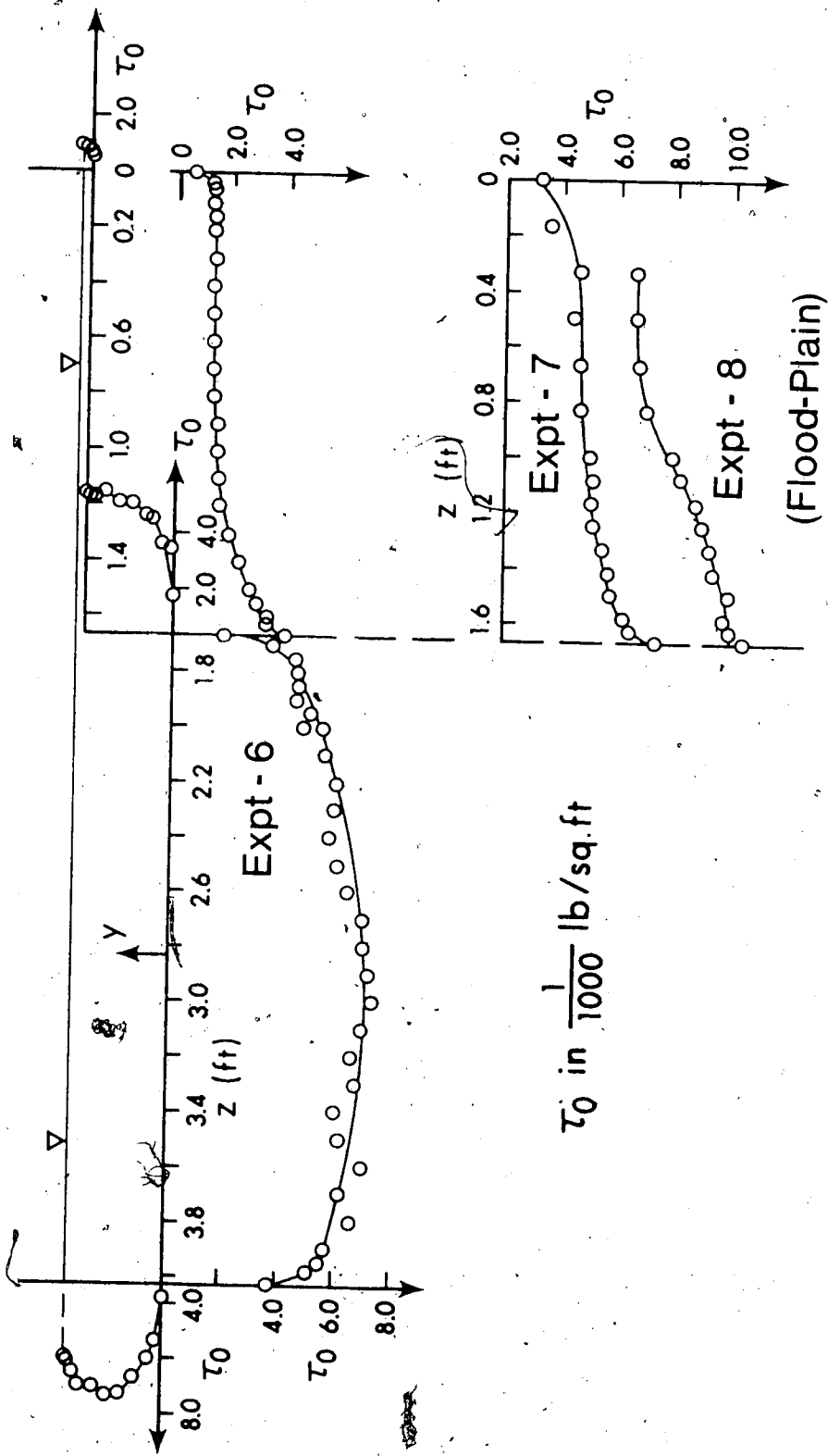
Figure 4.4 (cont.) Bed Shear Stress: Expts 4 & 5
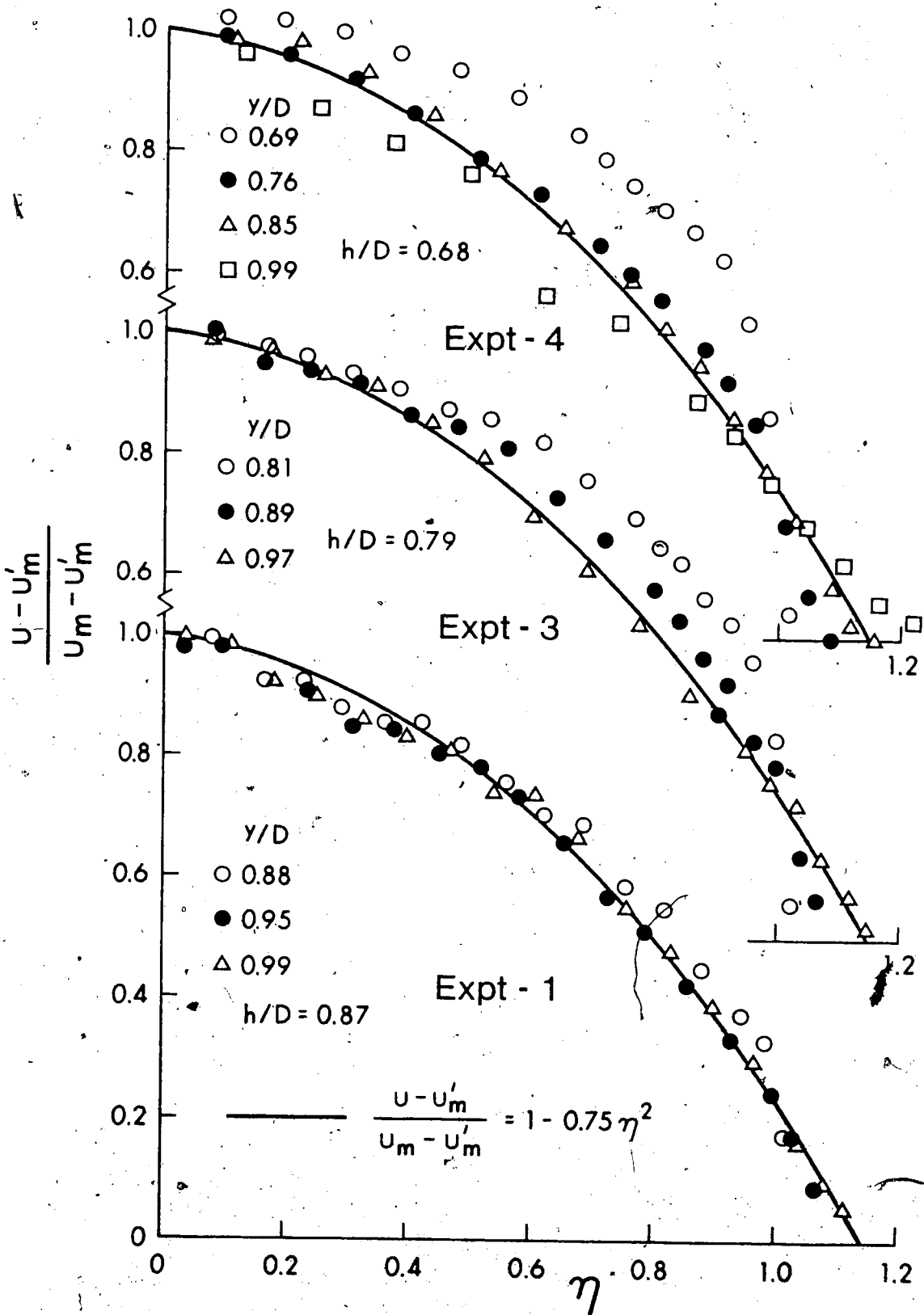
Figure 4.4 (cont.) Bed Shear Stress: Expts 6, 7 & 8

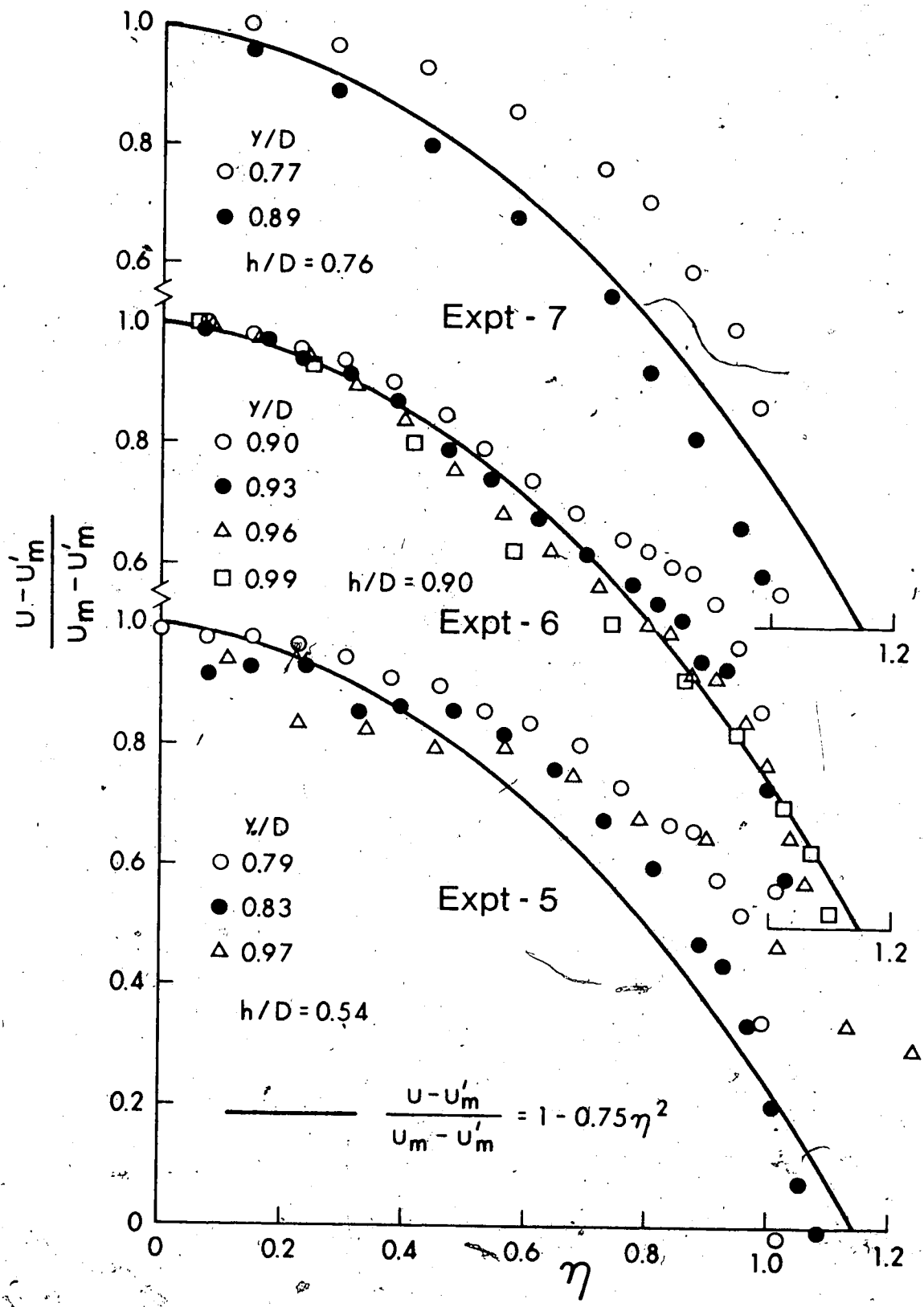Figure 4.5 Velocity Profile Similarity: Upper Part of Main Channel (Expts 1, 3 & 4)

Figure 4.5 (cont.) Velocity Profile Similarity: Upper Part of Main Channel (Expts 5, 6 & 7)

plain and assuming that in those unaffected regions, the
vertical velocity profiles (u(y) or u(y')) are described by
the logarithmic law, then:

$$\frac{u_m - u_\infty}{u_\infty} = \sqrt{\frac{C_{*m} \ D}{C_{*f} \ d}} \ [\ 1 + \frac{\log \frac{y \sqrt{C_{*m} \ D}}{y \sqrt{C_{*f} \ d}}}{\log \frac{C \ y' \sqrt{C_{*f}} \ gdS}{\nu}} \ ] - 1 \qquad (4.2)$$

wherein C is a constant equal to 9.06 and $C_{*m} = \tau_{om} / \gamma \ D \ S_o$ and
$C_{*f} = \tau_{o\infty} / \gamma \ d \ S_o$. The factors C_{*m} and C_{*f} could be obtained
from Figure A-2 in Appendix A. For the present experiments,
values of $(u_m - u_\infty)/(u_\infty)$ calculated from equations 4.2 are
compared with measured values. Figure 4.6 shows that the
calculated values agree reasonably well with the measured
values.

To predict u_m, $(u_m' - u_\infty)/(u_m' - u_\infty)$ was plotted
against y'/d for the seven experiments. It appears from
Figure 4.7 that $(u_m' - u_\infty)/(u_m - u_\infty)$ varies mainly with y'/d
and increases from about 0.2 for y'/d=0.0 to about 0.30
for y'/d=1.0. An average value of 0.25 could be suggested
for practical purposes.

The data for the length scale showed that for any
experiment, the variation of b_m with y' was small hence
average values for b_m/D for the whole range of y'/d were
obtained. These values were then plotted against D/d in
Figure 4.8. From Figure 4.8 it is seen that b_m/d increases
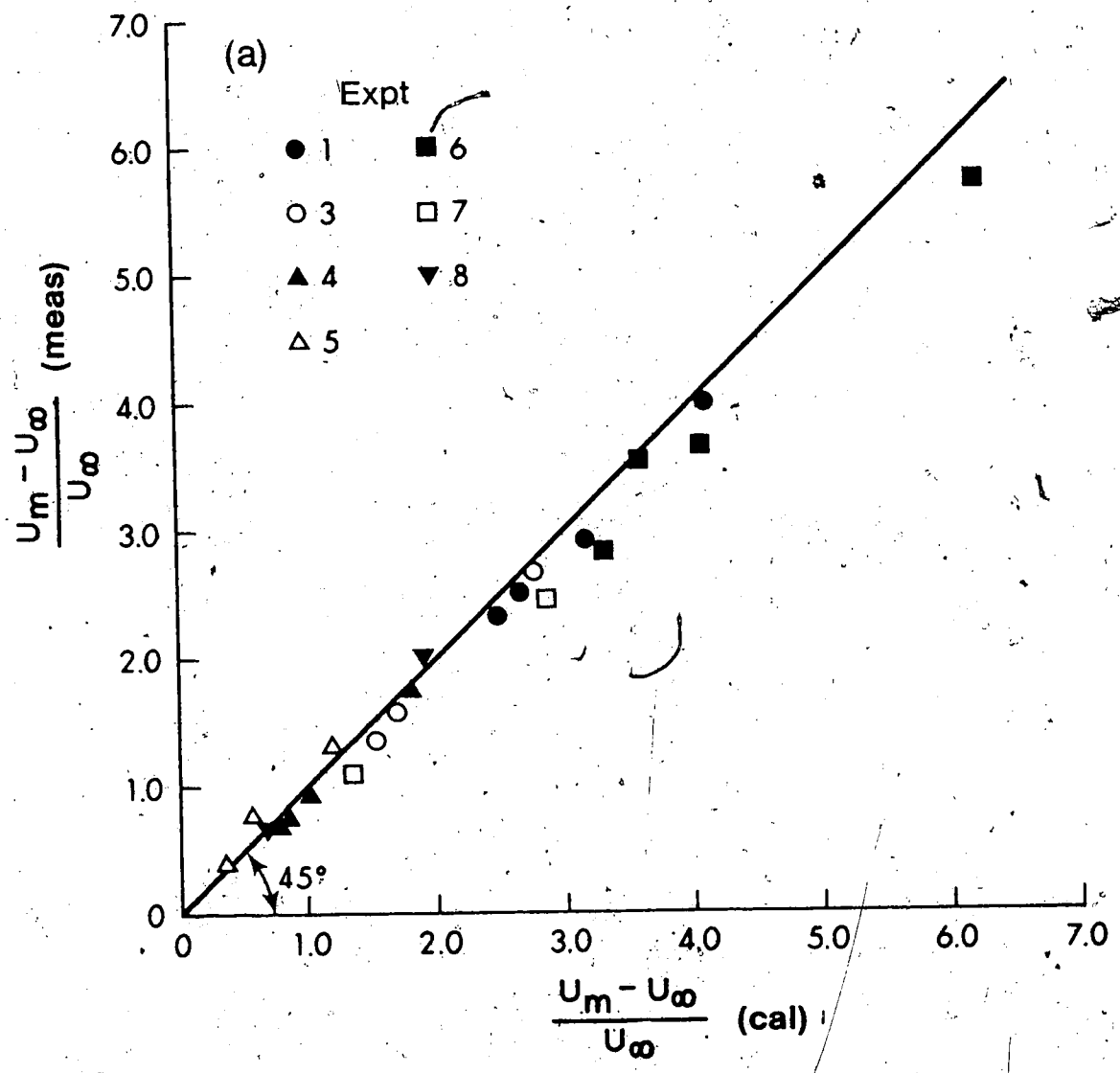linearly with D/d and could be described by the equation:

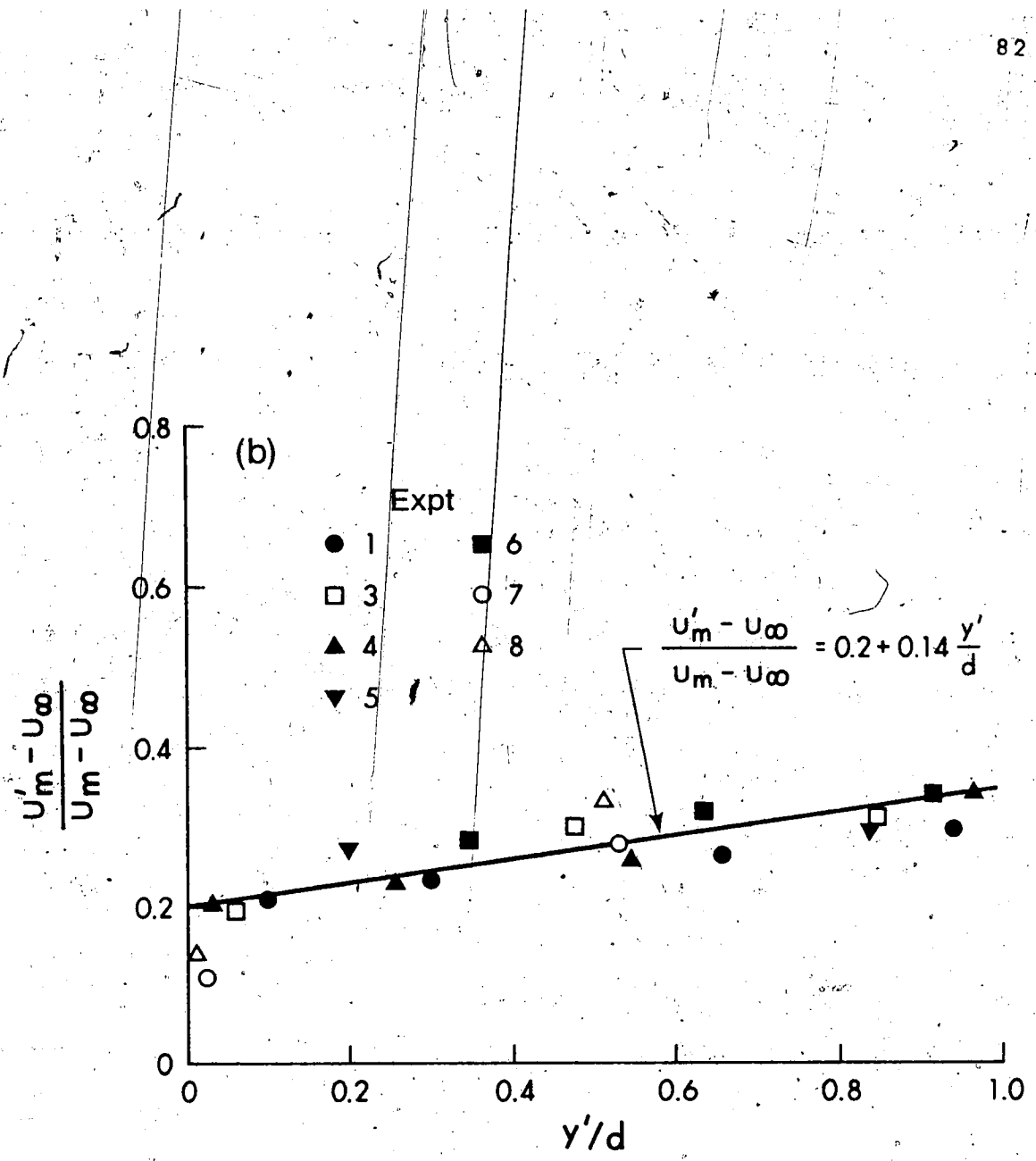Figure 4.6 Calculated Velocity vs. Measured Velocity

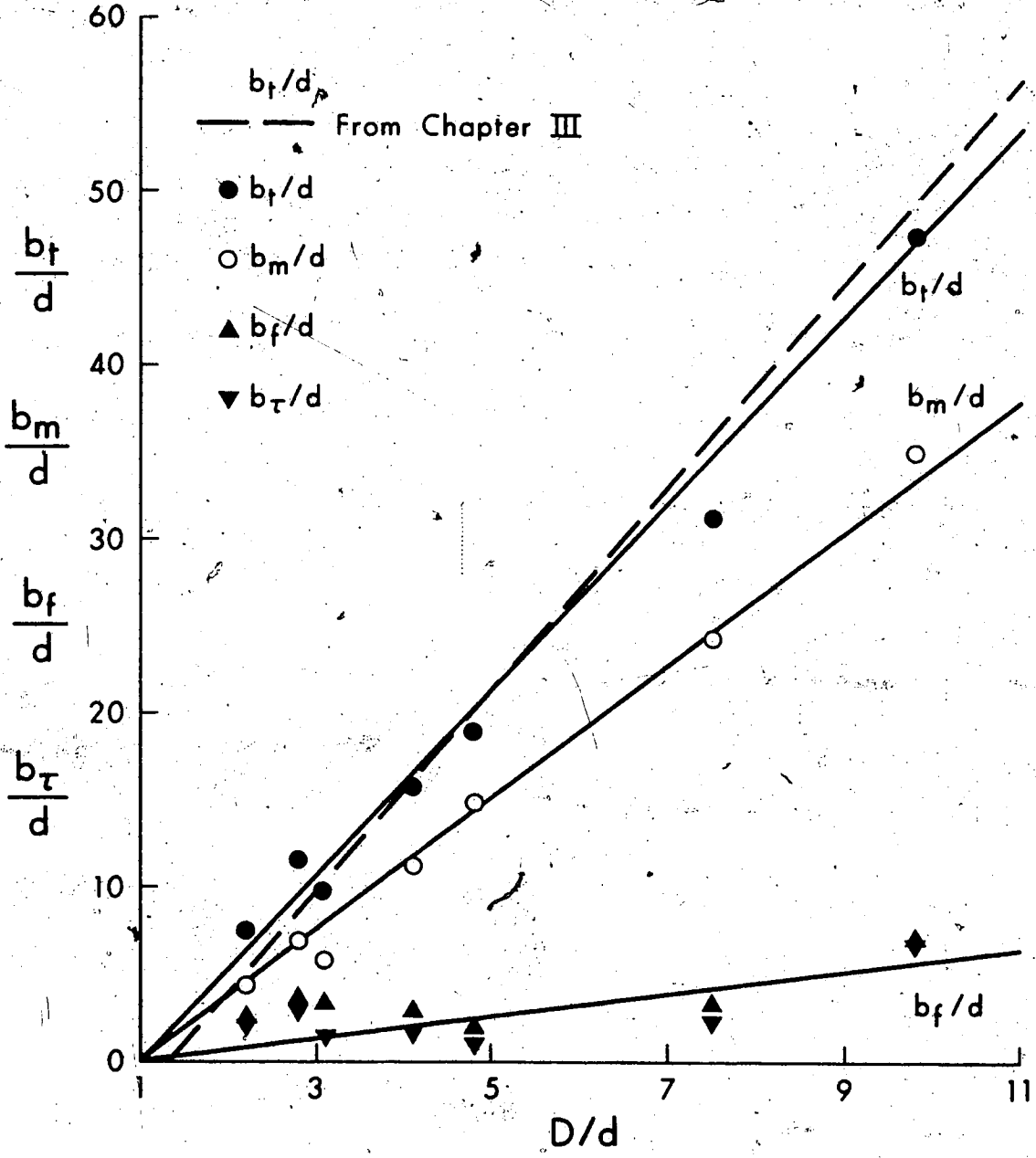Figure 4.7 Variation of Normalized Depth vs. Normalized Velocity

Figure 4.8 Length Scales: (b_f, b_m, b_t, b_τ)

$$\frac{b_m}{d} = 3.78 \left(\frac{D}{d} - 1 \right) \tag{4.3}$$

The velocity profiles in the flood plain are tested for similarity by plotting $(u - u_\infty)/(u_m' - u_\infty)$ versus z'/b_f where $b_f = z'$ where $(u - u_\infty)/(u_m' - u_\infty) = 0.50$. Figure 4.9 shows that, in general, these profiles are similar and could be described by the exponential equation:

$$f(\eta') = \frac{u - u_\infty}{u_m' - u_\infty} = e^{-0.693 \eta'^2} \tag{4.4}$$

where $\eta' = z'/b_f$. The undisturbed velocity in the flood plain could be predicted using the logarithmic law and then u_m' could be calculated using the results presented earlier. Figure 4.8 shows that the dimensionless length scale b_f/d increases linearly with D/d and could be described by the equation:

$$\frac{b_f}{d} = 0.64 \left(\frac{D}{d} - 1 \right) \tag{4.5}$$

The width of the momentum diffusion region could be seen to start from approximately the section in the main channel where u begins to decrease with z to the section in the flood plain where u reaches u_∞. Using equations 4.1, 4.3, 4.4 and 4.5 the total width of the length scale b_t, was calculated. The results plotted in Figure 4.8 show that b_t/d increases linearly with D/d and is described by the equation:
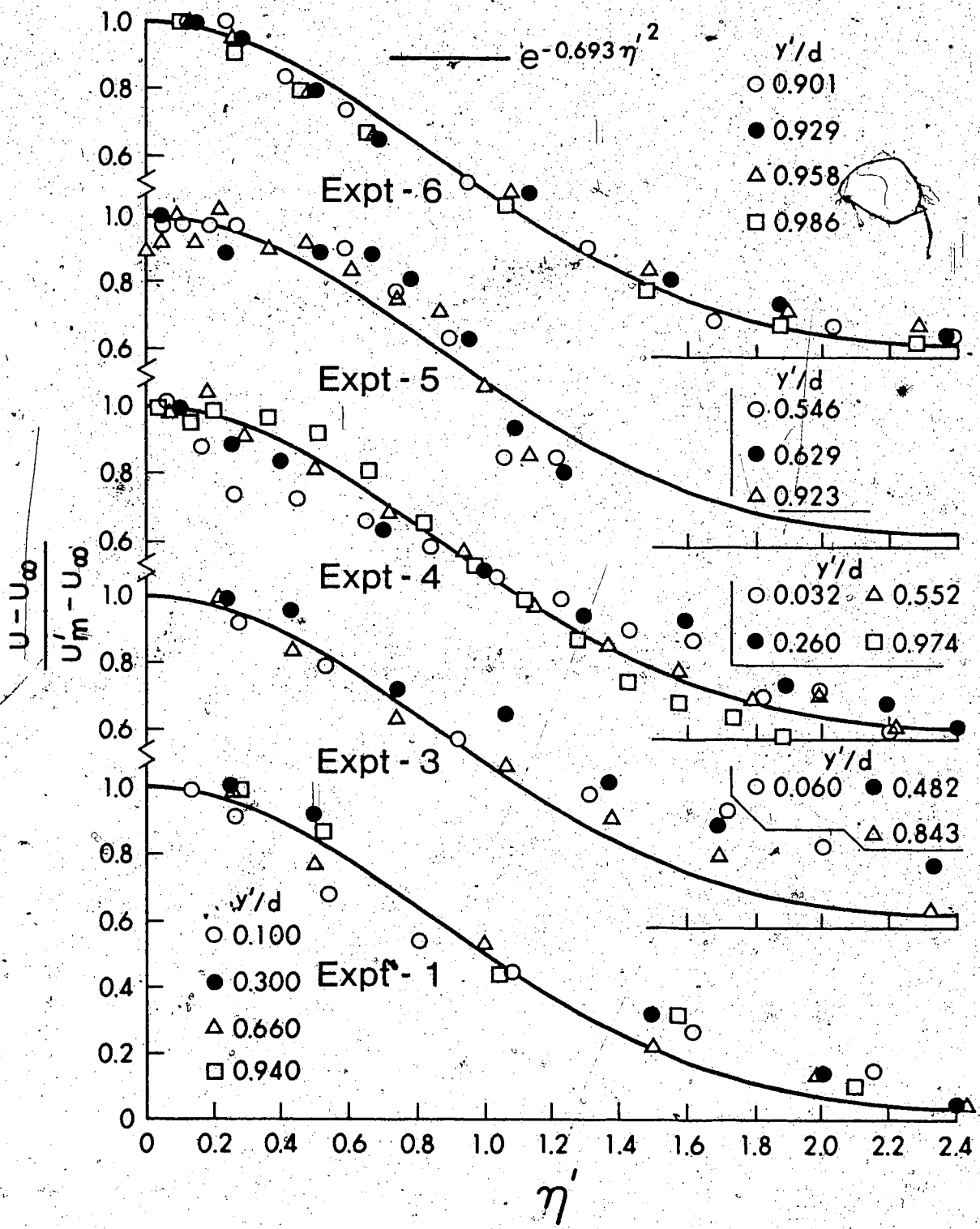
Figure 4.9 Velocity Profile Similarity: Flood Plain (Expts 1, 3, 4, 5 & 6)

$$\frac{b_t}{d} = 5.95\left(\frac{D}{d} - 1\right) \tag{4.6}$$

The dotted line in Figure 4.8 shows the width of the diffusion region from an earlier study (Chapter III) where the main channel was so narrow that it did not allow the full growth of the diffusion region.

The experimental results shown in Figure 4.4 indicated that the bed shear stress in the flood plain, was increased due to the interaction. Figure 4.10 shows that the profiles of the excess bed shear stress in the flood plain defined as $\Delta\tau_0 = (\tau_0 - \tau_{0\infty})$ are similar when $\Delta\tau_0/(\tau'_{om} - \tau_{0\infty})$ is plotted against z'/b_τ where $b_\tau = z'$ where $\Delta\tau_0/(\tau'_{om} - \tau_{0\infty}) = 0.5$. The similarity curve is well represented by the equation:

$$f(\eta_\tau) = \frac{\Delta\tau_0}{\tau'_{om} - \tau_{0\infty}} = e^{-0.693\eta_\tau^2} \tag{4.7}$$

The behaviour of the scale for the excess bed shear stress $(\tau'_{om} - \tau_{0\infty})/(\tau_{0\infty})$ and the length scale b_τ/d is shown in Figure 4.10. Both these scales, when expressed in a dimensionless manner, increase linearly with D/d and could be represented by the equations:

$$\frac{\tau'_{om} - \tau_{0\infty}}{\tau_{0\infty}} = 0.26\frac{D}{d} - 0.17 \tag{4.8}$$

and

$$\frac{b_\tau}{d} = 0.64\left(\frac{D}{d} - 1\right) \tag{4.9}$$
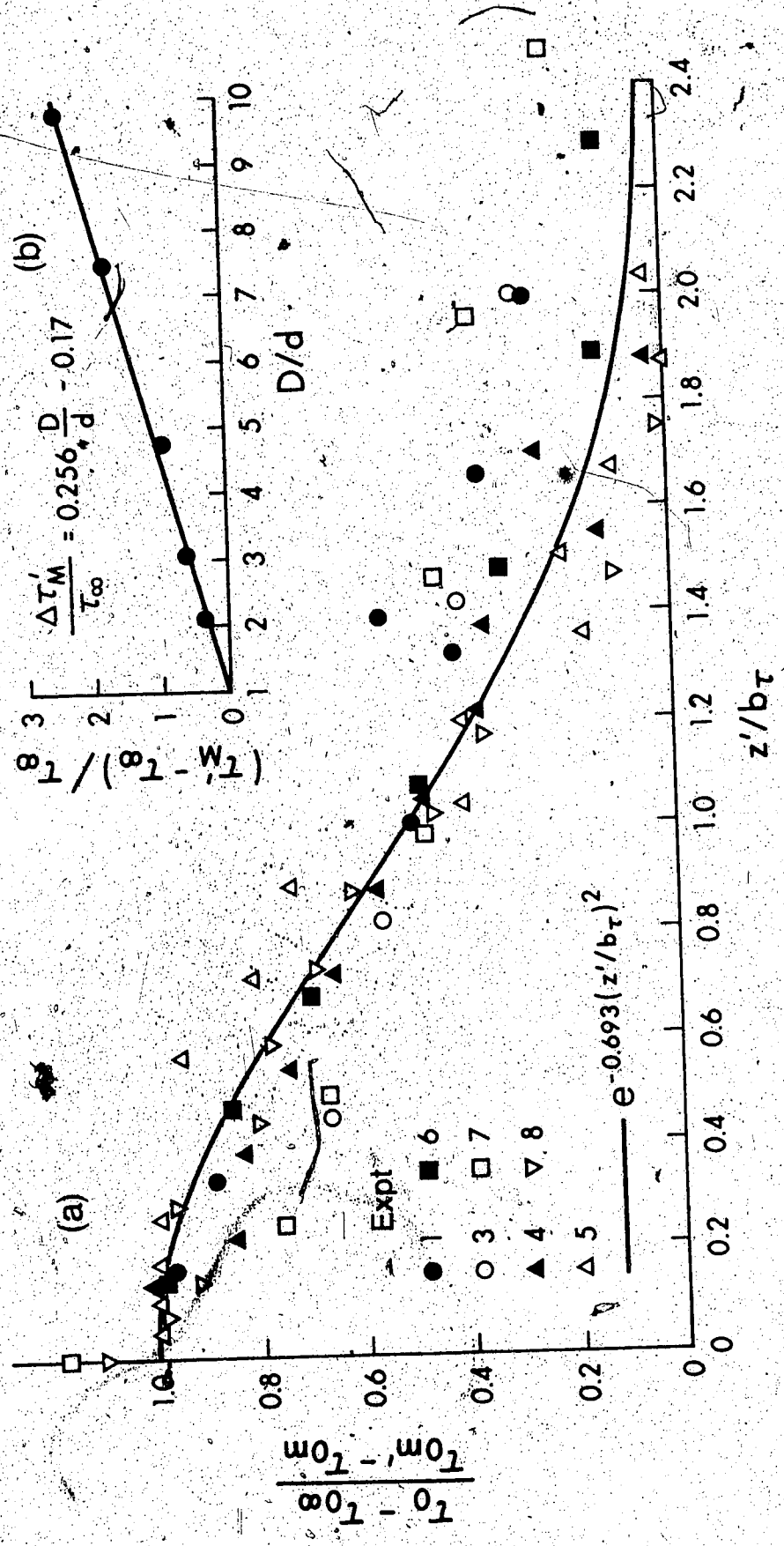
Figure 4.10 Bed Shear Stress Similarity: Flood Plain Channel (Expts 1 to 8)

Considering the bed shear stress in the main channel, it is known that it is reduced due to the transfer of momentum for the flood plain. The results shown in Figure 4.11 support this idea. If τ_{om} is the bed shear stress at approximately the middle of the main channel, which is apparently not affected by the lateral momentum transfer, and $\Delta\tau_o$ is the reduction in shear stress at any z due to the momentum transfer, Figure 4.11 shows that $\Delta\tau_o/\tau_{om}$ increases with $=z/B/2$ for each value of D/d. If $(\Delta\tau_o/\tau_{om})_m$ is the maximum value of the reduction as obtained from Figure 4.11, it is seen that $(\Delta\tau_o/\tau_{om})_m$ is mainly a function of D/d. For a D/d=10.0, $(\Delta\tau_o/\tau_{om})_m$ is about 0.20.

It was questioned as to whether the velocity distribution in the region affected by the lateral momentum transfer is still logarithmic. From Figure 4.12 for experiment 1 and other plots (not reproduced herein) it was found that in the portions of the main channel and flood plain that were not affected by the momentum transfer, the velocity distribution follows the logarithmic law:

$$\frac{u_m}{u_*} = 5.75 \log\left(\frac{y\, u_*}{\nu}\right) + 5.5 \qquad\qquad (4.10)$$

except in the narrow region close to the side walls. It was also found that in the interaction region, equation 4.10 describes the data well if the local value of u_* is used in the equation. This observation suggests a possible analytical attack on the interaction region combining the law of the wall and shear layer concepts. In the main channel, in the interaction region, the momentum transfer to
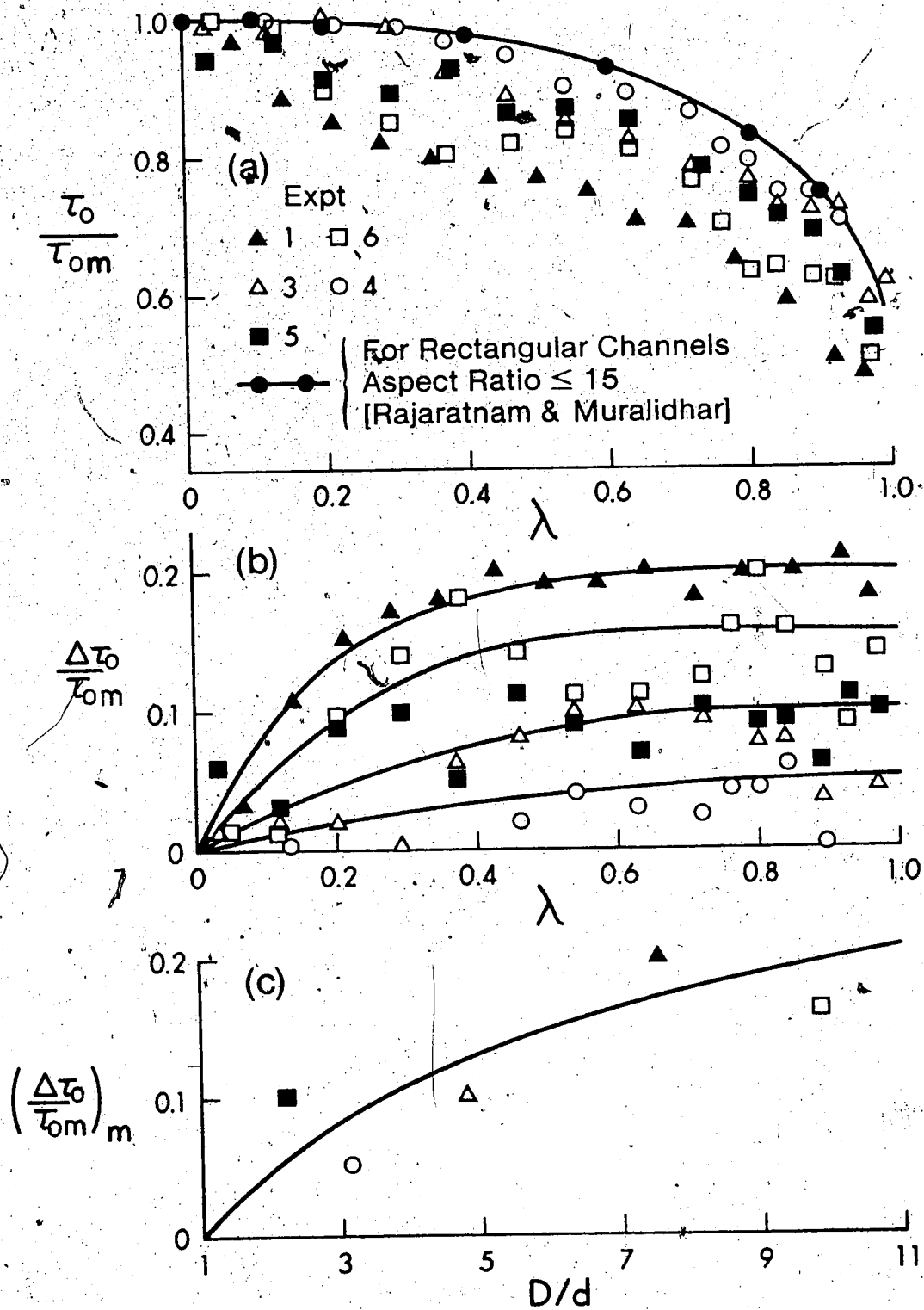
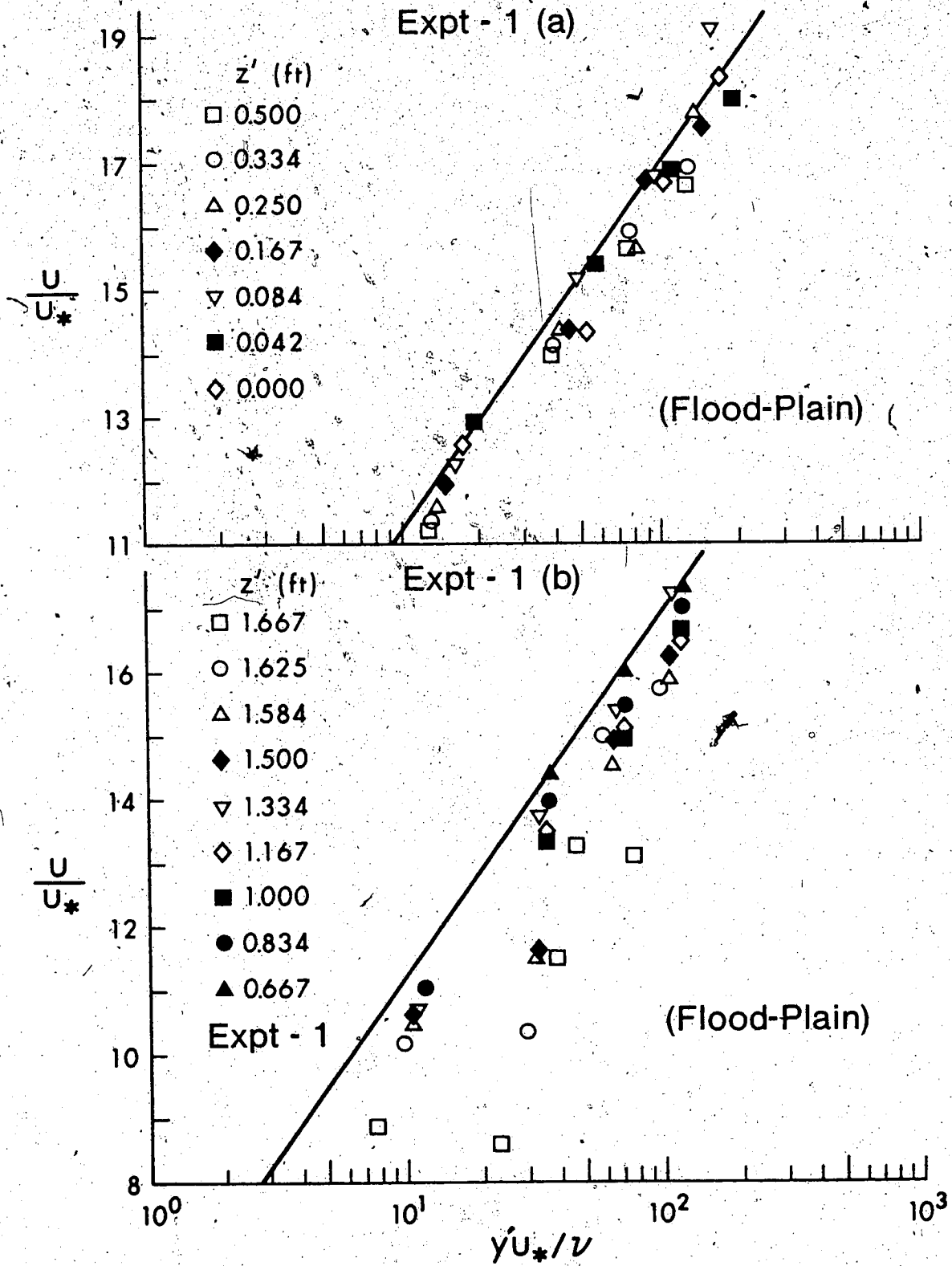Figure 4.11 Variation of Bed Shear Stress with D/d & λ
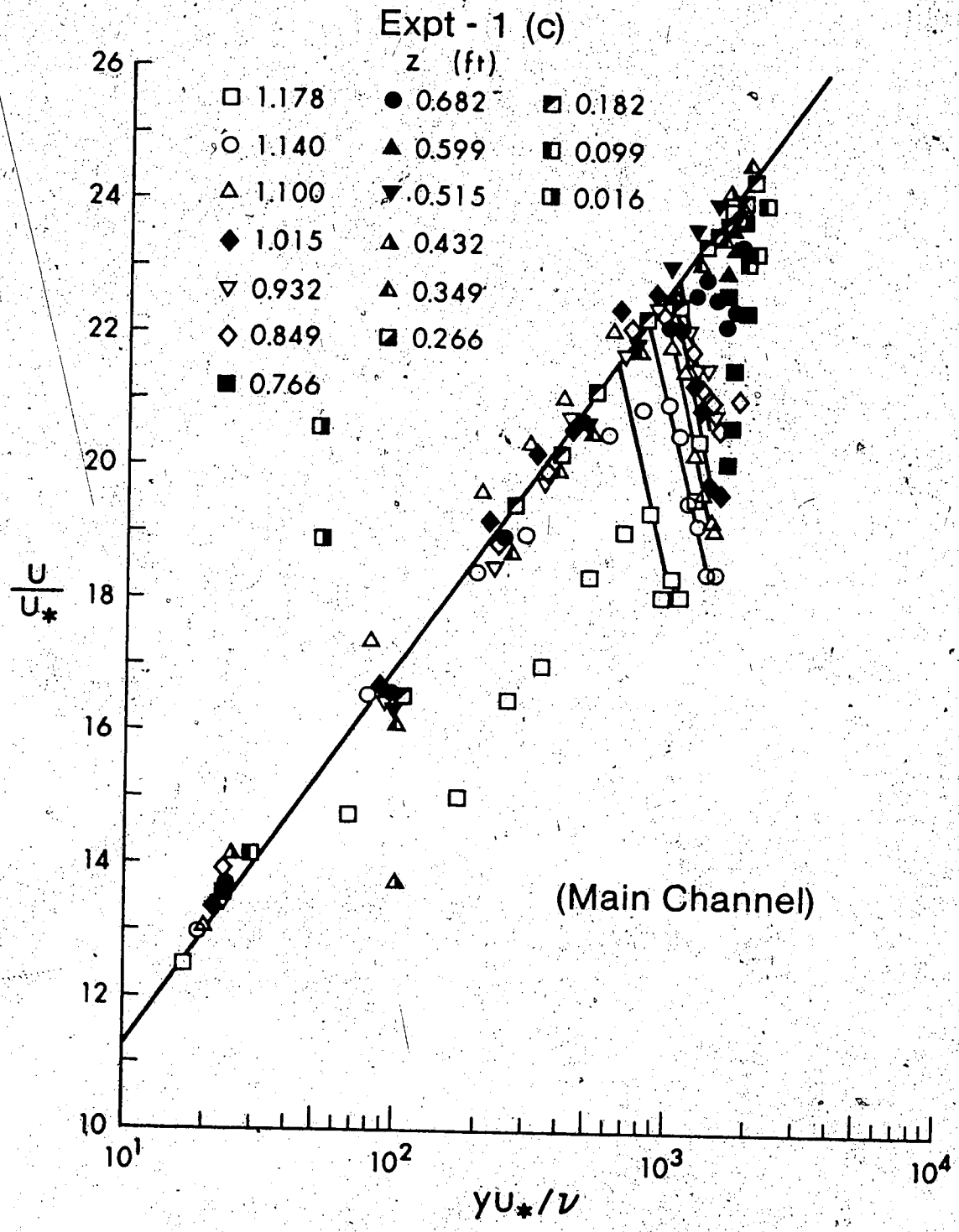
Figure 4.12 Velocity Distribution (u(y')): Log Law

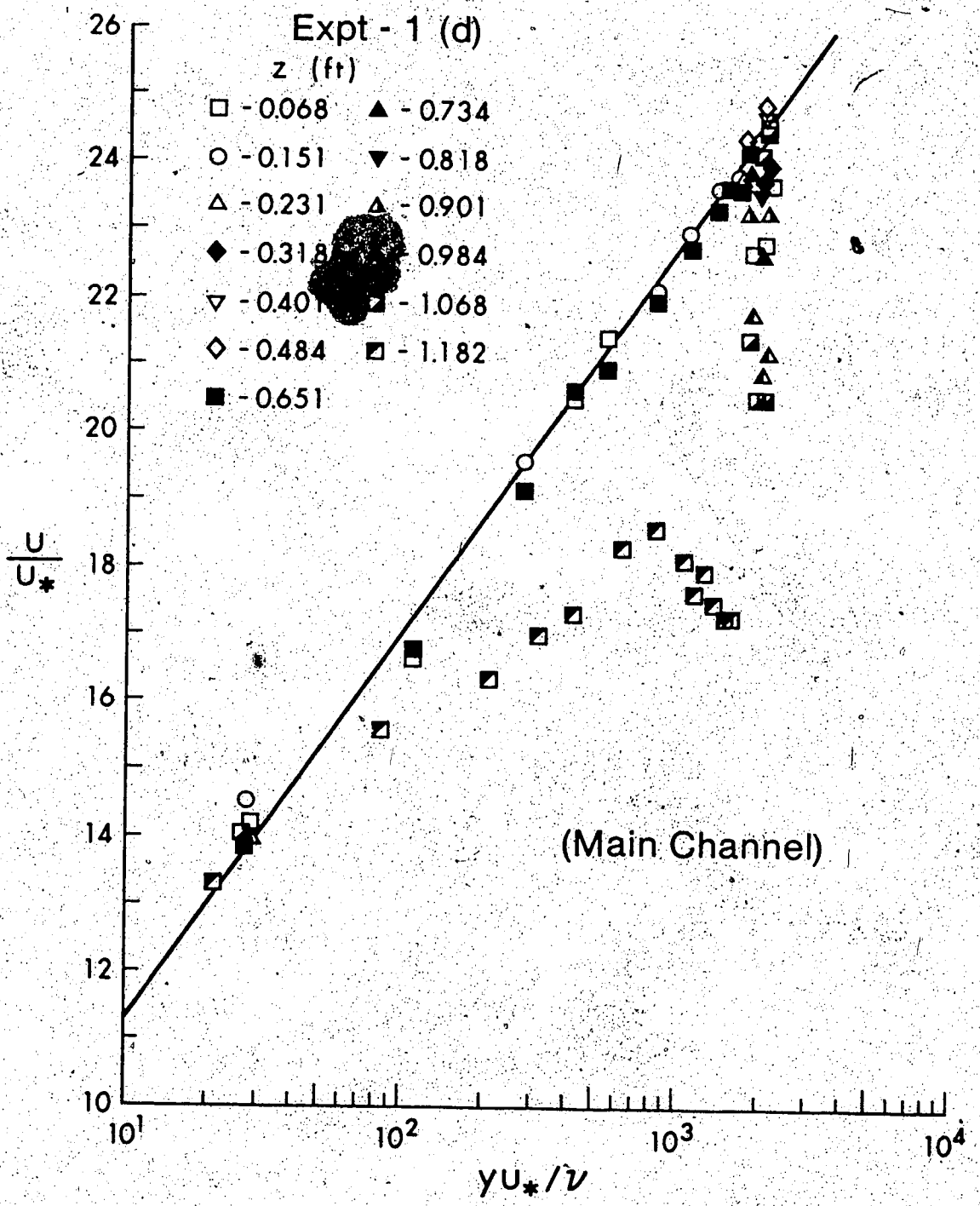Figure 4.12 (cont.) Velocity Distribution (u(y)): Log Law

Figure 4.12 (cont.) Velocity Distribution (u(y)): Log Law

the flood plain causes a significant dip (more noticeable than that in channels without a flood plain) in the velocity profile in the upper part of the flow. If y^* is the location of the start of the dip in the velocity profile (see Figure 4.12) in Figure 4.13 y^*/D is plotted against $\lambda = z/B/2$ for a number of experiments. One can at most, indicate some trends 'in Figure 4.13. It appears that for any given D/d, y^*/D decreases as λ increases and for λ close to unity, y^*/D attains values in the range of 0.45 to 0.7.

4.4 Kinematic Eddy Viscosity

It was shown that the vertical distribution of the velocity even in the region affected by the lateral momentum transfer is logarithmic. Average kinematic eddy viscosity in y direction ε_y, could then be shown to be equal to 0.067 $u_* d$.

Dye injection was adopted to find out the magnitude and variation of the lateral kinematic eddy viscosity ε_z an o see whether it was affected by the lateral momentum transfer in the interaction region. It can be shown the that rate of growth of a passive jet in a media with the same density as the fluid injected is a function of ε_z, x and u. The final working equation is given (lecture notes, Rajaratnam 1978) as:

$$b = 4.15 \sqrt{\frac{\varepsilon_z x}{u}}$$

(4.11)

where b is the half width of the plume at distance x from
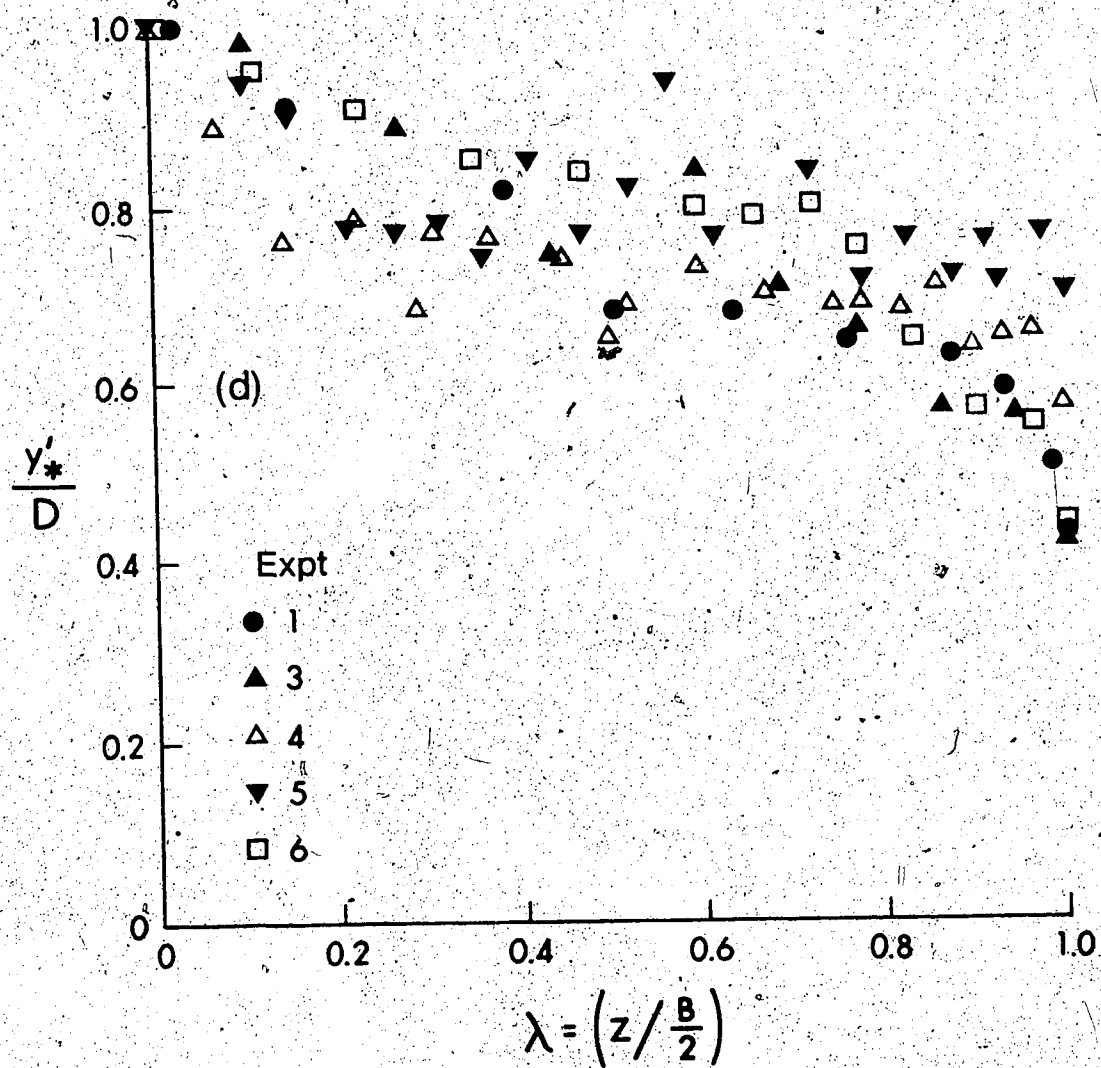
Figure 4.13 Location of Dip in Velocity Profiles: Main Channel

the nozzle and u is the velocity at the point where the nozzle is located.

Lateral distribution of the velocity was defined by equations 4.1 and 4.4 in the main channel and flood plain channel respectively. Therefore, ε_z could be calculated as follows:

$$\tau_{ozx} = - \rho \, \varepsilon_z \, \frac{\partial u}{\partial z} \qquad\qquad (4.12)$$

Equation 4.12 could be evaluated, since the values of τ_{ozx} could be obtained simply by considering the equilibriun condition for a column of water (see sketches in Figure 4.14).

Two series of dye test were conducted in the asymmetrical channel Type C. The dye had a density equal to the water and was injected through a one milimeter OD tube. The dye was injected parallel to the x direction at half depth on the flood plain. A constant head-tank provided the necessary head in such a way that the dye could flow with the same velocity as the surrounding flow. The velocity u and bed shear stress τ_o were measured for each profile. Each time the dye was injected, a few photos were taken from four feet (1.25 m) above the water surface. The photos provide a measure of the rate of expansion of the jet.

From equation 4.11 the value of lateral eddy viscosity ε_z was calculated. The values of ε_z, and ε_z at the level of $y'=d/2=0.05$ feet and $y'=0.005$ feet (1.5 and 0.15 cm) for experiment number 7 and $y'=d/2=0.09$ feet (2.75 cm) for experiment number 8 were obtained from the dye test. Figure
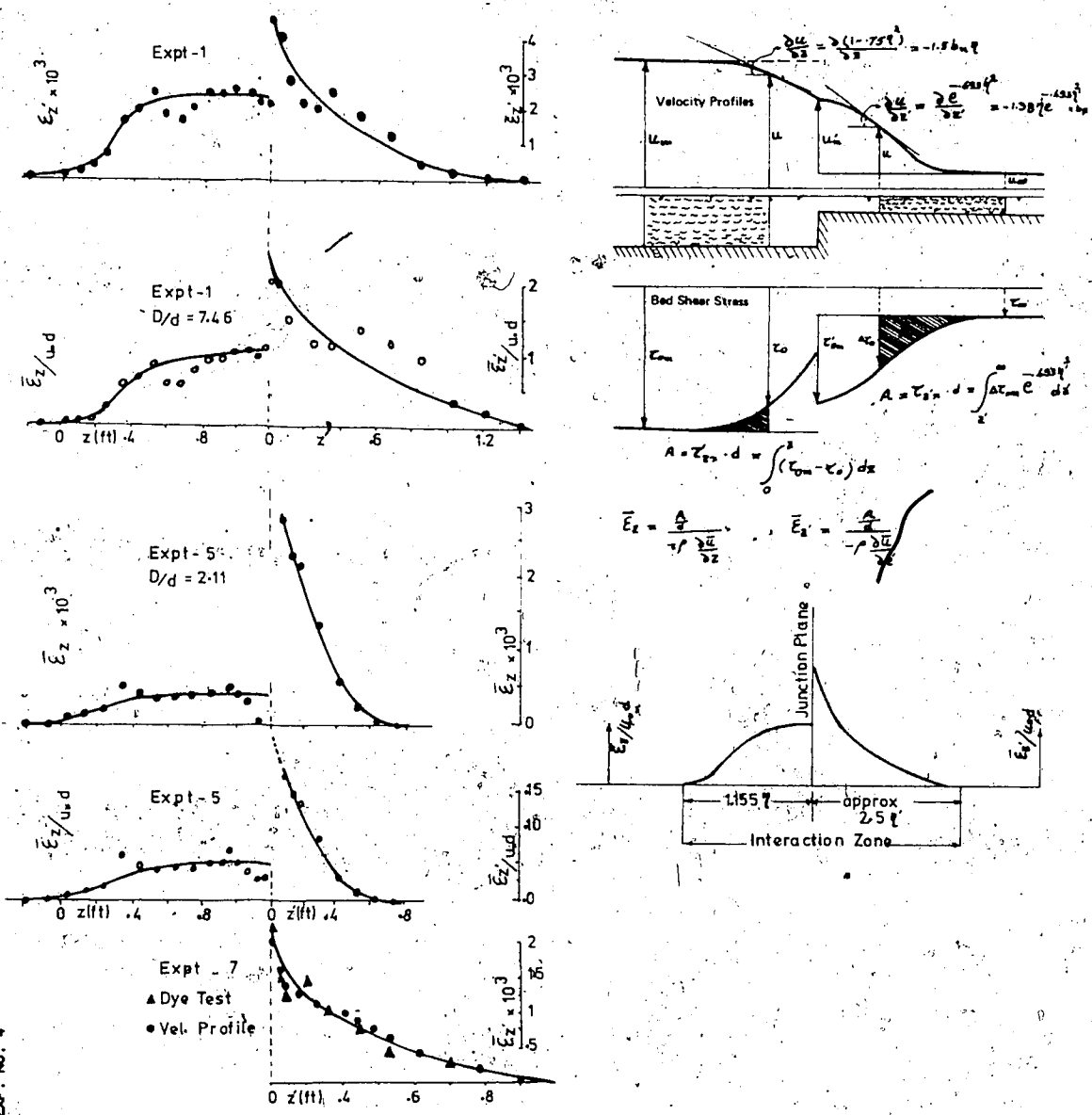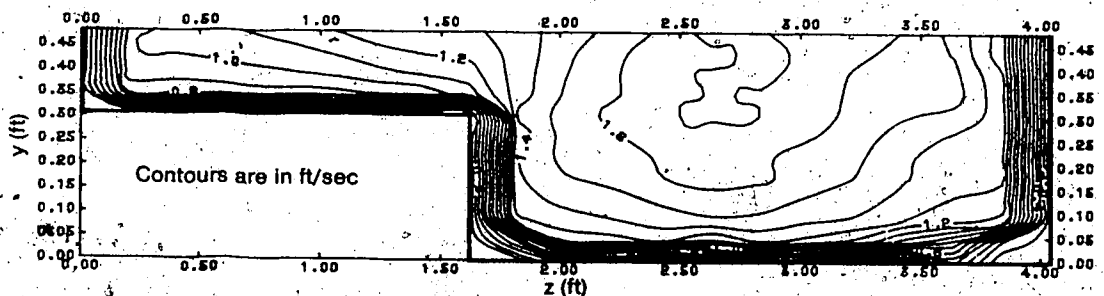
Figure 4.14 Eddy Viscosity

Figure 4.15 Cross-Sectional Isovel Map: Expt-4

4.14 shows the lateral distribution of ϵ_z and $\epsilon_{z'}$ for experiments with one large and one small value of D/d (experiment number 1, D/d=7.46 and experiment number 5, D/d=2.17). Experiment number 7 is also included.

Variation of the transverse-mixing coefficient $\epsilon_z/d\ u_*$, over the width of the channel is shown in Figure 4.14. Fischer (1973) showed that the transverse-mixing coefficient is a function of the aspect ratio. For a range of aspect ratios from 3 to 60, the transverse-mixing coefficient varies from 0.09 to 0.20. For each set of experiments, the aspect ratio is constant. Therefore, the variation of the transverse- mixing coefficient over the width of the channel in Figure 4.14 shows the effect of the interaction between the main flow and the flood plain flow on ϵ_z. It is shown that in the mixing region, ϵ_z or $\epsilon_{z'}$ is increased. The transverse- mixing coefficient in the interaction region decreases rapidly from the junction plane toward the flood plain bank and it decreases slowly toward the center of the main channel. Depending on the D/d, the transverse-mixing coefficient in this mixing region will assume appreciably larger values, more than the undisturbed value for a channel with the same aspect ratio of the flood plain or main channel.

A cross-sectional isovel map of experiment number 4 is shown in Figure 4.15. From this isovel map, one can visualize the zone of interaction, the direction of the momentum transfer and the change in the magnitude of the velocity.

4.5 Conclusions

The results presented in this chapter demonstrate that
the structure of the flow in the main channel with a flood
plain could be analysed using the concept of lateral
momentum transfer and by treating the interaction region as
a turbulent shear layer. The interaction between the main
channel and the flood plain flow produces increased
velocities and bed shear stresses in the flood plain and
causes reductions of velocities and bed shear stresses in
the main channel. These changes have been analysed using
similarity principles. It has been shown that in the upper
part of the flow (y>h), in the main channel and in the flood
plain area of the interaction zone, the lateral velocity
profiles are similar and can be described by equations 4.1
and 4.4 The related length scales, b_f and b_m in terms of d,
the depth of flow in the flood plain increase linearly with
D/d, which are defined by equations 4.3 and 4.5. Further
findings reveal that the velocity profiles in the vertical
direction are described by the logarithmic velocity
distribution law (equation 4.10) if the local bed shear
stress is used as the velocity scale, except in the upper
part of the flow in the main channel. Equations have also
been developed for predicting the revelant velocity scales
(equation 4.2 and Figure 4.6).

From the variation of the maximum bed shear stress with
aspect ratio shown in Figure A-1, and the lateral
distribution of the bed shear stress in the undisturbed
zones (main channel and flood plain) shown in Figure A-2,

the variation of τ_o in the interaction region in the main channel could be predicted (Figure 4.11). Equation 4.8 provides the magnitude of τ'_{om} at the junction plane. The lateral distribution of the excess bed shear stress in the flood plain is presented by the similarity curve, equation 4.7. The length scale for the bed shear stress in the flood plain varies linearly with D/d, equation 4.9. Proper manipulation of equations 4.7 and 4.9 provides τ_o in the affected region of the flood plain. This suggests possibilities of predicting the magnitude of the turbulent eddy viscosity for the interaction region analytically and this procedure is given in Figure 4.14. From this figure, it could be seen that the eddy viscosity in the junction plane is increased sharply.

5. Meandering Main Channel with Straight Flood Plains

Although several studies have been made on pipe bends and open channel bends, only a few investigators have studied meandering channels with flood plains. Rajaratnam & Muralidhar (Personal Communication) in 1967 collected a list of over 100 references related to the subject of open channel curves and pipe bends.

The fact is, because of the presence of centripetal acceleration, the water surface is superelevated; spiral motion is set up, and the velocity and boundary shear stress distributions will be modified accordingly. The flow characteristics will change from section to section. The effect of the bend extends in all directions. The bend is an obstacle to the flow, causing additional resistance besides the boundary resistance. As a result, there is extra energy loss and a backwater curve is created. In tight bends, separation may occur. In natural rivers, the flow is further complicated by irregular channel geometry and movable bed material. The presence of the flood plain brings additional complications to the study of momentum exchange between the flow in the meandering river and the flood plain flow. A brief literature review on curved was presented in Section 1.3. channels.

5.1 Flow in Curved Channels

A good review of the nature of the flow in the curved channel has been written by Rozovskii (1961). He accounts for the existing forces acting on the flow. Because of the

100

curvature of the channel, the streamlines are curved in plan
and this results in transverse inclination of the free water
surface. The extent of this superelevation can be evaluated
approximately by considering the equilibrium conditions for
a column of water on the bed. Actually, the three main
forces, namely the centrifugal force F_c, differential
pressure on the sides of the prism ΔP, and frictional force
F_f exerted on the column of fluid must be in equilibrium and
using this observation, one can derive an expression for
radial slope S_r. If frictional force is ignored one could
show that:

$$S_r = \alpha \frac{V_{ave}^2}{g\ r} \tag{5.1}$$

An expression for transverse circulation can be derived
by considering equilibrium for a volume element assuming the
radial component can be ignored.

$$S_r = \frac{V^2}{g\ r} \tag{5.2}$$

Since equation 5.2 is independent of z, this equation can
only be satisfied in two cases:

1. Straight channel, r=infinity and,

2. constant velocity, V=constant. Because of bed friction,
   the vertical velocity varies from a maximum at the top
   and a minimum value at the bed. The only place equation
   5.2 can be satisfied is where the velocity is equal to
   the average velocity.

   a. For particles moving with a higher velocity than the

average velocity, the centrifugal forces will exceed the differential pressure. Therefore, these particles will be displaced in a radial direction away from the center of curvature.

b. In the lower part of the flow, where the velocities are lower than the average velocity, the centrifugal force is smaller than the ΔP and particles will move toward the center of curvature.

Both transverse slope and helicodial circulation will change the velocity structure of the stream bend. The velocity components intensify the exchange of momentum in all directions especially in the longitudinal and radial directions in turbulent flows which leads to a redistribution of vertical and radial velocities. This greater change of momentum over the width of the curved channels in meandering channels with the flood plain channel adds an additional complication to the exchange of momentum between the main channel and the flood plain.

A brief discussion and analysis of the properties of streams in bends and a few available models are given in the following section.

5.2 Theoretical Considerations of Flow in a Bend

If a suitable cylindrical coordinate system is chosen, the Reynolds equation of motion and the continuity equation theoretically will give adequate base to solve the problem of flow in a bend. It is very unlikely that a complete solution to these equations of motion can be found. For an

approximate solution to this problem, a simplified form of
these equations usually based on the assumptions of fully
developed flow, (see Rozovskii 1961, B.C. Yen 1965, de
Vriend 1976,) flat bed, and or constant loss of energy for
an equal length of flow, could be established. Unfortunatly,
even in this simplified form, there are ten unknowns in
those four nonlinear differential equations. Therefore, at
least six more relations are necessary. Even with these
conditions, a complete solution to such a highly nonlinear
differential equation would still be impossible. Therefore,
further approximations and simplification have to be
introduced. The latest simplification brings restrictions on
the geometry of the channel. The distribution of the
tangential velocity components u_θ has to be assumed ahead of
time. Restrictions are as follows:

1. geometrical restrictions, which state the applicability
   of the model at the following points:
   a. the channel must be shallow which means a large
      aspect ratio (B/D>10.0);
   b. width of the channel and the radius to be of the
      same order of magnitude;
2. flow restrictions:
   a. at the core of the flow, all vertical profiles will
      assume a predetermined velocity distribution; most.
      investigators are suggesting the logarithmic
      velocity profile for their models;
   b. similarity assumption for the distribution of the
      lateral velocity components is valid;
   c. the shear stress effects must dominate the inertial

effects.

F. Engelund (1975) introduced his simple model by providing a relationship based on the above assumptions. His approach is as follows:

1. simplified equations of motion are:

$$\frac{u_\theta^2}{r} = \frac{\partial (g\ h)}{\partial r} + \epsilon \frac{\partial^2 v_r}{\partial y^2} \tag{5.3}$$

$$g\ S + \epsilon \frac{\partial^2 v_r}{\partial y^2} = 0.0 \tag{5.4}$$

where h the level of water surface;

2. geometry condition:

$$S\ r = S_o\ R \tag{5.5}$$

3. the slip velocity method was chosen for the distribution of u_θ over the depth. The logarithmic law was assumed near the bed and the parabolic distribution was assumed for the region away from the wall region.

4. Similarity assumptions are as follows:

$$v_r = \frac{U\ D}{r}\ f_1\left(\frac{y}{D}\right) \tag{5.6}$$

$$u_\theta = U\ \sqrt{\frac{R}{r}}\ f_2\left(\frac{y}{D}\right) \tag{5.7}$$

$$h = -\alpha\left(\frac{U^2}{g}\right)\frac{R}{r} \tag{5.8}$$

where U is some reference velocity.

After solving for the pair of ordinary differential equations and imposing boundary conditions to obtain the

values for the integration constants, Engelund obtained

expressions for f_1 and f_2.

More elaborate models are those of Rozovskii (1961),

B.C. Yen (1965) and de Vriend (1976). Besides the complexity

of their models, they do not offer a better solution of the

flow around the bends. Even with the use of these models,

prediction of the flow does not match the measurements and

in some sections the trend is in the opposite direction. In

chapter I, Section 1.3.2 some remarks were made on the

subject and it was indicated why analytical solutions,

considering present knowledge of flow in curved channels,

fail to predict the behavior of the flow. Also, it was

mentioned that most of the assumptions necessary to simplify

the equations of motion are not necessarily true.

5.3 Experiment and Experimental Results on Flow in Curved Channels

The details of the construction of the curved channel

were presented in section 2.3.3. Chapter II also described

the equipment used in connection with the measurement of the

slope, discharge, velocity and shear stress.

The measurements were made at the beginning of the

second loop at a distance of approximately 30 feet (9.15 m)

from the entrance. Eighteen feet (5.49 m) of the straight

main channel was connected with the first loop through a

gentle curve. It was believed that developed flow was

obtained at the exit of the first loop. The cross-sections

were located at 15 degree increments of θ from the first

section, located at the beginning of the second loop. The
sections in the bend were named by their angle in degrees
and also numbered from 1 to 15 where 1 corresponds to
entrance section and 15 corresponds to exit section of the
second meandering loop. All sections were perpendicular to
the longitudinal axis of the curved channel. At every
cross-section, nine vertical profiles were selected in such
a way that they were one inch (2.54 cm) apart from each
other. These profiles were named by the distance from the
inside wall of the curved channel (i.e. R2 means two inches
from the wall or a distance of 27 inches from the center of
the curve).

One experiment with depth of flow equal to 0.10 feet
(3.05 cm) was performed. Magnitude and the angle of
deviation of the velocity from the tangential direction were
measured and the velocity vector was resolved into the
tangential and radial components. The information obtained
at any point such as $x, y, z, R, \theta, V, u_\theta$ and v_r were entered
into a matrix for further processing of the data (i.e.
plotting the isovels etc.).

Figure 5.1 shows tangential velocity profiles for
cross-section numbers 1 to 15. Figure 5.2 presents radial
velocity profiles. Since the angle of deviation was small,
the tangential velocities and the velocity vector were
almost equal. Therefore, it was decided not to plot vector
velocity profiles. A quick examination of tangential
velocity profiles revealed that none of these profiles
followed logarithmic distribution. However, the aspect ratio
for this run was about 8.3 (B/D=8.3) which was not large
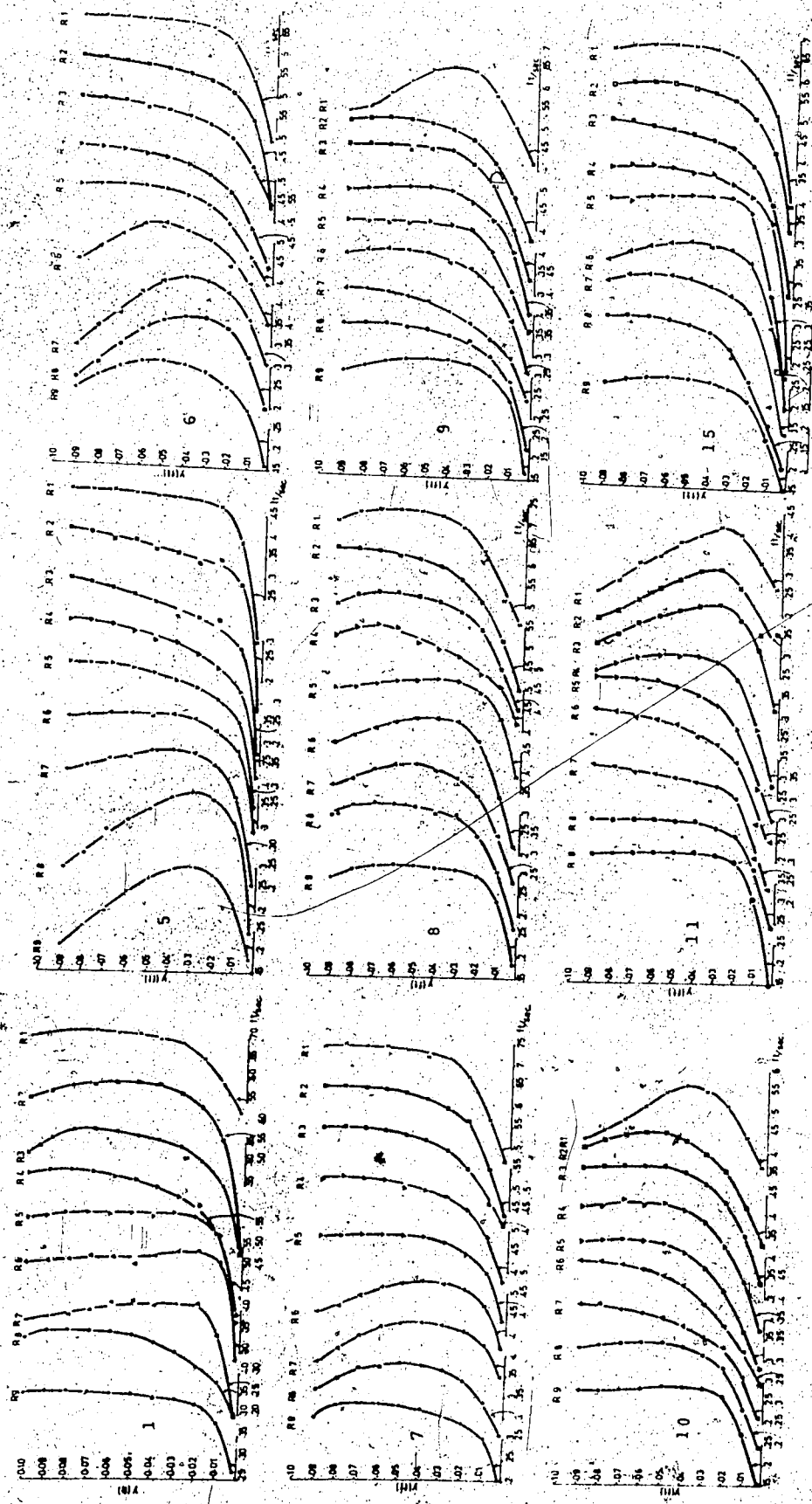
Figure 5.1 Distribution of Tangential Velocity in Curved Channel, Cross-Sections 1 to 15.
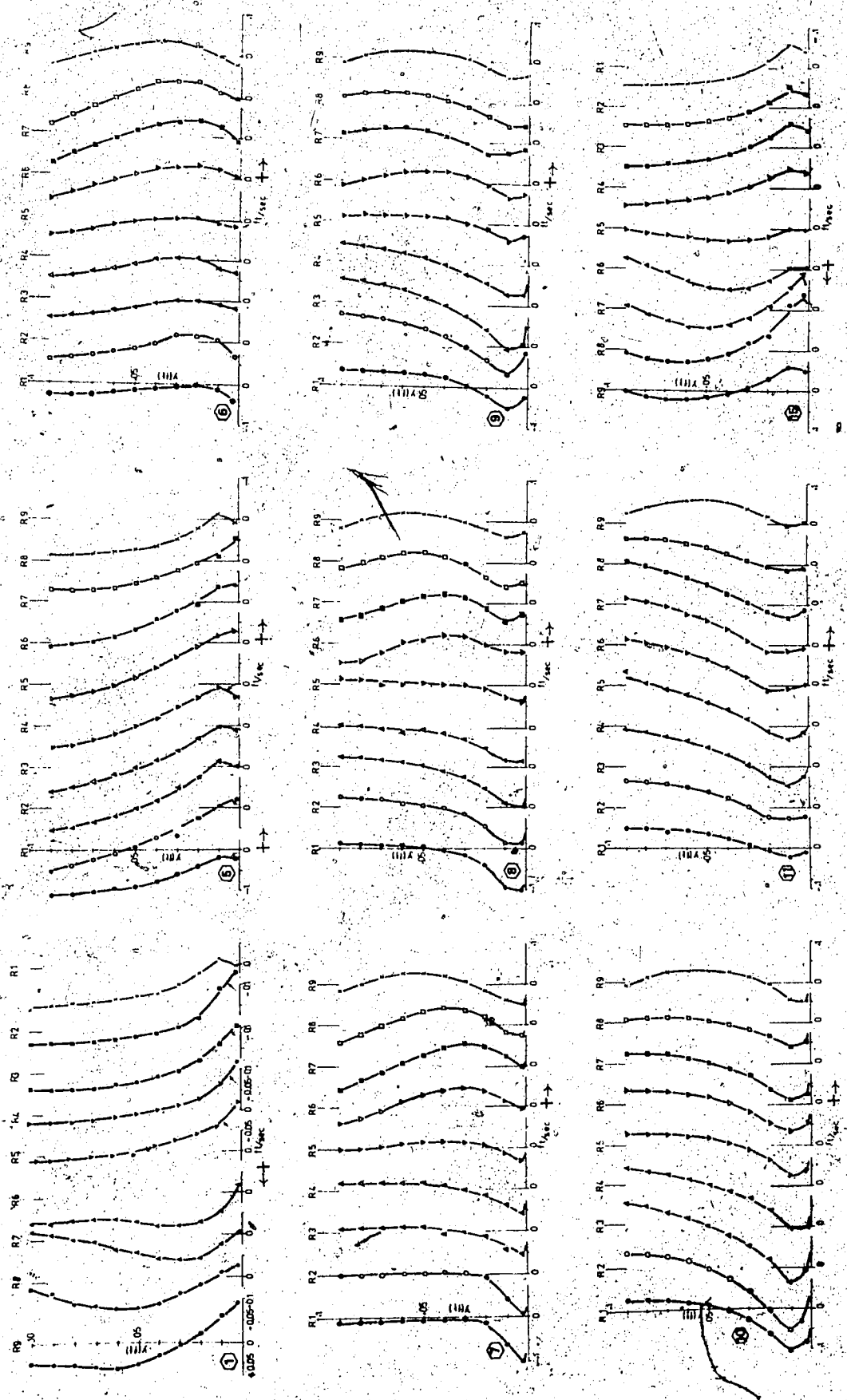
Figure 5.2 Distribution of Radial Velocity in Curved Channel, Cross-Sections 1 to 15

enough to neglect the effect of the side walls on the core
of the flow but it was similar to one of the B.C. Yen's
experiments, where he found that the velocity profiles in
the center of the channel could be described by the log-law.
The photos in Figure 5.3 shows the helicoidal motion of the
flow in the curved channel. In Figure 5.4 isovel maps of the
cross-sections are shown. The isovel contours of any given
cross-section are based on approximately 200 data points.
Surface II program (Sampson, 1978) was employed for
contouring the isovel maps and the Calcomp plotter was used
for drawing the isovel maps. Basically, these maps were
prepared for comparison with isovel maps of the main channel
with the flood plain. Lateral distribution of the depth
averaged tangential velocity is shown in Figure 5.5. It can
be seen from the figure that, these average tangential
velocity profiles are not the same. It can easily be noticed
that the maximum velocity at the beginning of the bend is
close to the inner wall and gradually shifts toward the
other side (outer wall). By the time the flow reaches the
end of bend and enters the next bend, the order of shifting
velocity is changed and again the maximum velocity will
occur near the inner wall.

Regarding the distribution of the velocity and
applicability of the defect law along the depth of flow, the
vector and tangential velocities were plotted and compared
with a theoretical curve. It was interesting to see that
none of these profiles obeyed the logarithmic law. The
dimensionless form of $u_\theta / u_{\theta max}$ vs. y/D is shown in Figure
5.7. As can be seen for the velocity profile located in
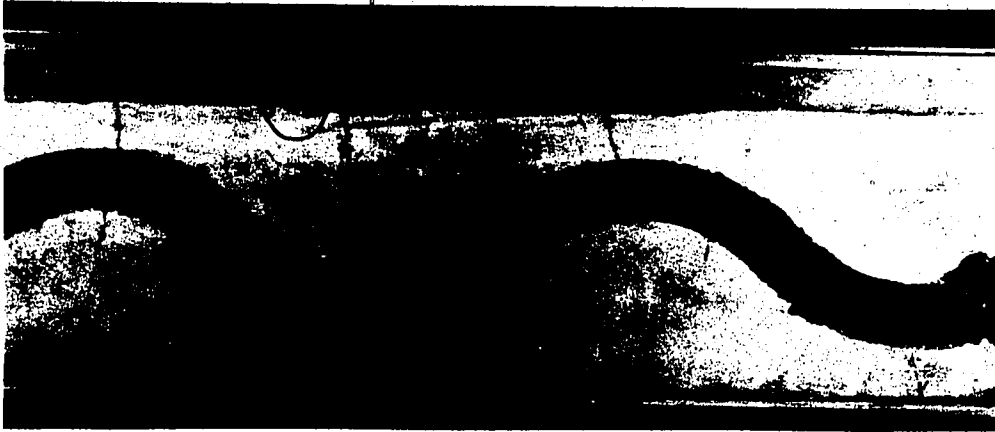
Curved Channel

Helicoidal Motion in the Curved Channel

Helicoidal Motion in the Curved Channel
Figure 5.3 Photograph : Helicoidal Motion
of the Flow in the Meandering Channel

CROSS-SECTION NO.6

CROSS-SECTION NO.5

CROSS-SECTION NO.1

CROSS-SECTION NO.9

CROSS-SECTION NO.8

CROSS-SECTION NO.7

CROSS-SECTION NO.15

CROSS-SECTION NO.11

CROSS-SECTION NO.10

Contours are in ft/sec

Contours are in ft/sec

Contours are in ft/sec
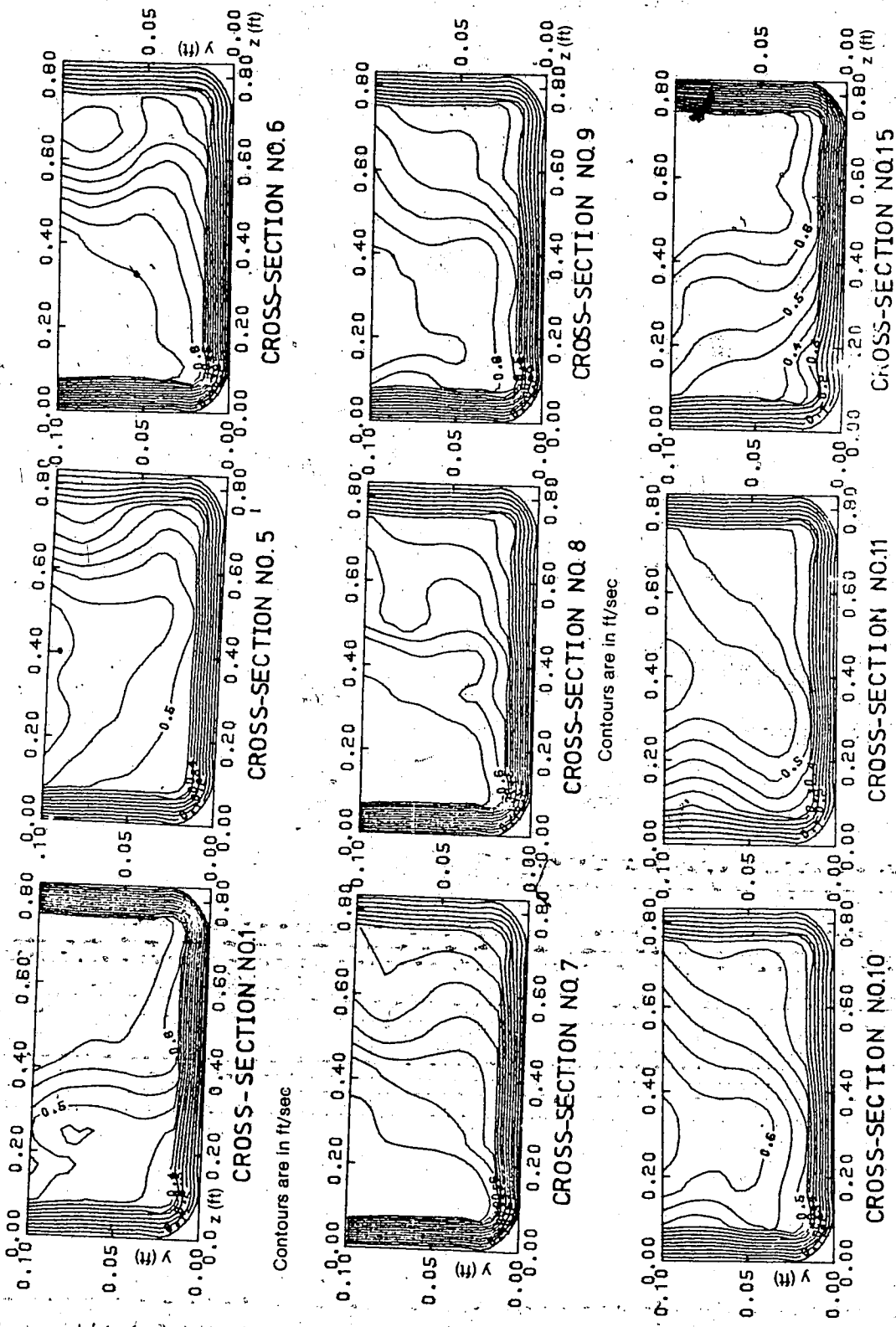
Figure 5.4 Cross-Sectional Isovel Map in Curved Channel (Cross-Sections No. 1 to 15)

Figure 5.6

Bed Shear Stress Distribution

τ / τ_{max}

Velocity Distribution

Scale for
Plan View
0ft   1ft

10 u_θ (ft/sec)
0ft   0.5
Velocity Scale

2 ——— 2   Cross-Section NO.2

FLOW

Figure 5.5 Lateral Distribution of Tangential Velocity
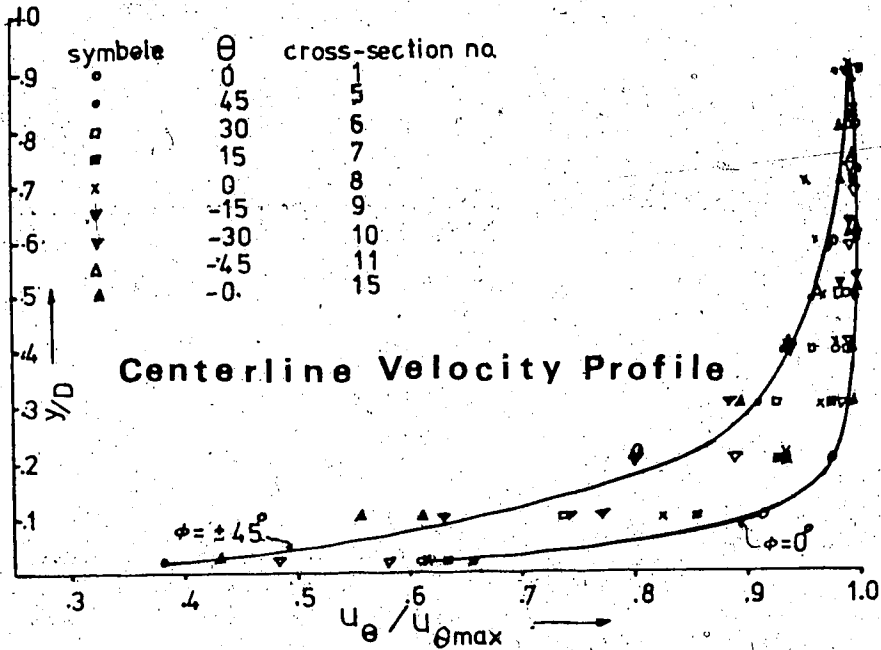
Figure 5.7 Variation of Velocity and Depth Along Centerline
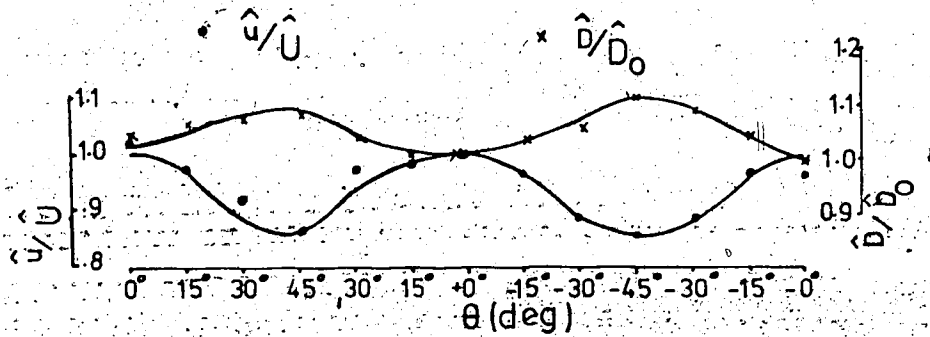
Figure 5.8 Non-dimensional Centerline Velocity Profiles in Curved Channel, Cross-Sections 1 to 15
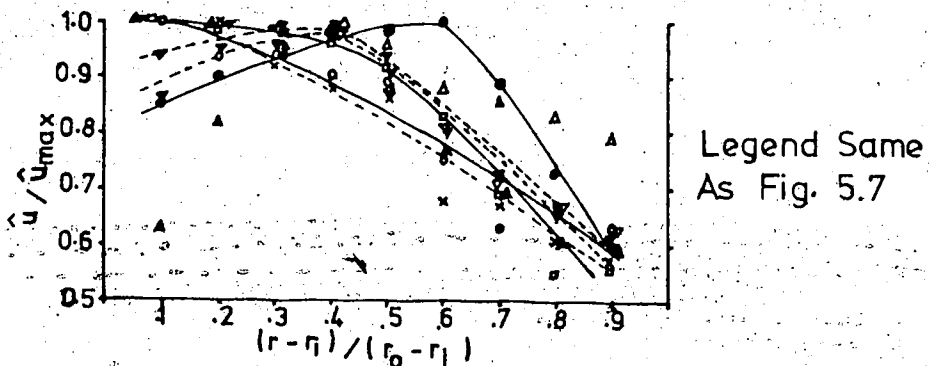
Figure 5.9 Non dimensional Lateral Distribution of Tangential Velocity in Curved Channel, Cross-Sections 1 to 15

cross-section number 1 ($\theta=0.0$ degree), the velocity
increases from zero (on the bed) to a maximum at a relative
depth of 0.2 ($y/D=0.2$). Then the velocity is constant up to
the water surface. However, in cross-section number 5 ($\theta=45$
degrees) the velocity increases with y and the maximum
occurs approximately near the water surface. Not only does
the vertical distribution of tangential velocity vary with
θ, but the magnitude of the velocity depends on the angle θ
i.e, the location of cross-section in the bend. The average
velocity of each cross-section $\hat{u}$ was computed for all the
profiles. If the average velocity of cross-sections 1, 8 and
15 which correspond to $\theta=0.0$ degrees is set to $\hat{U}$, then the
variation of $\hat{u}/\hat{U}$ with θ for cross-sections 1 to 15 is shown
in Figure 5.8. As was discussed in chapter I, the slope of
the main channel will change according to $S\cos\theta$.
Consequently, with the increase of θ the bed slope will be
reduced and therefore, the velocity which is proportional to
the water surface slope to some power will be decreased.
Subsequently, the continuity equation reveals that, any
reduction in the average velocity requires a higher average
depth of flow in order that an equal amount of flow passes
through all cross-sections. In the same figure, the
variation of $\hat{D}/\hat{D}_0$ (where $\hat{D}$ and $\hat{D}_0$ are the average depths of
the flow at any section and that at $\theta=0.0$ degrees) with θ is
shown. Apparently, the reduction of the velocity at $\theta=45$
degrees is about 14 percent ($\hat{U}$ at 45 degrees/$\hat{U}$ at $\theta=0.0$ is
equal to 0.86) and the increase of the depth of flow for the
same cross-section is about 11 percent. The discrepancy of
3% is possibly due to the error in the experimental

measurements.

Non-dimensional distribution of the depth averaged tangential velocity ($\hat{u}/\hat{u}_{max}$ where $\hat{u}/\hat{u}_{max}$ is the maximum value of $\hat{u}$) over the width of the channel $(r - r_i)/(r_o - r_i)$, where r_i, r_o and r are innermost radius, outermost radius and radius of the bend respectively, is shown in Figure 5.9. It can be seen from these lateral velocity distributions that, at cross-section number 1 the maximum velocity occurs near the inner wall and the lower velocities are located near the outer wall. As the flow goes around the bend, (i.e. as θ increases) the maximum velocity will shift toward the outer wall. Maximum shifting occurs at θ=45 degrees which is half of the central angle (θ_c=90 degrees). All of these distribution profiles can be superimposed on top of each other by rotating their ordinates around a point located at 20 percent of the depth and 95 percent of the maximum velocity. Once again, the importance of θ can be seen. As Choudhary & Narasimhan (1977) and Sieber & Gotz (1975) showed in their experimental results, the flow is indeed dependent on θ.

Generally, radial velocities are small compared with tangential velocity. The maximum radial velocity occurs near the bed and its magnitude is about 10 percent of the maximum tangential velocity. An attempt was made to find out if any of the similarity hypotheses suggested by previous authors can be adopted for the distribution of the radial velocity component. It seems that none of those similarity hypotheses hold perfectly, but generally the prediction of radial velocity and the measurements have the same trend.

The variation of the bed shear stress in the meandering channel can be seen in Figure 5.6. The maximum bed shear stress is located near the inner wall, but it is not symmetrical with respect to the crest of the curved channel (cross-section number 8). The maximum bed shear stress is located close to the inner wall and it can be as large as 2.15 times the centerline bed shear stress of the corresponding straight channel. The minimum bed shear stress usually occurs near the outer wall and is only 60 percent of the centerline bed shear stress of the equivalent straight channel.

5.4 Experiments on Meandering Channels with Flood Plains

Since the primary objective was to explore the characteristics of the flow in the meandering channel when the flow tops its banks, the flume and the equipment were set up for experiments in the curved channel in a straight valley. The discharge was increased until the depth of flow on the flood plain reached about one inch (d=2.54 cm). Uniform flow in the straight reach of the flume was ensured by manipulating the tailgate and observing the depth of flow in the different reaches.

The experimental arrangement and the instrumentation were the same as for the curved channel. While the velocity profiles in the main channel were measured in the same way as previously explained in curved channels without flood plain, the profiles on the flood plain were spaced 0.1 feet (3.0 cm) apart.

Two experiments in the meandering channel with a flood plain were conducted. The first experiment had the depth in the main channel equal to 0.20 feet (D=6.1 cm). Depth of the flood plain flow was about 0.08 feet (d=2.4 cm). For this run, cross-section numbers 1 to 15 were investigated in detail. For the second run, where D=0.235 feet (7.2 cm) and d=0.11 feet (3.35 cm), the velocity measurements were carried out for all the cross-sections (numbers 1 to 15), but only at a level of y=0.05 feet (1.5 cm).

5.5 Flow Visualization Results

Red dye with the same density as water was injected into the flow through a tube of 1.5 mm OD and 1.0 mm ID, with a constant head of 0.4 inch (1.0 cm) in order to clearly observe the flow path. To identify what is happening at different levels above the bed, three levels were chosen: one located directly on the bed, one at half the depth and another at the water surface. Cross-section number 1 (at the entrance of the second loop) was used as an injection section. Starting from the flood plain bank, the red dye spread as in any normal test in a simple rectangular channel. This part of the test where the dye spread up to a point of about 9 inches (c_1=22.9 cm) from the bank, showed that there is no measurable secondary current in this region. Consequently, this part of the flood plain channel is the minimum width of the flood plain (c_1=9 inches, 22.9 cm), where the flow in this area follows the alignment of the valley, which is straight (see photos in Figure

5.10(a)).

In the main channel, when the dye was injected below the flood plain level, helicoidal motion was observed (see photo in Figure 5.10(b)) as in the case of a curved channel without a flood plain. But, the helicoidal motion was not confined to the main channel. When a particle comes up above the flood plain, the spiral motion will continue on to the flood plain area. If the dye is injected above the flood plain, then the water has a tendency to move more or less straight in a width equal to the amplitude of the meander belt (see photo in Figure 5.10(c)). Therefore, it can be seen that the width of the main channel for the upper portion is equal to $c_2 = 20$ inches (50.8 cm). The other interesting observation was that the particle which is located just below the flood level, instead of going around the bend, simply went over the flood plain. Figures 5.10(a to c) illustrate these mechanisms of the flow.

5.6 Data Handling and Presentation of Results

In Chapter II the data acquisition system was described. It was used to record the information for each test. Then the data processing and analysis were carried out using the University of Alberta Computer. Due to some difficulties in Surface II Program, in regions of very steep gradients, sometimes the contours cross each other. Hence, the contours should be interpreted with some care.
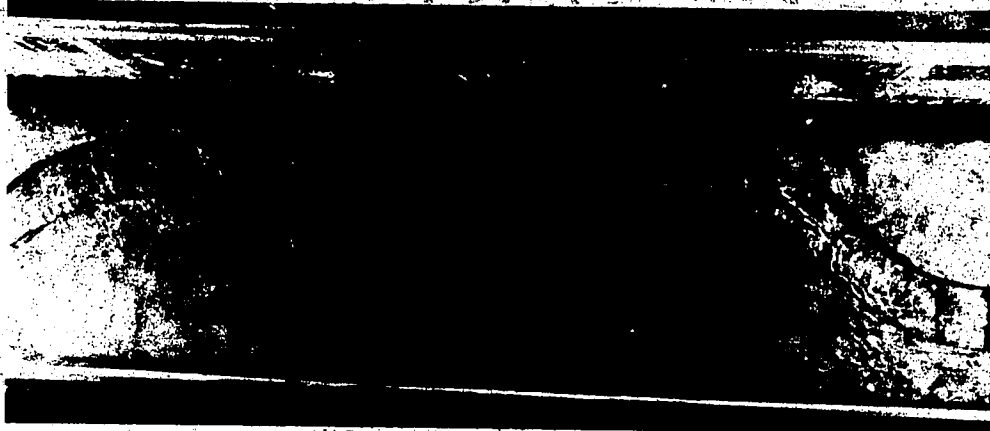
a; Flow: Flood Plain Channel
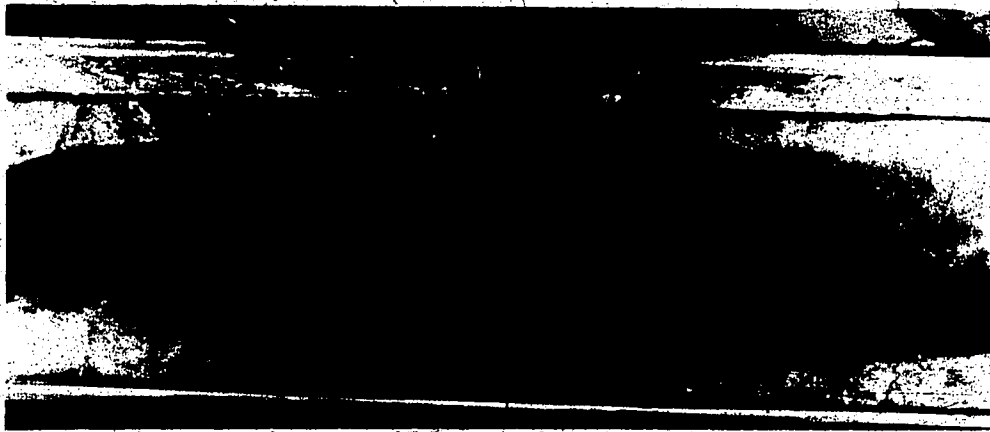
b; Lower Part of Flow: Helicoidal Motion
in the Meandering Channel
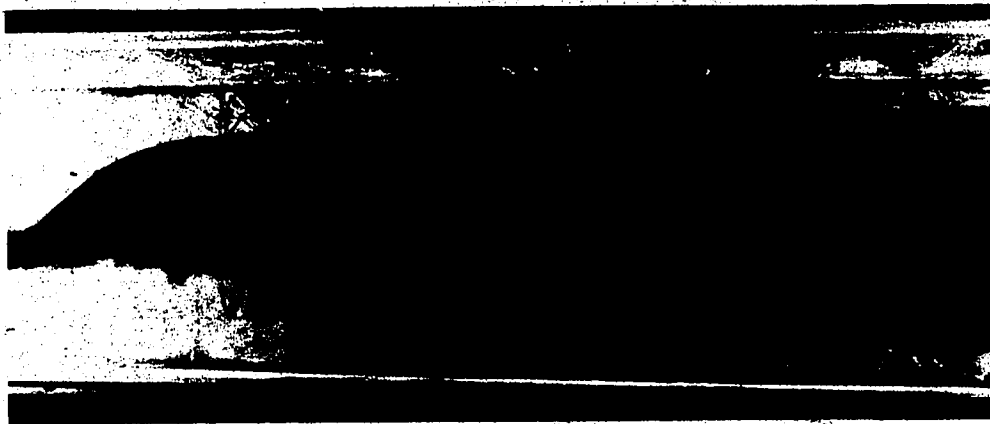
c; Upper Part of Flow: Straight Flow
in the Meandering Channel
Figure 5.10 Photograph : Effective Zone of Momentum Exchange
in the Meandering Channel with Flood Plain Channels

5.6.1 Velocity Distribution

The angle of the velocity vector and the distribution of the radial, vector and tangential velocities within the selected channel cross-sections (numbers 1 to 15) for run number 1 are presented in Figures 5.11 to 5.14. Since every cross-section had at least 40 vertical velocity profiles, it was decided to select a few representive profiles for the sake of brevity.

A quick glance at the vertical distribution of $\bar{\theta}$, the angle of the velocity with the tangential direction on the flood plain for the cross-section 1 to 15 in Figures 5.11(1) to 5.11(15) reveals that $\bar{\theta}$ ranges between -2 to +2 degrees except for the region close to the meandering main channel. The precision of the yaw probe in measuring the angle of the flow direction for $\bar{\theta}$ close to zero degree could be a few degrees (Rajaratnam & Muralidhar, 1969). Using the modified procedure of the yaw probe technique, it is estimated this inaccuracy could be reduced to a couple degrees. Considering the above inaccuracy, it is concluded that the velocity vector in the flood plain channel is parallel to the x axis.

Since the lower part of the flow in the meandering channel is bounded by the side walls, the flow is forced to flow more or less along the stream-lines of the curved channel. In the upper part of the flow, because of the absence of side walls, the flow has a tendency to move parallel to the x direction. The yaw probe in the meandering channel was always kept parallel to the local tangential direction of the curvature of the main channel at each section. Consider the profiles located at one inch (2.54 cm)
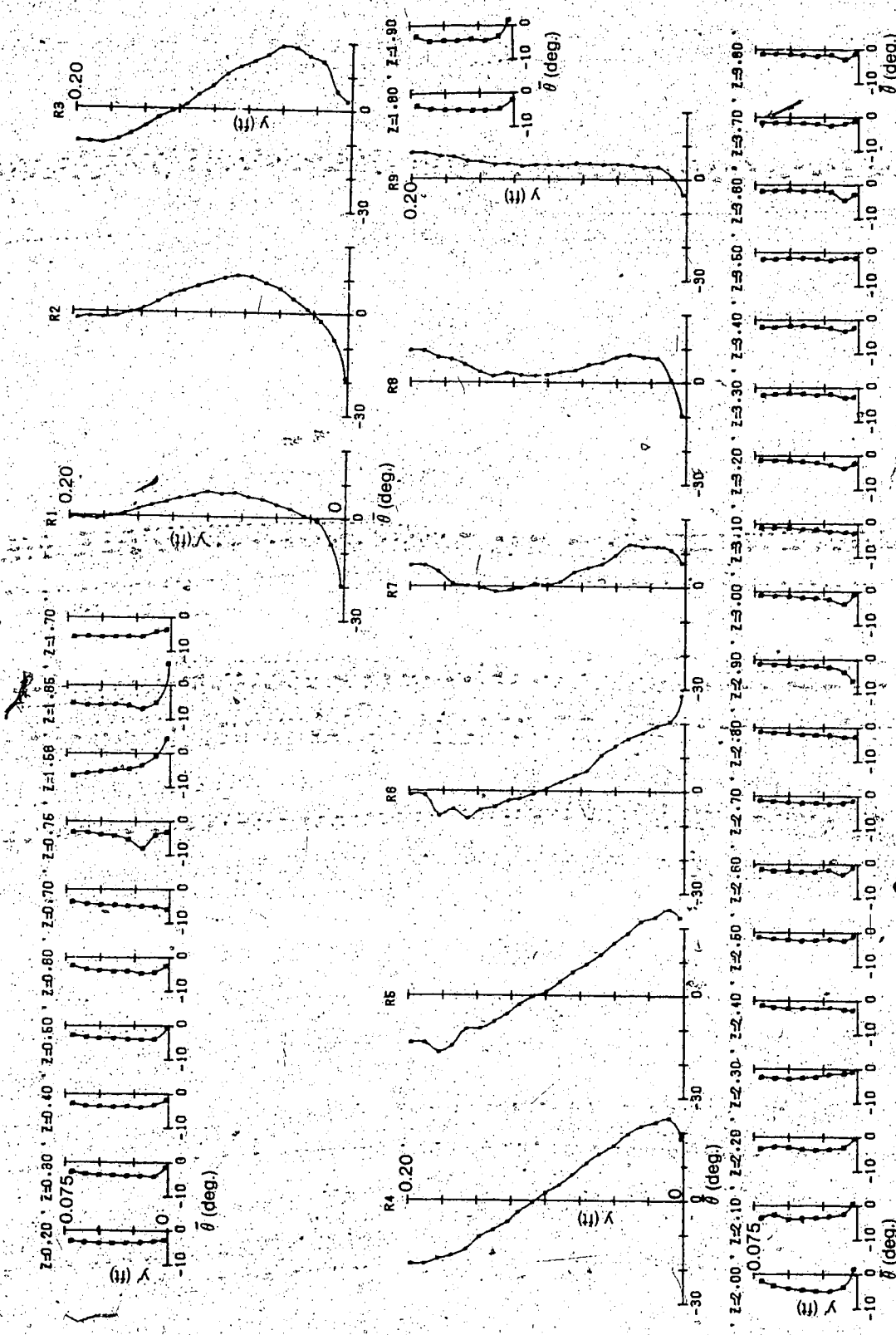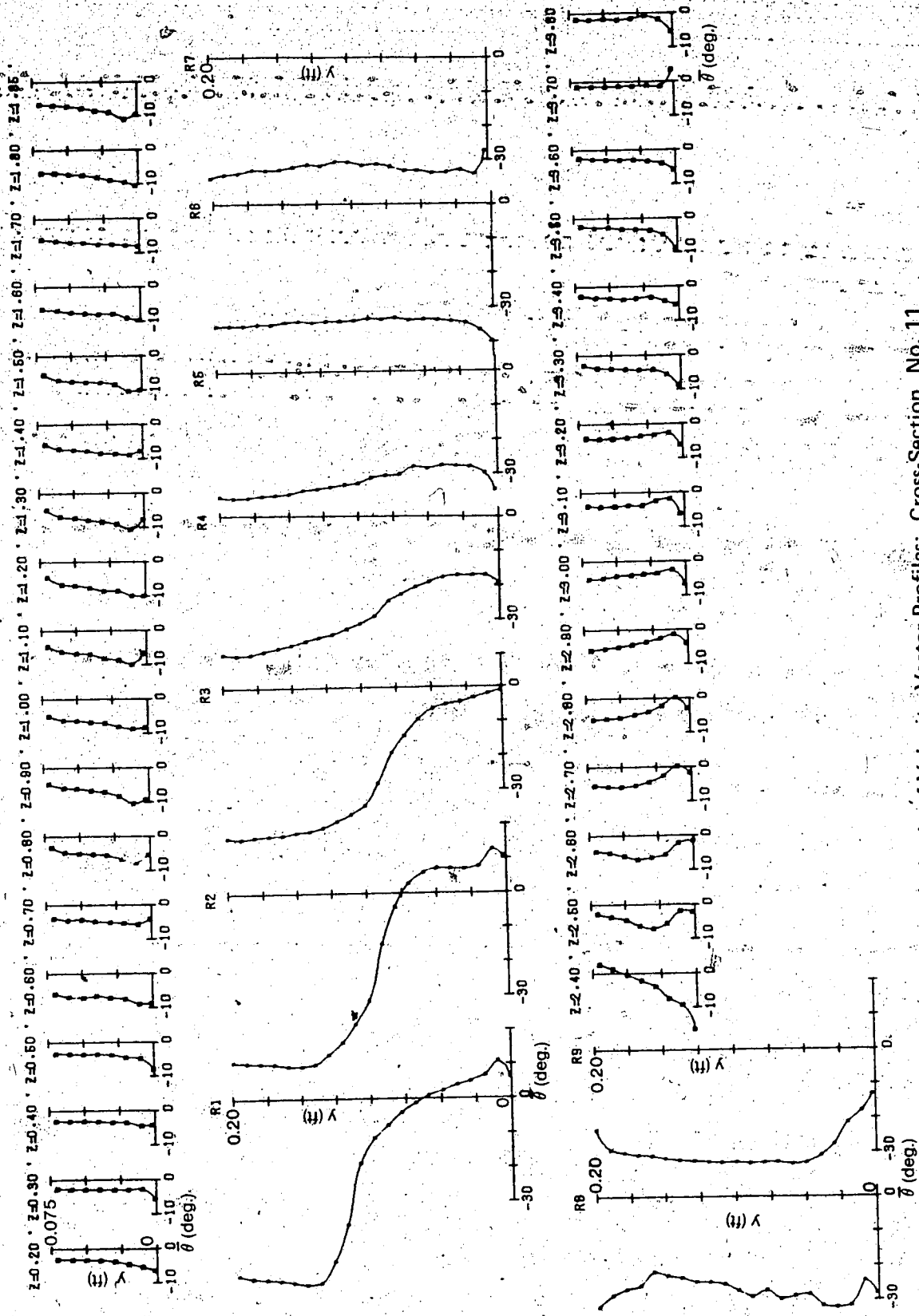
Figure 5.11(1) Angle of Velocity Vector Profiles, Cross-Section No. 1
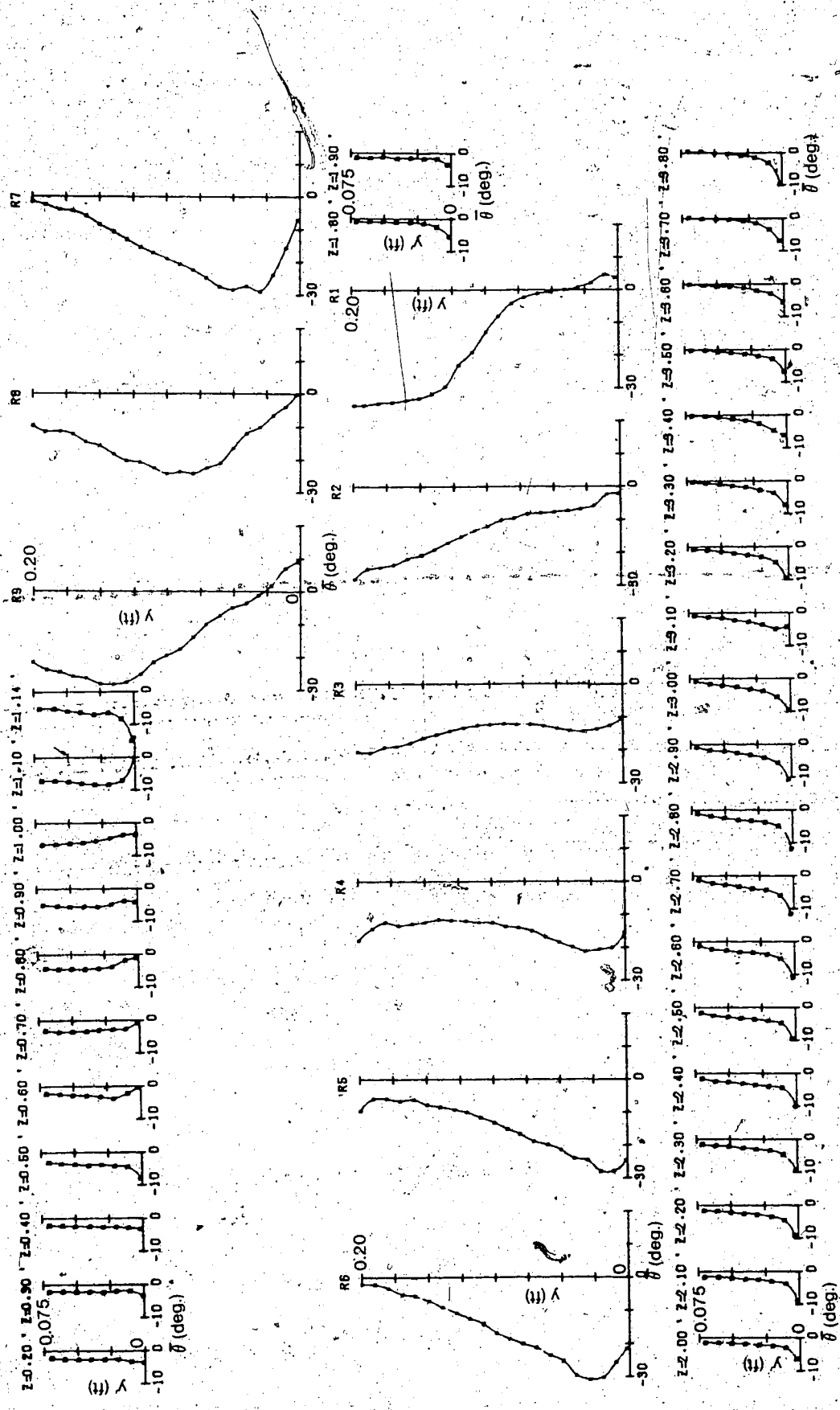
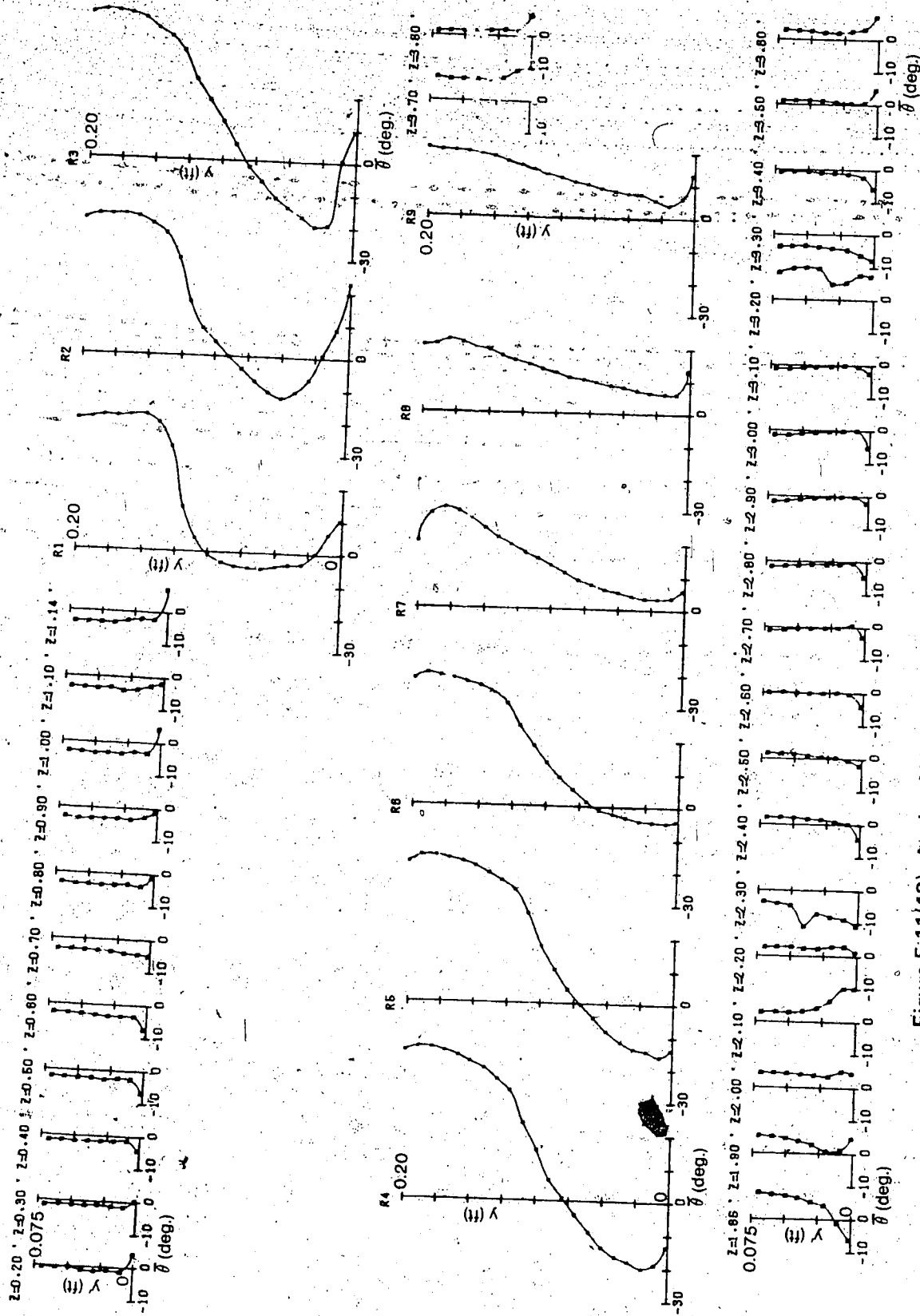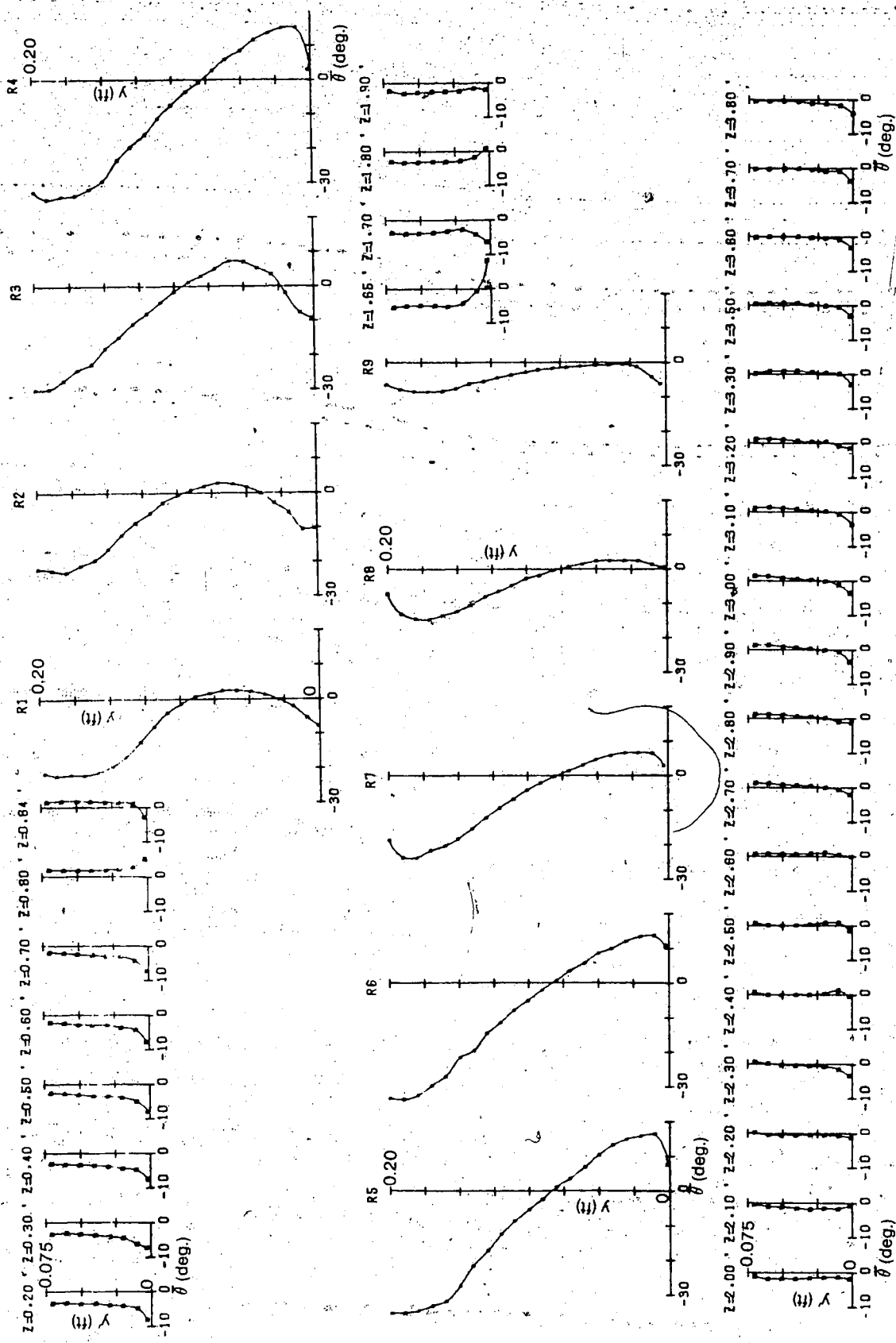Figure 5.11(3) Angle of Velocity Vector Profiles: Cross-Section No. 3
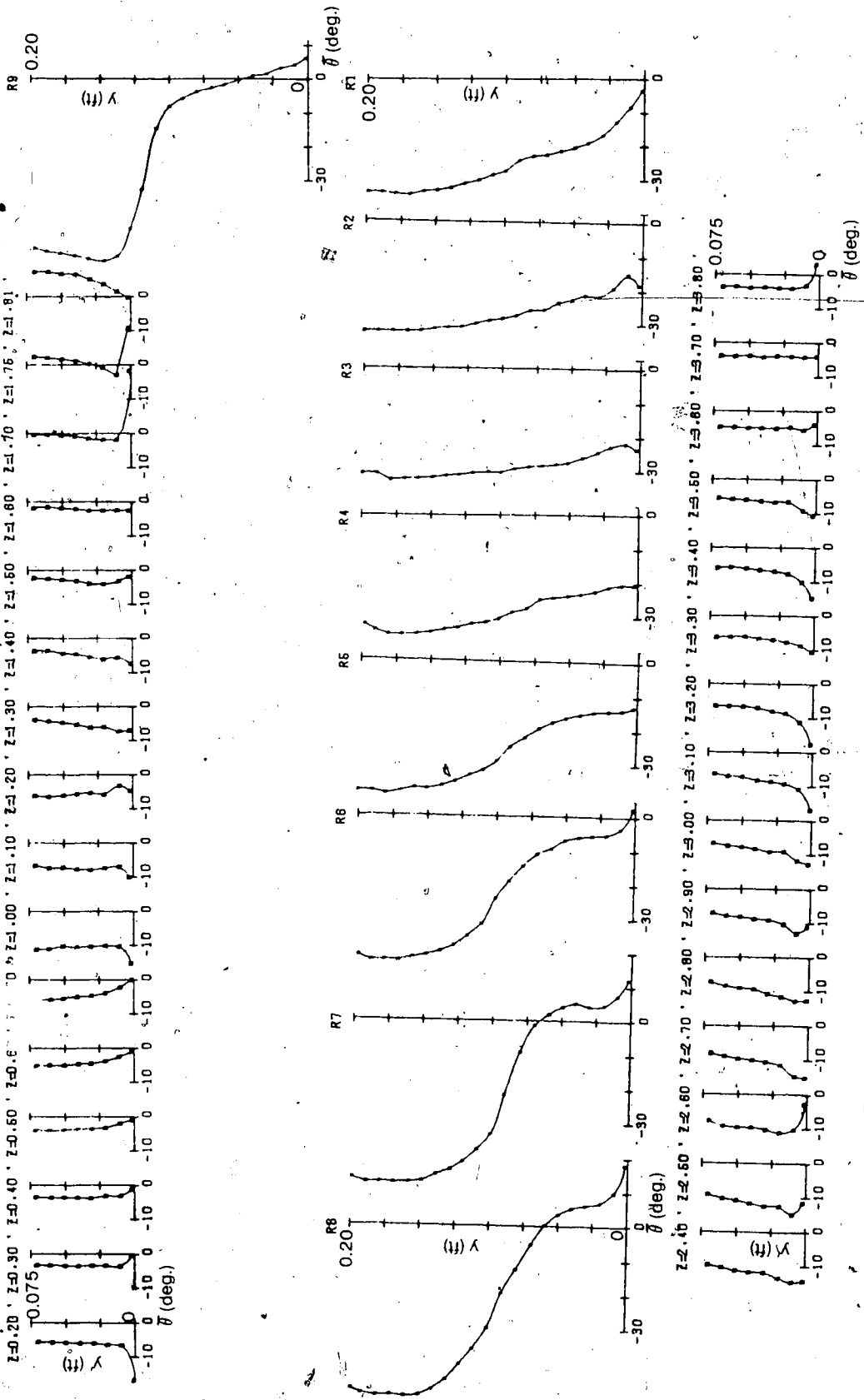
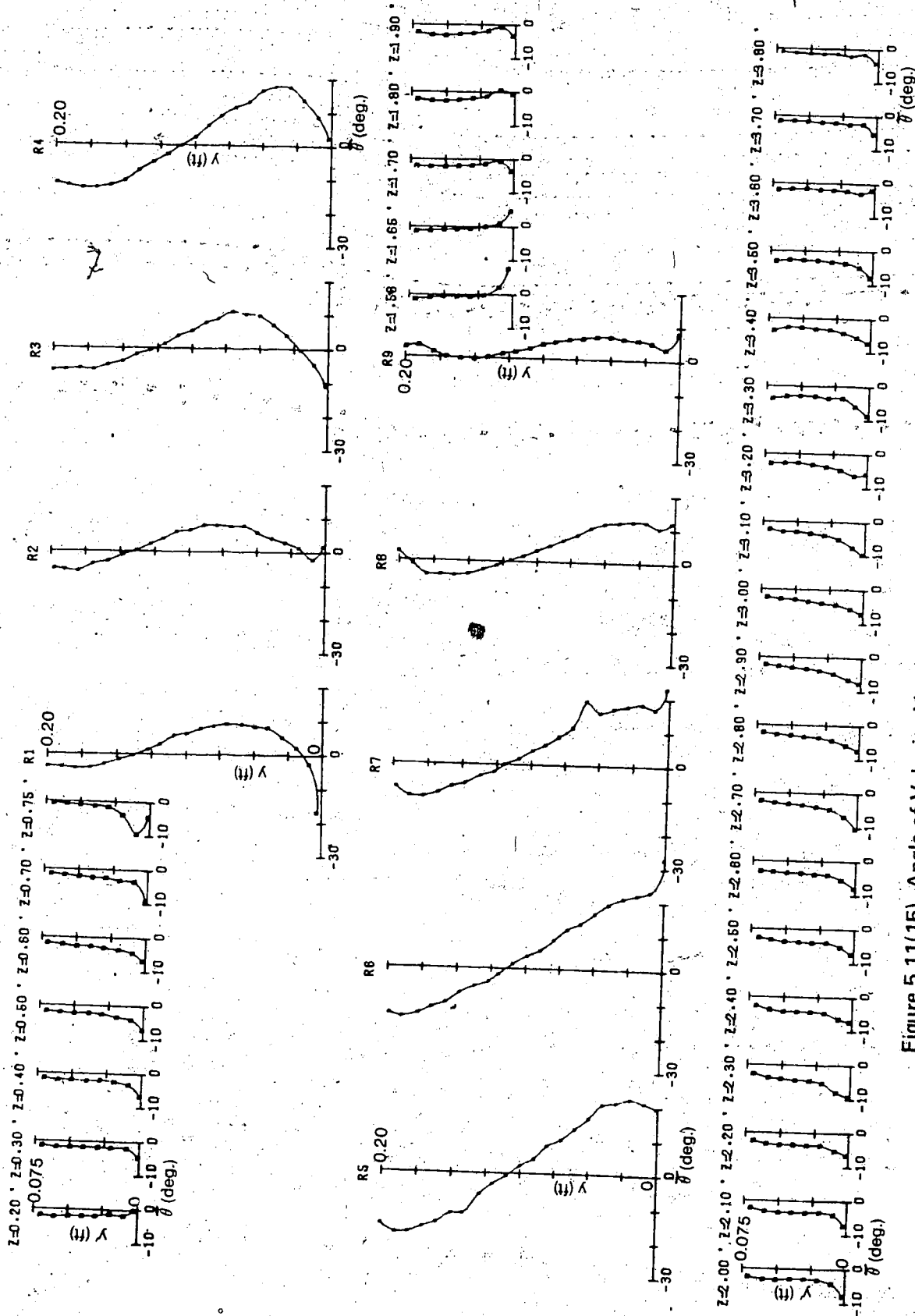Figure 5.11(5) Angle of Velocity Vector Profiles: Cross-Section No. 5
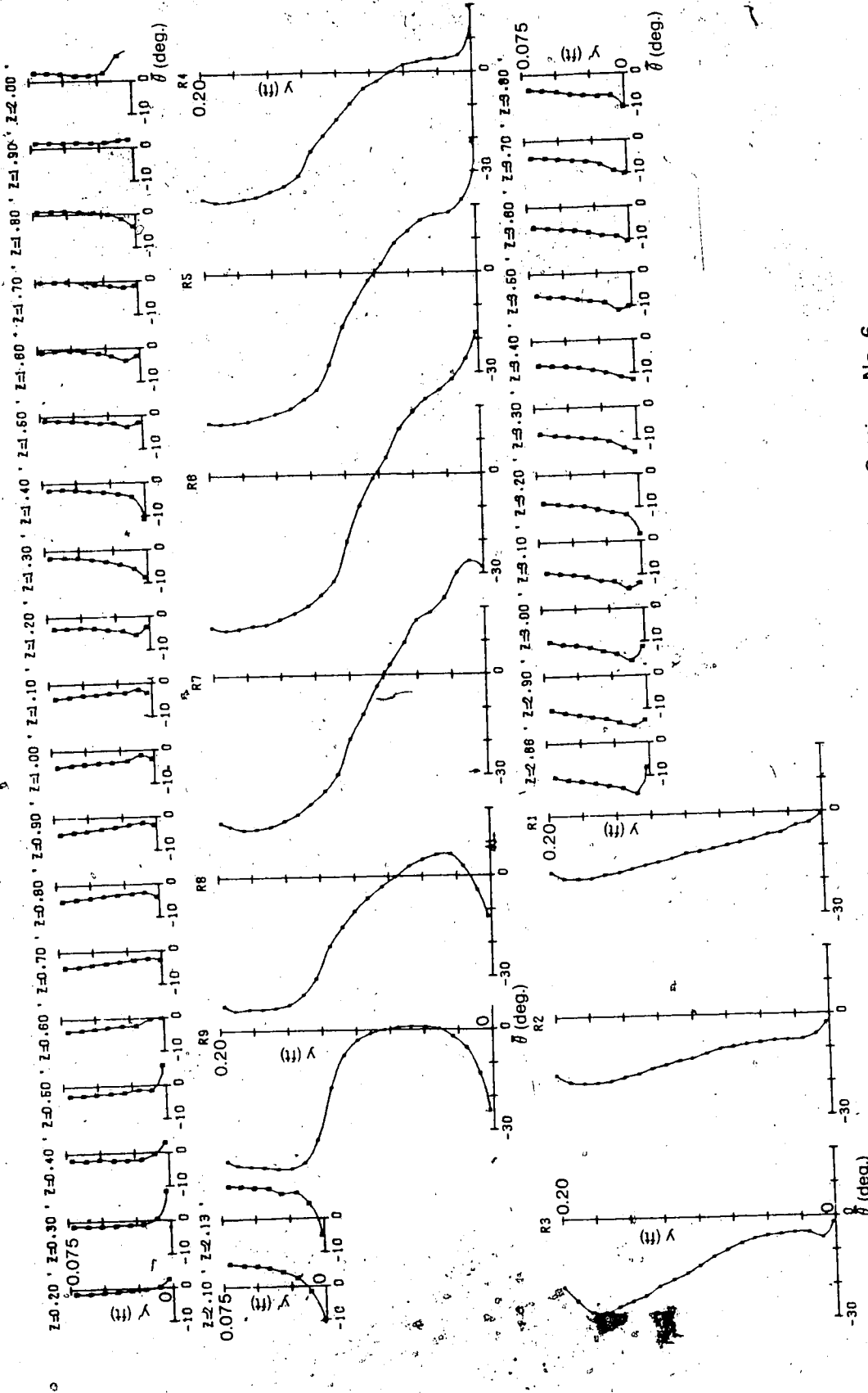
Figure 5.11(6) Angle of Velocity Vector Profiles; Cross-Section No. 6
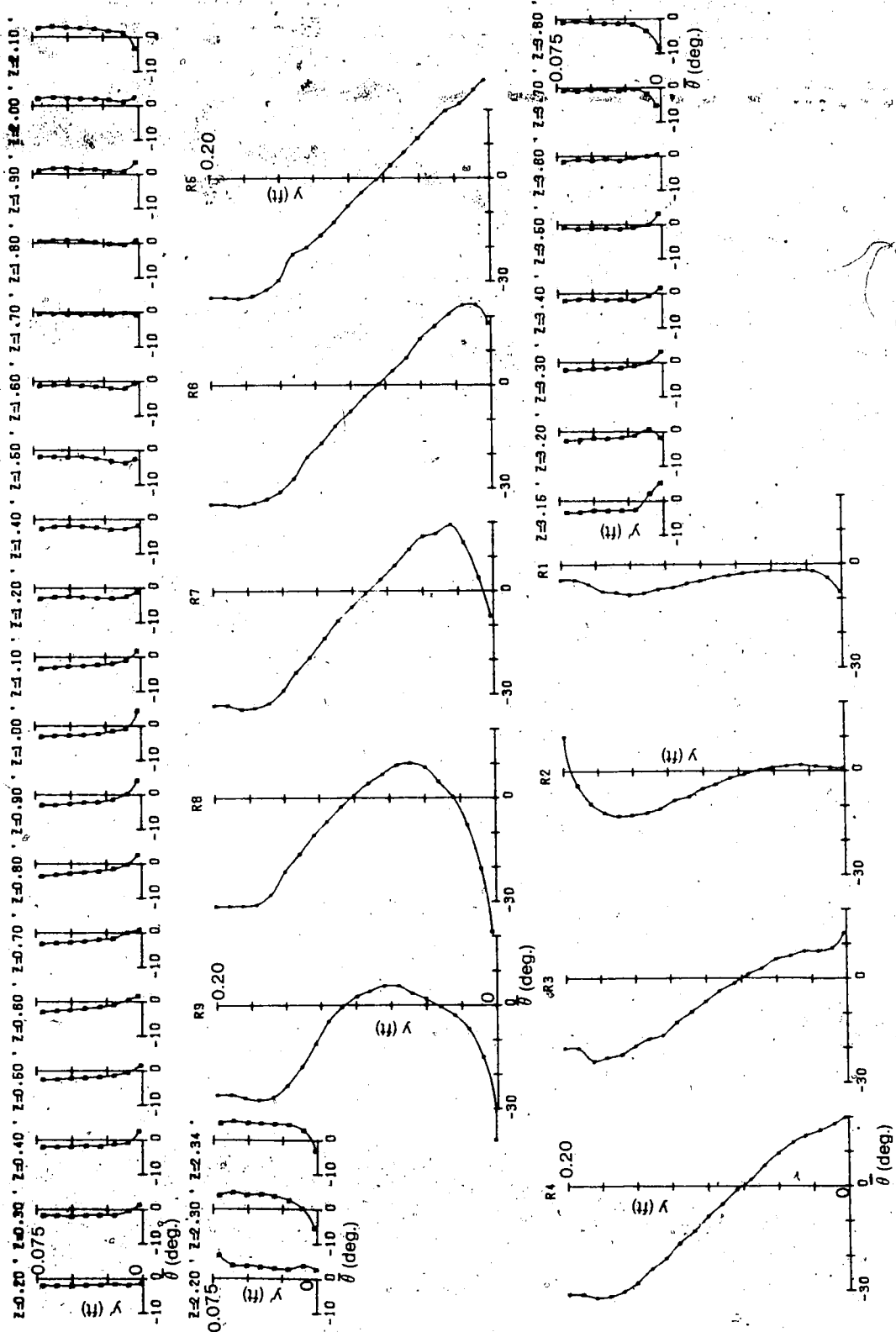
Figure 5.11(7) Angle of Velocity Vector Profiles: Cross-Section No. 7
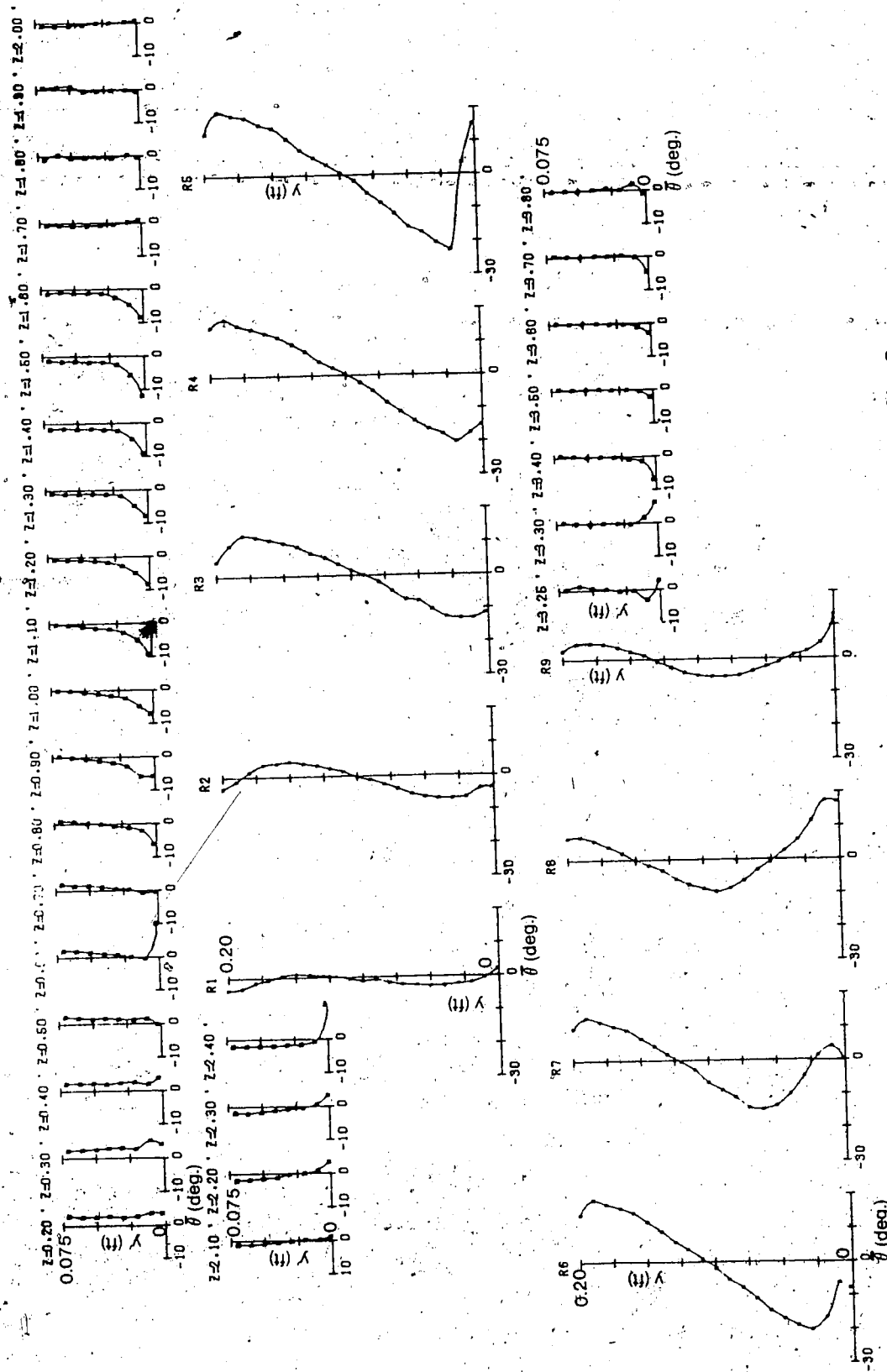
Figure 5.11(8) Angle of Velocity Vector Profiles: Cross-Section No. 8
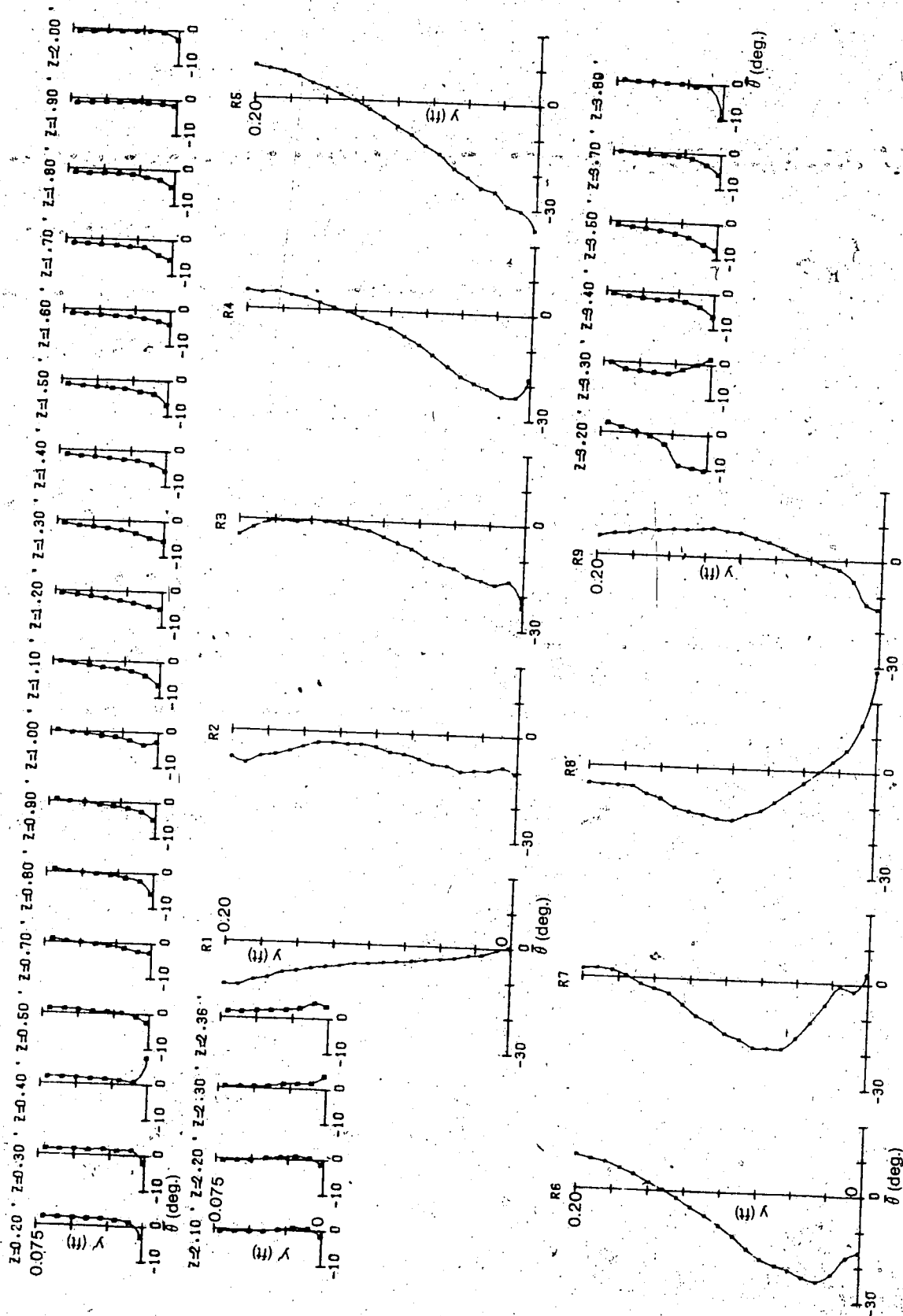
Figure 5.11(9) Angle of Velocity Vector Profiles: Cross-Section No. 9
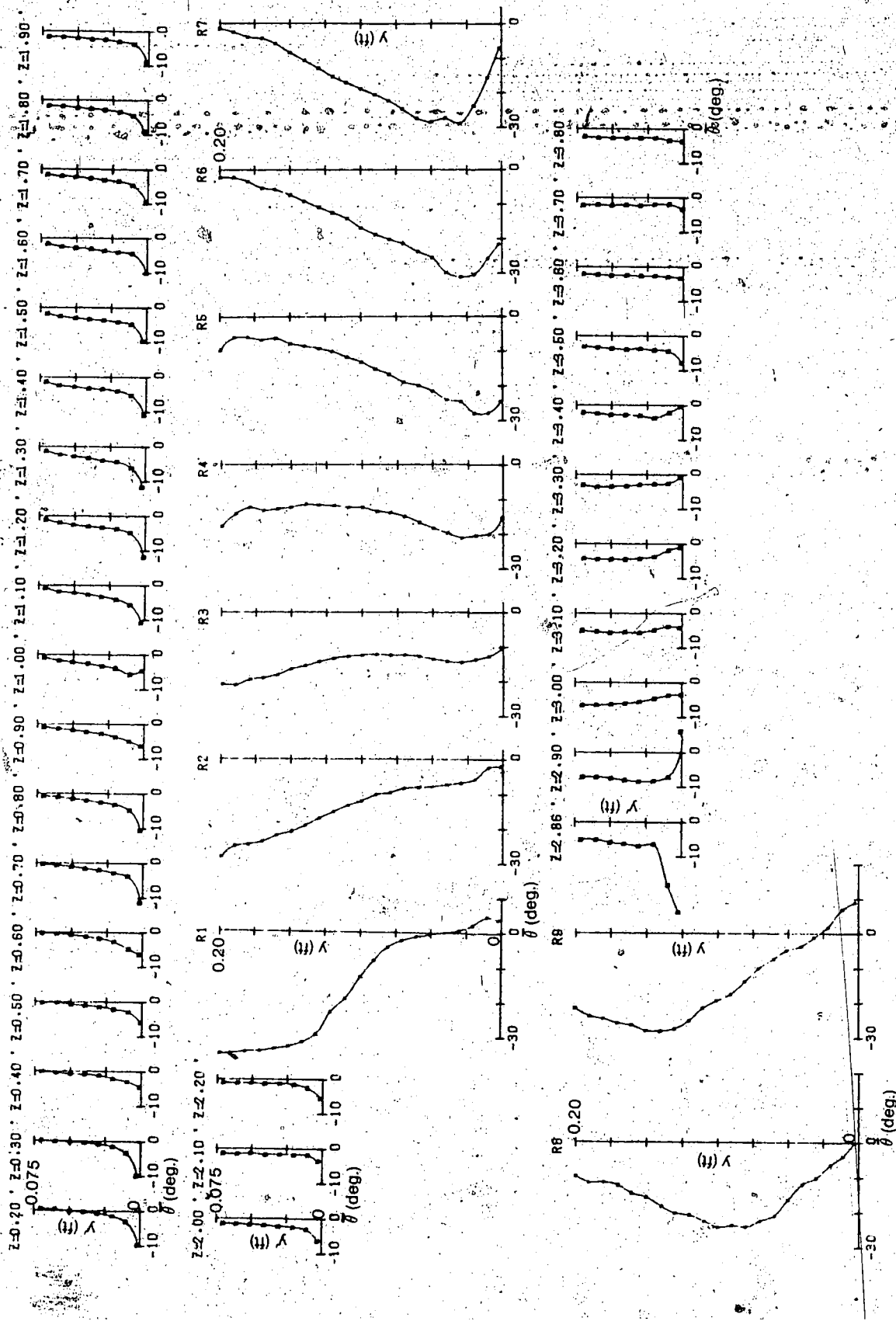
Figure 5.11(10) Angle of Velocity Vector Profiles: Cross-Section No. 10

Figure 5.11(11) Angle of Velocity Vector Profiles: Cross-Section No. 11

Figure 5.11(13) Angle of Velocity Vector Profiles; Cross-Section No. 13

Figure 5.11(14) Angle of Velocity Vector Profiles: Cross-Section No. 14

Figure 5.11(15) Angle of Velocity Vector Profiles: Cross-Section No. 15
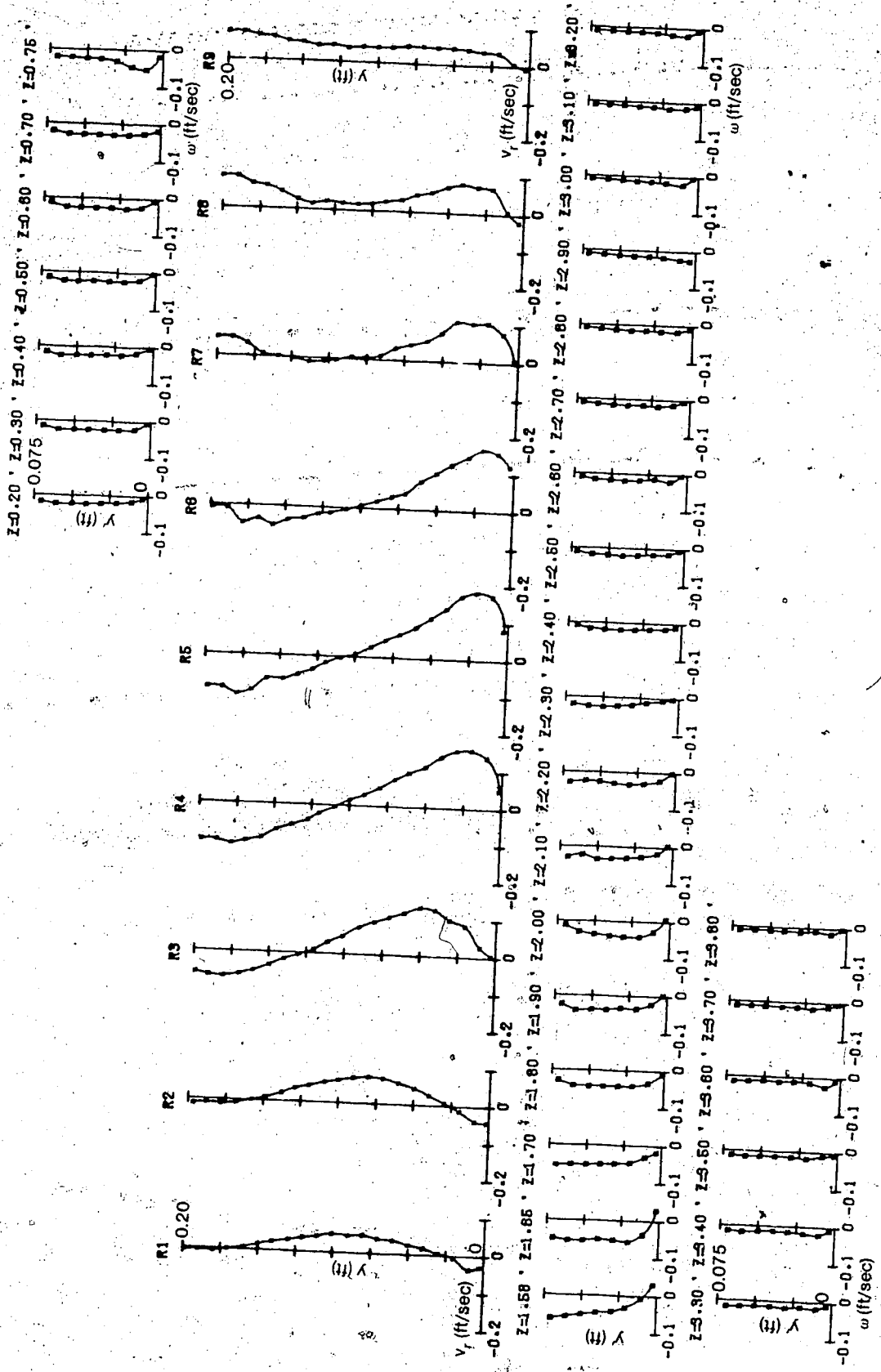
Figure 5.12(1) Radial Velocity Profiles: Cross-Section No. 1
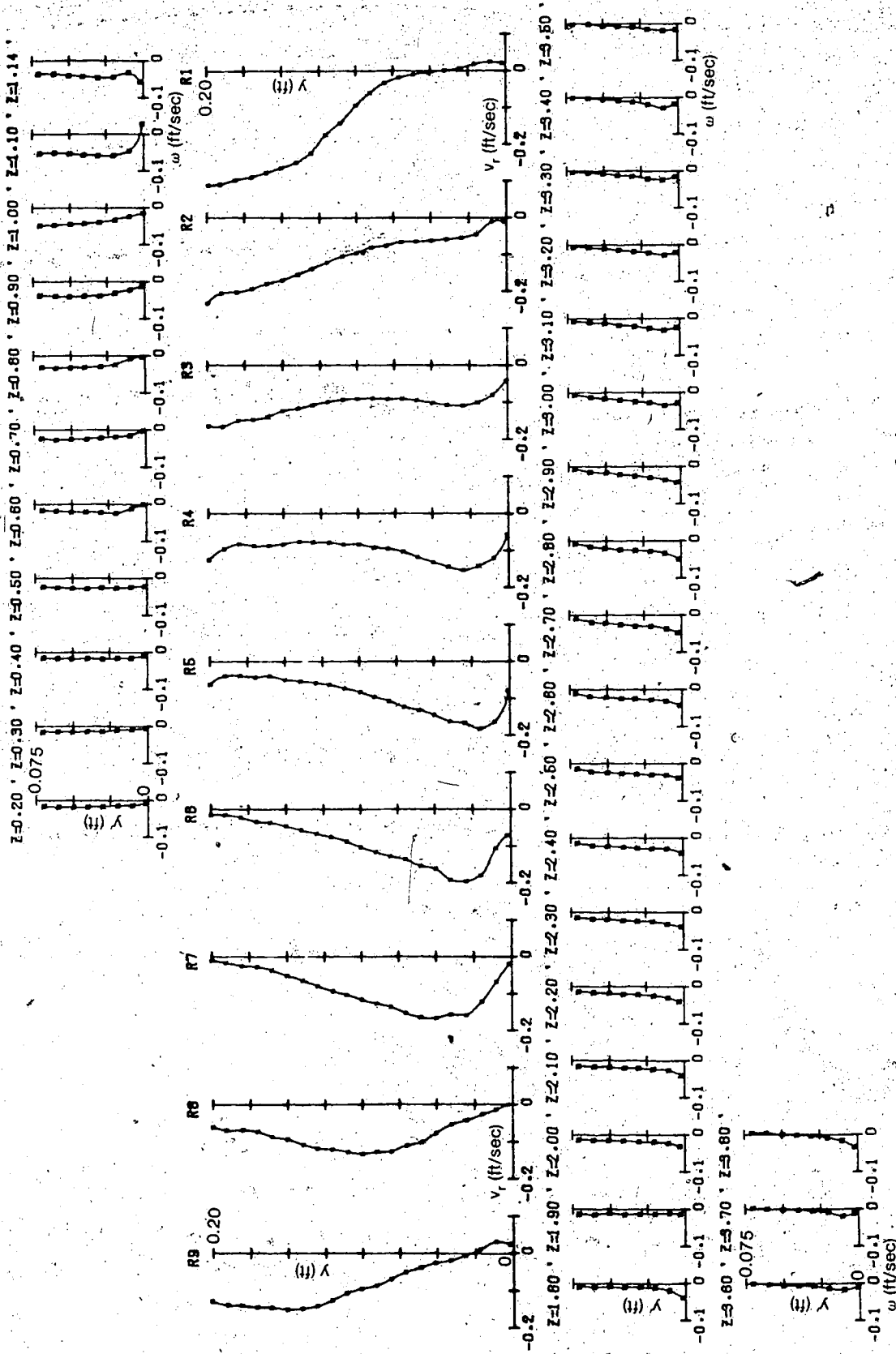
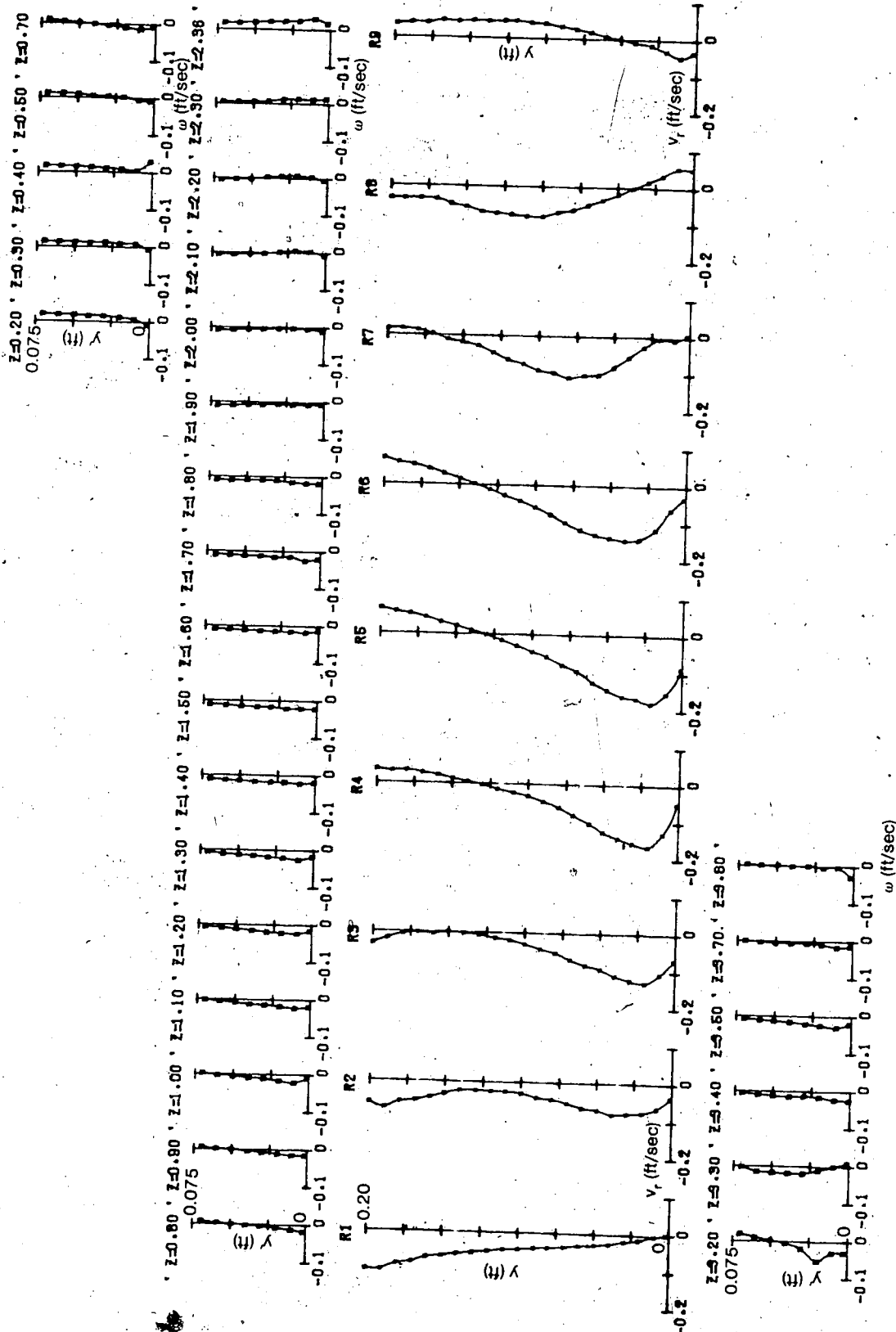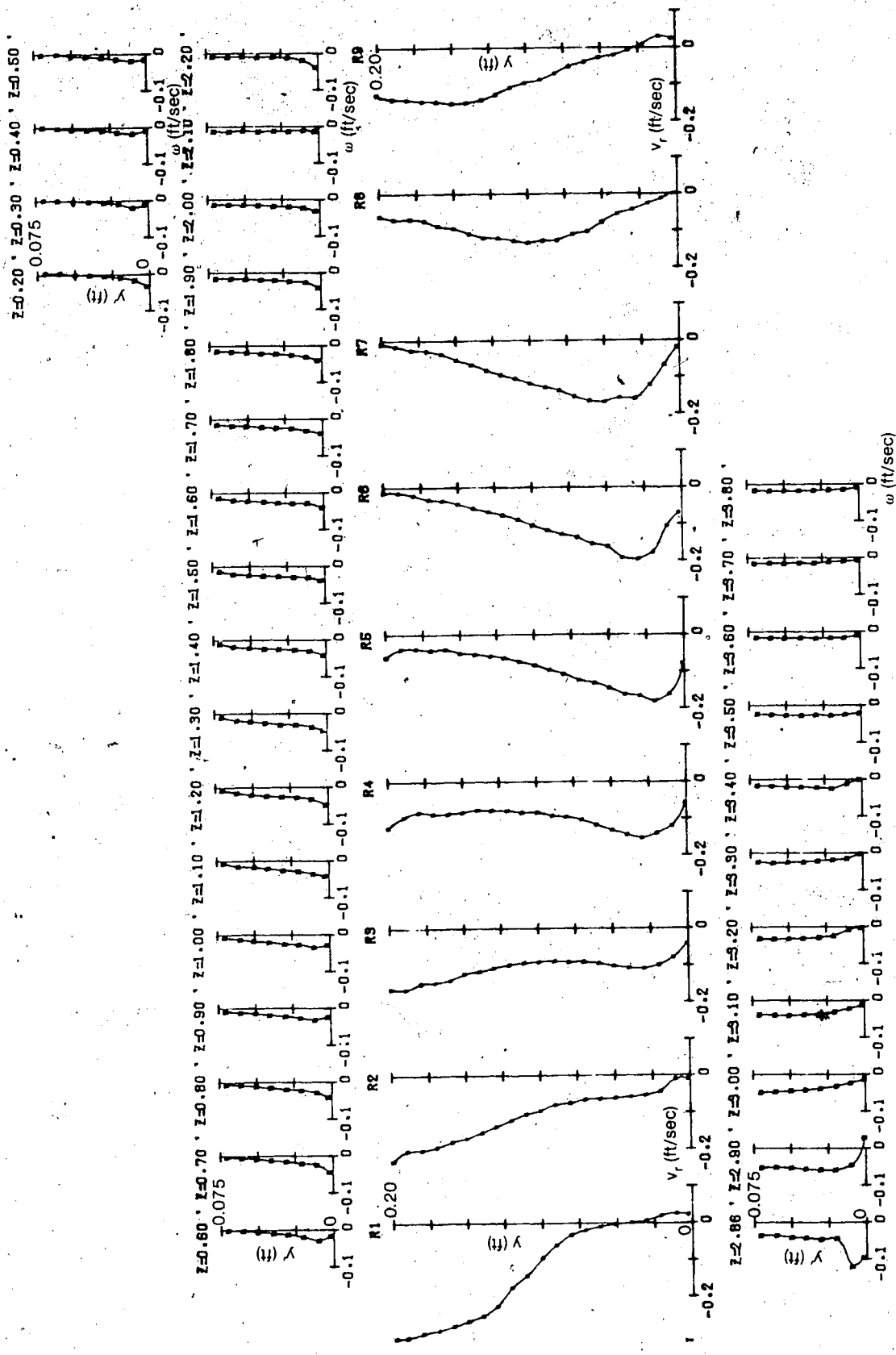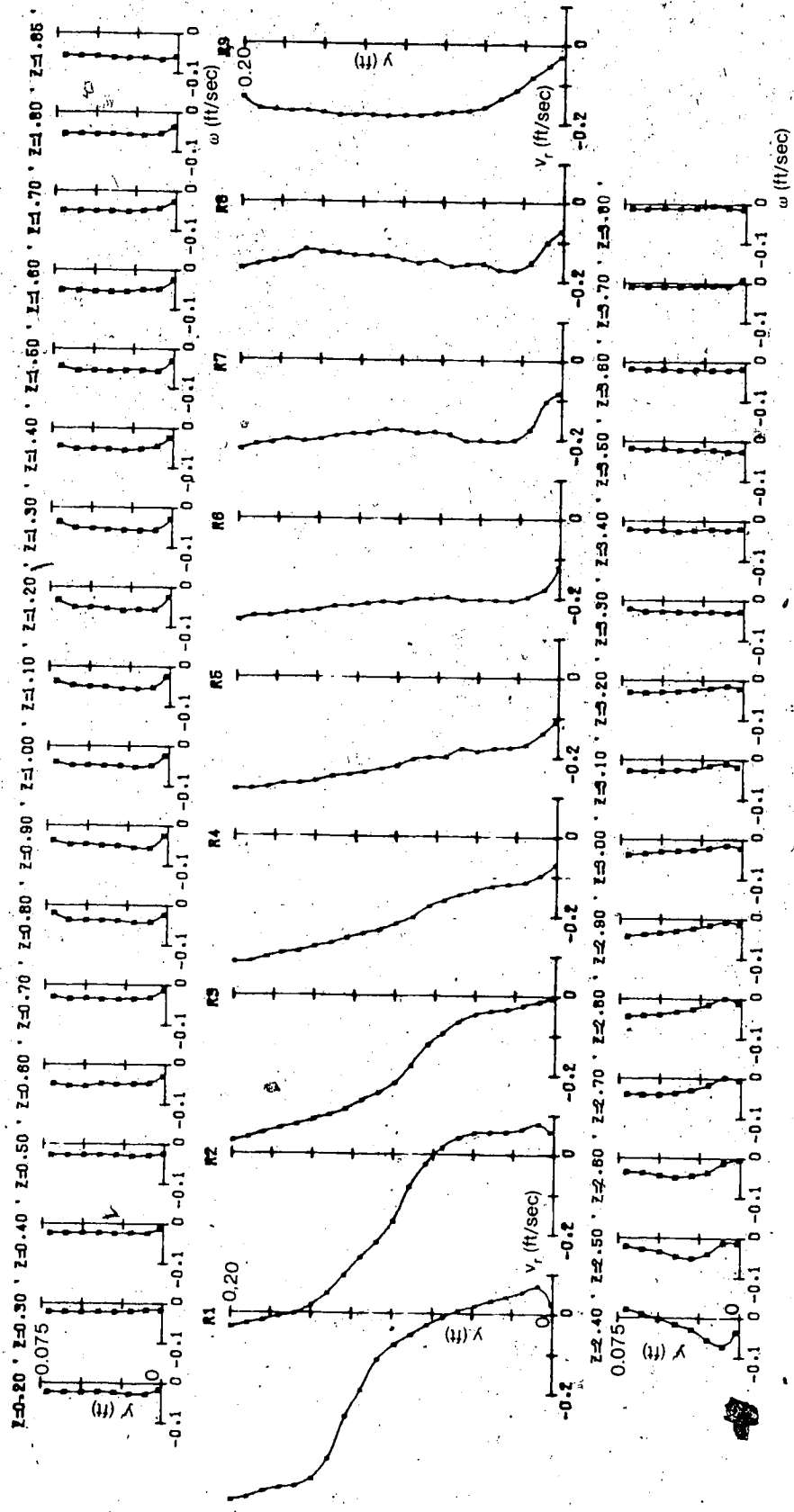Figure 5.12(3) Radial Velocity Profiles: Cross-Section No. 3
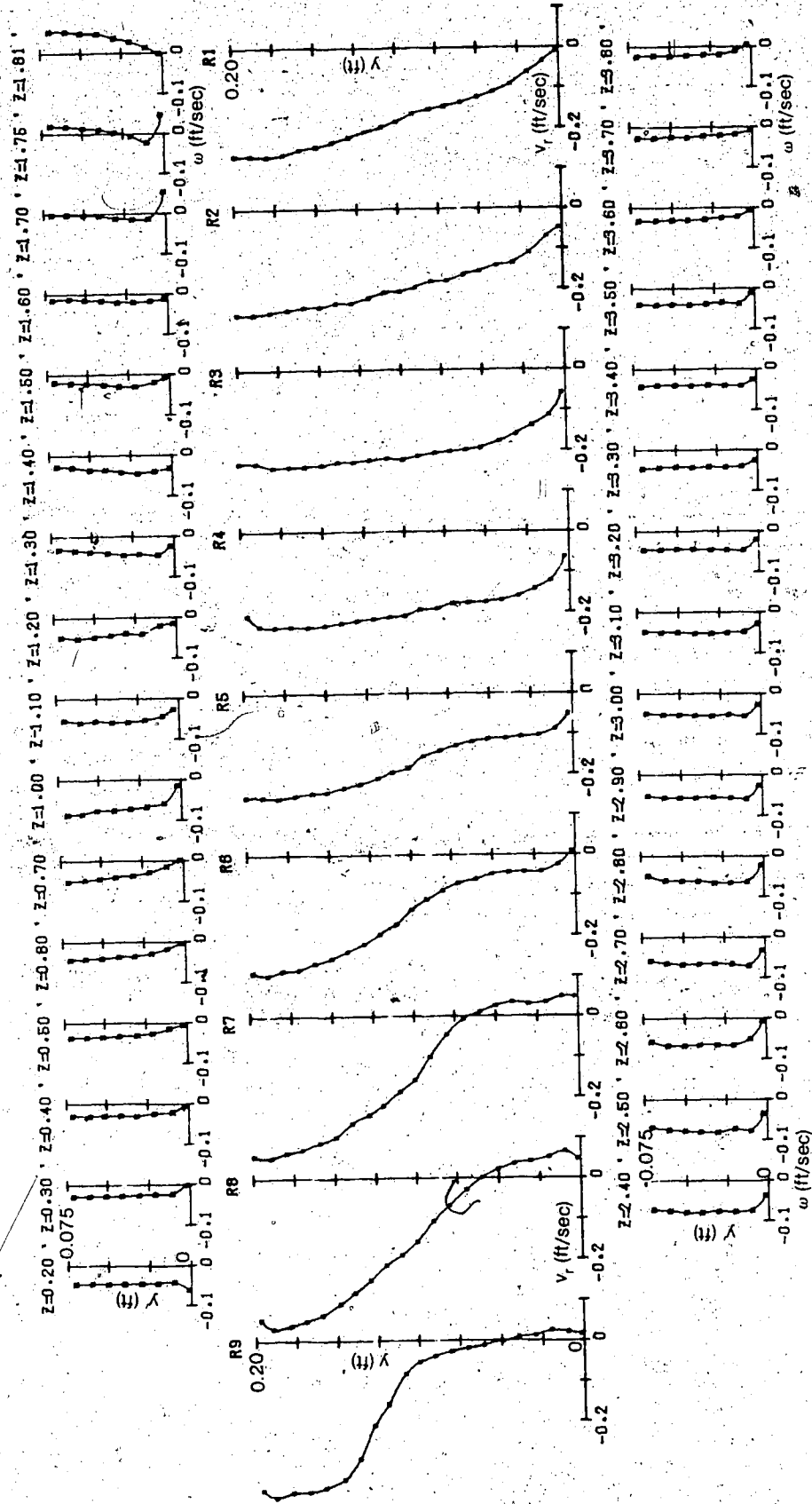
Figure 5.12(5)   Radial Velocity Profiles: Cross-Section No. 5
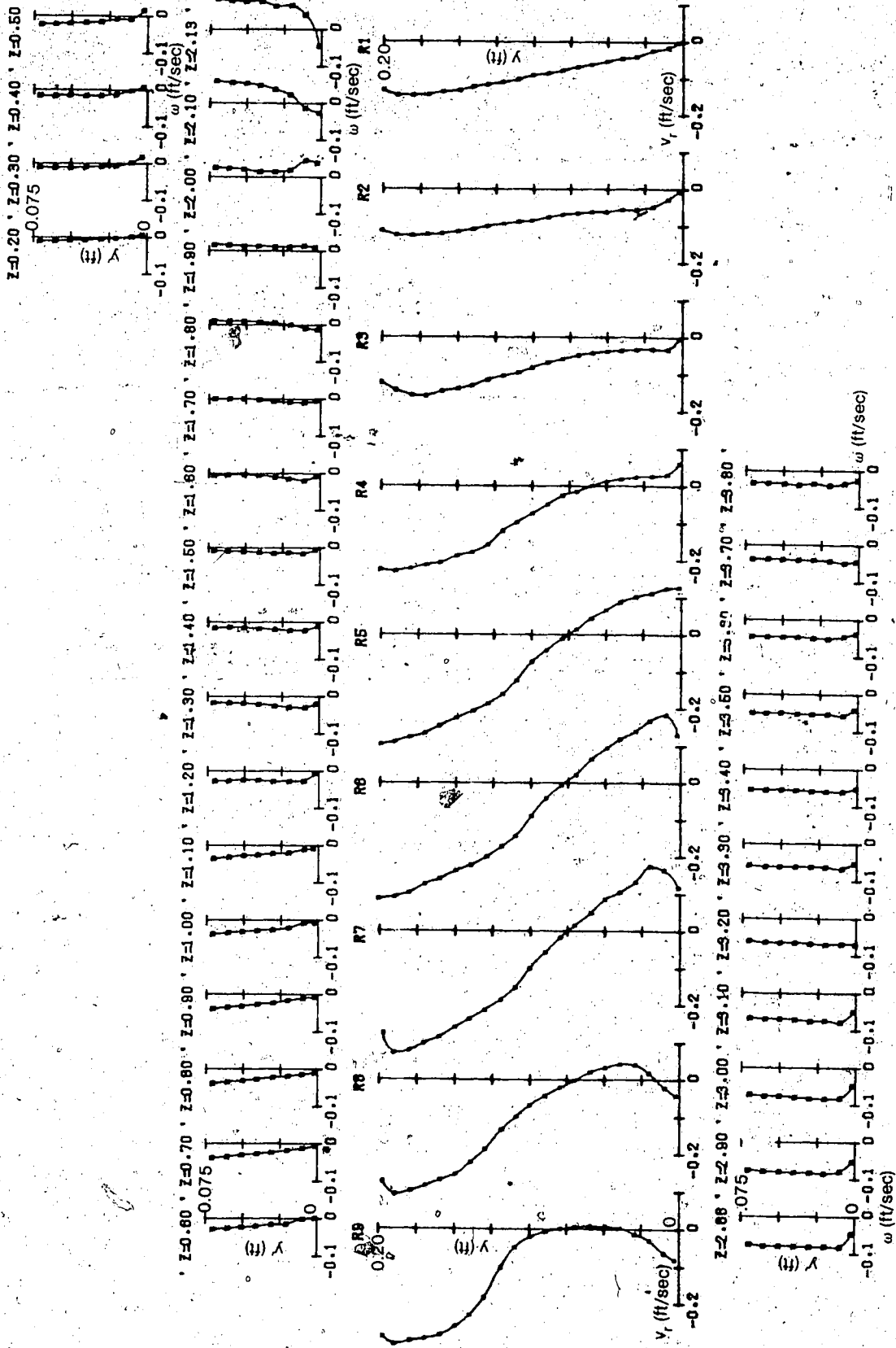
Figure 5.12(6) Radial Velocity Profiles: Cross-Section No. 6
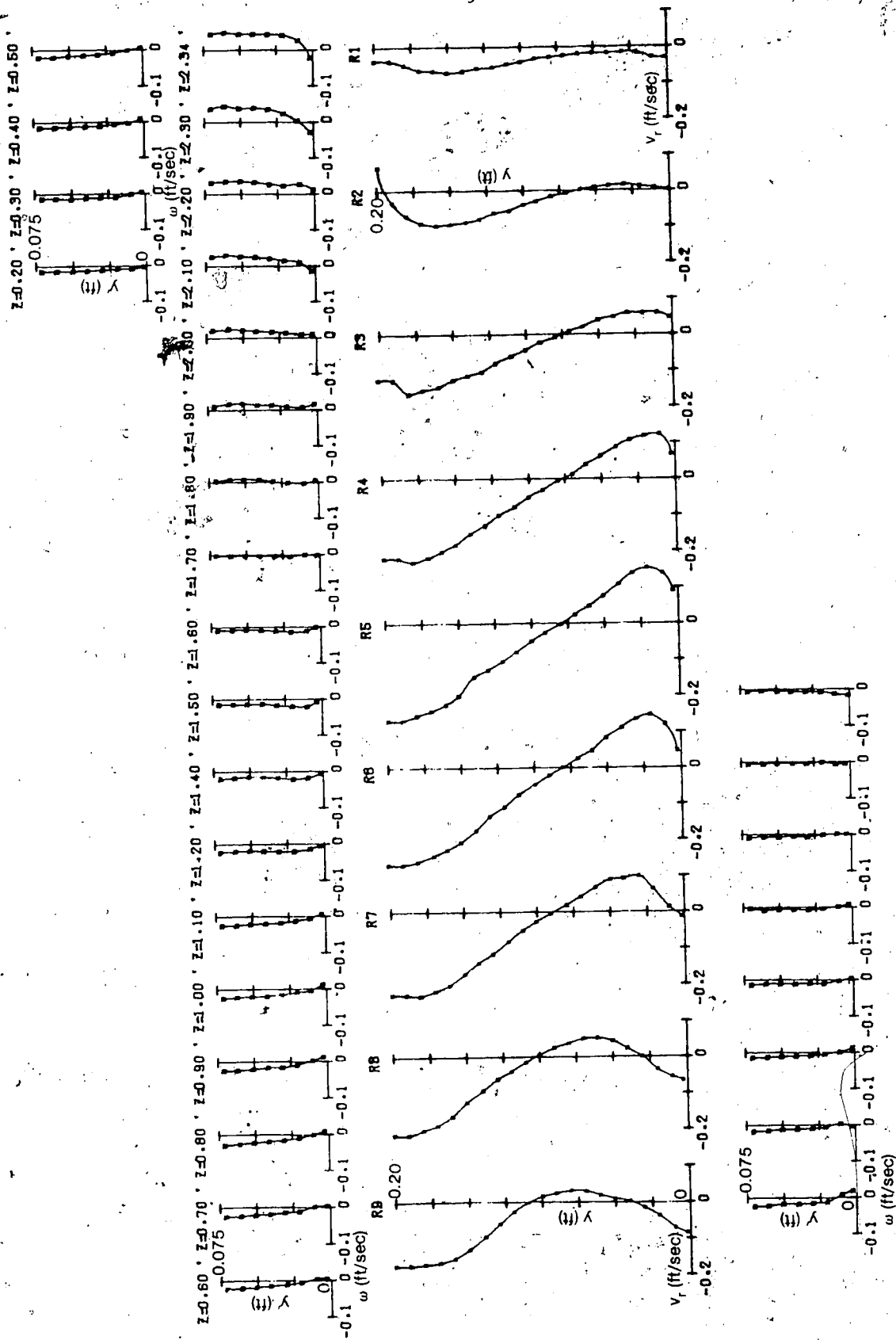
Figure 5.12(7) Radial Velocity Profiles: Cross-Section No. 7
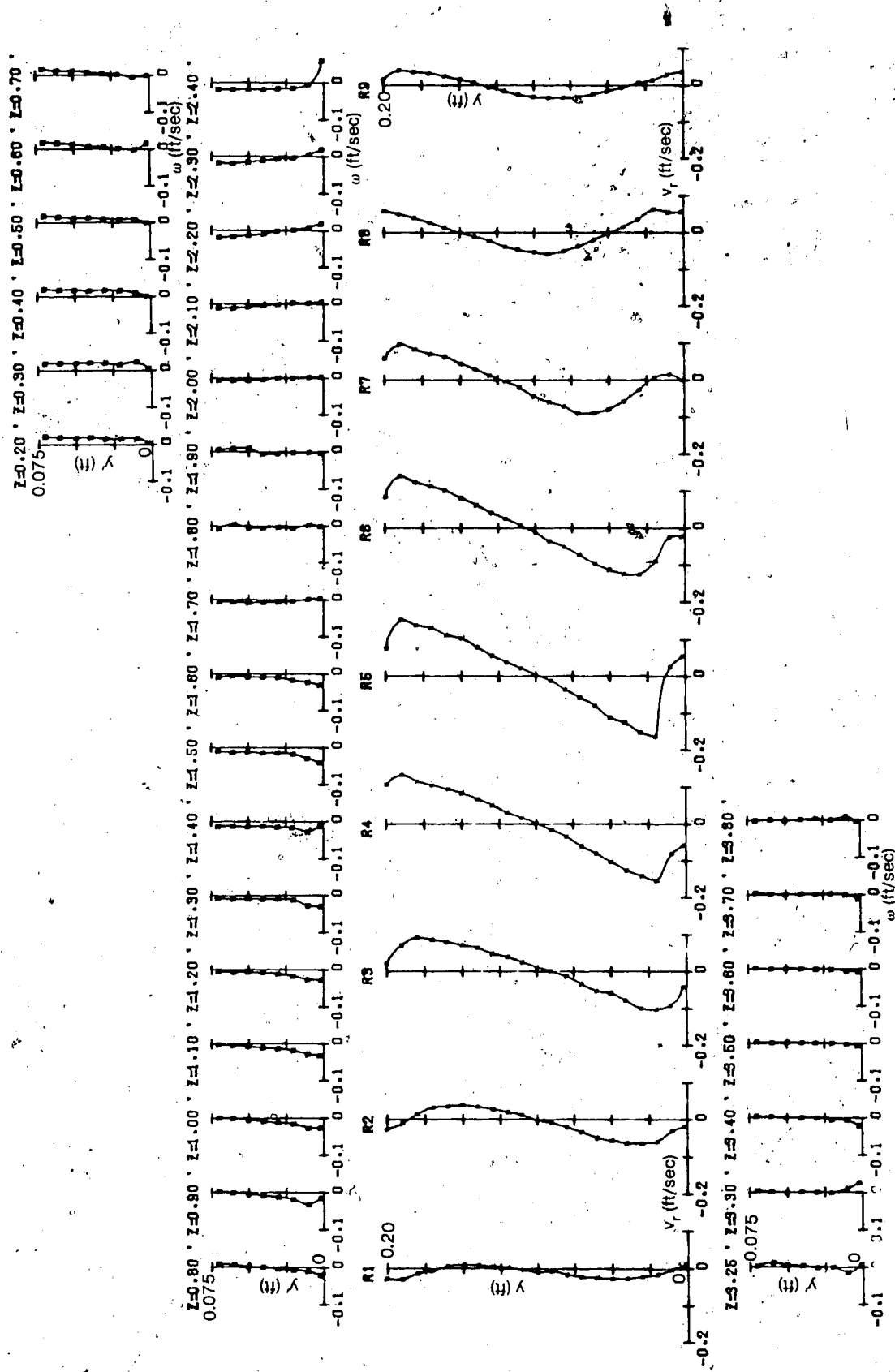
Figure 5.12(8)   Radial Velocity Profiles: Cross-Section   No. 8

Figure 5.12(9) Radial Velocity Profiles: Cross-Section No. 9

Figure 5.12(10) Radial Velocity Profiles: Cross-Section No. 10

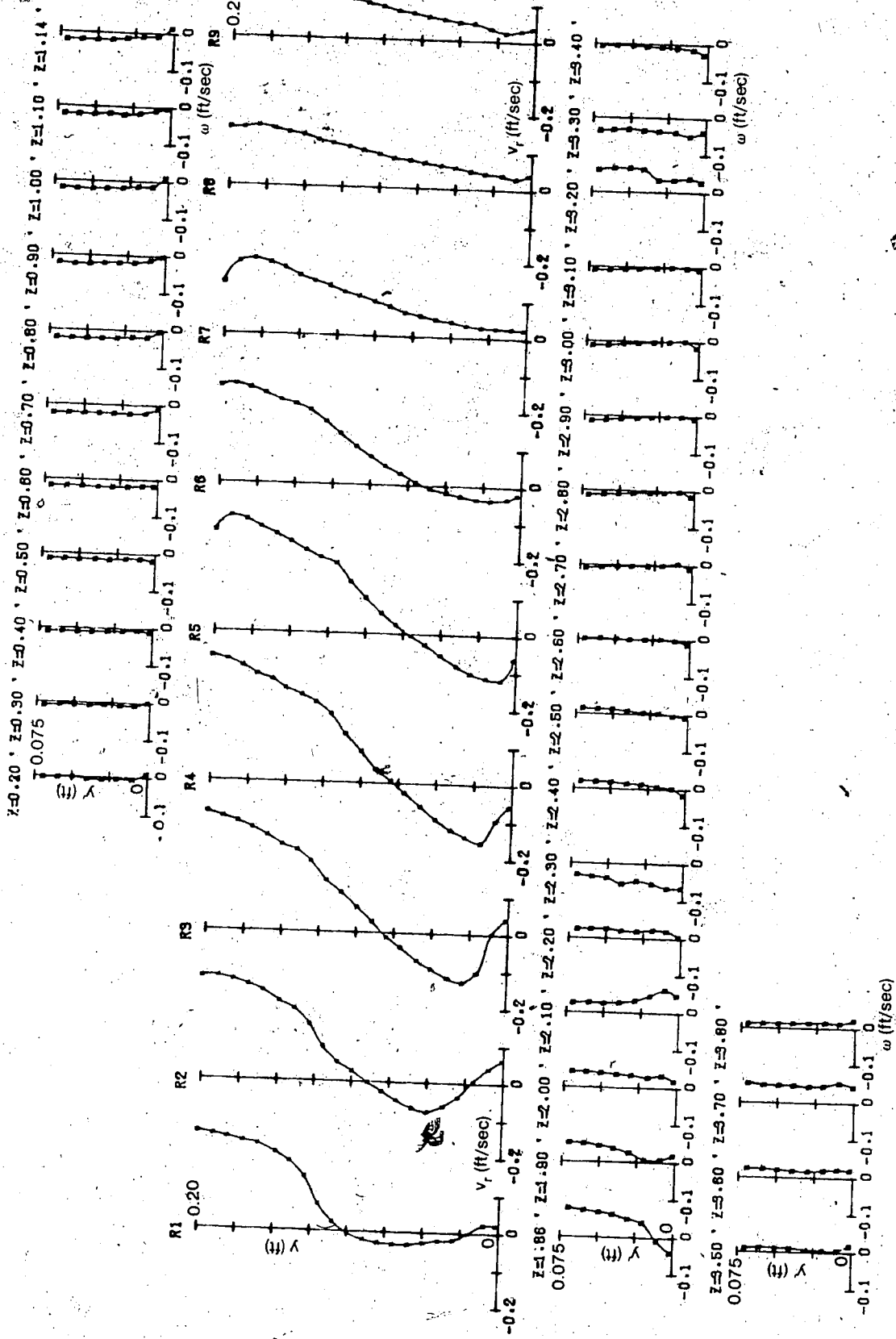Figure 5,12(11) Radial Velocity Profiles: Cross-Section No. 11

Figure 5.12(13) Radial Velocity Profiles: Cross-Section No. 13
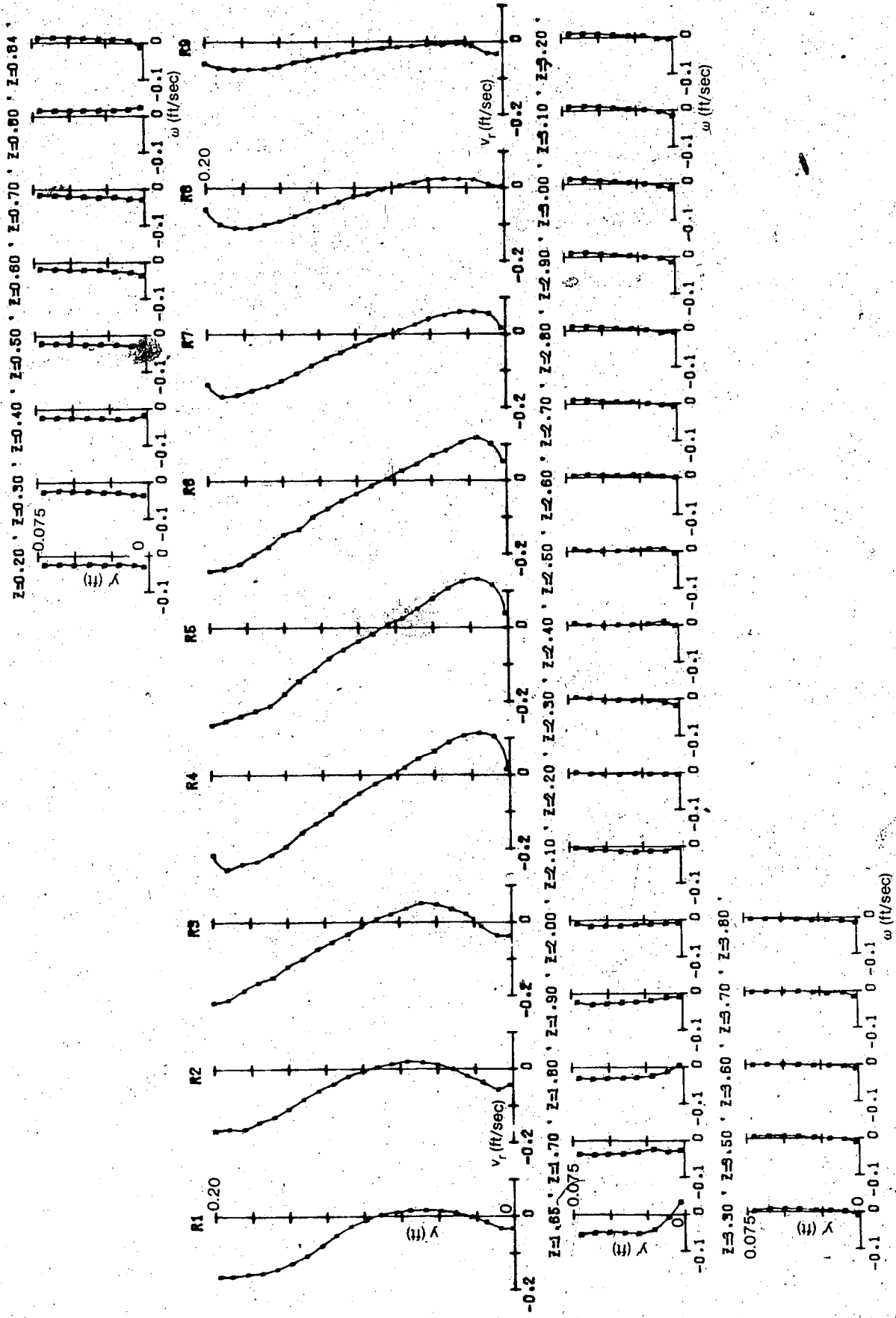
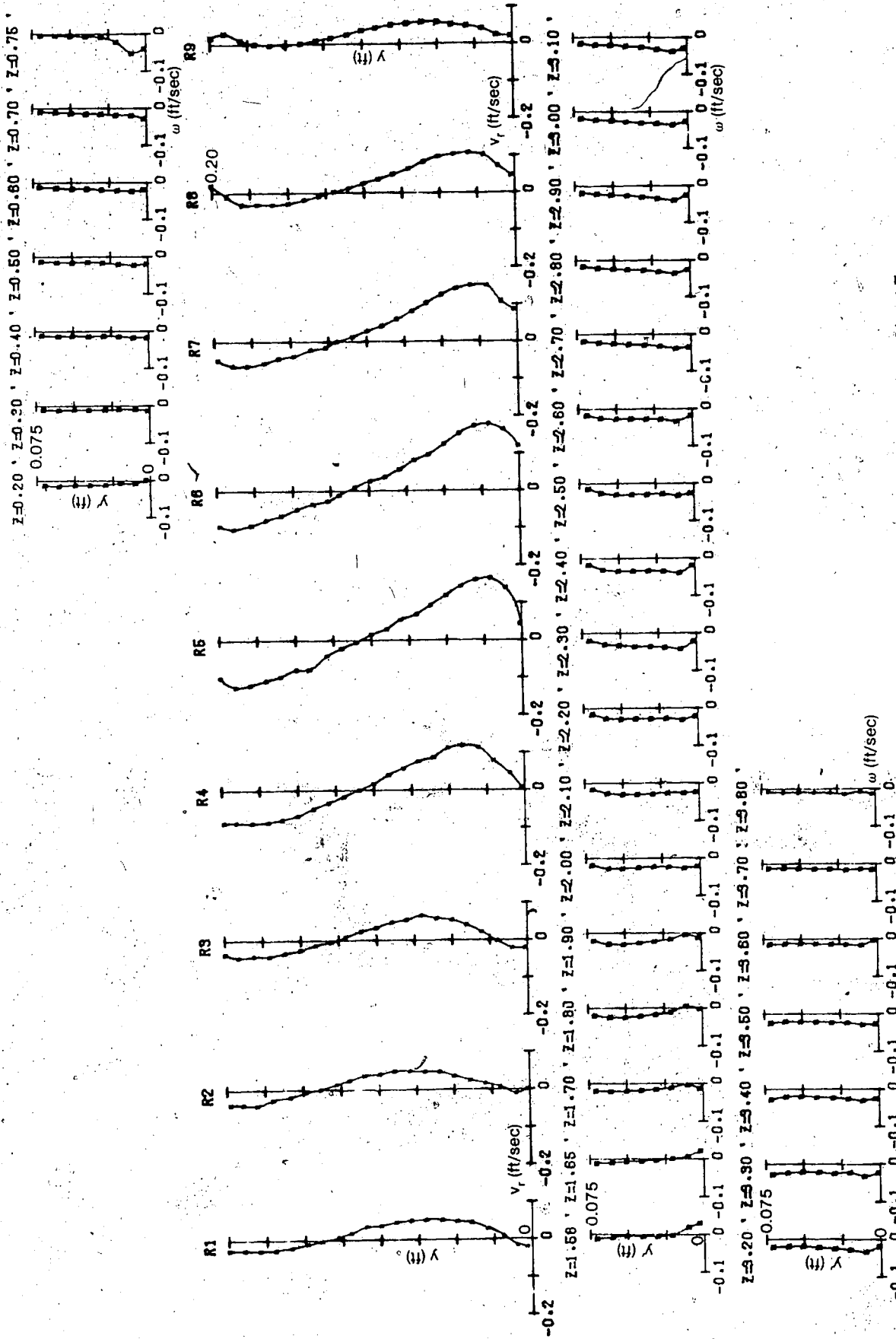Figure 5.12(14) Radial Velocity Profiles: Cross-Section No. 14

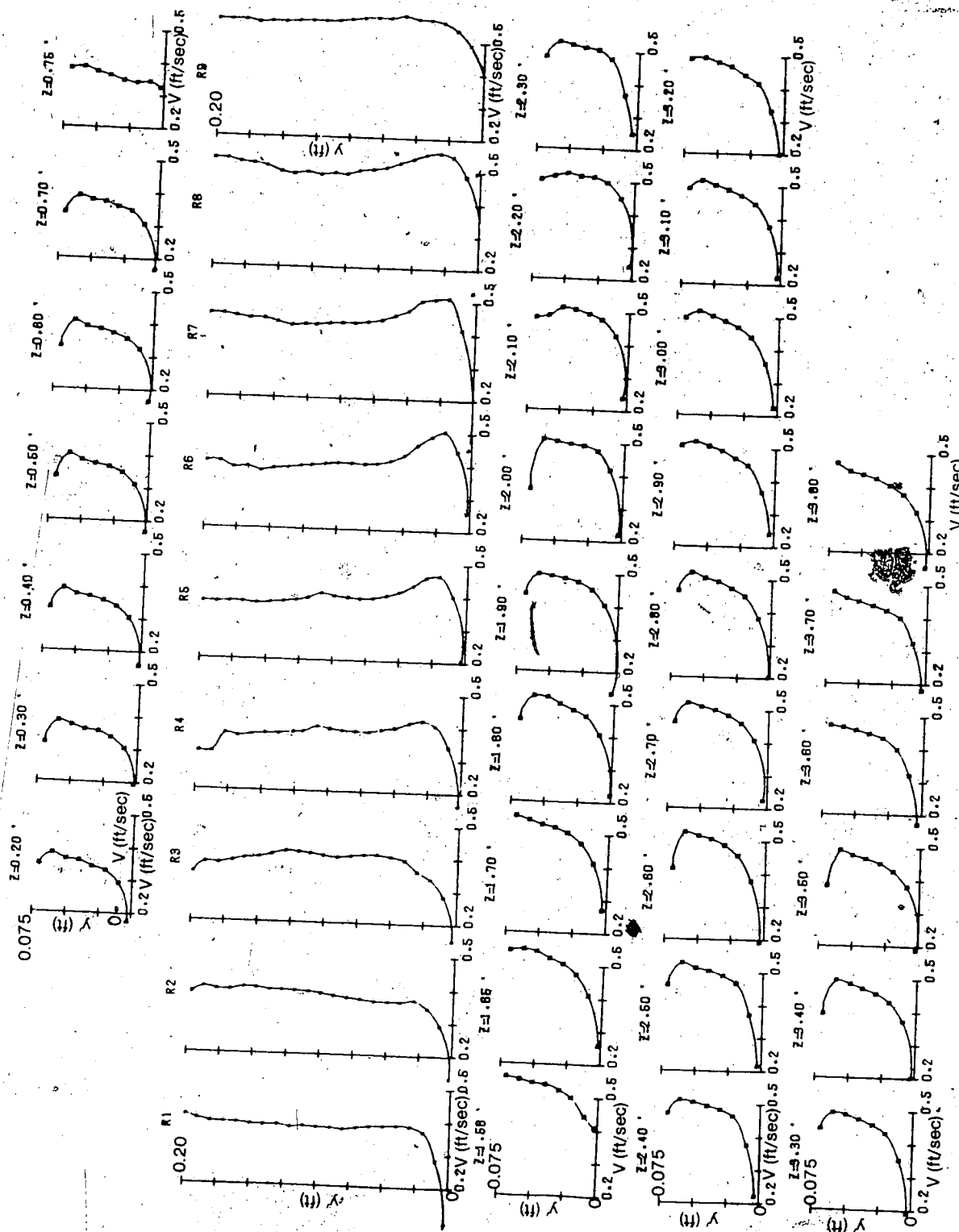Figure 5.12(15) Radial Velocity Profiles: Cross-Section No. 15

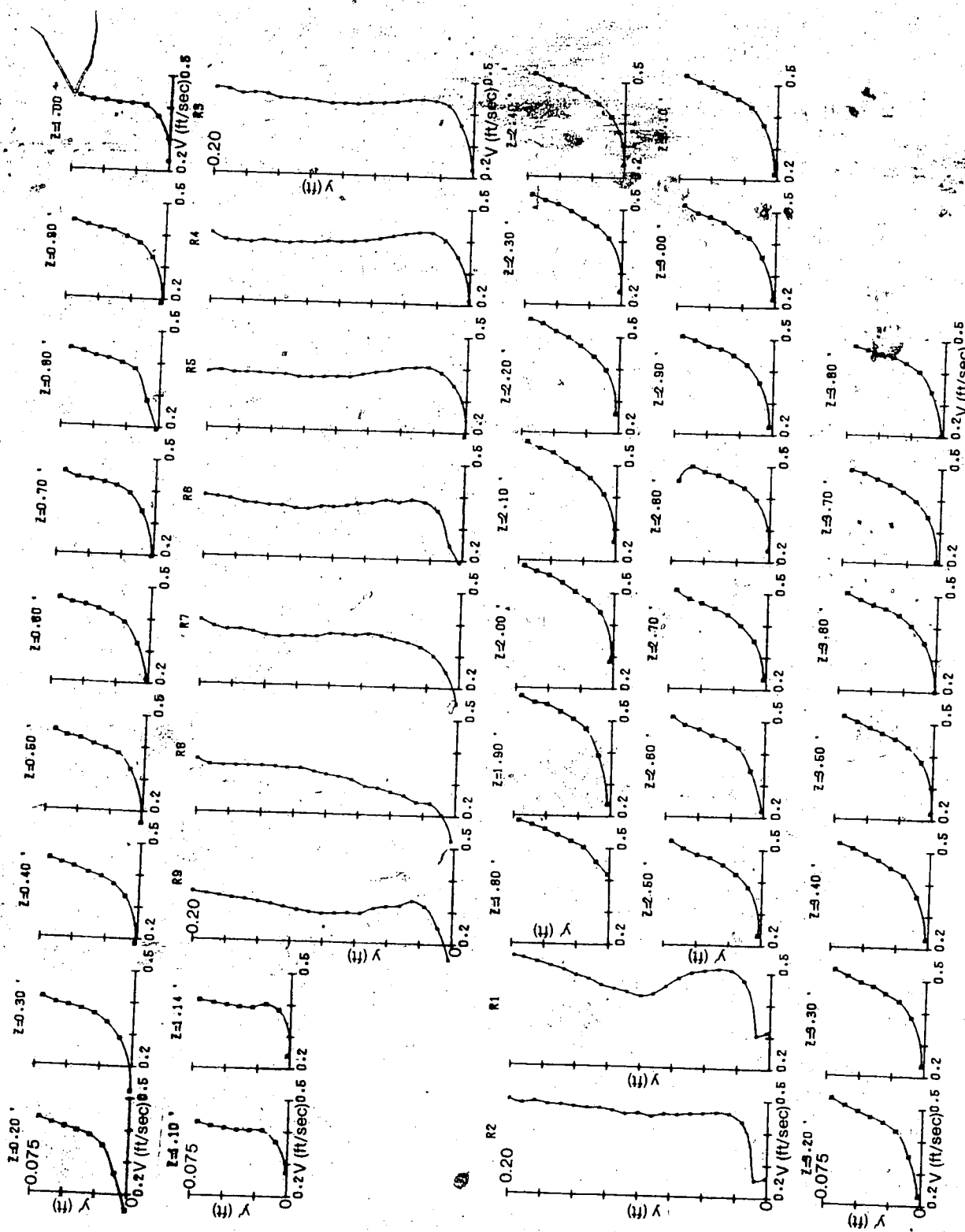Figure 5.13(1) Velocity Vector Profiles: Cross-Section No. 1

Figure 5.13(3) Velocity Vector Profiles: Cross-Section No. 3

Figure 5.13(5) Velocity Vector Profiles: Cross-Section No. 5

147

Figure 5.13(6) Velocity Vector Profiles: Cross-Section No. 6

Figure 5.13(7) Velocity Vector Profiles: Cross-Section No. 7

Figure 5.13(8) Velocity Vector Profiles: Cross-Section No. 8

Figure 5.13(9). Velocity Vector Profiles: Cross-Section No. 9
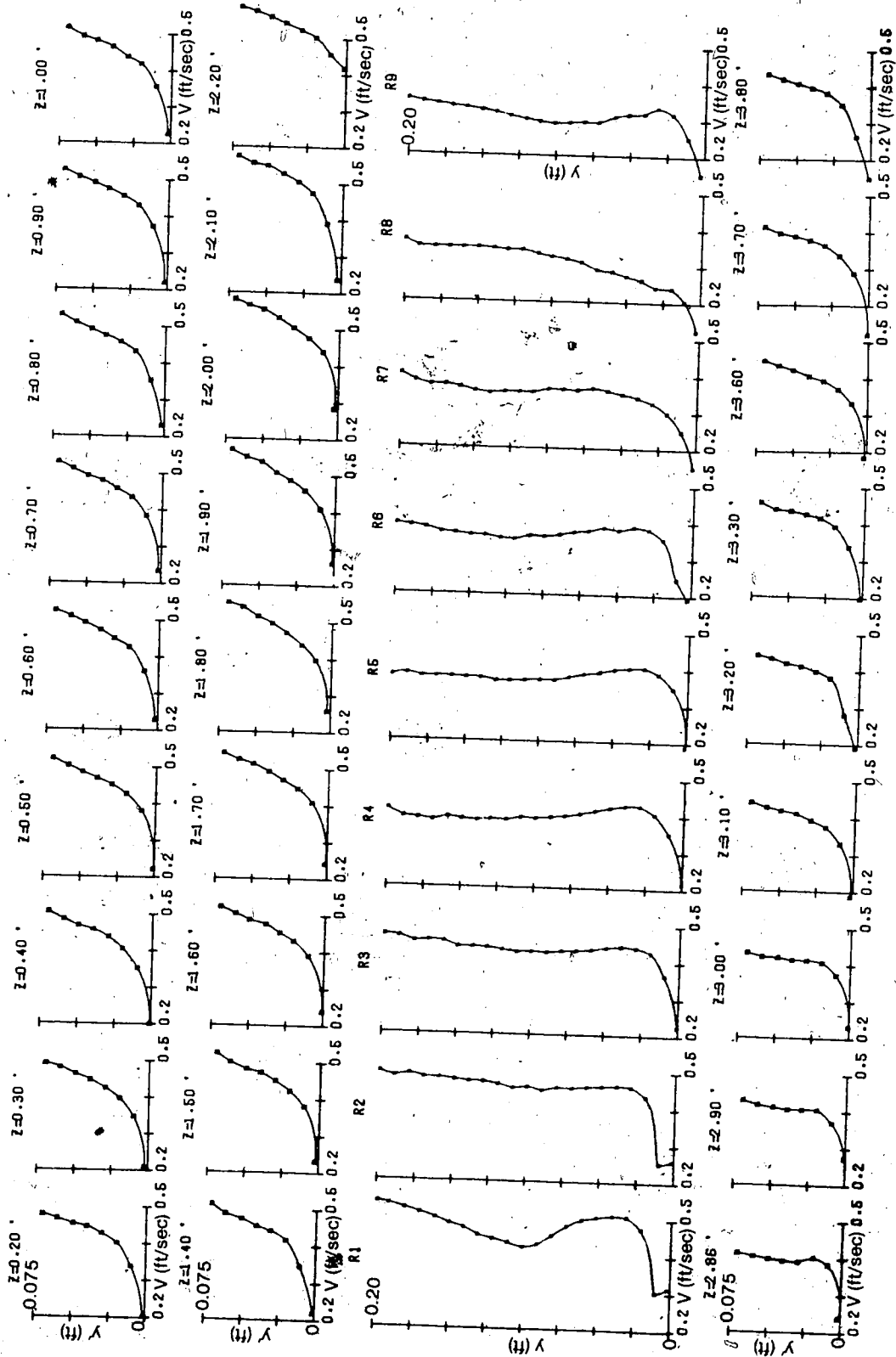
Figure 5.13(10) Velocity Vector Profiles: Cross-Section No. 10
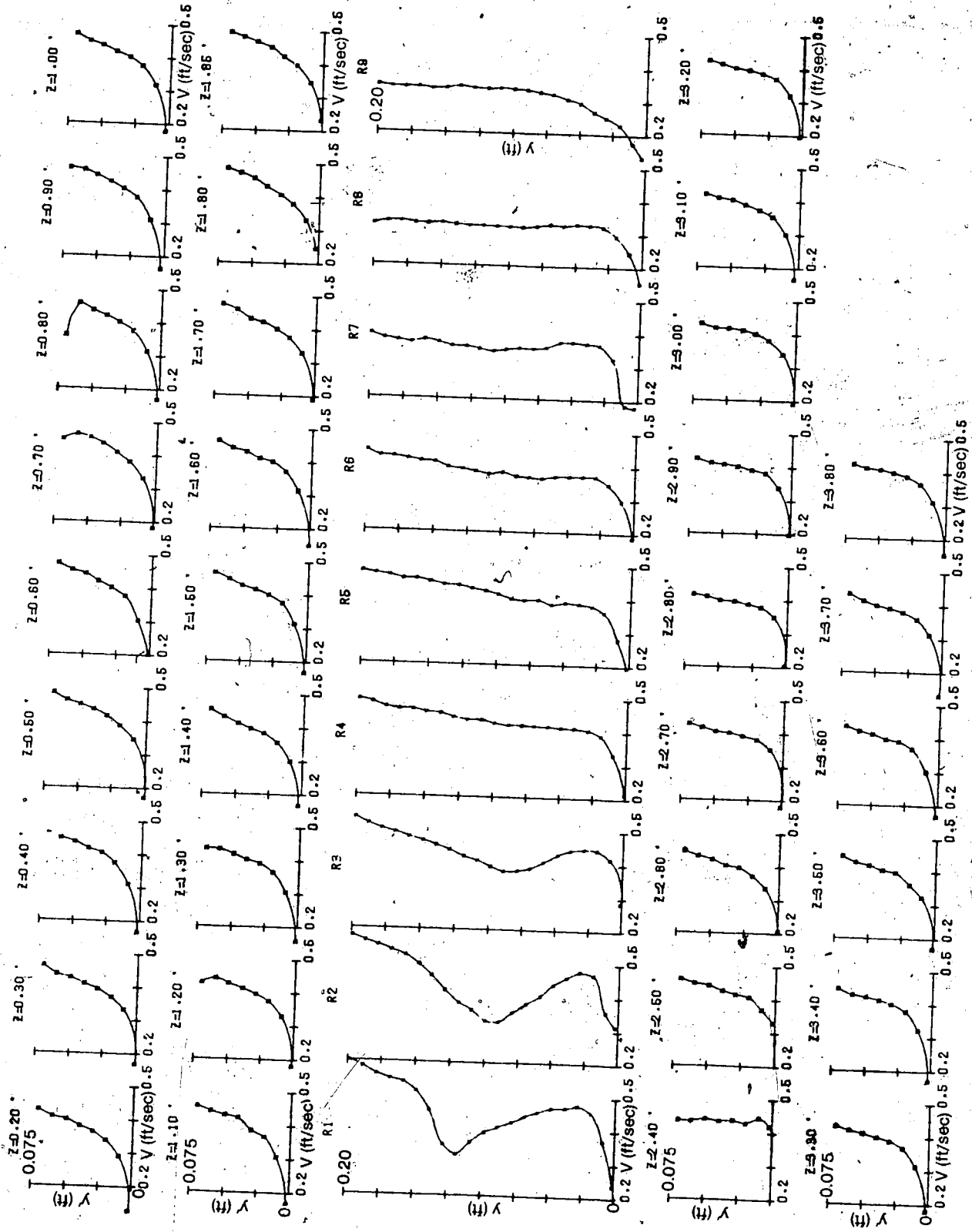
Figure 5.13(11) Velocity Vector Profiles: Cross-Section No. 11
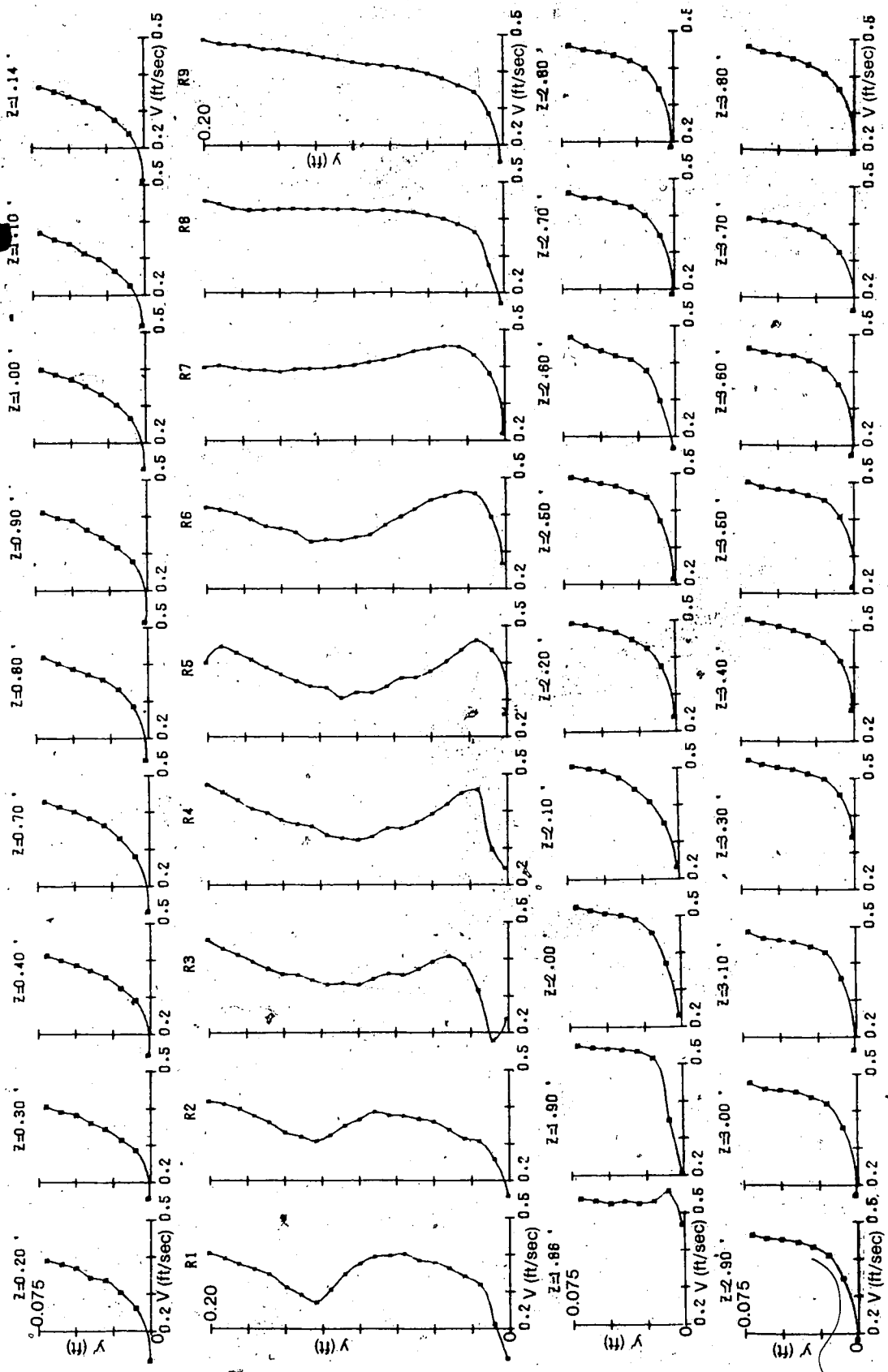
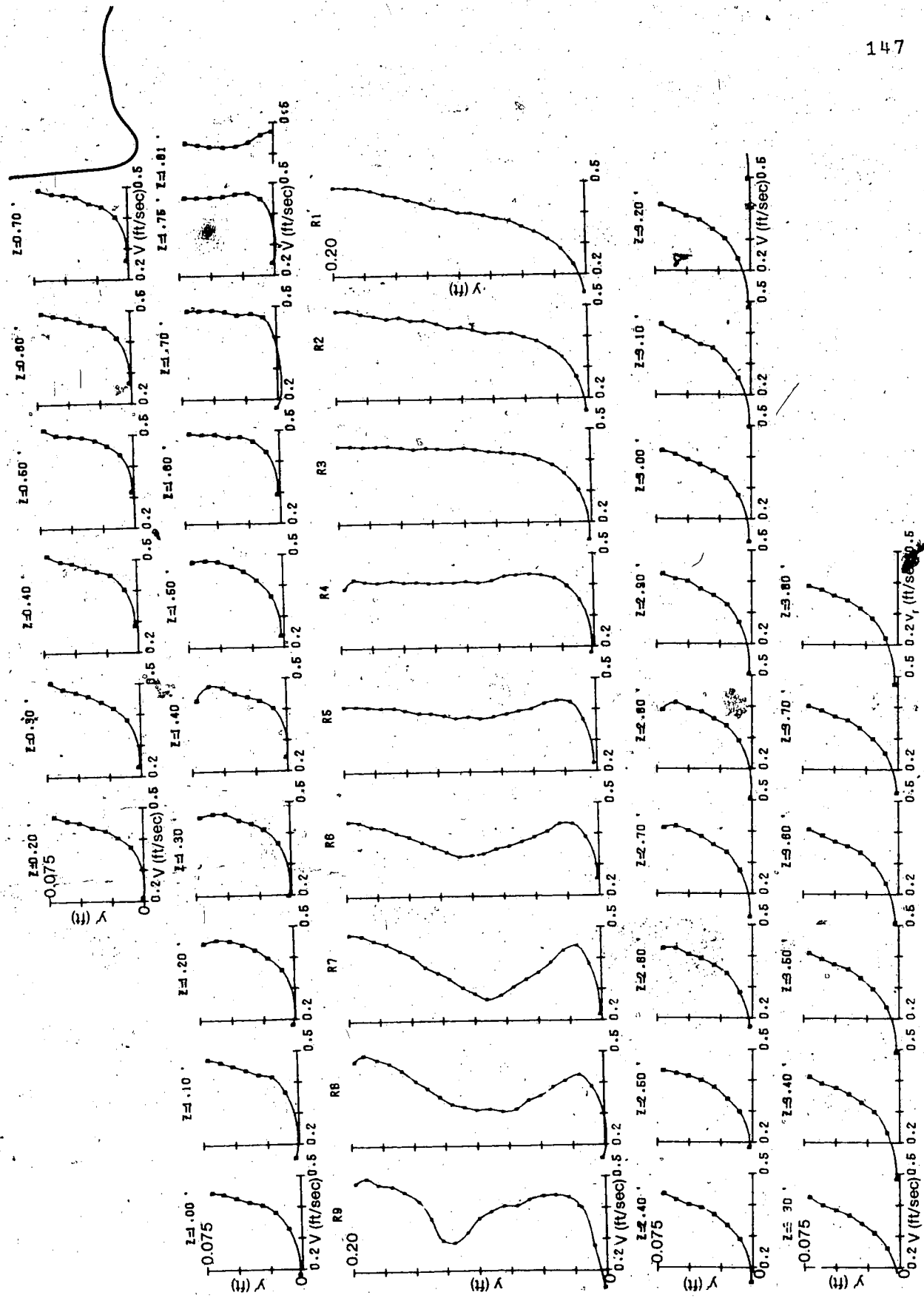Figure 5.13(13) Velocity Vector Profiles: Cross-Section No. 13

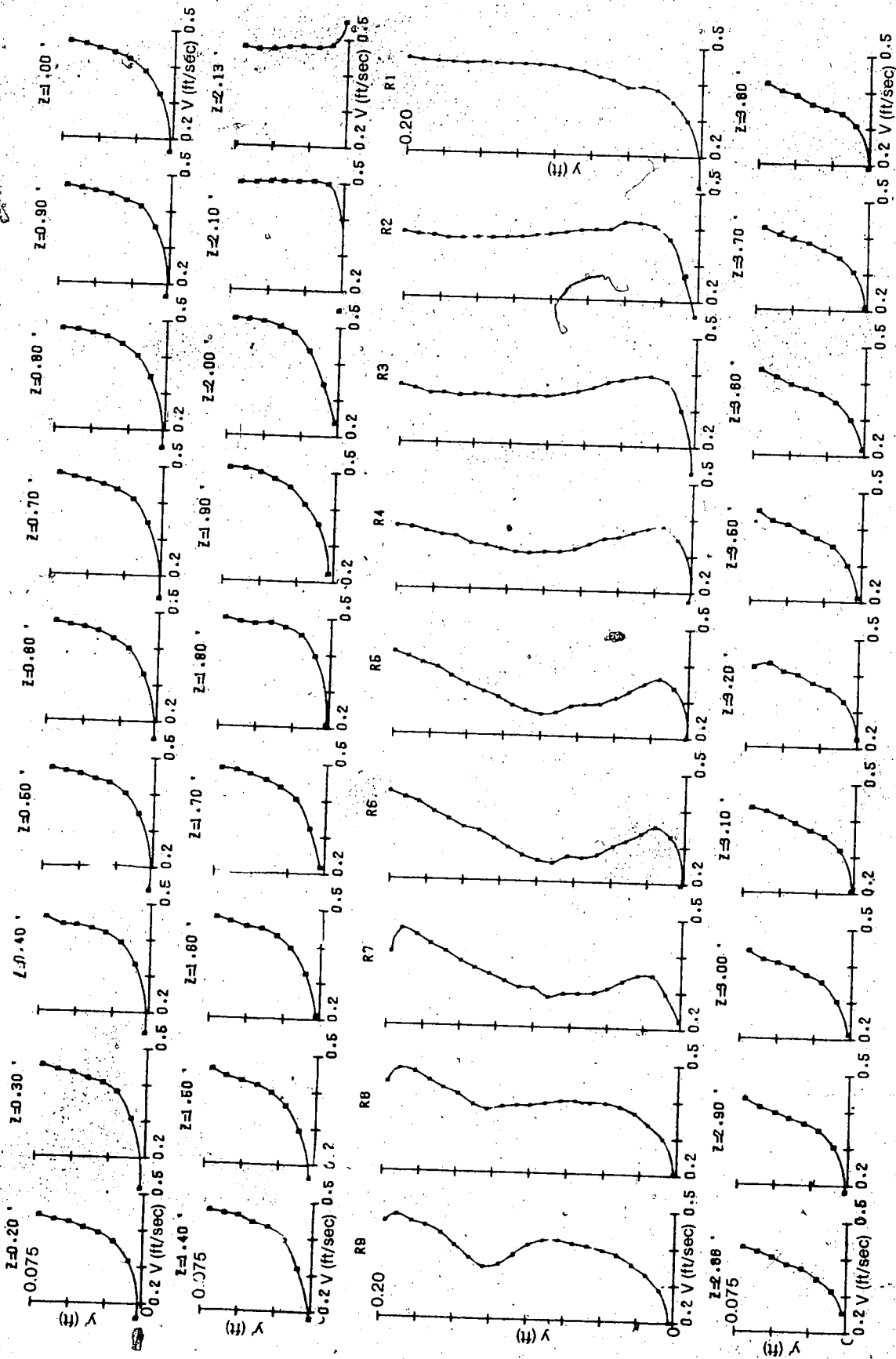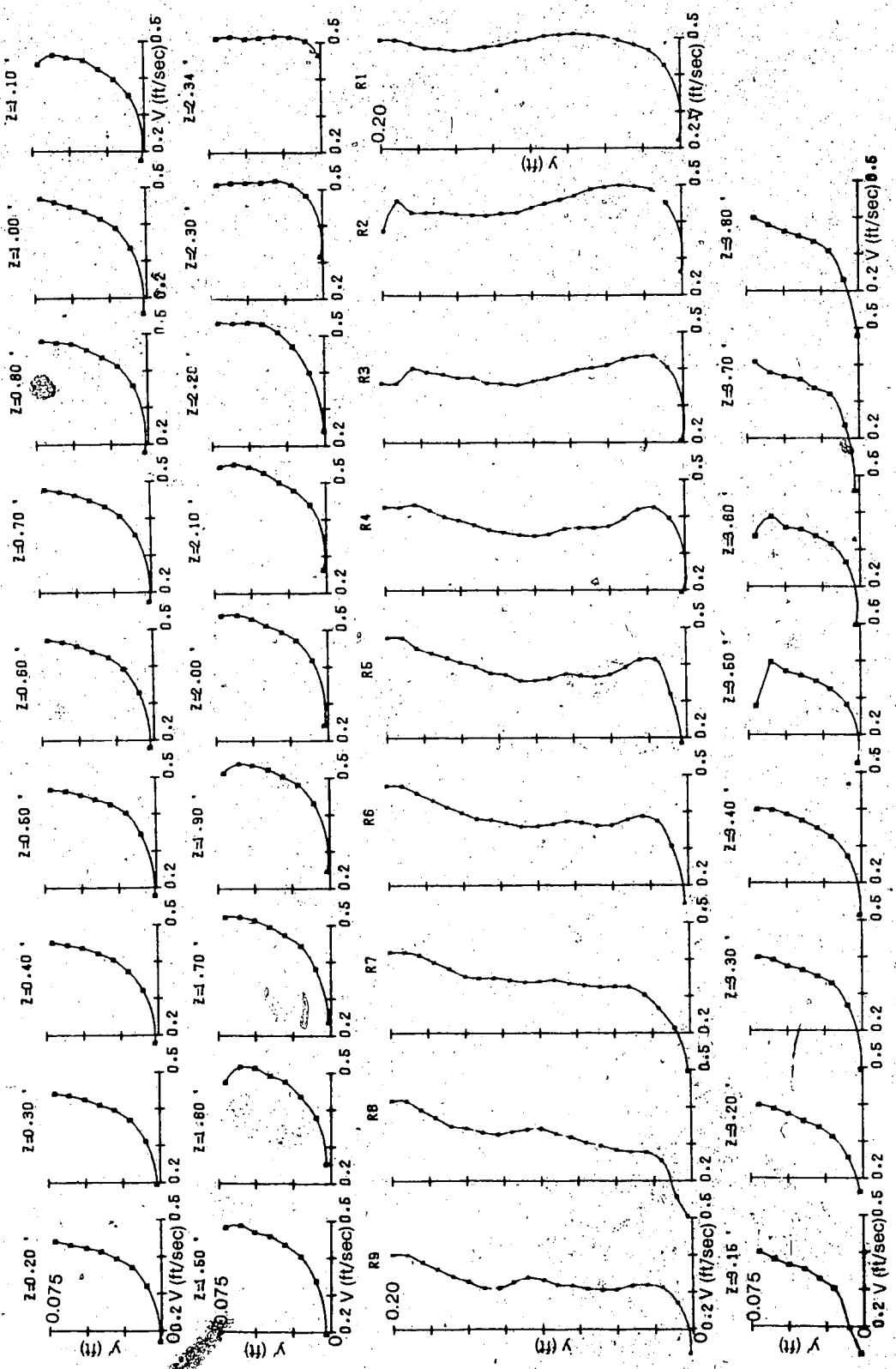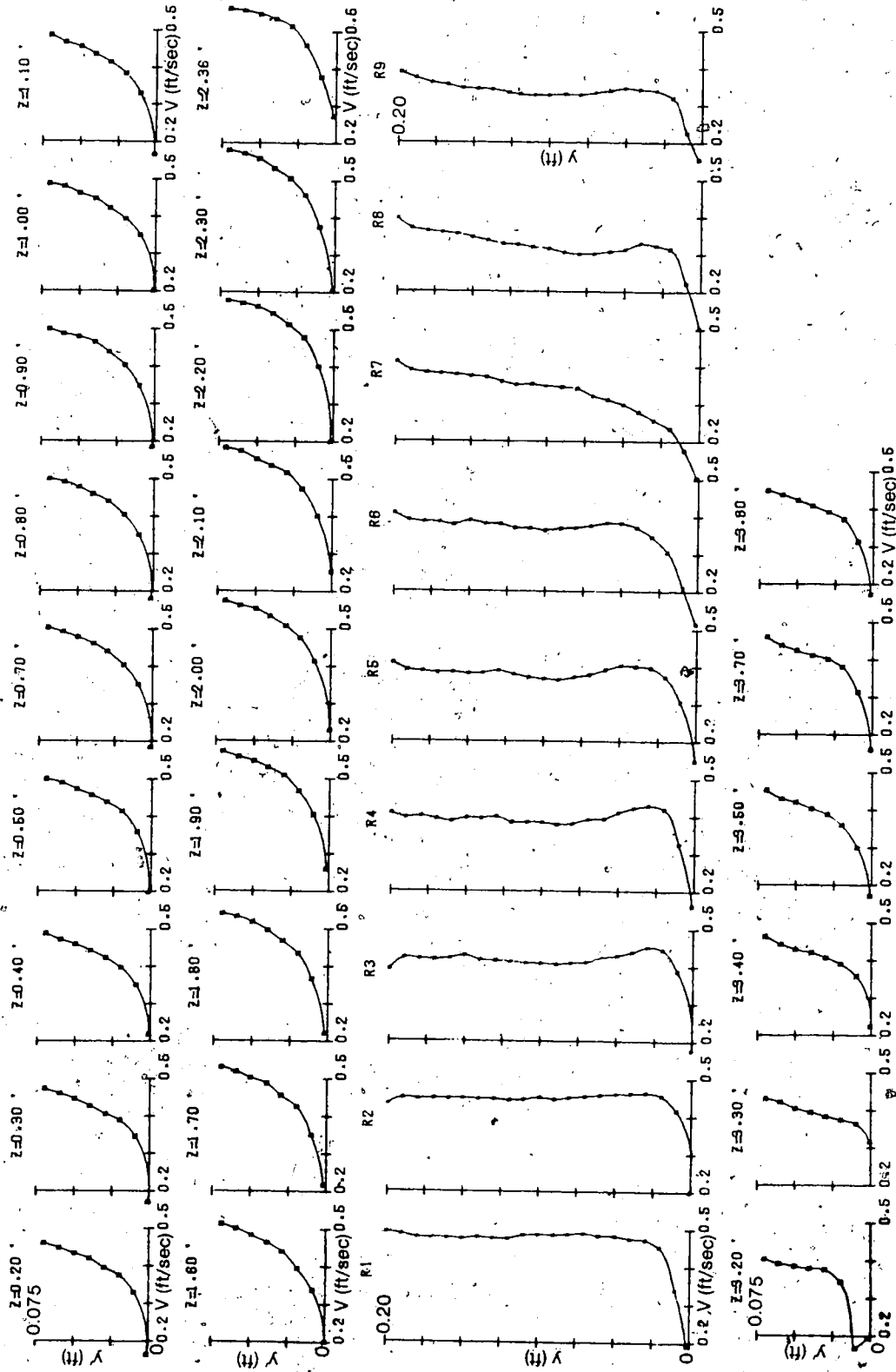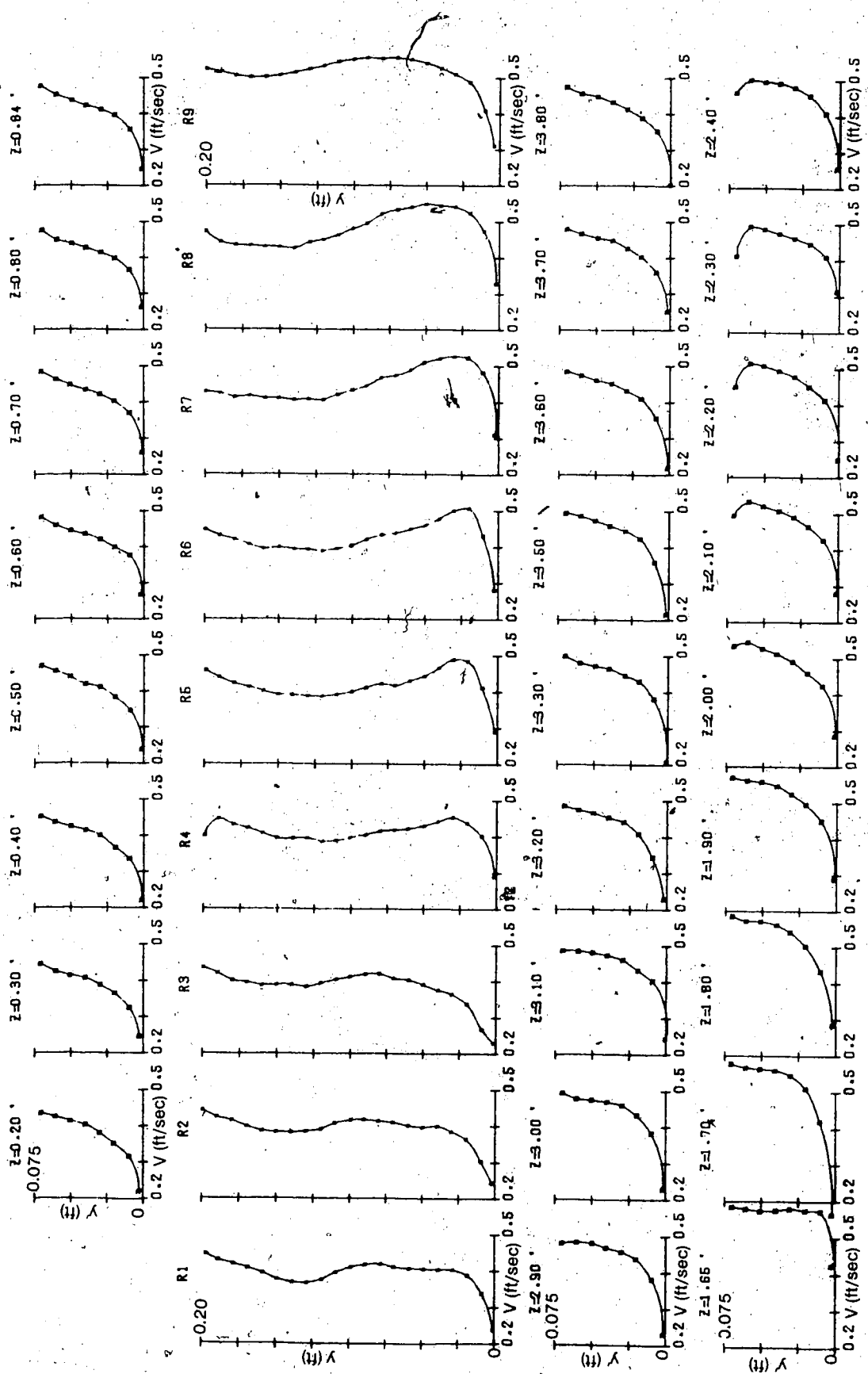Figure 5.13(14) Velocity Vector Profiles: Cross-Section No. 14

Figure 5.13(15) Velocity Vector Profiles: Cross-Section No. 15

Figure 5.14(1) Tangential Velocity Profiles: Cross-Section No. 1

Figure 5.14(3) Tangential Velocity Profiles: Cross-Section No. 3

158

Figure 5.14(5) Tangential Velocity Profiles: Cross-Section No. 5

Figure 5.14(6) Tangential Velocity Profiles: Cross-Section No. 6

Figure 5.14(7) Tangential Velocity Profiles: Cross-Section No. 7

162

Figure 5.14(8) Tangential Velocity Profiles: Cross-Section No. 8
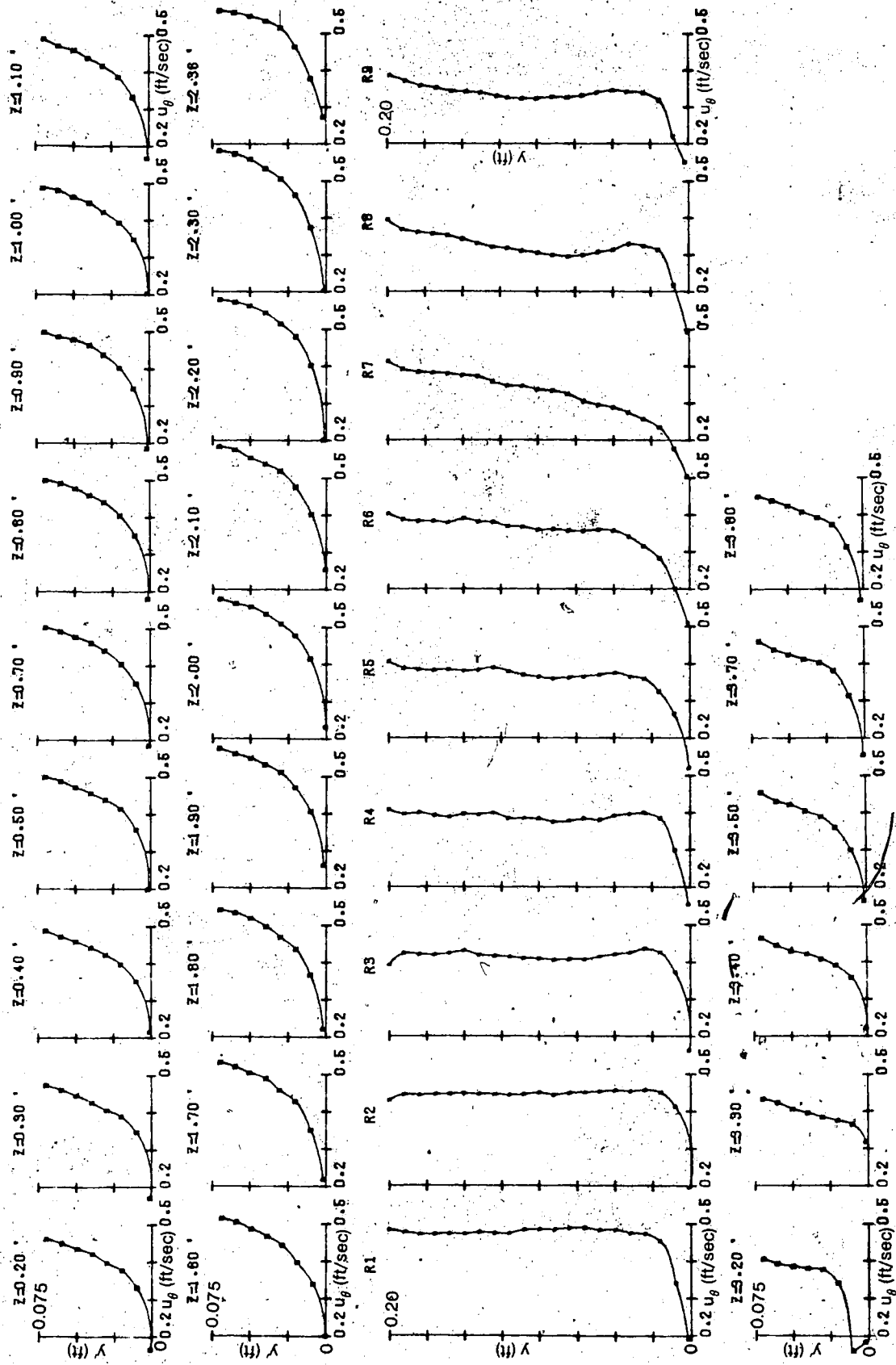
Figure 5.14(9) Tangential Velocity Profiles: Cross-Section No. 9
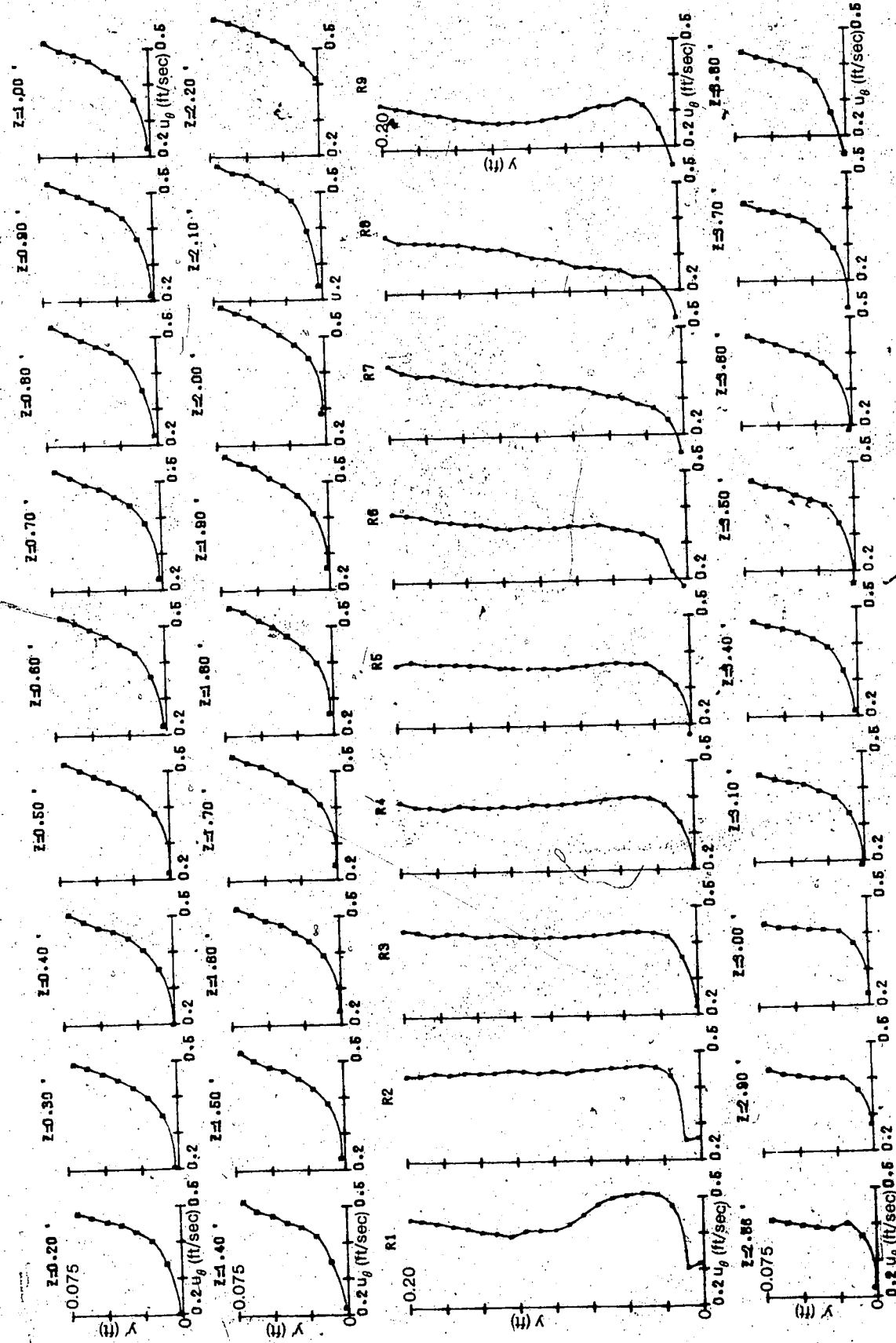
Figure 5.14(10) Tangential Velocity Profiles, Cross-Section No. 10
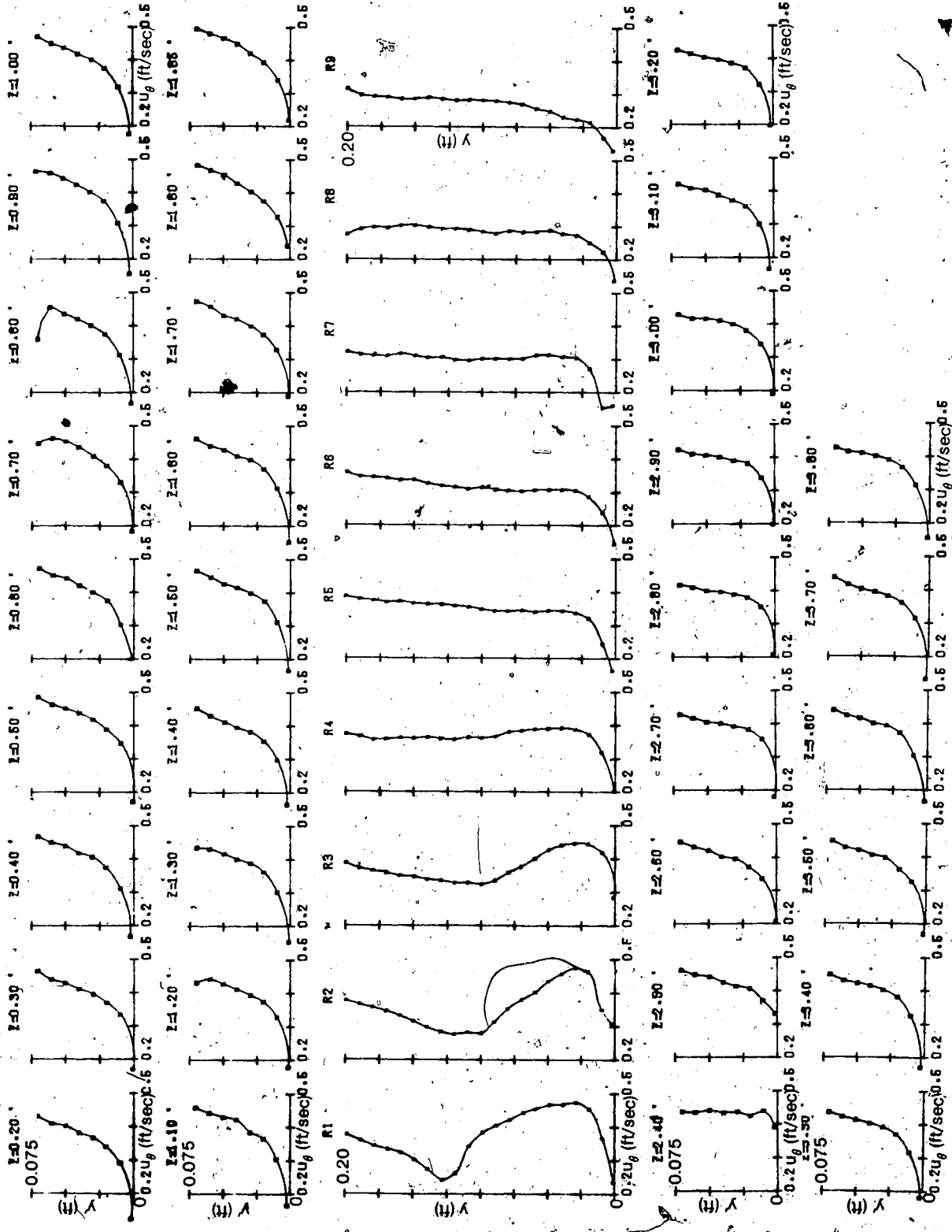
Figure 5.14(11) Tangential Velocity Profiles: Cross-Section No. 11
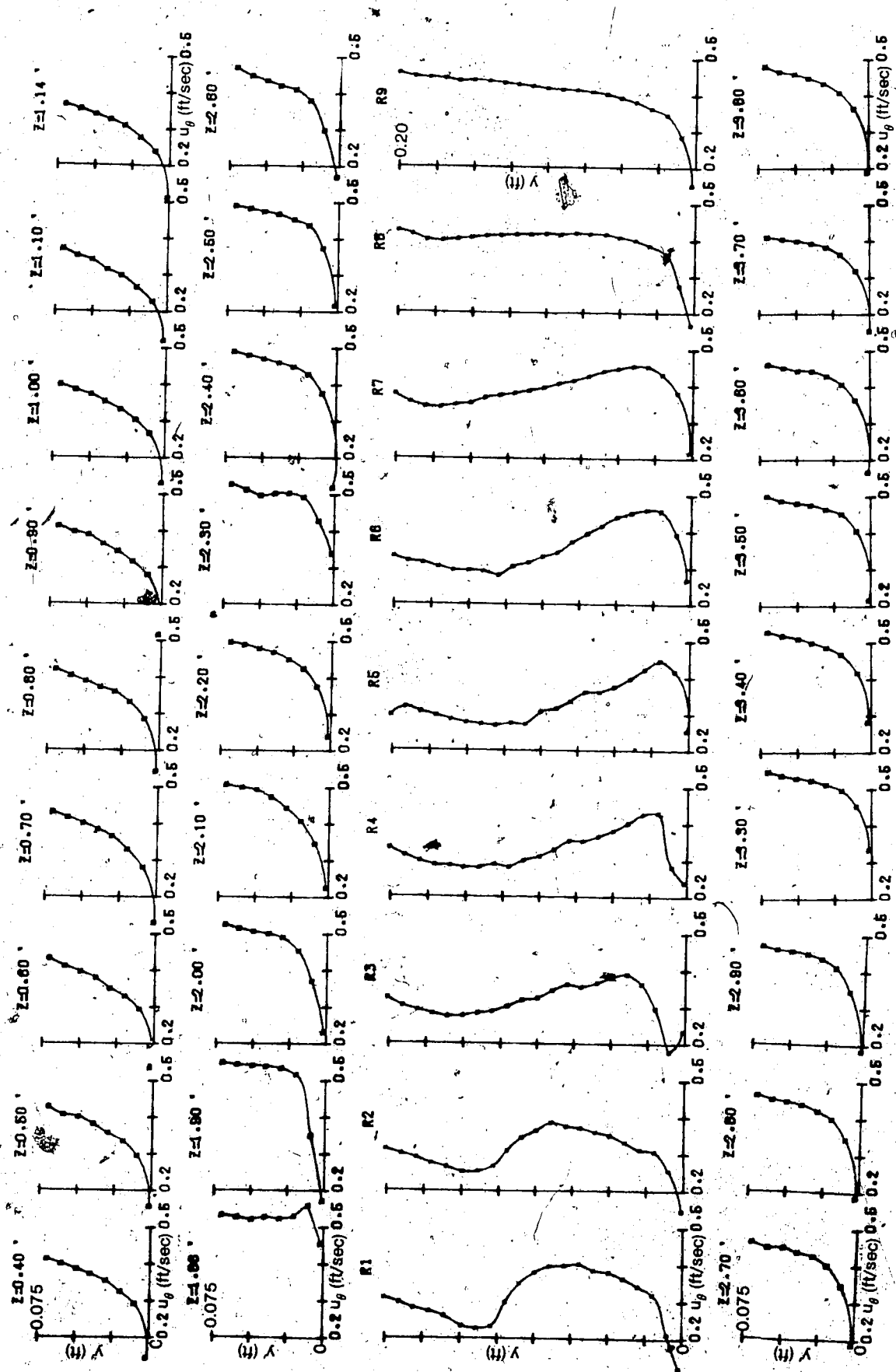
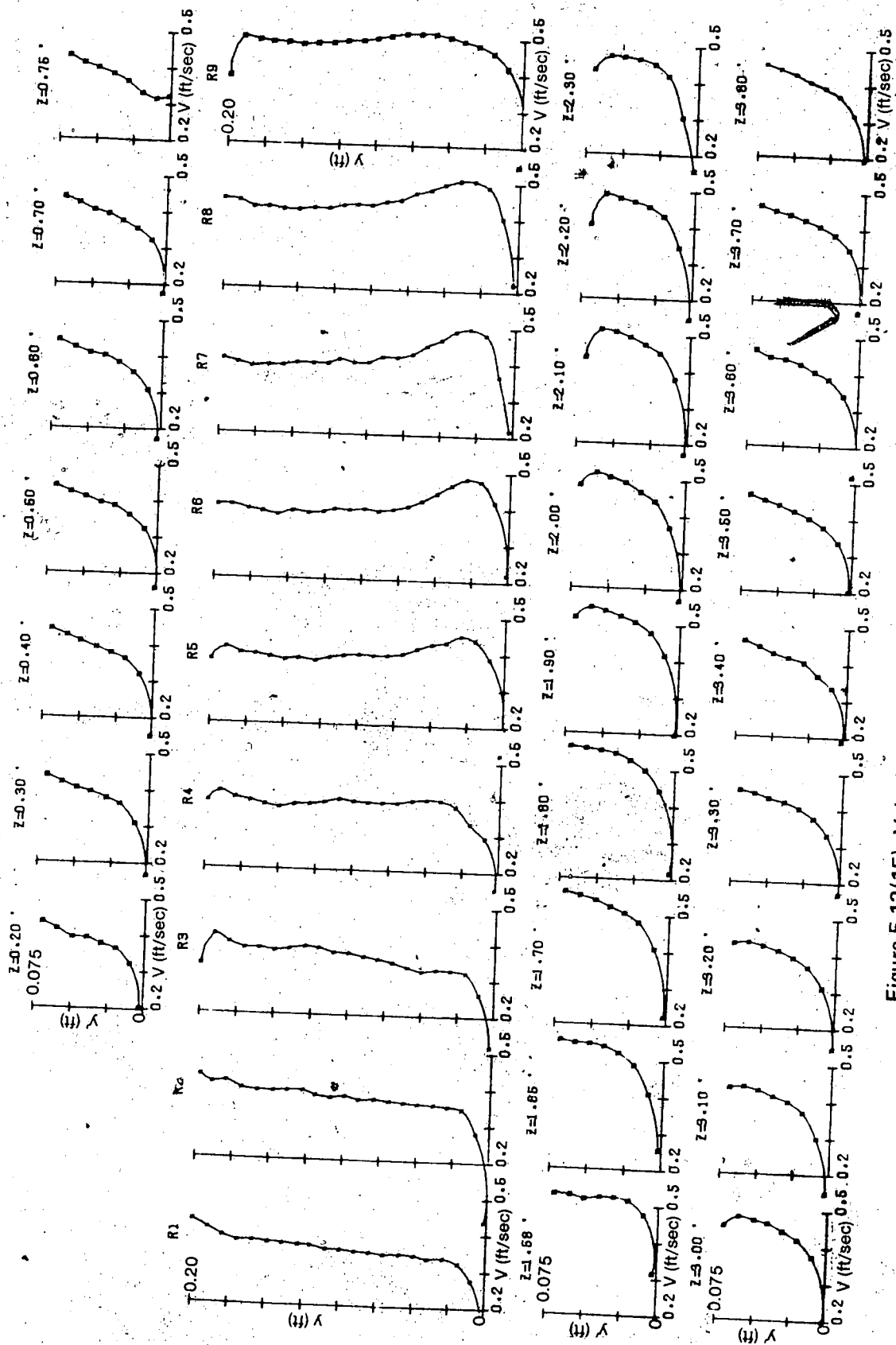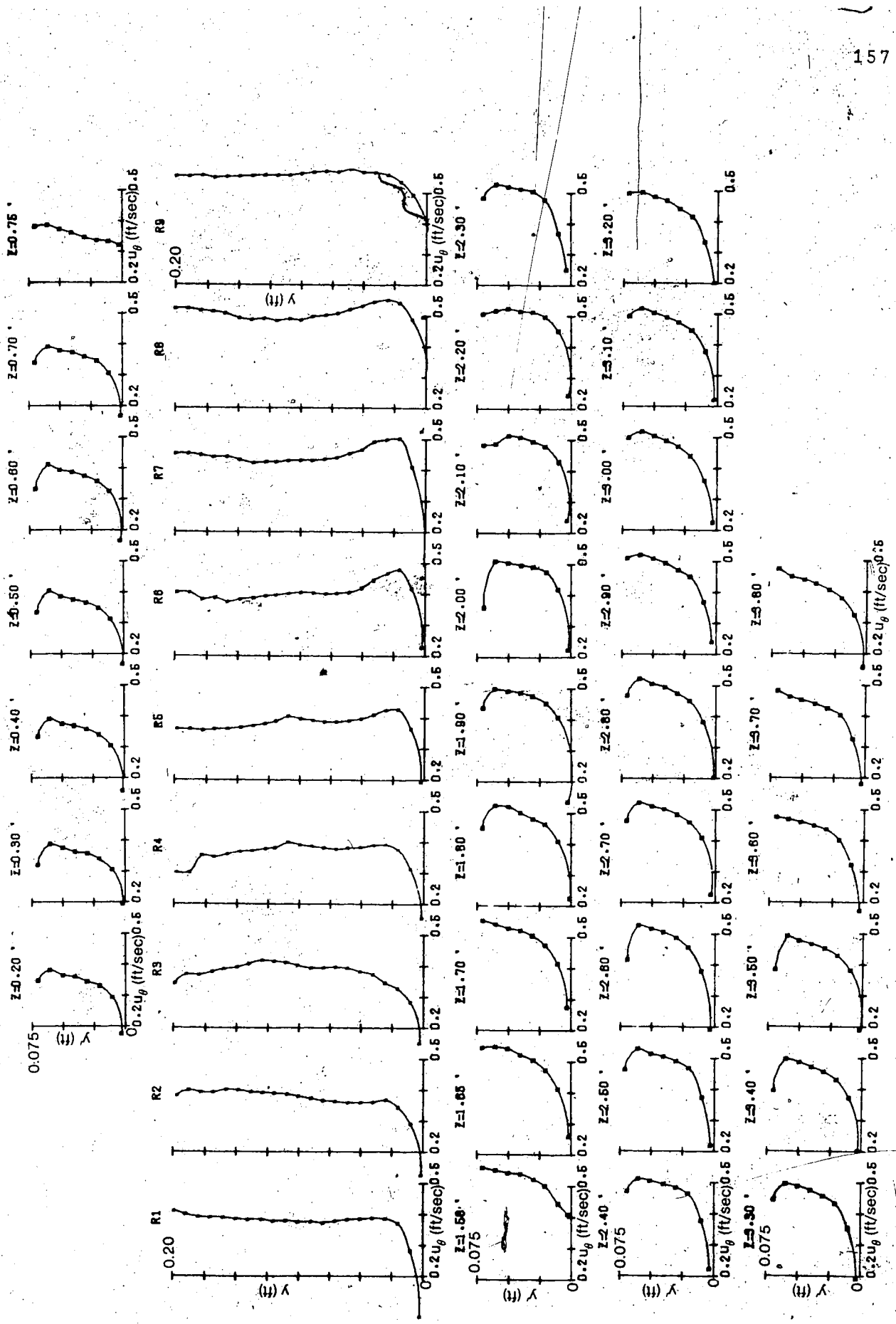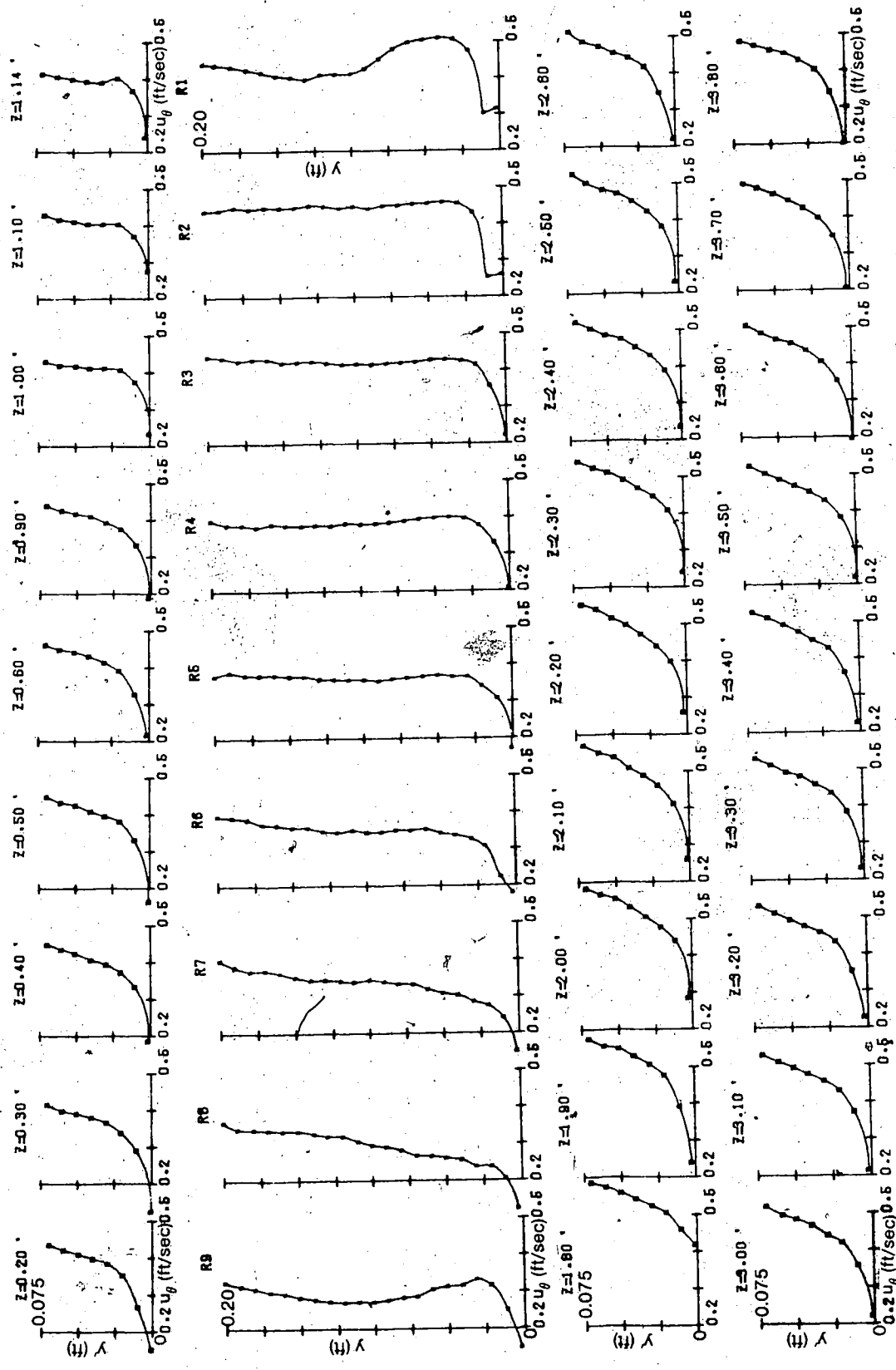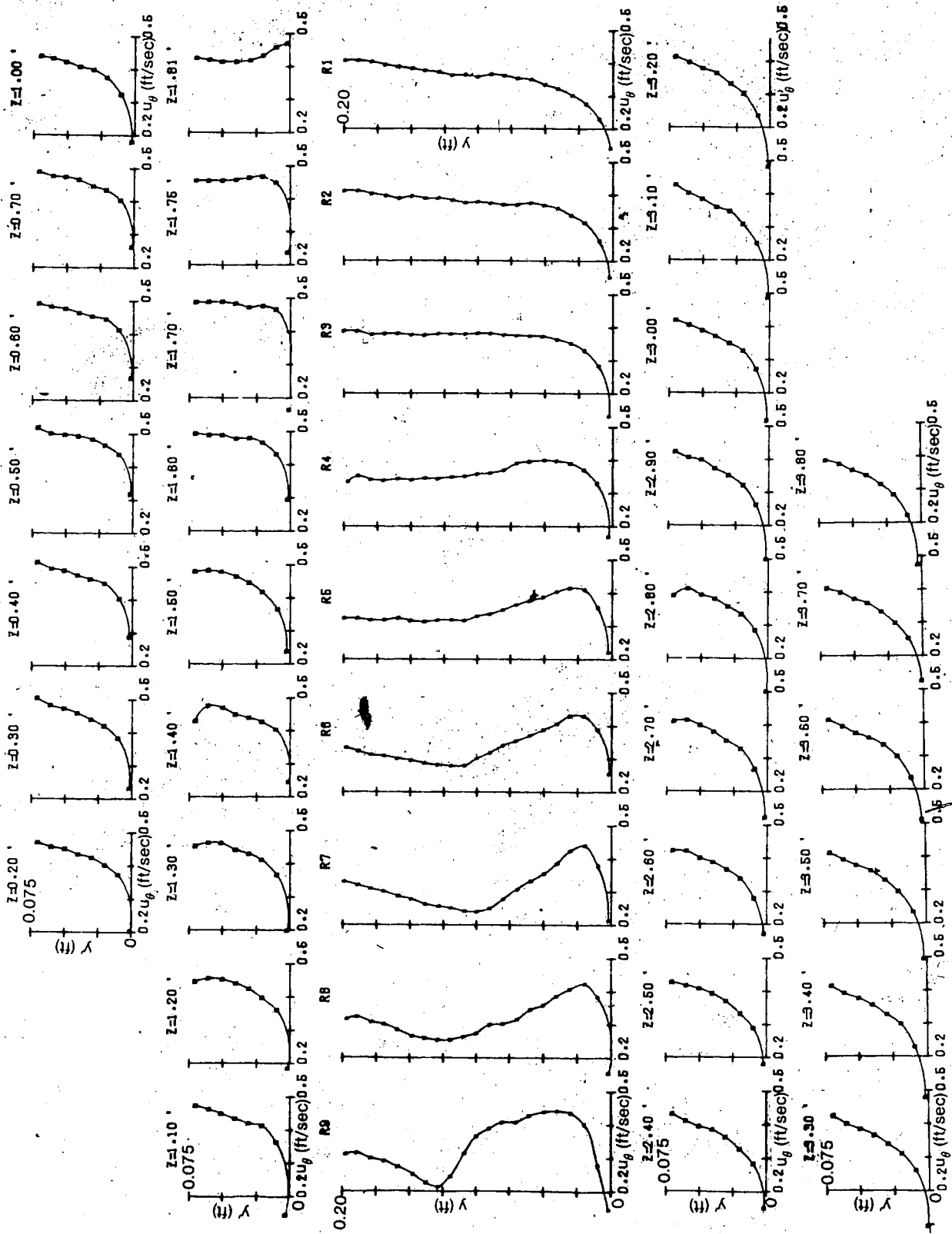Figure 5.14(13) Tangential Velocity Profiles: Cross-Section No. 13
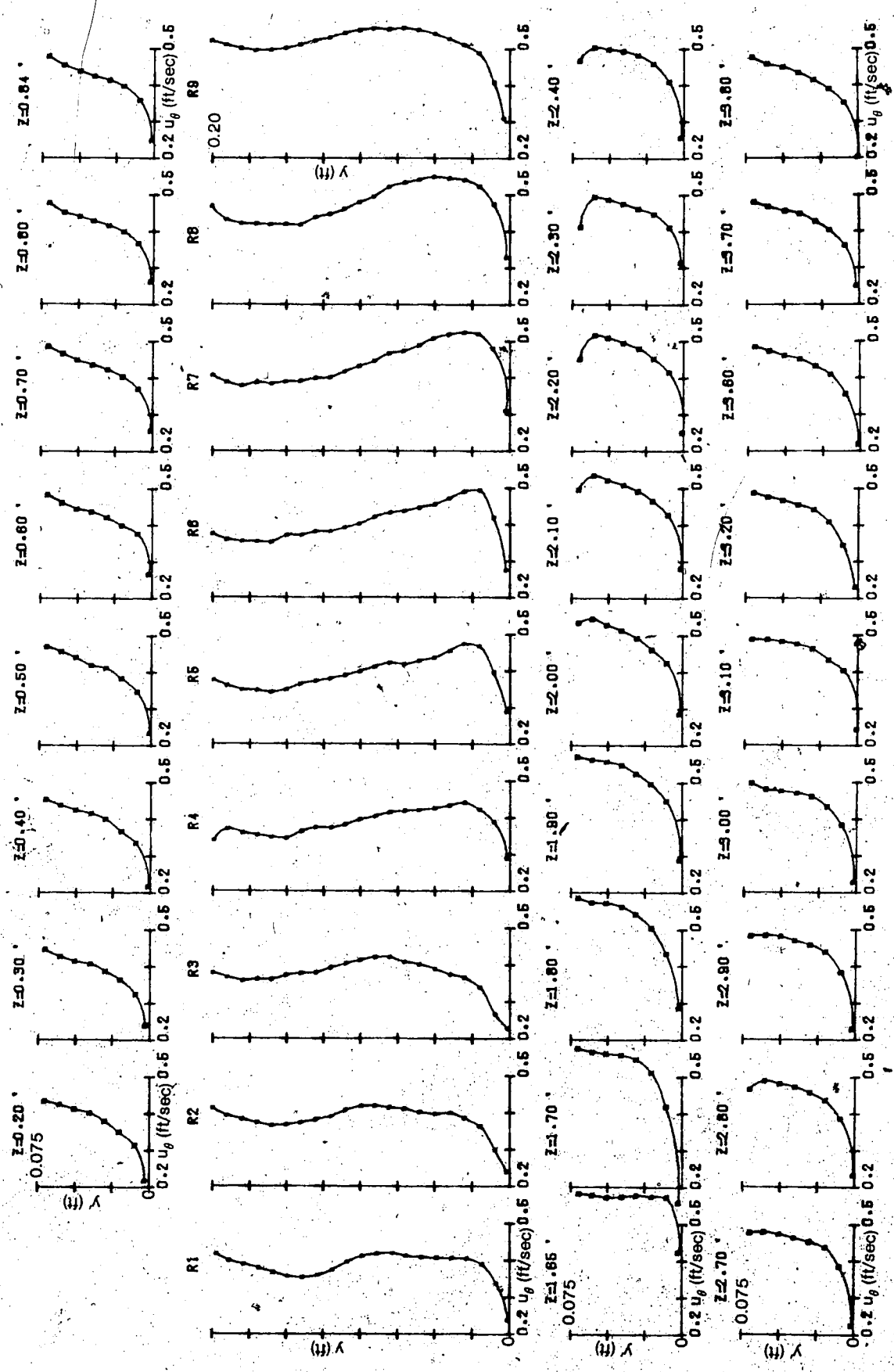
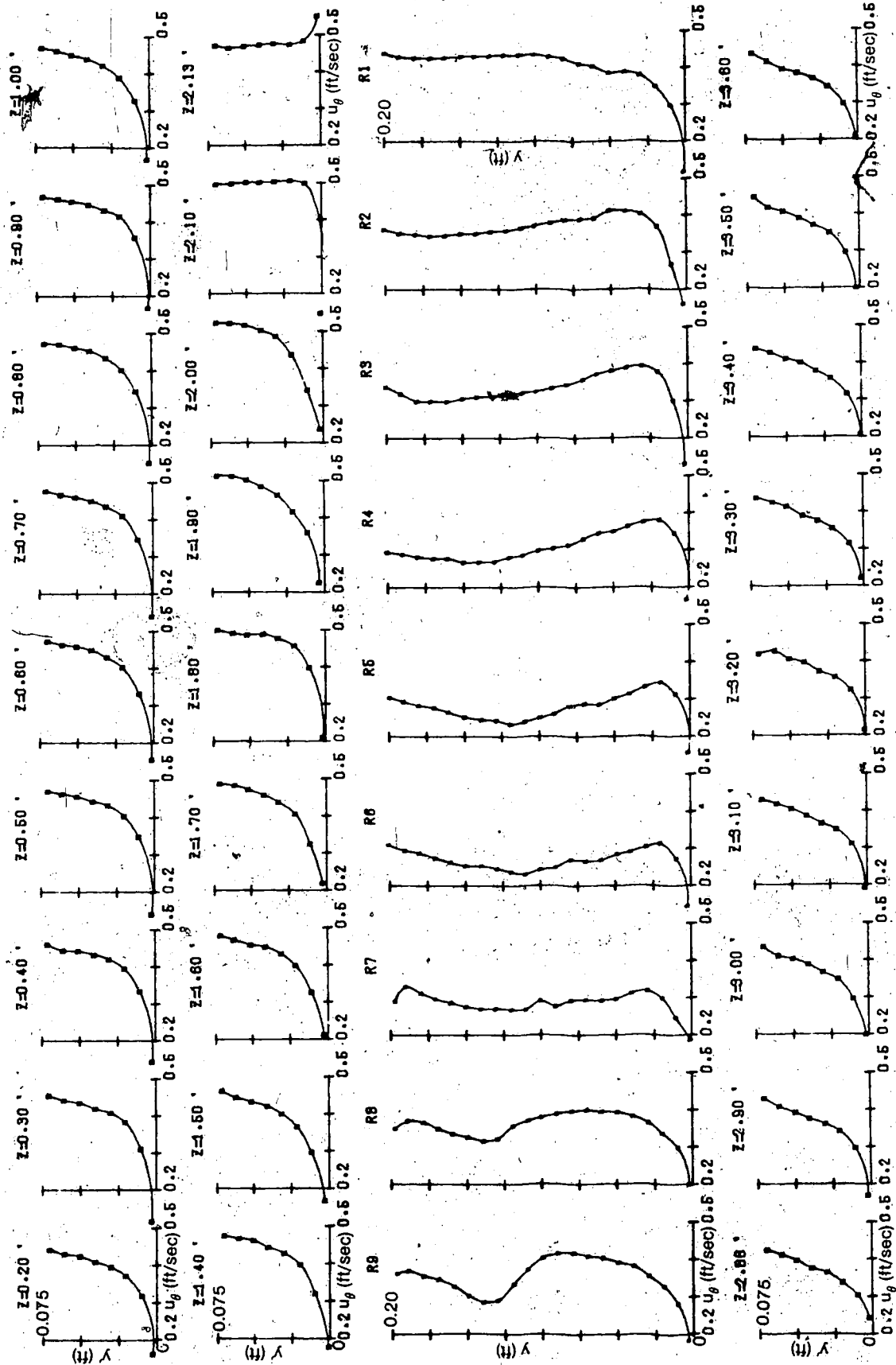Figure 5.14(14) Tangential Velocity Profiles: Cross-Section No. 14
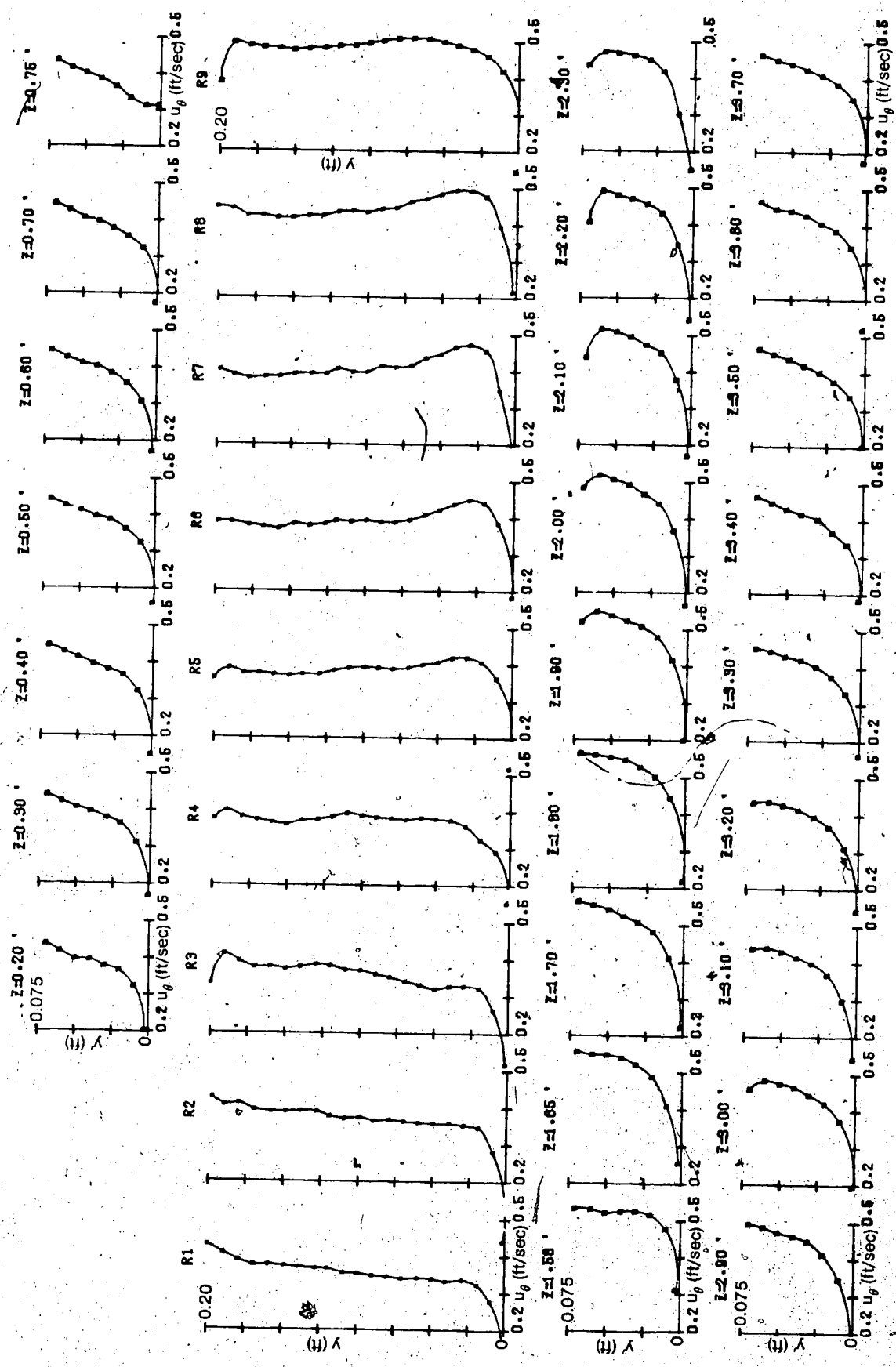
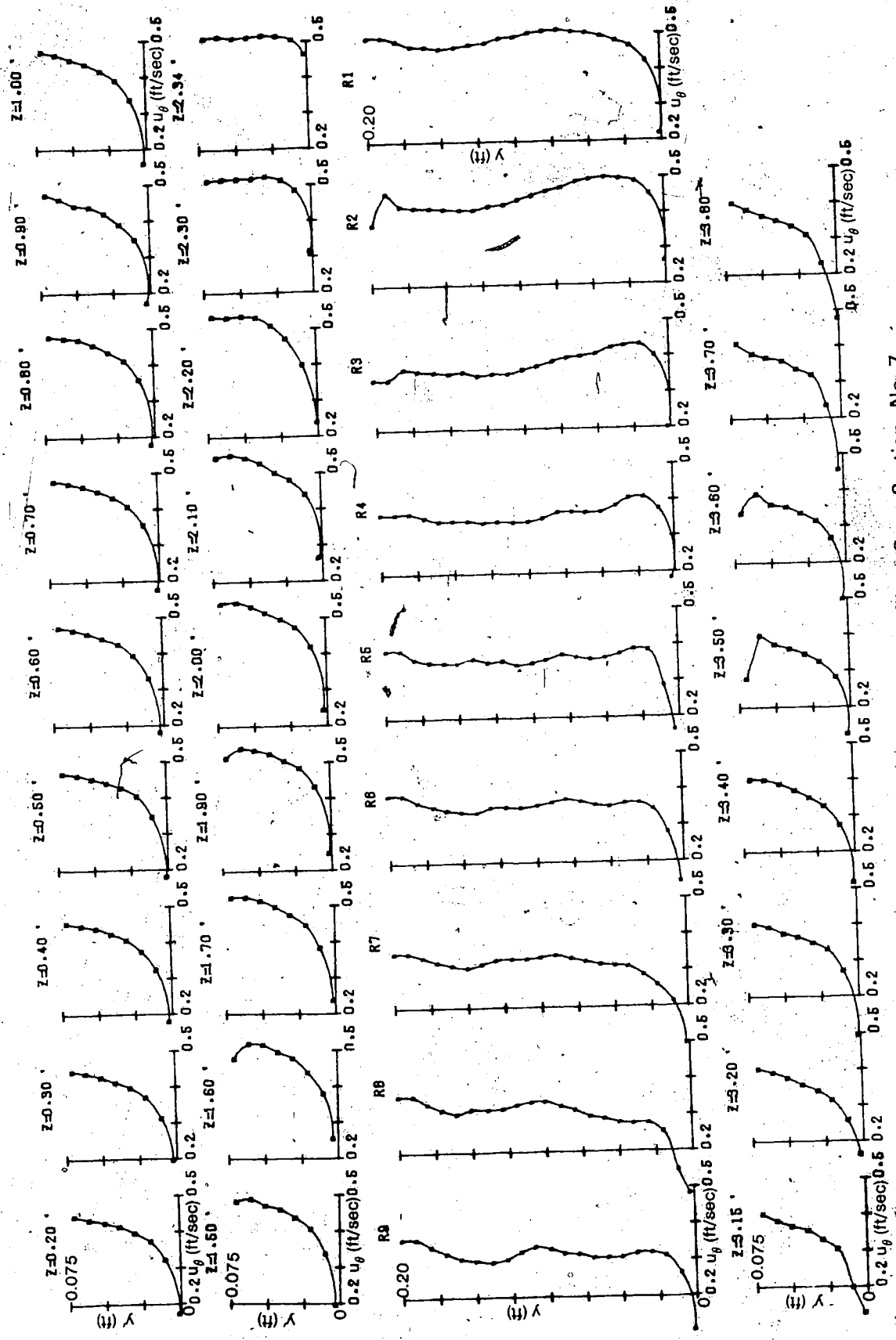Figure 5.14(15) Tangential Velocity Profiles: Cross-Section No. 15
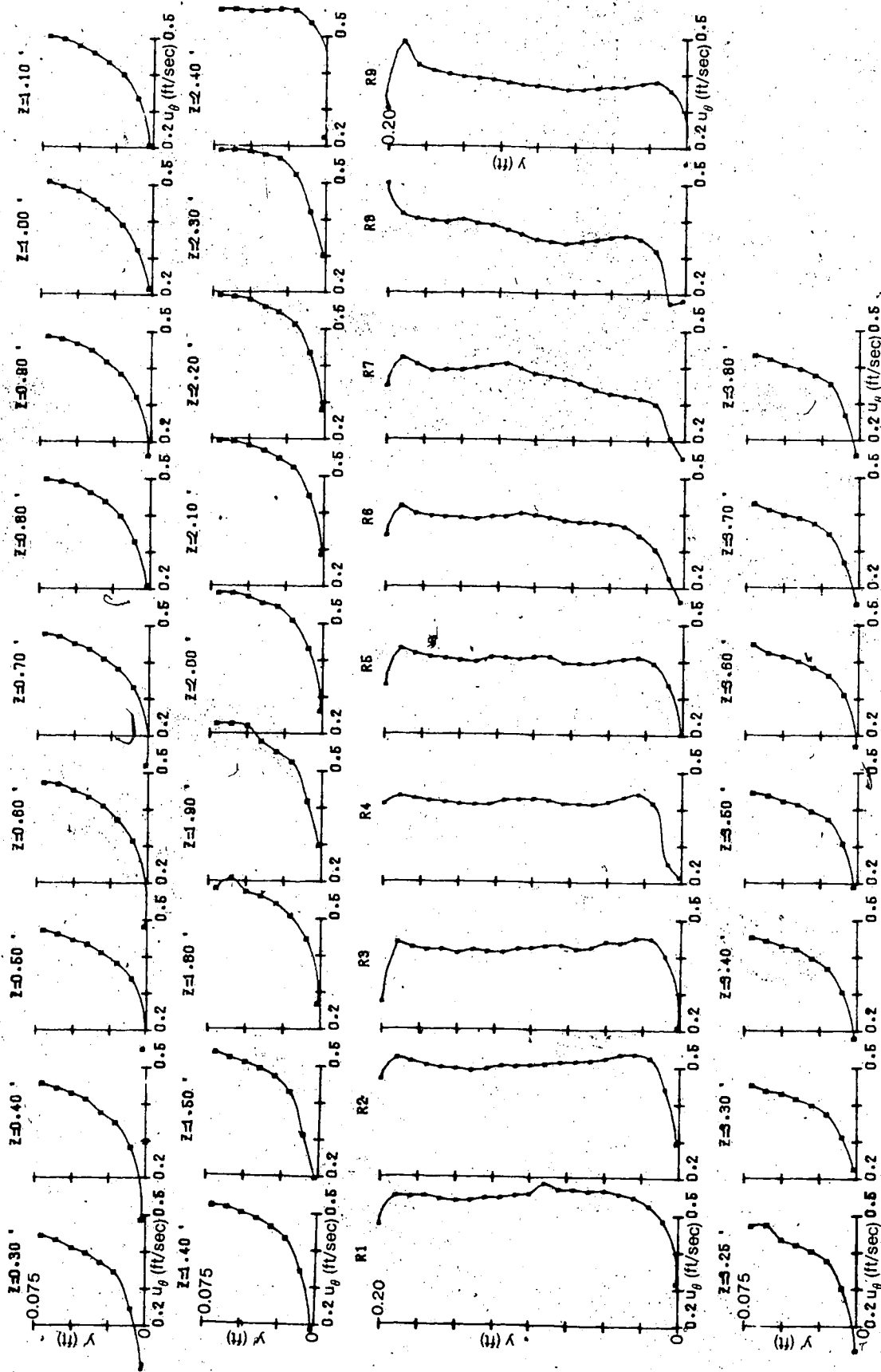
168

from the side wall in the main channel for cross-sections number 1 to 15 . One could clearly see from the profiles in Figures 5.11(1) to 5.11(15) that the angle of the velocity vector with respect to the local tengential direction $\bar{\theta}$, varies a little for the lower part of the flow (y=0.0 to h), but for the upper part of the flow (y=h to water surface), $\bar{\theta}$ varies in such a way that the velocity vector is parallel to x axis. For example, for R1 in Figure 5.11(3), where the cross-section is located at 30 degrees with respect to z, $\bar{\theta}$ has value of a few degrees when y=0.0 up to 0.1 feet and suddenly $\bar{\theta}$ increases to a constant value of about -30 . degrees from y=h=0.125 feet to n=0.20 feet.

It can be seen from Figure ▒▒▒ that the component of the velocity vectors in z direction (w) in the flood plain channel are negligible except in the region near the main channel which is affected by the secondary current in the. meandering channel.

Since the upper part of the flow in the meandering channel is flowing almost parallel to the x axis, the magnitude of v_r is very small whereas in the lower part of the main flow, the magnitude of v_r reaches up to 40 percent of the velocity vector.

The tangential and vector velocity profiles in the flood plain channel were replotted with u/u_* versus $\log \frac{y u_*}{\nu}$, where u simply replaced V and u_θ because there were no difference between the two velocities. From these plots (these are not presented here), it was found that the velocity distribution agreed well with the well known Karman-Prandtl equation (Schlichting, 1968) for a smooth

boundary:

$$\frac{u}{u_*} = 5.75 \log\left(\frac{y' \, u_*}{\nu}\right) + 5.5 \qquad\qquad (5.9)$$

even for the region near the main channel. It was noticed that near the free-surface there was a dip in the velocity profile (Rajaratnam & Muralidhar, 1968).

Figures 5.13 and 5.14 show that V and u_θ increase with y, the distance from the bed of the meandering channel rather rapidly and then assume an almost constant value up to the flood plain level. From this point on, if the profile is close to the outermost wall, the velocity decreases continuously to eventually become approximately constant near the water surface. Likewise, if the profile is near the innermost wall, the velocity increases continuously to become constant near the water surface. This behavior was noticed in the straight main channel with straight flood plains (Chapter III and IV).

From the above figures it was concluded that separating the effect of the momentum exchange due to the compound cross-section from the one due to the effect of the curved channel is difficult, if possible at all. A comparison of u(y) for flow with and without the flood plain shows a little difference for the lower part of the profile. For the upper part, above the flood plain level, as we should expect from the experience in straight channel, it should have a dip with approximately a constant velocity for each vertical profile. The dips in meander flows are not similar to the dips in the straight compound channels.

Figure 5.15 shows the lateral distribution of the tangential velocity $(u(z))$ for run number 1 at different levels above the flood plain (y'). For run number 2, $u_\theta(z)$ is presented for $y' = 0.05$ feet (1.5 cm) is shown in Figure 5.16. From Figure 5.15 it can be seen that u_θ increases with z, the distance from the side wall of the flood plain until it reaches almost a constant value. Due to the interaction between the curved channel and the flood plain, u_θ increases to a maximum value at the innermost junction plane between the main channel and flood plain. The tangential velocity in the main channel decreases rather rapidly toward the outermost junction plane between the meandering channel and flood plain channel. At the outermost junction plane, one could see a small increase in u_θ in the interaction zone, but eventually u_θ approaches a constant value and then will again decrease as the bank of the flood plain is approached. Due to the uniformity of the velocity profile in the upper part of the flow $(u_\theta(y))$, the curves of the lateral distribution of u_θ in the main channel for different levels above the flood plain level are the same.

Figures 5.15 and 5.16 clearly show that the velocity near the edge of the main channel and the flood plain has been increased because of the effect of the interaction between the two channels. As can be seen, the lateral distribution of the velocity over the flood plain on both sides of the main channel is not the same. On the convex side, over the flood plain, the velocity steadily increases up to the crest of the meander. Then it decreases until it reaches the meandering channel. However, the flow velocity
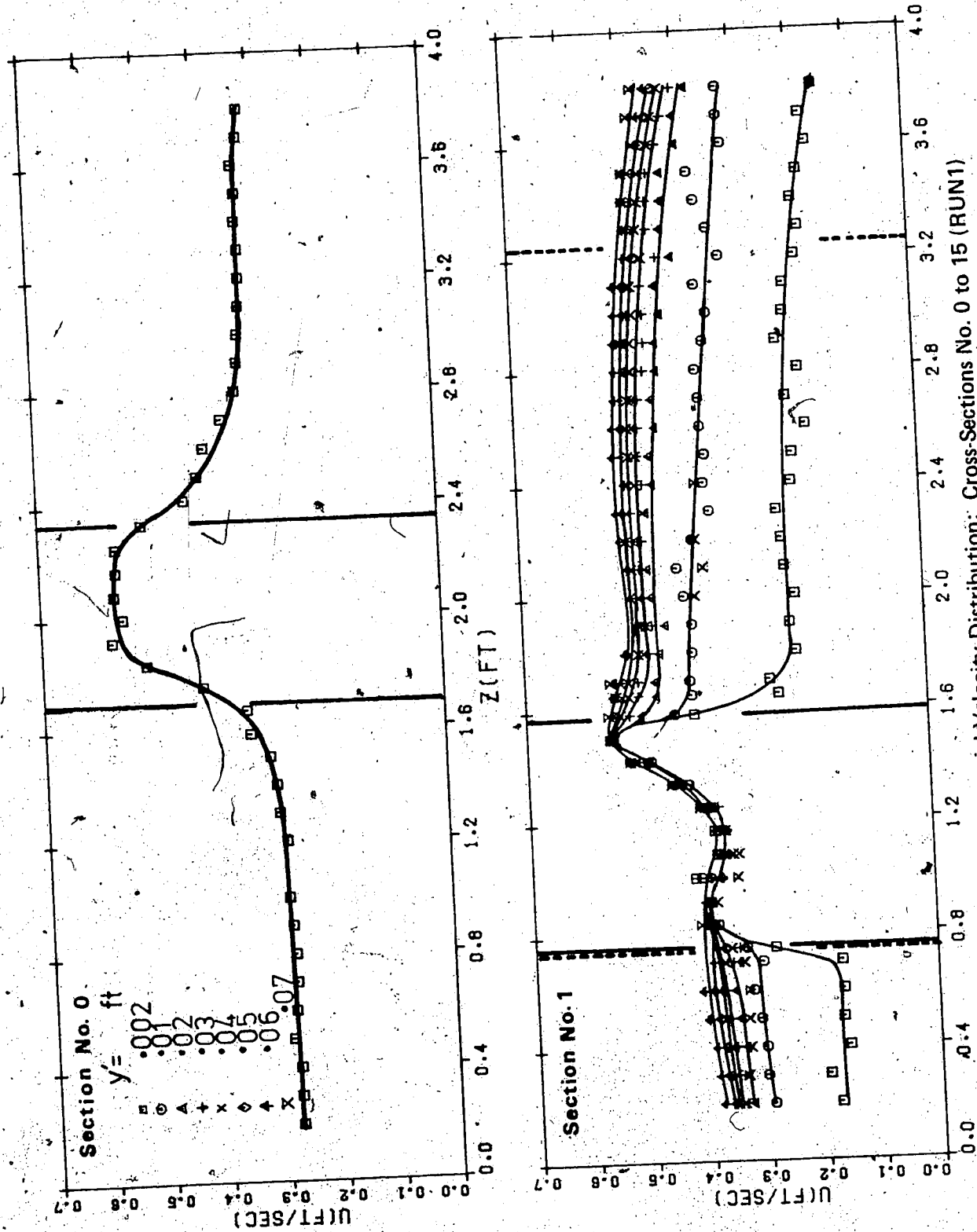
Figure 5.15 Lateral Tangential Velocity Distribution: Cross-Sections No. 0 to 15 (RUN1)

Figure 5.15 Continued

173

Section No. 7

Section No. 8

Figure 5.15 Continued

Section No.9

Section No.10

Figure 5.15 Continued

Section No.11
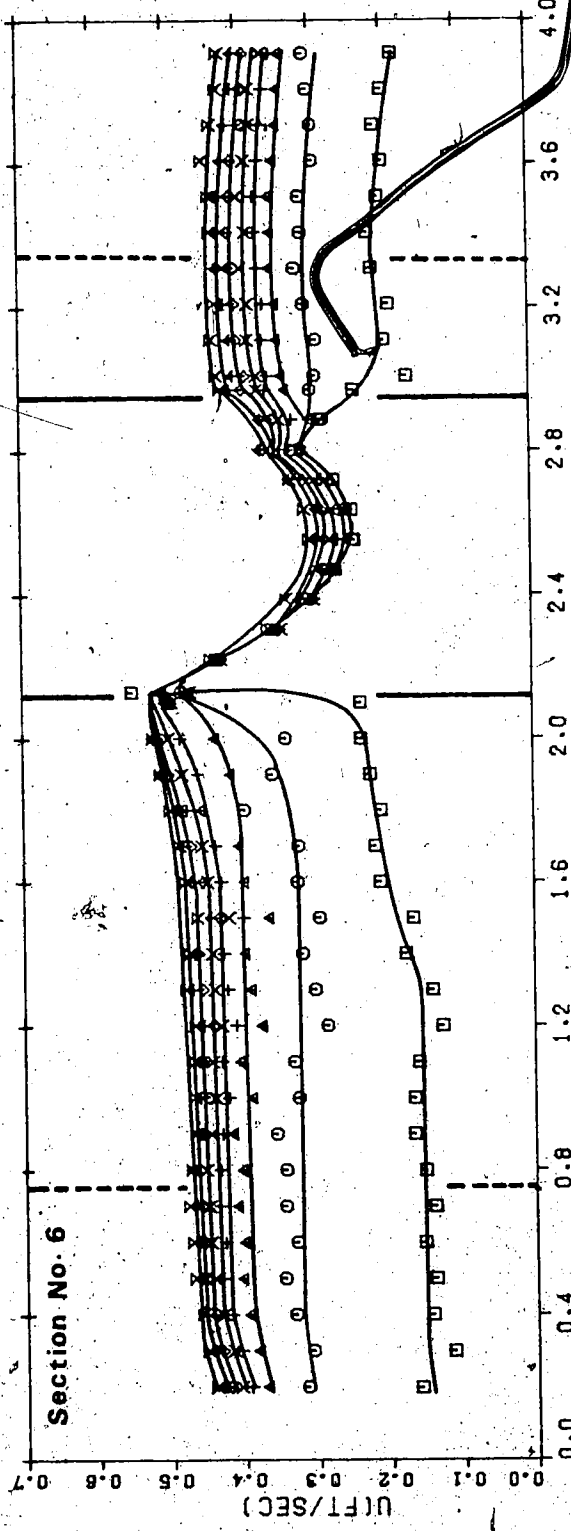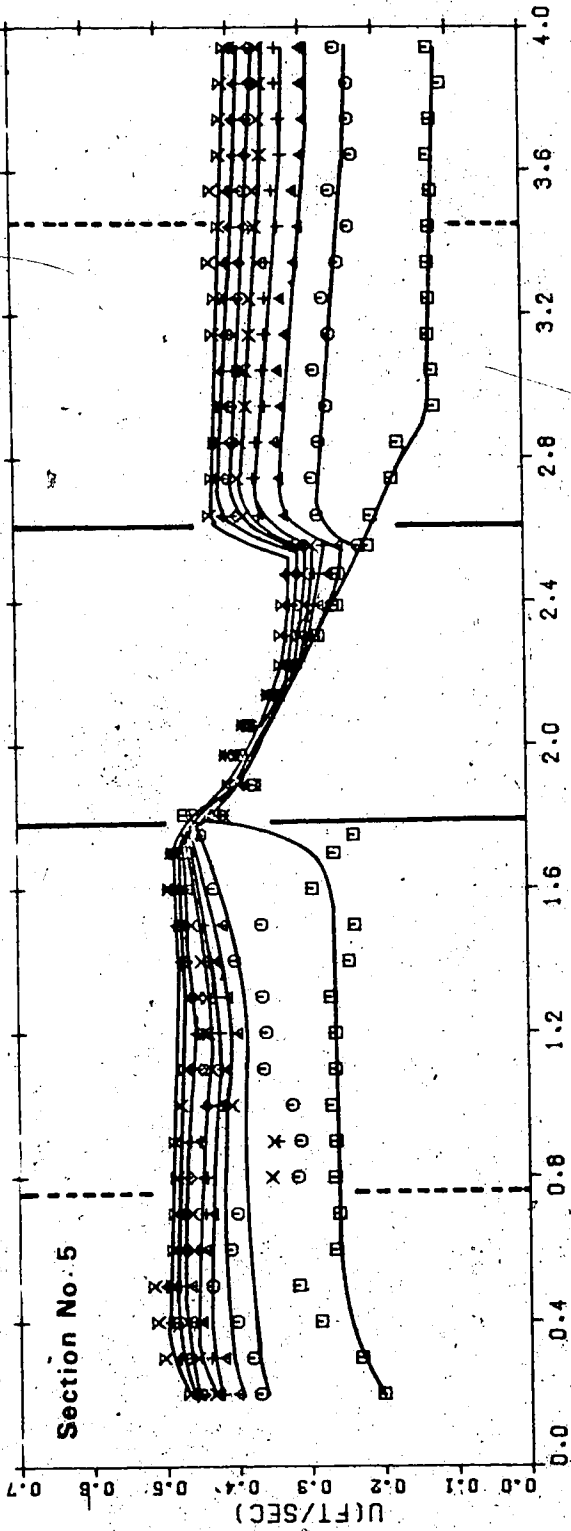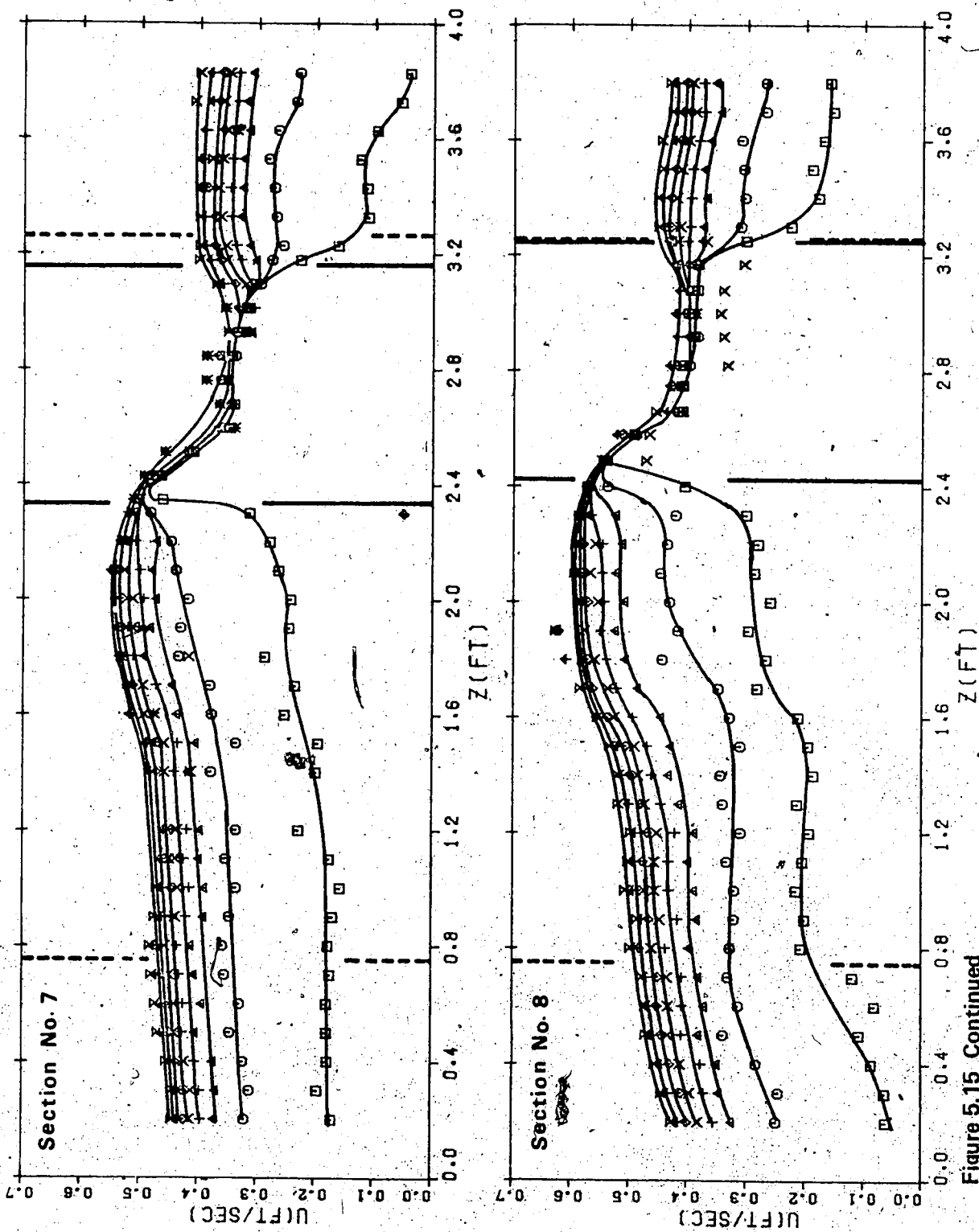
Section No.13

Figure 5.15 Continued

Figure 5.15 Continued
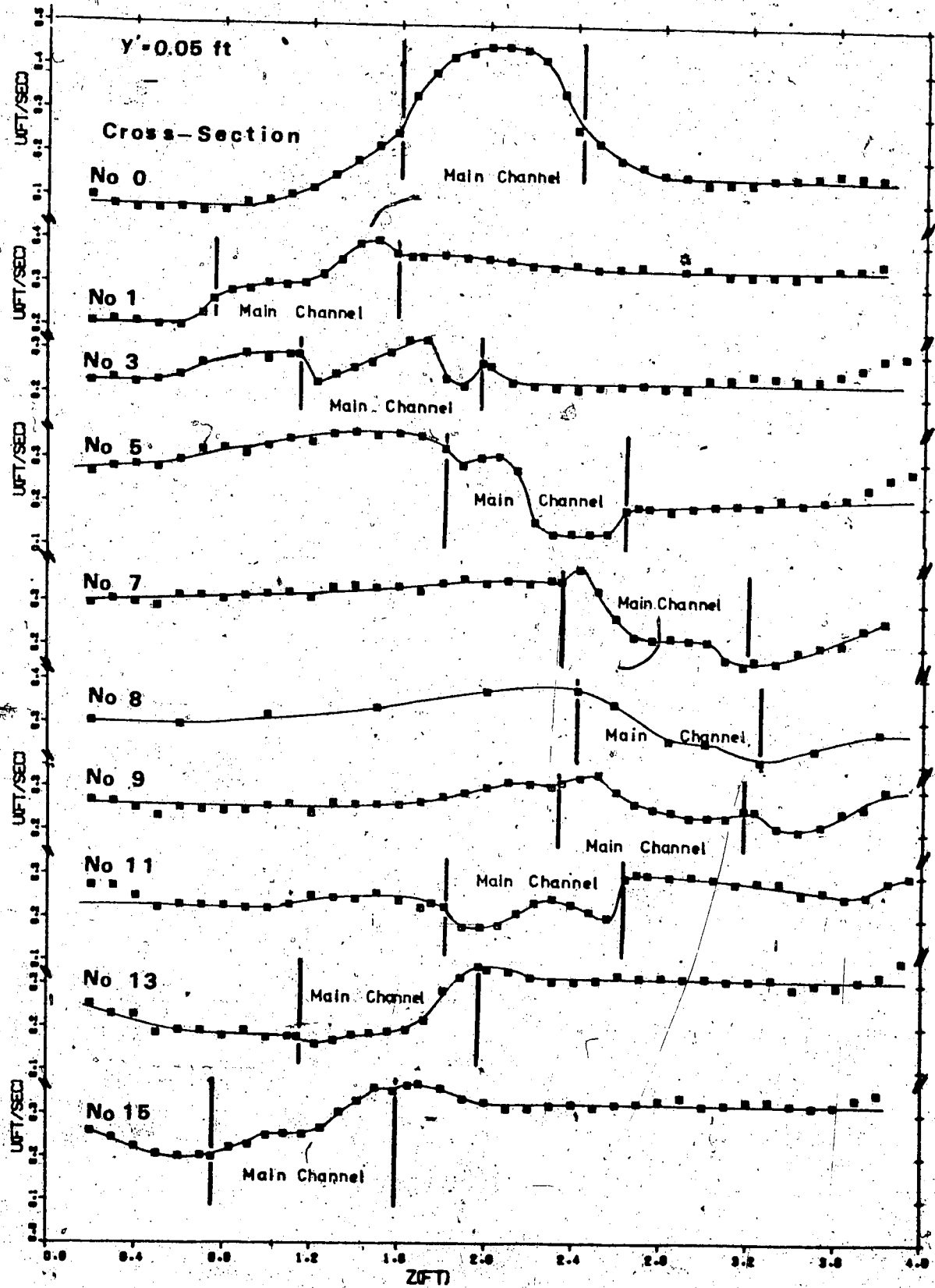
Figure 5.16 Lateral Tangential Velocity Distribution: Cross-Section No. 1 to 15 (RUN2)

over the flood plain on the convex side is always higher than on the concave side. Therefore, it was decided to draw isovel maps for different levels.

From Figure 5.11, which reveals the distribution of $\bar{\theta}$, one can conclude from the sudden change of $\bar{\theta}$ at $y=h$, that the velocity vector direction is changing from its direction in the main channel to becoming almost parallel to the x axis at the flood plain elevation. The sudden change of the direction and the magnitude of V suggests there is a rotational shear as well as a parallel shear in the horizontal (parallel to the meandering bed) plane.

5.6.2 Cross-Sectional Isovel

For cross-section numbers 1 to 15, maps of isovels for the tangential velocity were prepared. These cross-sectional isovel maps are shown in Figure 5.17. These maps show two important mechanisms of the flow.

Firstly, in the main channel below the flood plain level, the higher velocity will occur near the convex side (the innermost wall) at the beginning of the bend and will shift toward the concave (outermost wall) with increasing θ. Nevertheless, it will never occur close to the concave wall. The amount of shifting of u_θ can be seen by comparing the cross-section number 5 with cross-section number 11. They are located 45 degrees before the crest and past the crest of the meandering channel respectively.

Secondly, the meandering channel flow will affect the flood plain channel flow. As the result of the lateral momentum exchange between the two channels, increased
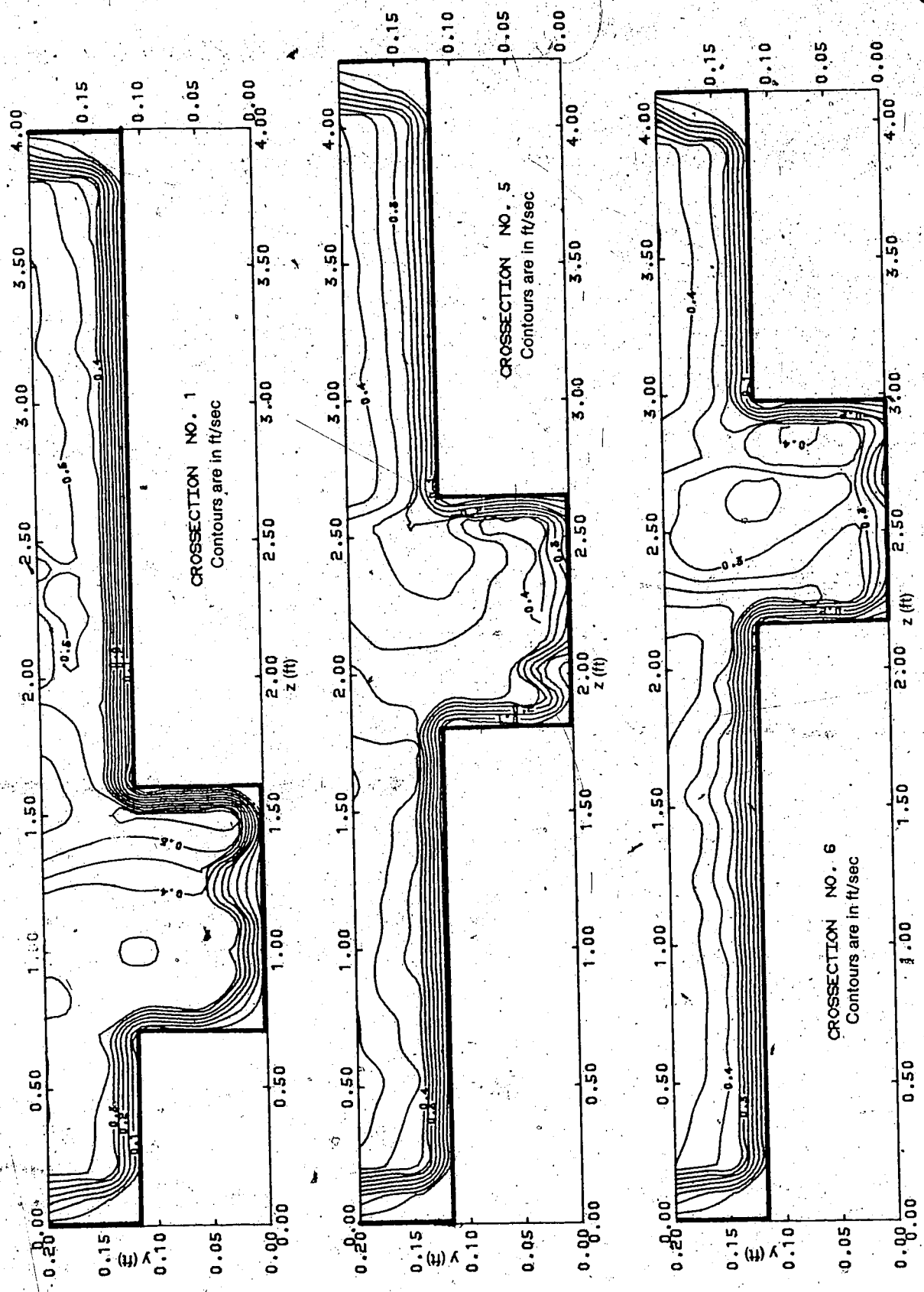
Figure 5.17 Cross-Sectional Isovel Map, RUN1

CROSSECTION NO. 1
Contours are in ft/sec

CROSSECTION NO. 5
Contours are in ft/sec

CROSSECTION NO. 6
Contours are in ft/sec

CROSSECTION NO. 7
Contours are in ft/sec

CROSSECTION NO. 8
Contours are in ft/sec

CROSSECTION NO. 9
Contours are in ft/sec

Figure 5.17 Continued

CROSSECTION NO. 10
Contours are in ft/sec

CROSSECTION NO. 11
Contours are in ft/sec

CROSSECTION NO. 13
Contours are in ft/sec

Figure 5.17 Continued

CROSSECTION NO. 14
Contours are in ft/sec

CROSSECTION NO. 15
Contours are in ft/sec

Figure 5.17: Continued

velocities will occur on the flood plain area. The approximate zone of interaction can be distinguished in the channel. Once again, comparison of the two cross-sections (numbers 5 and 11) will show that they are not identical. They differ mainly with regards to the acceleration and deceleration of the flow on the flood plain and the effect of θ. The isovel maps for the main channel at these sections are not the same.

5.6.3 Isovel Map

For the entire second loop at different levels above the flood plain, $u_θ$, φ, V and ω, (where φ the angle of the velocity vector with the x axis), contours are shown in Figures 5.18, 5.19, 5.20 and 5.22 for run number 1. For run number 2 the same contour maps for the level $y'=0.05$ feet (1.15 cm) are shown in Figures 5.21, 5.22.

Figures 5.19, and 5.21 show that the deviation of the angle of the vector velocity from the x axis ranges from -20 to +20 degrees, which mostly covers the main channel and its surrounding area. These maps, by themselves, suggest that the radial velocity component in the main channel and its neighbourhood in the flood plain (interaction zone) are large by comparison with the flow on the flood plain area far away from the main channel.

Figures 5.19 and 5.21 also show the variation of the angle of deviation of the velocity vector φ, from the x direction, (φ being negative if the rotation of V to x is clockwise). Figure 5.22 shows isovel maps of the radial velocity component. These contour maps are given for y'
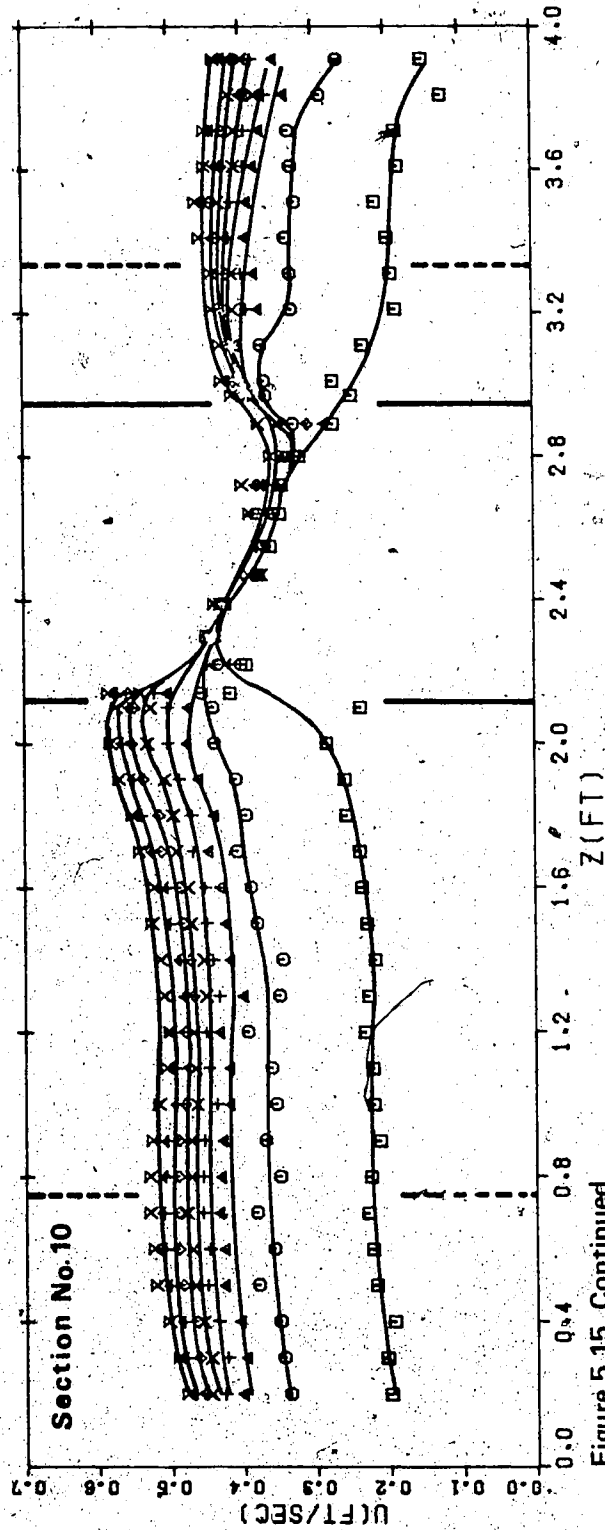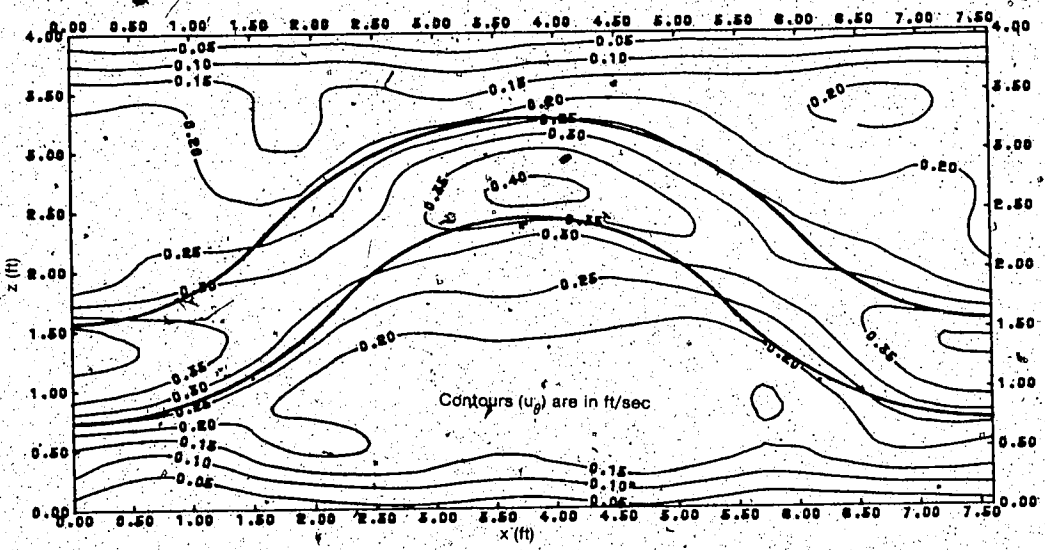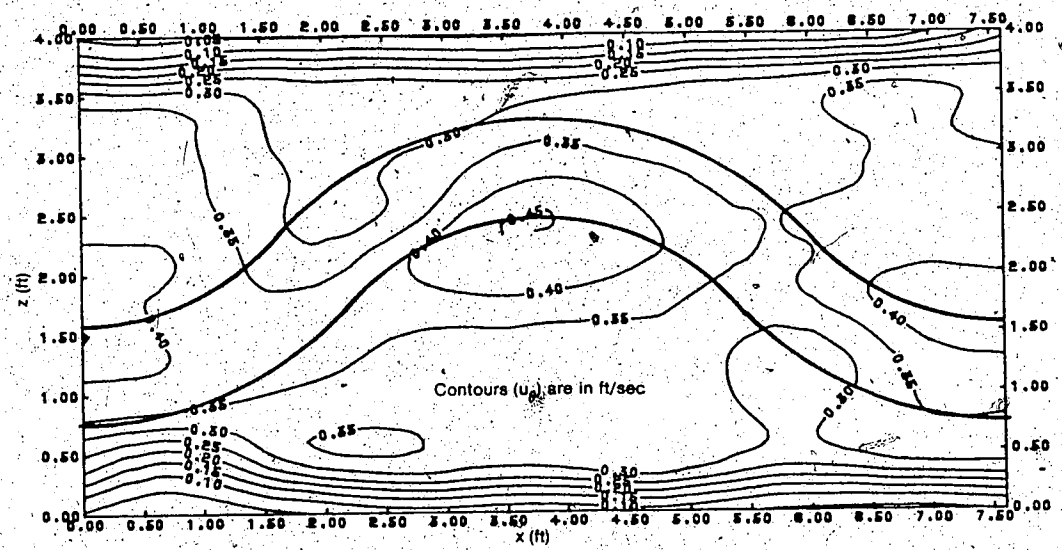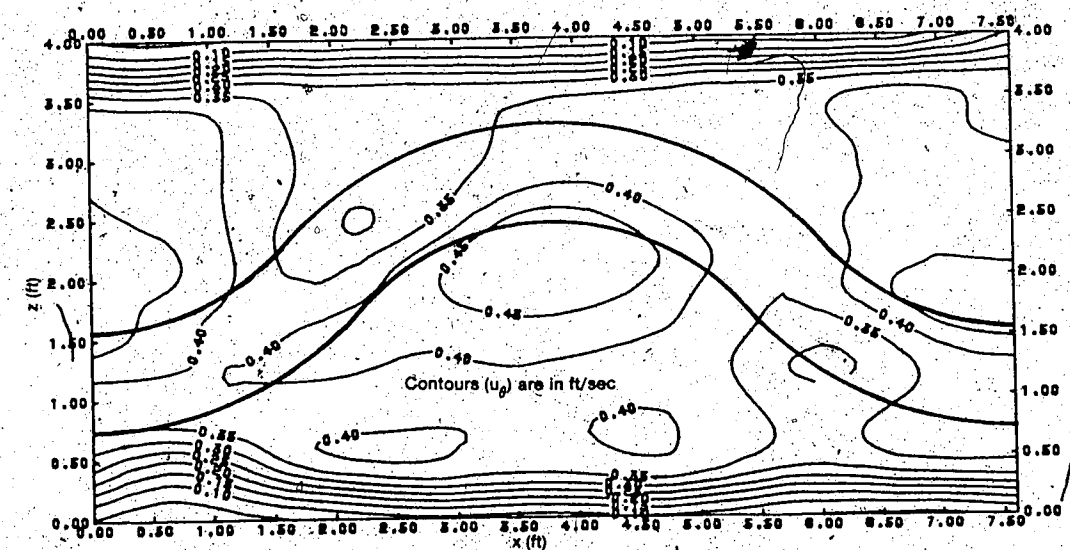
Figure 5.18 Tangential Velocity Isovel Maps at Different Level of y : RUN1
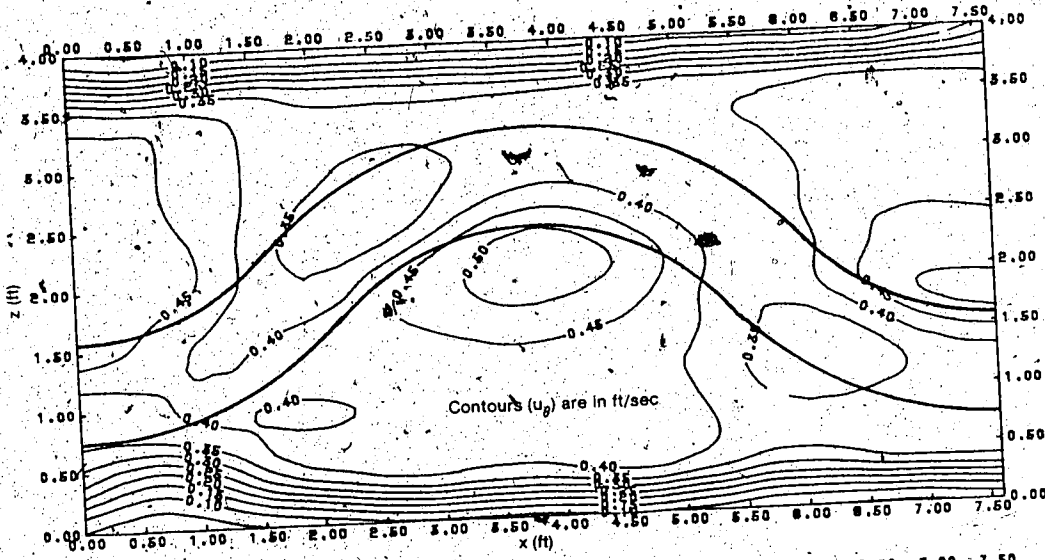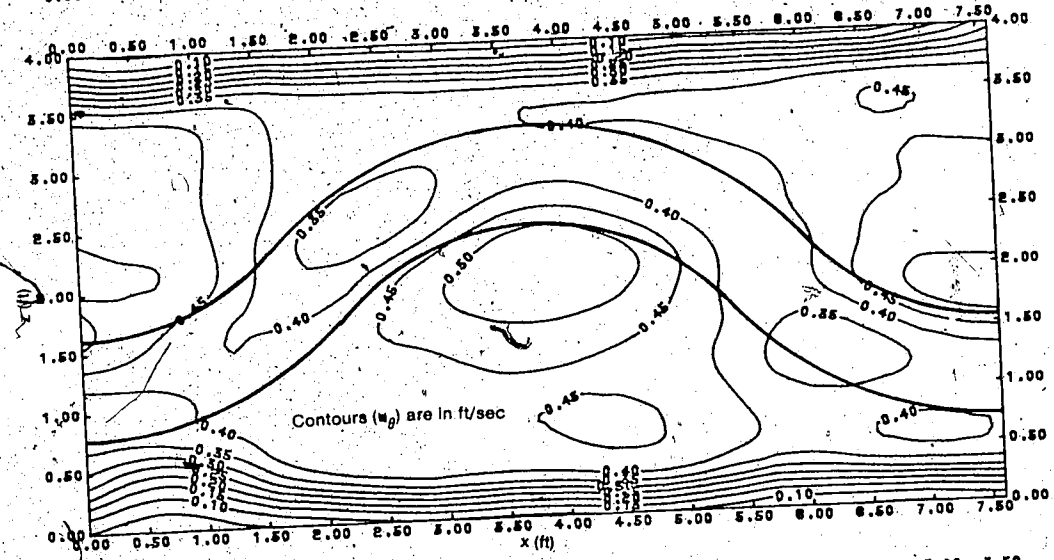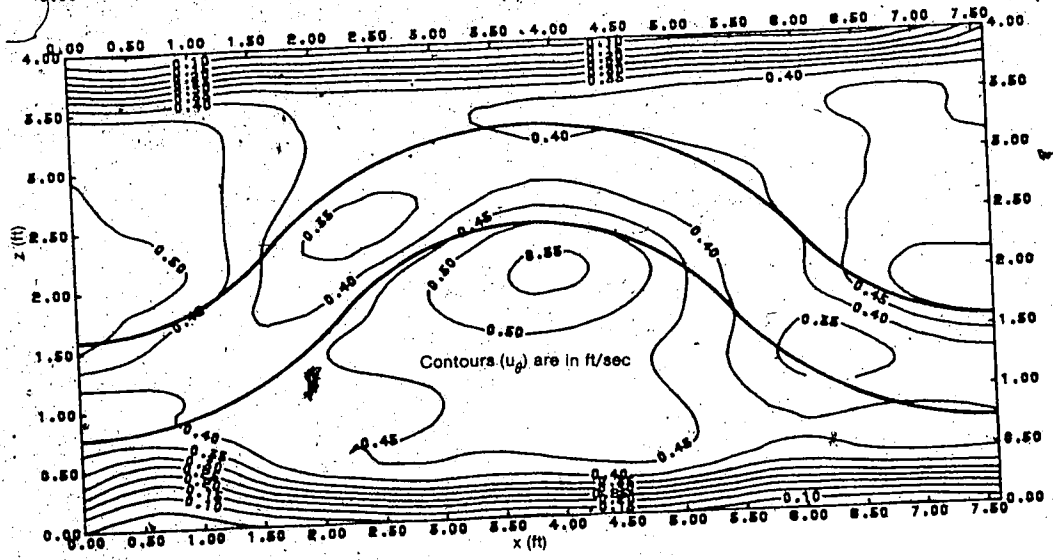
Figure 5.18 Continued

Figure 5.18 Continued

Contours (u_θ) are in ft/sec

Contours (u_θ) are in ft/sec

Figure 5.18

Contours (ϕ) are in degrees
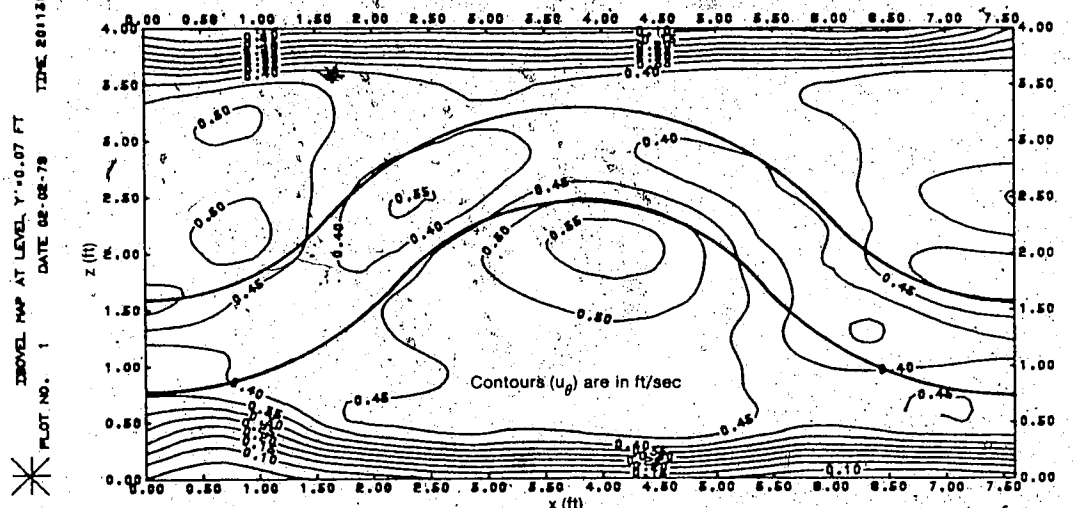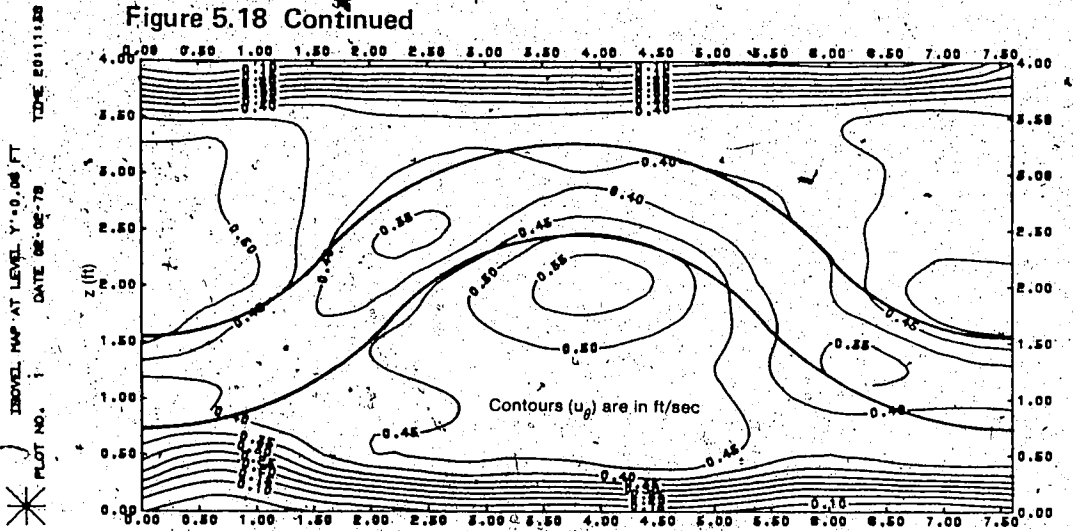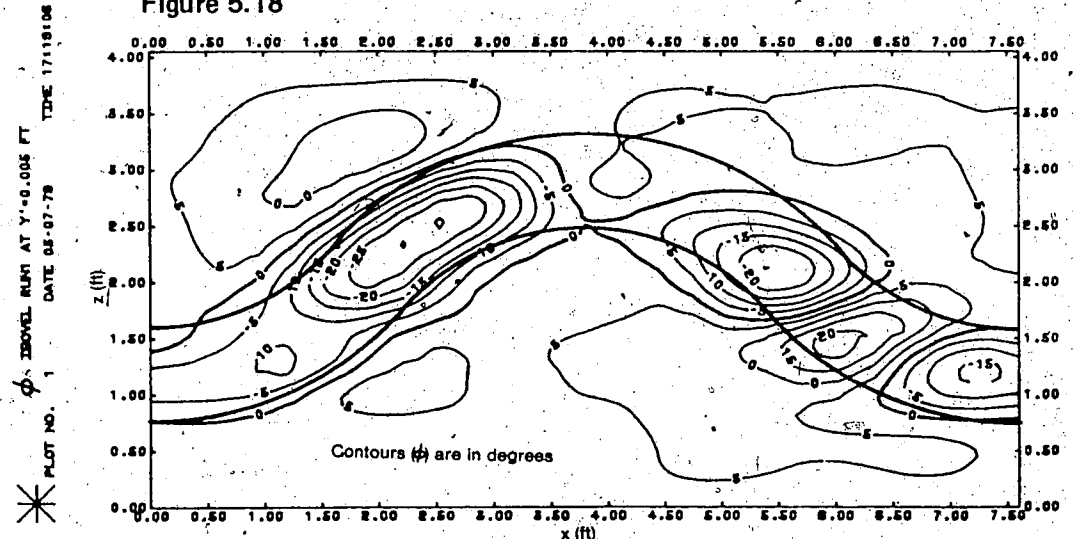
Figure 5.19 Angle of Velocity Vector Countur Map at y′ = 0.005 Feet: RUN1

Contours (V) are in ft/sec

Contours (V) are in ft/sec

Contours (V) are in ft/sec
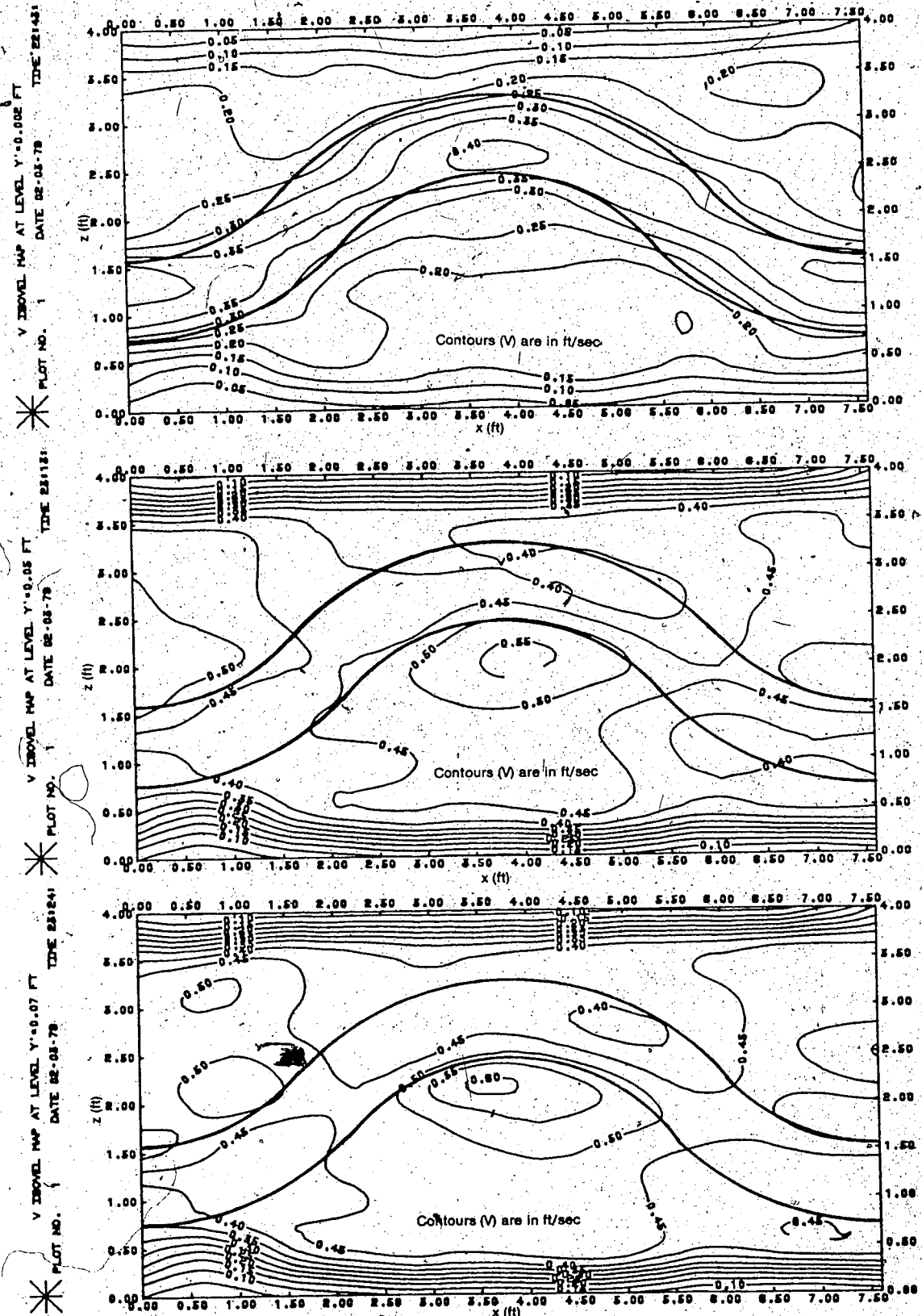
Figure 5.20 Velocity Vector Isovel Maps at Different Level of y′: RUN.1
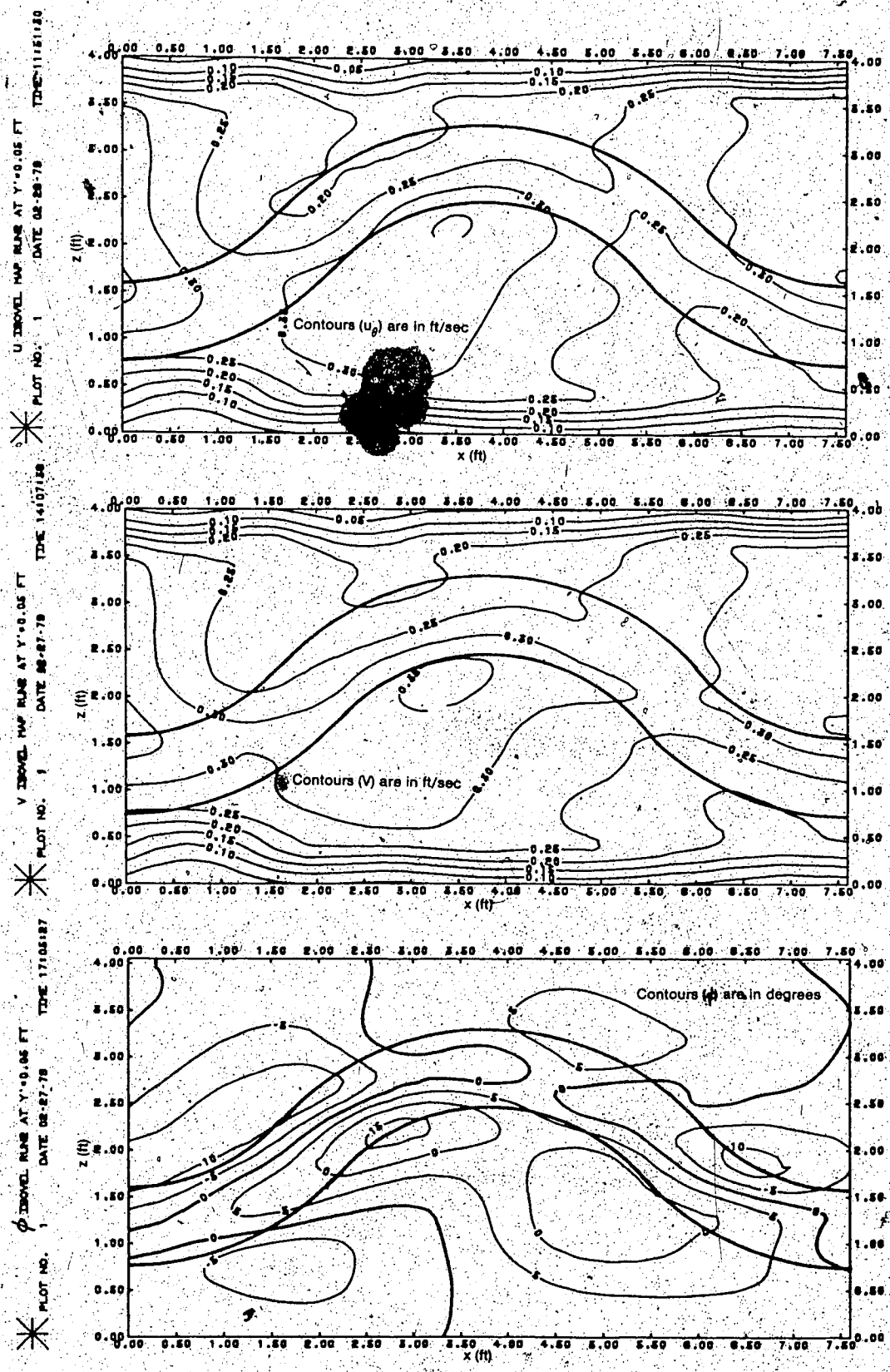
Figure 5.21 u_θ, V and ϕ Contur Map at y' = 0.05 Feet: RUN 2
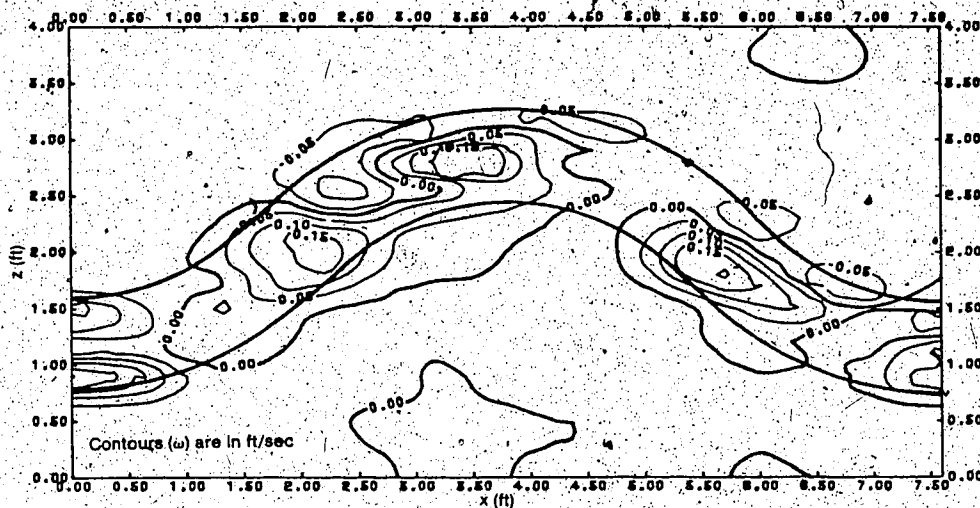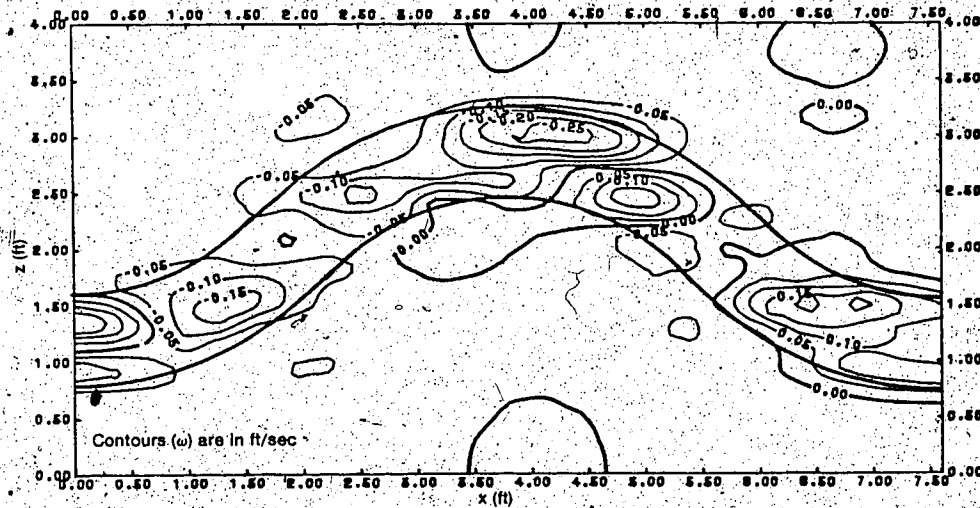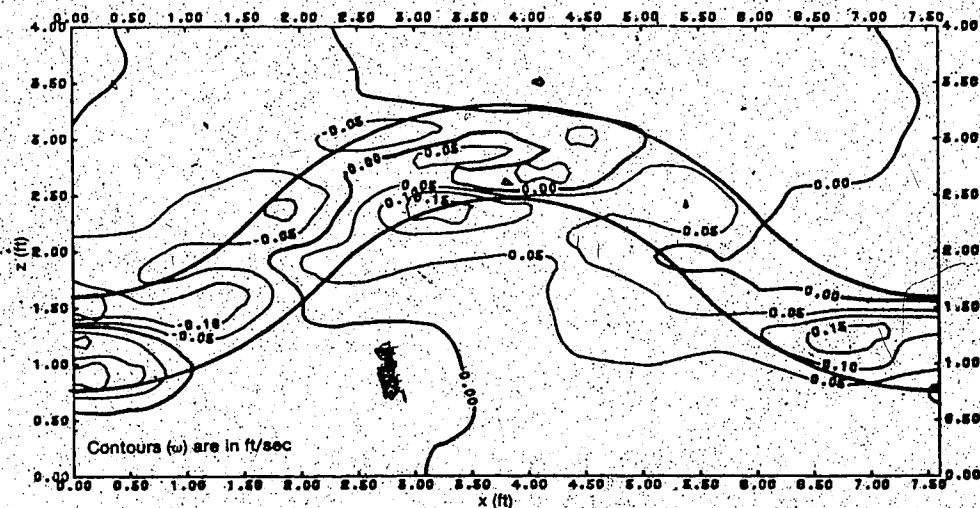
Figure 5.22 Radial Velocity Isovel Map: RUN1 & RUN2

=0.003 and 0.04 feet (0.9 and 12.2 mm) for run number 1 and y'=0.05 feet (1.52 cm) for run number 2. Figures 5.19 and 5.22 provide evidence of the flow exchanges between the meandering main channel and the flood plain, confirming the existence of secondary currents and showing that the magnitude of the lateral velocity component could reach (at some locations) be as much as 50% of V. One should also notice the divergent and convergent patterns, even in the straight channel.

Tangential and vector velocity contour maps looked alike for each y' and therefore, V isovels are presented in Figure 5.20 for only three levels y'=0.002, 0.04 and 0.07 feet (y'=0.6 mm, 1.2 cm and 2.2 cm) The isovel maps in Figure 5.20 and 5.22 show that the maximum velocity contour is located near the convex wall, but they are not symmetrical with respect to the crest of the meandering curve. This is because the behaviour of the flow approaching the crest is not the same as the behaviour of the flow past the crest. Another comment can be made about the acceleration and deceleration of the velocity vector by noticing the closed contours for equal values of φ.

Figure 5.22 shows contours of the lateral velocity component at level y'=0.003 and 0.04 feet (0.9 mm and 12.2 mm) for run number 1 and y'=0.05 feet (15.2 mm) for run number 2. This figure clearly shows the zones of the flood plain disturbed by the main meandering channel and also the magnitude of the secondary current.

It was concluded that the helicoidal currents were not confined to the main channel and spread to a broader area

equal to the width of the meander loop. The exact contribution of the momentum exchange from the curved channel and the compound cross-section to the lateral velocity redistribution is not known. But, qualitatively, the effect of the curved channel and the exchange of momentum for u(z) could be seen from lateral tangential velocity profiles.

5.7 Discussion on Interaction Results

There is an absence of sound knowledge about the flow in curved channels, even in the simplest cross-section (rectangular). Addition of flood plains to meandering channels brings additional difficulties. In light of the study described in chapters III and IV, transfer of momentum will take place from the region of high velocity to the region of the lower velocity (in the case of straight channel from the main channel to the flood plain channel). In the case of meandering channels with flood plains, one should expect the transfer of momentum to occur between the high and low region of the velocity.

The secondary current, which is generated in the meandering channel because of the curvature of the main channel, will transport momentum in and out from the meandering channel to the flood plain. The helocoidal motion in the lower part of the curved channel is confined in the main channel because of the presence of the solid walls. However, in the upper part of the flow, the absence of solid boundaries allows the helicoidal motion to continue on to

the flood plain. Therefore, in Figure 5.22 an isovel map for the lateral component of the velocity vector v_r, for a few selected cross-sections is shown. The secondary currents are mostly confined to a region equal to the total width of the meander.

The flow above the flood plain level has a tendency to flow more or less in the x direction. Because of changes in the depth of the flow in x direction, the flow will accelerate in the deeper part (on the main channel) and will slowly decelerate on the shallow part (in the flood plain) by excess friction. Comparison of the lateral tangential velocities of cross-section numbers 1 to 15 with the symmetrical cross-section number 0 (i.e. see Figure 5.16) will bring the following points to light:

1. increased velocity in the flood plain channel due to exchange of momentum between the main flow and the flood plain flow,

2. decreased velocity in the main channel due to interaction. However, the lateral tangential velocities retain their features such as higher velocities near the innermost wall and lower near the outermost wall,

3. due to the acceleration and the deceleration mechanisms, at the beginning of the bend, the velocity on the flood plain will increase up to cross-section number 8 (the crest cross-section) and decrease gradually,

4. the sudden change of the direction of the velocity velocity in the main channel at plane z=h introduces a rotational shear in this plane.

In most cross-sections the lateral velocity profiles near

the convex edge of the flood plain bears the maximum
velocity which normally is associated with high shear
stress. Therefore, at high flood flow the convex edge of the
flood plain will be eroded and the channel will straighten
out.

5.8 Conclusions and Comments on Further Direction

The present study of flow field in a smooth rigid
boundary model of a curved channel and a meandering channel
in a straight flood plain valley has led to the following
qualitative conclusions.

The logarithmic velocity distribution law may be
applicable only in the immediate region close to the bed of
the curved channels (about 20% of the depth of flow). It is
shown that the distribution of $u_\theta(y)$ in the core of flow is
mostly uniform. The magnitude of u_θ is dependent on $\cos\theta$.
Also, there is a relationship between D, u_θ and θ. The
normalized lateral velocity distribution $u_\theta(z)$, for
different cross-sections has been studied. They are similar
if the distribution curves rotate around the point of
intersection of all distribution curves, where it is located
at 20% of B from the innermost wall of the curved channel.

The shear stress near the convex region of the
meandering channel was about 2.5 times as large as that for
a uniform channel of the same width and for the same
hydraulic radius and discharge.

The interaction between the inbank and overbank flows
results in lateral momentum transfer which, in turn,

produces increased flood plain velocity and increased bed shear stresses. This interaction also causes reductions in the meandering channel velocity. The lower part of the flow in the main channel bounded by the side walls, flows more or less parallel to the boundary. The upper part of the flow above the flood plain level flows parallel to the x direction. This change of the direction of the flow in a horizontal plain will cause an additional rotational shear between the adjacent horizontal plains. At this stage of the study, no attempt was made to determine the magnitude of the rotational shear stresses nor the effect on reduction of the discharge due to this extra shear.

An interesting observation was the acceleration of the flow from the main channel to the flood plain up to the middle of the loop in the flood plain area. At this point the flow started to decelerate until it reached the end of the loop.

5.9 Further Direction

The existing models for prediction of the flow in a curved open channel are not adequate for describing the flow. This is the case mainly because the models ignore the fact that θ is one of the most important parameters. Besides that, the assumptions made to simplify the equation of motion can not be justified (fully developed flow, logarithmic law, etc.).

With this state of knowledge for flow in curved channels, the addition of a flood plain makes the problem

.even more difficult. Hence it might be advisable to first

tackle the problem of flow in curved channels and then

attempt to solve the problem of flow in curved main channels

with flood plains.

6. Summary of Conclusions

6.1 Concept of Interaction between Main Channel and Flood Plain Flows

The concept of the momentum transfer from high to low velocity region by turbulent mixing was tested in the case of a main channel (region of high momentum) with a straight flood plain (region of low momentum). The lateral transfer of momentum from the main channel to the flood plain channel results in the creation of a mixing region between the main channel and the flood plain.

The velocity and boundary shear stress distributions were measured for a range of flow conditions in a rectangular compound cross-section channel with both straight symmetrical and asymmetrical flood plains and also for a meandering main channel with straight flood plains. A series of figures show the relationships between boundary shear stress, aspect ratio and relative roughness for rectangular channels. Methods of estimating the local boundary shear stress, velocity and discharge for a simple rectangular channel and a compound cross-section channel shape are described.

6.2 Wide Main Channel and Wide Flood Plain Channel

For a straight wide main channel with a wide flood plain, the interaction between the main channel and the flood plain flows has been studied experimentally. The results have demonstrated the transport of the longitudinal

197

momentum from the main channel to the flood plain. The lateral velocity profiles in the flood plain and the main channel above the level of the flood plain, if viewed with respect to the undisturbed flood plain velocity, have been found to be approximately similar. Empirical correlations have been found for the velocity and length scales. It seems the structure of the flow in a main channel with a flood plain could be analysed using the concept of lateral momentum transfer and by treating the interaction region as a turbulent shear layer. The vertical velocity profiles can be described by logarithmic velocity distribution law. This suggests analytical possibilities of predicting the magnitude of the turbulent eddy viscosity for the interaction region.

The bed shear in the flood plain near the junction plane with the main channel is increased considerably and the main channel bed shear is decreased because of the interaction between the main channel and the flood plain flows. These changes have been analysed using similarity ideas. Some estimates of this penetration distance could perhaps be made using the results on turbulent compound shear layers. The scale factors for the shear stress distribution have been developed and D/d has been found to be the main parameter to indicate the extent of the interaction between the main channel and flood plain flows.

There is a reduction in carrying capacity in the compound cross-section channel due to the flow interaction. It is possible to express this reduction of the discharge analytically. The results of one experiment with a rough

flood plain is included.

6.3 Meandering Channel in a Straight Valley

Flow in a curved channel and meandering channel in a straight flood plain valley was also studied.

The logarithmic velocity distribution law may be applicable only in the immediate region close to the bed of the curved channel for about 20% of the depth of flow. It is shown that the vertical distribution of the velocity in the core of flow is mostly uniform. The magnitude of the velocity is dependent on the angular position of the section. Normalized lateral velocity distributions for different cross-sections are similar. The bed shear stress near the convex region of the meandering channel was about to 2.5 times as large as that for a uniform channel of the same width and for the same hydraulic radius, roughness and discharge.

The interaction between the inbank and overbank flows results in lateral momentum transfer which, in turn, produces increased flood plain velocity and increased the bed shear stresses. This interaction also causes reductions in the meandering channel velocity and bed shear stresses. The lower part of the flow in the main channel bounded by the side walls flows more or less parallel to the boundary. The upper part of the flow above the flood plain level flows parallel to the x direction. This change of the direction of the flow in horizontal plain will cause an additional rotational shear between the adjacent horizontal planes. At

this stage of the study, no attempt was made to determine either the magnitude of the rotational shear stresses or the effect on reduction of the discharge due to this extra shear.

The flow accelerates from the main channel to the flood plain up to the middle of the loop in the flood plain area. At this point the flow starts to decelerate until it reaches the end of the loop. The present results on the meandering channel with flood plains could be considered to constitute only an exploratory study.

NOTATIONS

The following symbols are used in this report:

A, B, C, k and k_1 to k_6 = constants

B = width of the main channel

b = width of flood plain channel

b_f = length scale for flood plain

b_m = length scale for main channel

b_t = total length scale

b_τ = shear length scale

b' = width of first flood plain channel

b'' = width of second flood plain channel

c_1 = minimum width of the flood plain channel

c_2 = maximum width of the flood plain channel

D = depth of main flow

d = depth of flow in flood plain

d' = depth of flow in flood plain at second level in multi-stage flood plain

F = Froude number

f = function

g = acceleration due to gravity

h = depth of main channel, below the level of flood plain

h' = depth of main channel below the second level of the flood plain in multi-stage flood plain

h_o = static pressure head

h_1 = dynamic pressure head of hole No.1 of the yaw probe

h_2 = dynamic pressure head of hole No.2 of the yaw probe

h_3 = dynamic pressure head of hole No.3 of the yaw probe

k_s = Nikuradse sand roughness

1_* = value of z' where $\Delta \tau_o = 0.0$

L = length of meander channel

1_{en} = entrance length

1_{ex} = exit length

1_w = wave length

p = pressure

p_o = static pressure

p_1 = pressure of hole No.1 of the yaw probe

p_2 = pressure of hole No.2 of the yaw probe

p_3 = pressure of hole No.3 of the yaw probe

Q = discharge

R = centerline radius of bend

r_i = innermost radius of bend

r_o = outermost radius of bend

S = slope

S_o = slope of channel (bed slope)

S_r = water surface slope in radial direction

S_w = water surface slope

T = length of tangent

U = reference velocity

u = velocity in the longitudinal (x) direction

u_θ = tangential velocity

u_m = value of u for z=0.0

u'_m = value of u for z=B/2

u_o = value of u for y=h

u_∞ = undisturbed value of u in the flood plain for any y'

u_* = shear velocity

$u_{*\infty}$ = undisturbed shear velocity

V = velocity vector

v_r or ω = radial velocity

x = longitudinal distance

y = vertical distance from bed of main channel

y' = vertical distance from bed of flood plain

y^* = loction of the dip in the main channel

z = lateral distance from the centerline of main channel

z' = lateral distance for flood plain (z=B/2, z'=0.0)

η, η' = dimensionless lateral distances

θ = angular coordinate

$\bar{\theta}$ = angle of attack for the yaw probe

θ_c = central angle of bend

ν = kinematic viscosity of water

k = Von Karman universal constant

τ_o = bed shear stress

τ_{om} = τ_o at z = 0.0

τ'_{om} = τ_o at z=B/2 or z'=0.0

$\tau_{0\infty}$ = undisturbed τ_0 in the flood plain

$\Delta\tau_0$ = τ_0 in flood plain minus $\tau_{0\infty}$

$\hat{\tau}_{om}$ = τ_{om} with side walls of the main channel extended to total depth

$\tilde{\tau}_*$ = average longitudinal shear stress in the junction plane

ϕ = angle of deviation of velocity vector from longitudinal direction of channel projected on horizontal plane, positive outward

$(-)$ave = average value for section

$(\hat{})$ = mean value

λ = wave length

ε = eddy viscosity

ρ = density of water

γ = specific weight of water

References

Allen, J. and Seh Per Chee, "The Resistance To The Flow Of Water Round A Smooth Circular Bend In An Open Channel," Proceeding ICE, London, Volume 23 No. 1, 1962, pp. 422-434

Ananyan, A.K.: "Fluid Flow In Bends Of Conduits," Israel Program for Scientific Translation, Jerusalem, 1965.

Bagnold, P.A.: "Some Aspects Of The Shape Of River Meanders," USGS, Paper No.6611, 1960.

Brus-Chacinskii, T.M.: "Helical Flow In Open Channel Bends - Factors In Meandering Phenomena," Dock and Harbour Authority, London, August, 1955.

Udai Vand Choudhary and Sampathiengar Narasimhan: "Flow In 180 Degree Open Channel Rigid Boundary Bends," Proceedings of the ASCE, Journal, Hydraulics Division, Volume 105, No. Hy6, 1977, pp.651-657.

Chow, V.T., Open Channel Hydraulics, McGraw-Hill Book Co. Inc., N.Y., 1959.

Cruff, R.W.: "Cross-channel Transfer Of Linear Momentum In Smooth Rectangular Channels," U.S. Geological Survey, Water Supply, pp.1592-B, 1965.

de Vriend, H.J.: "A Mathematical Model Of Steady Flow In Curved Channels," Report No.76-1, Communication on Hydraulics Department of Civil Engineering, Delft University of Technology 1976.

Einstein, H.A. and Harder, J.A.: "Velocity Distribution And The Boundary Layer At Channel Bends," Transactions, American Geophysical Union, Volume 35, No.1, 1954.

Ellis, L.B. and Joubert, P.N.: "Turbulent Shear Flow In A
    Curved Duct," Journal of Fluid Mechanics 1974, Volume
    62, part 1, pp.65-84.

Engelund, F.: "Instability Of Flow In A Curved Alluvial
    channel," Journal of Fluid Mechanics 1975, Volume 72,
    Part 1, pp.145-160.

Engelund, F.: "Flow And Bed Topography In Channel Bends,"
    Proceedings of ASCE, Journal, Hydraulics Division,
    Volume 100, No.Hyll, November, 1974, pp.1631.

Eskinazi, S. and Yeh, H.: "An Investigation On Fully
    Developed Turbulent Flows In A Curved Channel," Journal
    of Aero Sciences, 1956, Volume 23, No.1 pp.23-75.

Fischer, H.B.: "Longitudinal Dispersion and Turbulent Mixing
    in Open-Channel Flow," Annual Review of Fluid Mechanics,
    Volume 5 1973 pp. 59-78 .

Gessner, F.B. and Jones, J.B.: "On Some Aspects Of Fully
    Developed Turbulent Flow In Rectangular Channels,"
    Journal of Fluid Mechanics, 1965, Volume 23, Part 4,
    pp.689-713.

Ghosh, S.N. and Jena, S.B.: "Boundary Shear Distribution in
    Open Channel Compound," Proceedings, Institute of Civil
    Engineers, London, England, Volume 49, August 1971,
    pp.417-430.

Ghosh, S.N. and Roy, N.: "Boundary Shear Distribution in
    Open Channel Flow." Proceedings ASCE, Journal Hydraulics
    Division, April 1970, pp.967-994.

Goncharov, V.N.: "Dynamics of Channel Flow," Israel Program
    for Science Translation, Jerusalem, 1964.

Hegly, V.M. transalted by Chilton, A., and Wright, A.: "Flow

in Earthen Canals of Compound Cross-Section,"
Proceedings ASCE, p.36, November 1937.

Henderson, F.M.: "Steady Flow in Sinusoidally Varying
Channels," Proceedings 1st Aust. Conference on
Hydraulics and Fluid Mechanics, Pergamon Press, 1962.

Hollick, Makeolm: "Boundary Shear Stress Measurement by
Preston Tube," ASCE, Journal of Hydraulics Division,
p1053.

Hollingshead, A.B.: "Boundary Shear Stress Distribution in
Open Channel Flow," Doctoral Thesis, Department of Civil
Engineering, University of Alberta, Edmonton, 1972.

Ikeda, S: "On Secondary Flow and Bed Profile in Alluvial
Curved Open Channel," Proceedings of XVIth Congress of
the IAHR, Sao Paulo, 1975, Volume 2, Paper B-14.

Keulegan, G.H.: "Laws of Turbulent Flow in Open Channels,"
National Bur. Standards, Journal of Research, Volume 21,
1938.

Kikkawa, Hidea, Ikeda, Syunsuke, and Kitagawa, Akira: "Flow
And Bed Topography in Curved Open Channels," ASCE,
Journal of Hydraulics, Division of Hydraulics,
p.1327-1342, 1976.

Kikkawa, H., Ikeda, S., Ohkawa, H., and Kawamura, Y.:
"Secondary Flow in a Bend of Turbulent Stream,"
Transactions of the JSCE, Volume 5, 1973, p.100.

Langbein, W.B. and Leopold, L.B.: "River Meanders - Theory
of Minimum Variance," USGS, Prof. Paper 422-H, 1963.

Leopold, L.B., Bagnold, R.A., Wolman, M.G., and Brush, Jr.
L.M.: "Flow Resistance in Sinuous or Irregular
Channels," Geologic Survey Professional Paper 282-D,

USGS: 1960.

Leopold, L.B. and Langbein, W.B.: "River Meanders,"
Scientific American, June, 1966, Volume 214, No.6,
pp.60-70.

Mockmore, C.A.: "Flow Around Bends in Stable Channels,"
Transactions ASCE, Volume 109, 1944, pp.593-628.

Mockmore, C.A.: "Comprehensive Studies on the Meandering of
Alluvial Streams," Transactions ASCE, Volume 119, 1954,
pp.335-360.

Myers, W.R.C.: "Momentum Transfer in a Compound Channel,"
Journal of Hydraulic Research, 1978, No.2, pp.139-150.

Myers, W.R.C. and Elsawy, E.M.: "Boundary Shear in Channel
with Flood-Plain," Proceedings of ASCE, Journal
Hydraulics Division, July 1975, pp.993-946.

Patankar, S.V., and Pratap, V.S.: "Prediction of Turbulent
Flow in Curved Pipes," Journal of Fluid Mechanics 1975,
Volume 67, Part 3, pp.583-595.

Patel, V.C.: "Calibration of the Preston Tube and
Limitations on its Use in Pressure Gradients," Journal
of Fluid Mechanics, Volume 23, 1965, pp.185-208.

Pratap, V.S. and Spalding, D.B.: "Numerical Computations of
the Flow in Curved Ducts," The Aeronautical Quarterly,
Volume XXVI 1975, p.219-228.

Preston, J.H.: "The Determination of Turbulent Skin Friction
by Means of Pitot Tubes," Journal of Royal Aeronautical
Society, Volume 58, 1954, pp.109-121.

Rajaratnam, N.: "On the Preston Tube with a Hemispherical
Nose," Civil Engineering, England, November 1965,
- 1642.

Rajaratnam, N., and Ahmadi, R.: "Interaction Between Main
Channel and Flood-Plain Flows," Departmental Report,
Civil Engineering, University of Alberta, 1978, Also
Published in ASCE, Journal of Hydraulics Division, May,
1979, pp.573-587.

Rajaratnam, N., and Ahmadi, R.: "Hydraulics of Channels with
Flood-Plains," Departmental Report, Civil Engineering,
University of Alberta, 1979.

Rajaratnam, N., and Muralidhar, D.: "Yaw Probe Used as
Preston Tube," The Aeronautical Journal of the Royal
Aeronautical Society, December 1968.

Rajaratnam, N., and Muralidhar, D.: "Boundary Shear Stress
Distribution in Rectangular Open Channels," La Houille
Blanche, Grenoble, France, No.6, 1969, pp.603-609.

Rowe, M.: "Measurements and Computations of Flow in Pipe
Bends," Journal of Fluid Mechanics 1970, Volume 4,
pp.771-783.

Rozovskii, I.L.: "Flow of Water in Bends of Open Channels,"
Israel Program for Scientific Translations, Jerusalem,
1961.

Sampson, R.J.: Surface II Graphics System (Revision one)
published by Kansas Geological Survey, Lawrence, Kansas,
U.S.A. 1978.

Schlichting, H.: "Boundary-layer Theory" English Translation
published by McGraw-Hill Book Co. Inc., New York 1968
(Sixth Edition).

Sellin, R.H.: "A Laboratory Investigation Into the
Interaction Between the Flow in the Channel of a River
and that over its Flood-Plain," La Houille Blanche,

Grenoble, France, No.7, 1964, pp.793-802.

Shukry, Ahmad: "Flow Around Bends In An Open Flume,"
Transactions ASCE,Journal, Volume 115, 1950, pp.751-788.

Siebert, W., and Gotz, W.: "A Study on the Deformation of
Secondary Flow in Models of Rectangular Meandering
Channels," Proceedings of XVIth Congress of IAHR, Sao
Paulo, 1975, Volume 2, Paper B-18.

Smith, C.D.: "Flood Stage in a Valley with a Meandering
Channel," Research Report HY-77-01, April 1977,
University of Saskatchewan, Saskatoon.

Soliman M.M., and Tinney, Roy: "Flow Around 180 Degree
Bends in Open Rectangular Channels," Proceedings of ASCE,
Journal of Hydraulics Division, July, 1968.

Tingsanchali, Tawachai, and Ackerman, Norbert L.: "Effects
of Overbank Flow in Flood Computation," ASCE Hydraulics,
1976, pp.1013-1033.

Toebes, G.H. and Sooky, A.A.: "Hydraulics of Meandering
Rivers with Flood-Plains," Proceedings ASCE, Journal of
Waterways and Harbors Division, May 1967, pp.213-236.

Tracy, H.J.: "The Structure of a Turbulent Flow in a Channel
of Complex Shape," USGS, Paper 983, 1976.

Vogel, H.D., and Thompson, P.W.: "Flow in Riverbends," Civil
Engineering, May 1933,.

Wolman, M.G. and Leopold, L.B.: "River Flood-Plains: Some
Observations on Their Formation," Geological Survey
Professional Paper 282-C, USGS, 1957.

Wright, R.R. and Carstens, M.R.: "Linear-Momentum Flux to
Overbank Sections," Proceedings ASCE, Journal Hydraulics
Division, September 1970, pp.1781-1793.

Yarnell, D.L. and Woodward, S.M.: "Flow of Water Around 180

    Degree Bends," Technical Bulletin, No. 526, U.S.

    Department of Agriculture, 1936.

Yen, C.B.: "Characteristics of Subcritical Flow in a

    Meandering Channel," Institute of Hydraulic Research,

    University of Iowa, Iowa City, 1965.

Yen, B.C. and Yen, C.L.: "Water Surface Configuration in

    Channel Bends," Proceedings of the ASCE, Journal

    Hydraulics Division, Volume 97, No. HY2, February 1971,

    p. 303.

Zheleznyakov, G.V.: "Interaction of Channel and Flood-Plain

    Streams," Proceedings IAHR Congress, 1971, Paris, Volume

    5, pp. 145-148.

APPENDIX A

A-1 Turbulent Flow in Rectangular Channels

Perhaps the most simple cross-section in an open channel is a rectangular one. Even in a simplified case like a straight channel with rectangular cross-section, the equations of motion for turbulent flow, along with the continuity equation cannot be solved. In order to formulate an approximate solution, it is required to adopt empirical assumptions. It is necessary to supplement the original hypothesis with additional hypotheses which may vary from case to case. The form of certain functions, or at least certain numerical values, must be extracted from experiments. In order to ignore the effect of the side walls, one must always assume the channel is very wide. Cruff (1965), and subsequently Rajaratnam & Muralidhar (1969), obtained considerable experimental data for smooth rectangular channels. Rajaratnam & Muralidhar (1969), in their paper, presented the variation of maximum bed shear stress with respect to aspect ratio. In addition, they expanded upon the distribution of bed shear stresses and wall shear stresses.

This study presents some supplementary measurements on the shear stress and velocity distribution in smooth and rough channels. Together with the data available from Cruff (1965), Rajaratnam & Muralidhar (1969) and Ghosh & Jena (1971) and supplementary measurements in a smooth and rough rectangular channels, the author was able to relate the effect of wall (aspect ratio) and the bed roughness with

212

aximum bed shear stresses. Furthermore, the distribution of
bed and wall shear stresses with width and depth of flow
respectively was obtained. Further, the average
cross-sectional velocities for the entire section in both
cases, smooth and rough, were compared with average
velocities obtained by dividing discharge by cross-sectional
area.

A-2 Experimental Arrangements and Experiments

The experiments were performed in an eight inch (20.2
cm) wide, seven inch (17.8 cm) deep and 60 feet (18.3 m)
long channel with adjustable slope. Water entered the flume
from a constant head reservoir provided with suitable
screens. The discharge was measured by means of an
orifice-meter located in the supply line to the head-tank.

The height of the water surface was measured with point
gauges. The water surface slope was measured by a pressure
transducer. In order to obtain uniform flow, the tail gate
was adjusted until the water surface slope for the middle 20
feet (6.1 m) of the flume, coincided with the bed slope. The
test section was located in the middle of the flume.
Velocities were measured using a 1/8 inch (3mm) external
diameter Prandtl-type pitot static tube. The same Prandtl
tube also served as the Preston tube for the smooth
boundary.

In the case of the smooth boundary, most data were
taken from the work of Rajaratnam & Muralidhar (1969).
Complementary runs were conducted to verify the average

curve and to fill the gap between data points.

In the case of the rough bed with smooth walls, data were obtained from a Departmental report by Rajaratnam (1967-1969), from Ghosh & Jena (1971) and from several experiments conducted by others. Further experiments were conducted with pre-molded rubber mats with hemispheres of 1 inch (2.54 cm) and 1/2 inch (12.7 mm) in diameter.

All data were chosen in such a way that the Froude number varied from 0.10 to 0.70. Velocity and the boundary shear stress distributions were obtained in one half of the channel. If y is the normal distance above the bed and if z denotes the transverse distance from the centerplane of the channel, then $\lambda = z/(B/2)$ and $\eta = y/D$, where B is the width of the channel and D is the depth of water and the range of λ was from zero up to about 0.95 and η ranged from 0.005 up to almost 1.0.

A-3 Velocity Distribution

a. Smooth Boundary:

The velocity data on the centerline of the channel as well as off the centerline were plotted with u/u_* versus $\log \frac{y u_*}{\nu}$, where u_* is the shear velocity, equal to $\sqrt{\tau_0/\rho}$, at the foot of the corresponding normal line, and ρ is the mass density of water. It was found that the velocity distribution agrees well with the well known Karman - Prandtl equation:

$$\frac{u}{u_*} = 5.75 \log\left(\frac{y\, u_*}{\nu}\right) + 5.5$$

even for values of λ as large as 0.95. It was noticed that near the free-surface, there is a dip in the velocity profile.

b. Rough boundary:

The present semi-empirical methods for computation of turbulent flow in open channels are based essentially on the work of Keulegan (1938). For rough boundaries, Keulegan uses the Karman - Prandtl velocity distribution equation as

$$\frac{u}{u_*} = A \log\left(\frac{y}{k}\right) + C$$

where k is the roughness height and C is a coefficient. For the densely packed sand roughness of Nikuradse, k becomes k_s and $C=8.5$. Rajaratnam used an averaged value of u_* based on $\gamma\, r\, S_o$ where γ is the specific weight of the fluid, r is the hydraulic radius and S_o is the bed slope, to evaluate the value of A. He found for 4 types of roughness the value of A ranging from 7.40 to 6.32.

A-4 Distribution of Boundary Shear Stresses

Based on existing data from literature and several supplementary experiments, a plot of the aspect ratio (B/D) versus $\tau_{om}/\gamma\, D\, S_o$, for different values of D/k_s in shown in
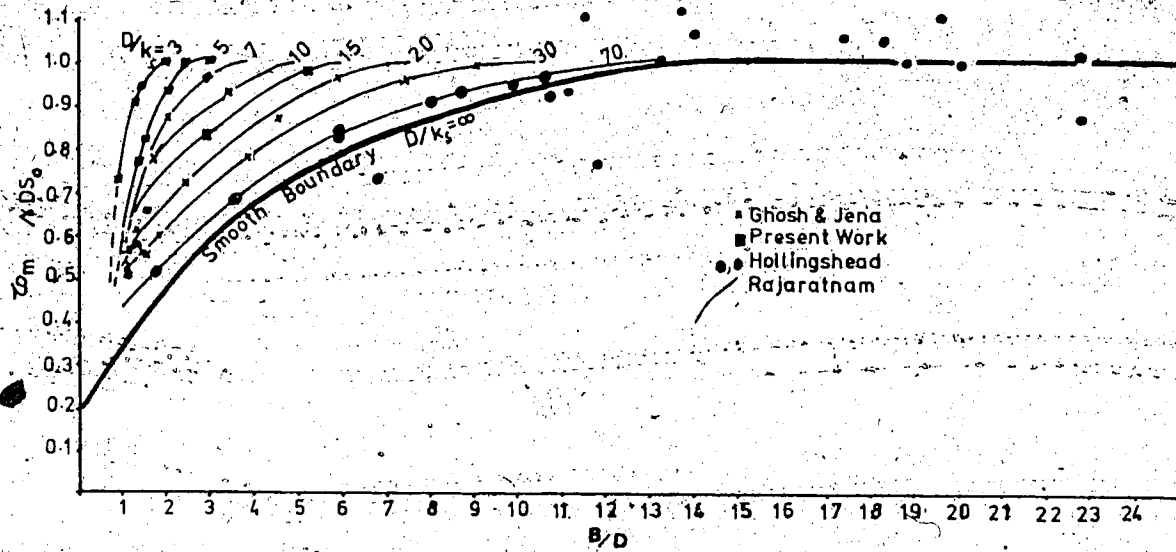
Figure A-1 Centerline Bed Shear Stress for Rectangular Channels: Smooth & Rough Boundary
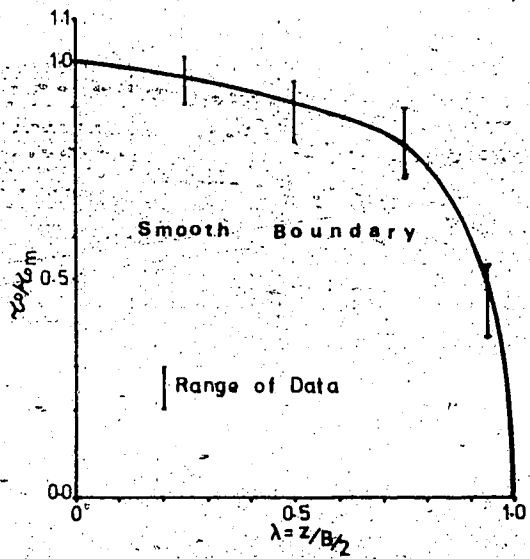

Figure A-2 Lateral Distribution of Bed Shear Stress for Rectangular Channels: Smooth Boundary
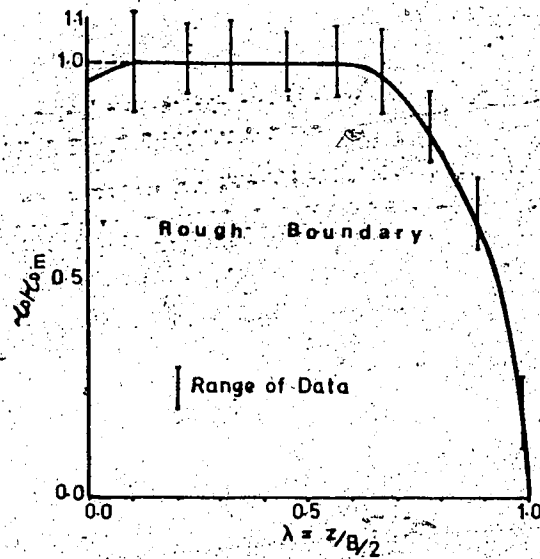
Figure A-3 Lateral Distribution of Bed Shear Stress for Rectangular Channels: Rough Boundary

Figure A-1, where τ_{om} is the centerline shear stress. From Figure A-1, it could be seen that for $D/k_s=3.0$, $\tau_{om}/\gamma D S_o$ becomes equal to one for an aspect ratio of two whereas for the channel with smooth boundaries, the corresponding value of the aspect ratio is about 14.5. In the case of the smooth boundary for which $D/k_s=\infty$, supplementary experiments confirmed that the average curve obtained by Rajaratnam and other investigators is fairly good. Figure A-2 shows the distribution of τ_o/τ_{om} versus on the bed for the smooth boundary. Figure A-3 shows the distribution of τ_o/τ_{om} versus for the rough bed with smooth walls. There is quite a scatter of the points in this plot, caused basically by the variation of D/k_s. At this stage of the work, it was not possible to label the different curves for various values of D/k_s. An average curve is all that could be drawn.

A-5 Average Velocity Prediction

For smooth boundaries, $u=(u_*/k)\ln(y/y_o)$ where $k=0.40$, $y_o=m\nu/u_*$ and $m=9$. If $\hat{U}$=average velocity in the vertical profile, after integration with proper boundary condition:

$$\frac{\hat{U}}{u_*} = 5.75 \log\left(\frac{D u_*}{\nu}\right) + 3.0$$

One more integration with $\hat{U}$ from $z=0.0$ to $z=B/2$ will give an average velocity for the cross-section. By noticing that:

$$\left(\frac{\tau_o \text{ at any point}}{\tau_{om} \text{ at centerline}}\right) = \frac{u_*}{u_{*o}}$$

and fitting an equation to the curve in Figure A-2, one can

proceed with the integration to obtain the final result as

$$\frac{V}{u_{*o}} = 5.75 \log(\frac{D u_{*}}{\nu}) + 2.75 \qquad\qquad (A-2)$$

Compared with an earlier empirical equation (Chow, 1959) which reads:

$$\frac{V}{v_{*}} = 5.75 \log(\frac{r v_{*}}{\nu}) + 2.75 \qquad\qquad (A-3)$$

wherein v_{*} is shear velocity, based on the hydraulic radius rather than the depth of flow. It is seen that the constant 3.25 is higher because the hydraulic radius r is always smaller than D, the depth of flow.

For a rough boundary the governing equation is:

$$\frac{u}{u_{*}} = 5.75 \log(\frac{y}{k}) + C \qquad\qquad (A-4)$$

Upon integration from the bed to water surface the average velocity is given by:

$$\frac{\bar{U}}{u_{*}} = 5.75 \log(\frac{D}{k_{s}}) + 6.0 \qquad\qquad (A-5)$$

(where k_{s}=Nikuradse sand roughness)

Once more, integration from the centerline to the wall, using Figure A-3 and proceeding in the same way as in the case of the smooth boundary, the average velocity for the cross-section is given by:

$$\frac{V}{u_{*o}} = 5.75 \log\left(\frac{D}{k_s}\right) + 5.25$$

$$(A-6)$$

By knowing the aspect ratio and D/k_s, from Figure A-1 one can obtain τ_{om}, and hence u_{*o} and using Equation A-6, V can be calculated.

These results are similar to those Keulegan (1938) who evaluated these coefficients using arbitrary shear stress profiles and the experimental data of Bazin.

APPENDIX B

B-1 Channels with Flood Plains at Two Levels

Often successive increments of overbank deposition are
responsible for building a flood plain. The erosion of the
main channel bed and the edge of the flood plain creates a
narrow strip of intermediate flood plain level. A detailed
study by Wolman & Leopold (1957) showed that the deposition
on the flood plain does not continue indefinitely. The flood
plain area can be transformed into a terraced surface by
some tectonic or climatic changes. A terrace overflows less
frequently than a flood plain. When a flood plain and its
adjacent terrace are flooded during a very high flood, the
compound cross-section will have at least three or more
different bed elevations.

Only one experiment was conducted with the multi-level
flood plain channel. The dimensions of the multi-flood plain
were presented in Chapter II. (see Figure 2.2d). Figure B-1
shows the distribution of $u(y)$, $u(y')$ and $u(y'')$. It can be
seen from the profiles that the velocity in the main channel
increased with y and the maximum velocity will be obtained
just below h (first flood plain elevation). The velocity
will continue to increase at lower rates up to $y = h$ and
from here to the water surface will remain almost constant.
The lateral velocity profiles are shown in Figure B-2.
Considering the uppermost flood plain (second level of the
flood plain), the velocities will increase continuously as
one moves towards the first level of the flood plain. The
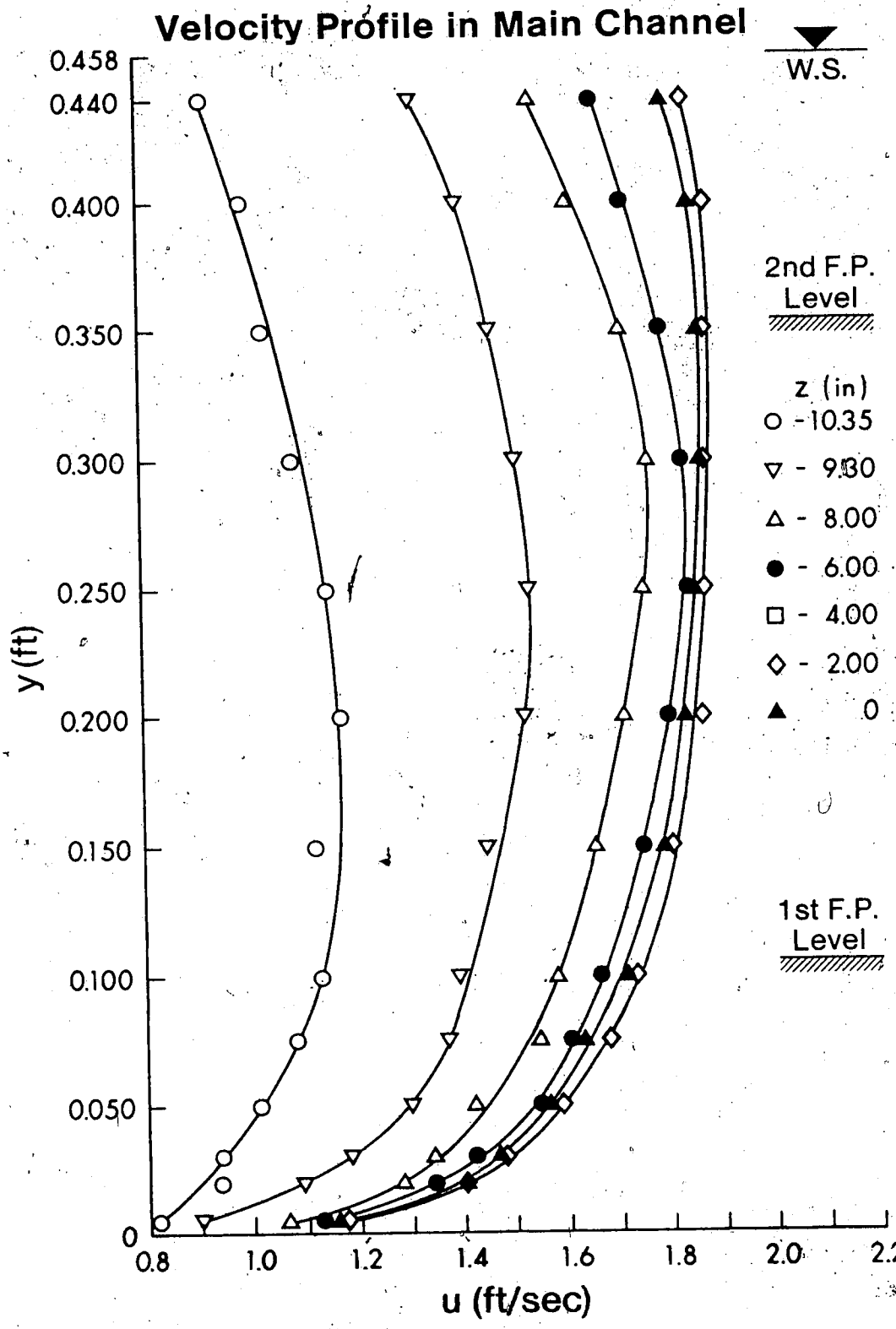first stage flood plain evidently acts as a main channel for

Velocity Profile in Main Channel

Figure B-1 Undisturbed Velocity Profiles: Main Channel

Velocity Profile
In Main Channel

▼ W.S.

z (in)
○ 2.0
▽ 4.0
● 6.0
△ 8.0
□ 9.0
◇ 9.5

2nd F.P.
Level

1st F.P.
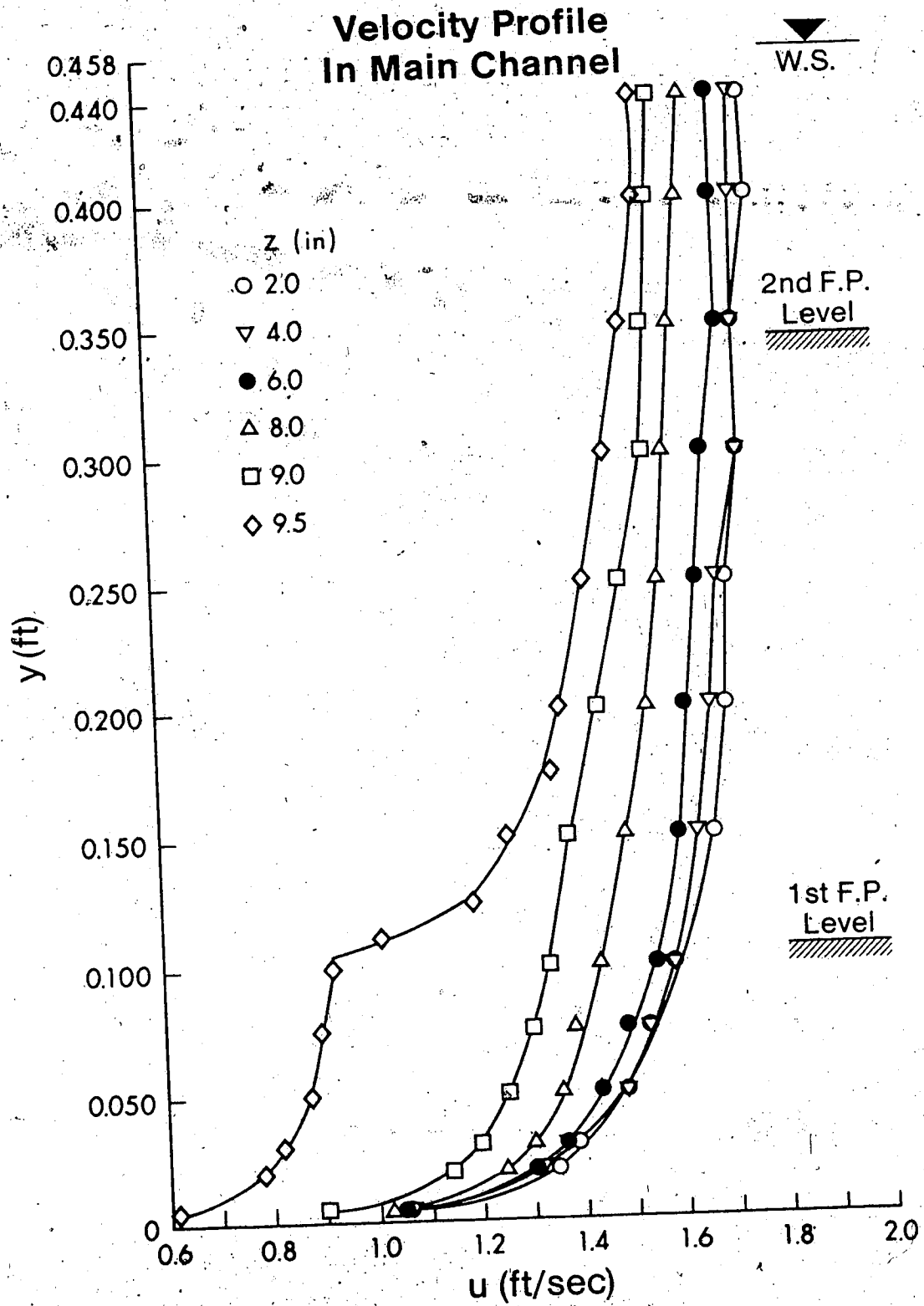Level

y (ft)

u (ft/sec)

Figure B-1 (cont.) Disturbed Velocity Profiles: Main Channel

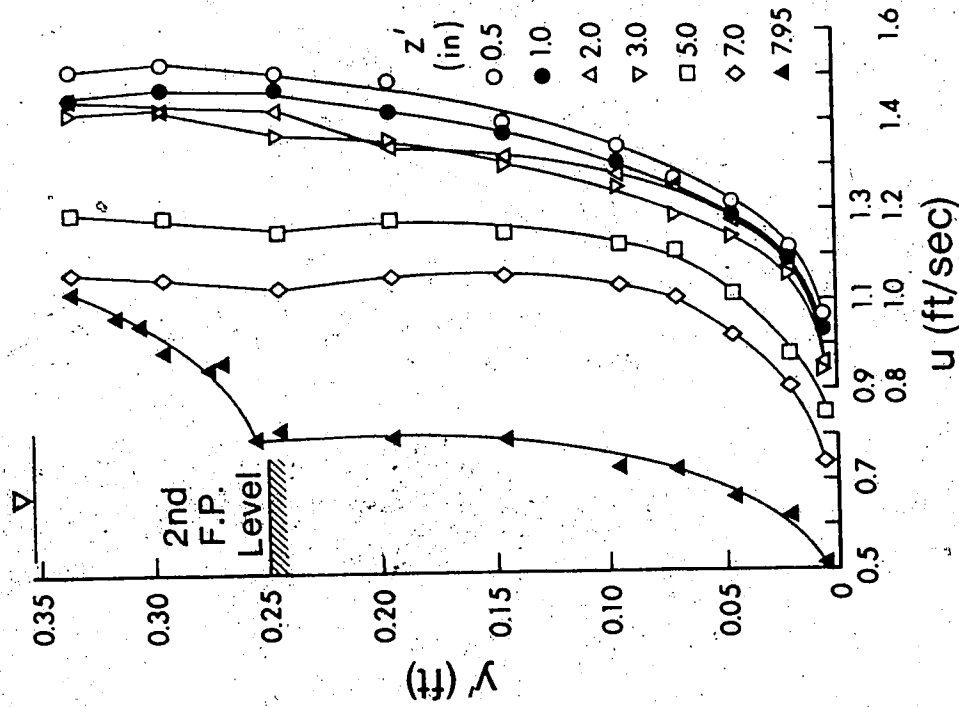**Velocity Profile in Second Flood Plain Level**

Figure B-1 (cont.) Velocity Profiles: Second Flood Plain Level

Velocity Profiles in First Flood Plain Level
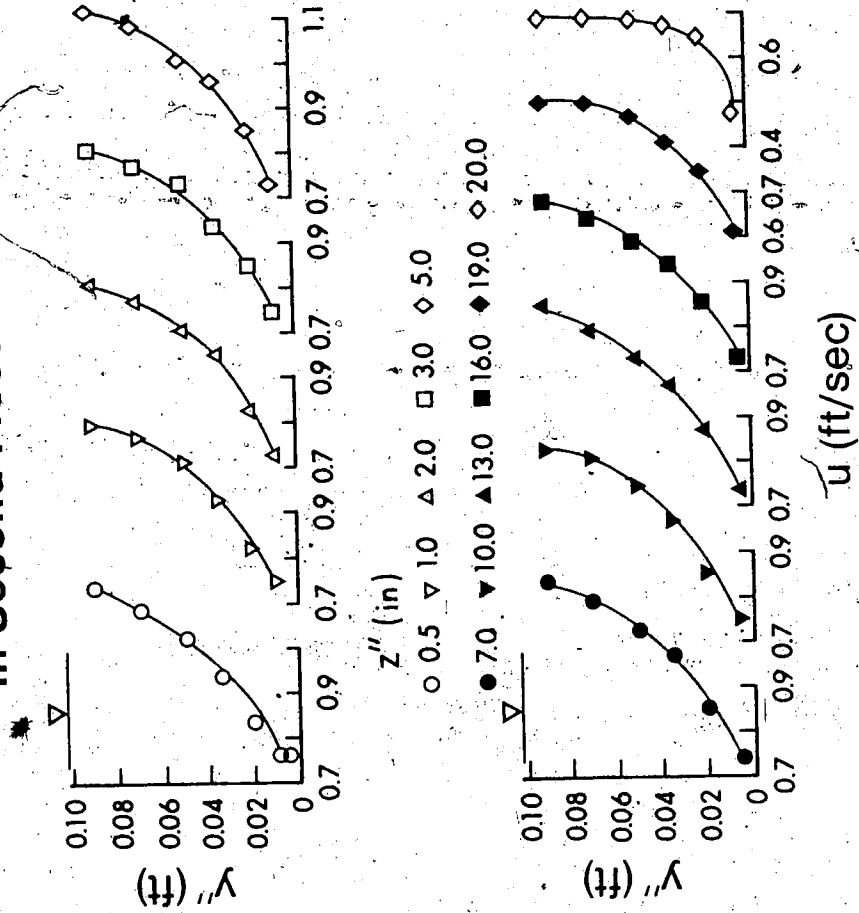
Figure B-1 (cont.) Velocity Profiles: First Flood Plain Level

Multi-Flood Plain
Lateral Velocity Profile

Bed & Wall Shear Profile
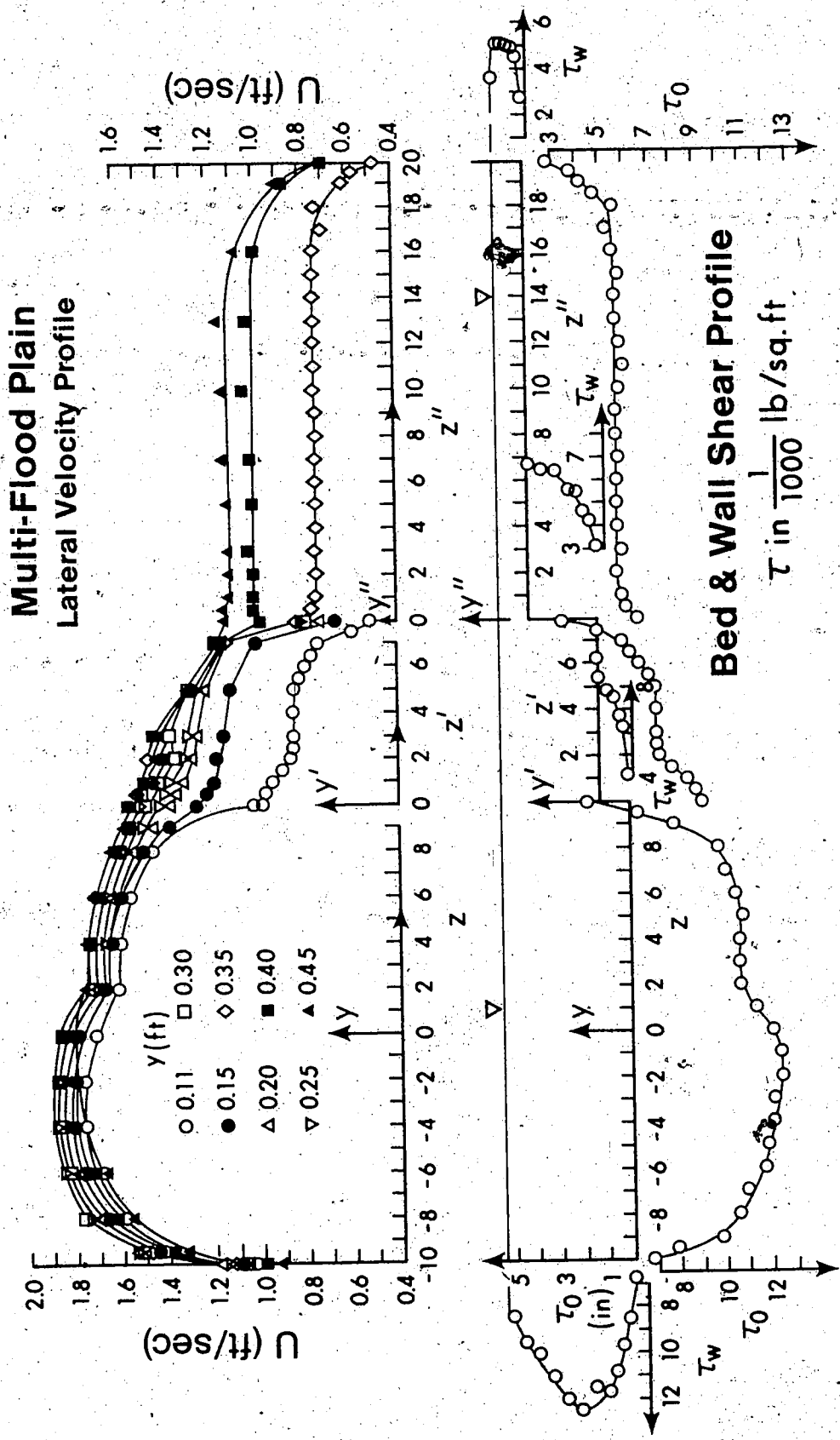τ in $\frac{1}{1000}$ lb/sq.ft

Figure B-2 Lateral Velocity & Bed Shear Stress Distribution

the second stage flood plain. The velocity continues to increase from the first stage flood plain to the main channel.

The variation of the bed shear stress with z', z'' and z''' is also shown in Figure B-2. In the main channel the bed shear stress decreases from a maximum value of τ_{om} to zero at the main channel wall which is attached to the first flood plain. In the first flood plain channel, τ_o decreases continuously from a maximum at the junction plane to approach an undisturbed value of $\tau_{0\infty1}$. Then τ_o will again decrease as it reaches the junction plane of the two flood plains. The part of the first flood plain area close to the main channel acts as a flood plain for the main channel. The other part of the first flood plain acts as main channel for the second flood plain level. τ_o on the second flood plain level will continue to decrease from the junction plane to approach an undisturbed value of $\tau_{0\infty2}$ and then τ_o will decrease as the bank of the second flood plain is approached.

B-2 Analysis of Experimental Results

From lateral velocity distributions one can see that the curve consists of two parts. The first curve looks the same as the lateral velocity distribution of a main channel with a flood plain channel having a width of the main channel equal to b' and the depth of flow equal to d'. For the second part of the curve, one should consider the main channel width equal to b' and the depth of flow equal to d'

and the flood flow width and depth the same as the second flood plain channel.

The lateral velocity distribution curves at a level $y > (h+h')$ for the above two single compound channels could easily be calculated and plotted. If these two plots are superimposed in such a way that the origin of the z axis coincides with the edge of the first and second level flood plain channels, the lateral velocity profile of the multi-level flood plains will form. Using the results obtained from Chapter IV, the two separate lateral velocities were calculated and plotted. Superposition of the two produced the final lateral velocity distribution which agreed very well with the measurements.

P-3 Conclusions

For a straight multi-level flood plain channel, the interaction between any pair of adjacent channel flows will take place. The channel adjacent to the main channel should be treated as a simple flood plain for the main channel and the same channel will serve as a main channel for the second flood plain and so on. It is possible to obtain the lateral distribution of u or τ_o by superposition of the related curves calculated for a simple compound cross-section.